

AN ANALYSIS OF THE TEMPERATURE
PROFILES OF SOME ANTARCTIC LAKES

T.G.L. SHIRTCLIFFE

Submitted for the degree of
Doctor of Philosophy

Department of Physics
Victoria University of Wellington
New Zealand
December, 1967.

ABSTRACT:

The temperature profiles of certain lakes in Taylor Valley, Victoria Land, Antarctica, are shown to be consistent with the hypothesis that these lakes were formerly cold brine pools; that their levels were raised by the addition of fresh water; and that they have since been heated principally by the absorption of sunlight.

The temperature profile of a lake in Wright Valley, Victoria Land, is shown to be consistent with the hypothesis that this lake was formerly warm and stable, as are those Taylor Valley lakes which were analysed; that the addition of a further large quantity of fresh water caused instability and limited convection; and that the heat source is again absorbed sunlight. The study of this lake requires an understanding of convection in the presence of a gradient of solute concentration. A survey of existing knowledge of this type of convection shows that it is inadequate for the task. Experiments which provide the necessary information are described.

CONTENTS

	Page	
Chapter 1	Introduction	1
Chapter 2	Non-convecting lakes	6
2.1	Lake Bonney: Description and measurements	6
2.1.1	Introduction	6
2.1.2	Measurements	8
2.2	Lake Bonney: Analysis	13
2.2.1	Basis	13
2.2.2	Seasonal effects	14
2.2.3	Steady state solution	15
2.2.4	Non-steady state solution	16
2.2.5	Initial conditions	16
2.2.6	Boundary conditions	18
2.2.7	Solution	19
2.2.8	Evaluation of the parameters	23
2.2.9	Manual optimisation	24
2.2.10	Values	26
2.2.11	Computer optimisation	27
2.2.12	Results	30
2.2.13	Discussion	32
2.3	Other applications	34
2.3.1	Lake Fryxell	34
2.3.2	Lake Joyce	36
2.3.3	Lake Bonney, eastern lobe (Hoare et al.)	37
2.3.4	Lake Bonney, western lobe	37
2.3.5	Summary and comment.	40
Chapter 3	Convecting lakes	42
3.1	Introduction	42
3.2	Lake Vanda	43
3.3	Convection	45

	Page	
3.3.1	Basic work	45
3.3.2	Non-linear temperature profiles	48
3.3.3	Overstability	49
3.3.4	Thermosolutal convection	50
3.3.5	Finite amplitude effects in thermosolutal convection	54
3.3.6	Experiments: marginal stability	57
3.3.7	Experiments: finite amplitude	59
3.3.8	Summary	62
Chapter 4	Laboratory experiments.	63
4.1	Experimental arrangement	63
4.1.1	Background	63
4.1.2	Optical equipment	65
4.1.3	Thermal equipment: instability indicator	68
4.1.4	Thermal equipment: bottom temperature	69
4.2	Experiments	70
4.2.1	Stability	70
4.2.2	Results	71
4.2.3	Periods of the oscillations	73
4.2.4	Turner - Stommel layers	74
4.2.5	Expansion of sugar solutions	77
4.3	Analysis and discussion	79
4.3.1	Stability experiments	79
4.3.2	Accuracy	80
4.3.3	Interpretation	80
4.3.4	Value of Rec	83
4.3.5	Periods of the oscillations	83
4.3.6	Turner - Stommel layers	85

	Page
Chapter 5 Lake Vanda	87
5.1 A model of the Turner-Stommel layers	87
5.1.1 Introduction	87
5.1.2 The model	88
5.1.3 Limitations	90
5.2 The development of Lake Vanda	92
5.2.1 Basis of the investigation	92
5.2.2 Application of the numerical model	94
5.2.3 Results	96
5.2.4 Conclusion	98
 Appendices:	
1. Correction of radiometer readings	100
2. Equilibrium between a Victoria - Land lake and its environment	103
3. Algol program to optimise parameters in a theoretical temperature profile	108
4. Interpretation of the experiment of Turner (1965)	114
5. Optics of the scanning schlieren system	120
6. Calibration of the optical system and determination of its accuracy.	125
7. Analysis of results of stability experiments	129
8. Numerical model of layered thermosolutal convection	132
Acknowledgments	147
References	148
List of symbols used	155

ILLUSTRATIONS

		<u>Page</u>
Fig.1	Map of McMurdo region of Victoria land.	3
2	Lake Bonney, showing locations of measuring stations.	9
3	Lake Bonney isotherms.	9
4	Light intensities in Lake Bonney.	11
5	Lake Bonney temperature profile.	16
6	Lake Bonney chloride concentration profile.	17
7	Increase of temperature with time due to absorption of solar radiation.	22
8	Increase of temperature with time due to geothermal flux.	23
9	Increase of temperature with time due to rearrangement of initial temperature distribution.	24
10	Quantities used in the calculations.	25
11	Increase of temperature with time at several specified depths.	26
12	Lake Bonney temperature profile.	33
13	Bathymetry of channel, Lake Bonney.	35
14	Lake Fryxell temperature profile.	36
15	Lake Joyce temperature profile.	38
16	Lake Bonney temperature profile (Hoare et al.)	38
17	Lake Bonney (western lobe) temperature profile.	39
18	Lake Vanda temperature, conductivity and density profiles.	44
19	Stability diagram, thermosolutal convection.	52
20	Density and Re.	64
21	Optical system.	66

		<u>Page</u>
Fig.22	Temperature measuring system. ,	70
23	Differential thermocouple record, run S8.	72
24	Differential thermocouple record, run S4.	73
25	Cells, run S15.	74
26	Profile after 3.5 hrs, run T1.	76
27	Schlieren observation after 50 min., run T2.	77
28	Profile after 62 min., run T2	77
29	Sequence of observations, run T4.	78
30	$\frac{\delta z}{\delta \theta}$ versus α , expansion coefficient measurements.	79
31	Expansion coefficient, sugar solutions.	80
32	Stability diagram using linear Re.	81
33	Stability diagram using cell heights.	82
34	Stability diagram using non-linear (cubic) Re.	83
35	Numerical model, run T4. Calculated profiles.	91
36	Numerical model, Lake Vanda. Calculated profiles.	99
A1	Directivity of the radiometer.	101
A2	Former state of Lake Bonney.	107
A3	Turner's experiment: heat flux.	115
A4	Turner's experiment: turbulent transfer coefficients.	115
A5	Turner's experiment: potential energy effects.	116
A6	Hypothetical profiles of concentration and temperature.	116
A7	Origin of diffraction effects.	124
A8	Calibration profile.	126
A9	Decay of profile by diffusion.	127
A10	Typical printout from UPHS 05.	132
A11	Starting and running solutions in the convection model.	133

TABLES

- I Temperatures measured in Lake Bonney.
- II Light intensities in Lake Bonney.
- III Laboratory measurements on samples from Lake Bonney.
- IV Calculated parameters.
- V Observed periods of oscillation.
- VI Cell heights.
- VII Calculated periods of oscillation.
- AI Measurements of transparency of ice cover.

Chapter 1
Introduction

The first recorded observation that Antarctica contains lakes of considerable size seems to have been that of Scott (1905). To reach the Polar Plateau he had ascended the Ferrar Glacier, and on returning from the Plateau he made a detour to investigate its northern arm, which is now known as the Taylor Glacier. After following this large glacier for a day, he was surprised to find that it ended not at the sea but in an inland basin several miles long, the bottom of which was occupied by "a shallow frozen lake". Beyond the lake the valley floor rose for some distance before an exit was found through a series of defiles. Further down, another lake could be seen, but no outlet to the sea was visible, and the party retraced its steps to Ross Island by way of the Ferrar Glacier.

The lake which occupied the "very curious valley" through which Scott and his companions tramped was named by them Lake Bonney. Scott was mistaken in his belief that it was shallow and frozen since, as will be seen, his own measurements imply that it was about 20m deep at the time, and the ice was probably only 2m thick. He appears to have regarded both the "frozen" lakes which he saw as fossil remnants of a former extension of the Taylor Glacier.

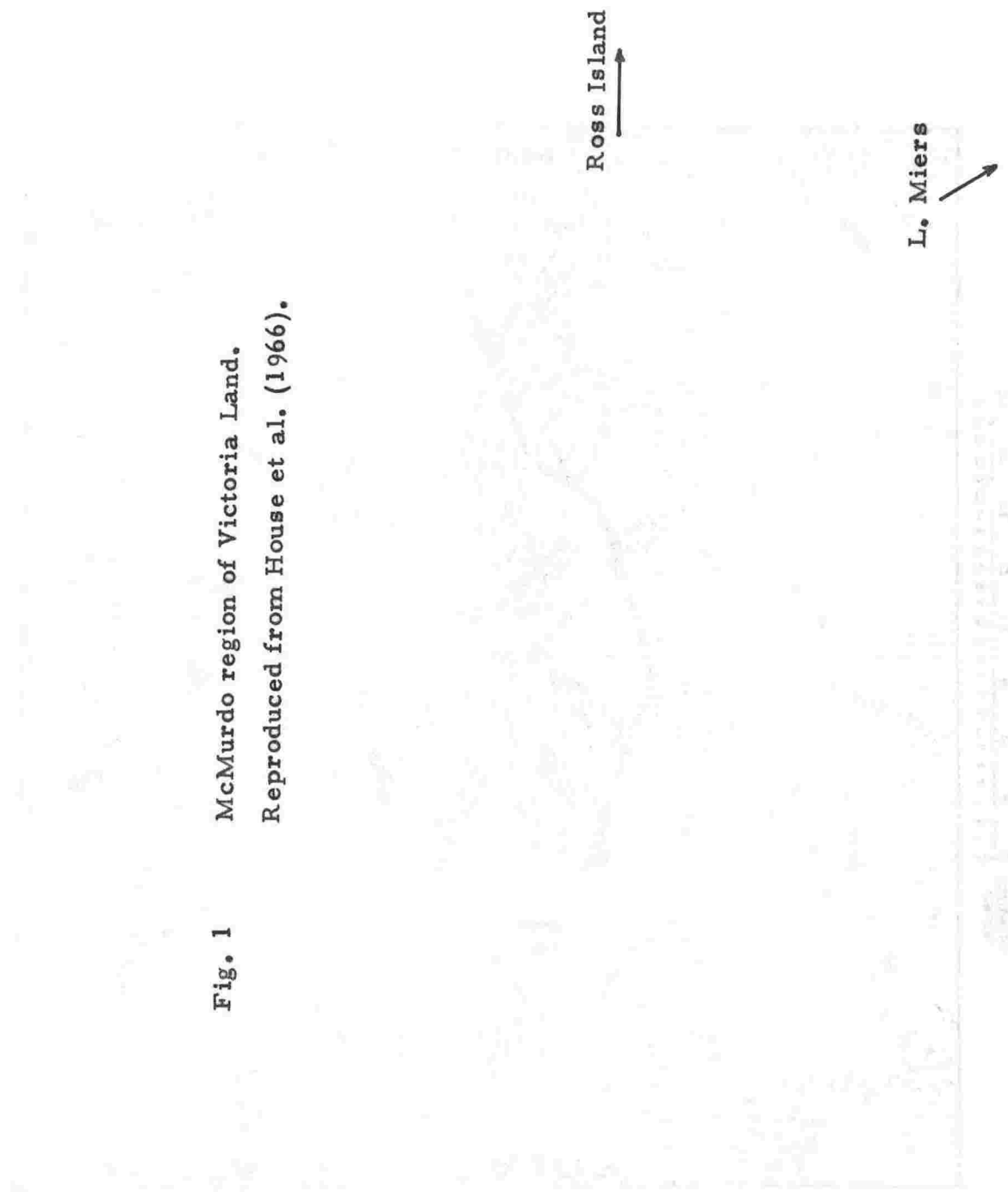
Some smaller lakes were found by Shackleton's (1909) expedition at Cape Royds, on Ross Island. One of these, Clear Lake, contained fresh water, while the others were saline. Blue Lake was 8m deep and frozen to within 1.6m of bedrock in the winter of 1908; it had apparently not thawed completely for at least three seasons. Coast Lake and Green Lake, both about 1.5m deep, were completely thawed in the summer, but while the former froze solid in the winter, a few inches of highly saline water remained in the latter. Hutchinson (1957)

regarded these lakes as being practically the only examples to be found of lakes permanently insulated by ice from changes at the earth's surface, and referred to them as "amictic". In fact they are probably too small to be truly amictic; Lake Bonney and others in the Taylor Valley are better examples.

A thorough investigation of the Taylor Valley was made by a party during Scott's second expedition, 1910-13 (Taylor, 1922). Once again the approach was made by way of the Ferrar Glacier, but this time the valley was followed to the coast. This party visited all the lakes now known as Bonney, Henderson, Popplewell, Chad, Hoare and Fryxell (see fig.1), but the only observation relevant to the present investigation was that the level of Lake Bonney had risen markedly since 1903. The difference was sufficient to cause Scott to ponder its origin in his journal (Scott, 1913).

It was not until the summer of 1960/61 that an expedition was mounted specifically to investigate the lakes of Victoria Land. The result was the unexpected discovery that they contained considerable depths of water, and that moreover the temperature of this water was well above freezing point (Angino et al., 1962; Armitage and House, 1962; Goldman, 1962; Angino and Armitage, 1963). This expedition investigated Lakes Vanda, Vida, Bonney and Fryxell on the mainland, in addition to the smaller lakes at Cape Royds and Cape Evans, on Ross Island. The expedition was regarded as a reconnaissance and was concerned primarily with biological and chemical aspects. In consequence, the curious fact that the lakes (except for Vida) contained liquid water in a region whose average temperature is about -20°C received little attention. Except in the case of Lake Fryxell, where solar radiation was thought to account for part of the heating, it was suggested that geothermal effects were responsible.

Fig. 1
McMurdo region of Victoria Land.
Reproduced from House et al. (1966).



During the 1961/62 summer Lake Bonney was investigated again by Angino et al. (1964), and the origin of its high temperatures was considered in more detail. The conclusion was reached that hot springs probably existed under the lake, solar radiation being an inadequate source of heat. During the same season Lake Vanda was studied by Wilson and Wellman (1962). The maximum temperature in this lake is about 25°C, compared with only 7.5°C for Lake Bonney. However it was shown that even such a high temperature could be maintained by the absorption of sunlight, since convection was inhibited by a stable gradient of salt concentration, and heat loss by conduction was very slow.

The following summer, Ragotzkie and Likens (1964) visited Lakes Bonney and Vanda, and an expedition from Victoria University of Wellington studied Lake Bonney (Shirtcliffe and Benseman, 1964). Further VUW expeditions investigated a number of lakes during the 1963/64 and 1964/65 summer seasons; results have so far been published concerning Bonney (Hoare et al., 1964), Fryxell (Hoare et al., 1965; Henderson et al., 1966), Vanda (Hoare, 1966) and Miers (Bell, 1967) only.

From all these investigations it appears that there are certain features which characterise the lakes of Victoria Land. They are all ice-covered, the thickness of ice being such as to allow a balance between the annual depth increment due to meltwater, the annual accretion at the bottom of the ice cover, and the annual loss of ice through ablation at the surface; this thickness is about 3-6m generally. The lakes are fed by fresh meltwater from the surrounding glaciers during the summer. They have no outflow, except for Lake Miers, which overflows intermittently. They contain large quantities of various salts in solution, the strength of the solution being greater at depth; the resulting density gradients inhibit convection in the lakes to varying degrees. Finally, some sunlight penetrates the ice cover, and provides a weak heat source which may have a significant long-term effect in the absence of convection.

It is clear that the relationship between these lakes and their environment is quite different to the case of lakes in other, more temperate, areas. In particular, because convection is inhibited, there exists a possibility that palaeoclimatic information may be stored in the profiles of temperature and solute concentration. Such information would be of obvious value in the study of an area such as Antarctica, in view of its likely influence on the climate elsewhere and the lack of direct observations in the past. This work is an attempt to account for the observed profiles, in the hope that this information can be recovered.

Scope of the work. The work which is described in this thesis began with the expedition to Lake Bonney led by the author in January 1963. The aim of that investigation was to test the hypothesis that absorbed sunlight is the major source of heat in the lake. A detailed analysis of the results has already been published (Shirtcliffe, 1964), and shows clearly that the hypothesis is correct. This analysis is repeated here in chapter 2, and extended both to give more information about Lake Bonney, and also to describe other similar lakes.

Consideration of the heat balance in Lake Bonney is simplified by the apparent absence of convection. Since all heat flow is conductive, it is possible to discuss the problem in terms of exact solutions of the equation governing heat conduction. Some of the Victoria Land lakes are subject to limited convection, however, which raises additional problems of analysis. The most interesting such lake on which information is available is Lake Vanda. Here the convection occurs in a series of layers, the distinction between the layers being maintained by the downward stepwise increase of salinity. The question of convection is taken up in chapter 3, and it is clear from this discussion that existing knowledge of the character of convection in the presence of a solute concentration gradient is not sufficient to allow an analysis of the heat balance in Lake Vanda to be made.

Chapter 4 describes laboratory experiments which were conducted in order to clarify the nature of thermosolutal convection. The experiments cover both the question of the stability criterion which governs the onset of such convection, and also the nature of its fully developed form.

Finally in chapter 5 the discussion returns to Lake Vanda. It is shown first that the observed development of thermosolutal convection in layers can be predicted quite well by a simple numerical model. The nature of this model is such that, although it is tested only against experiments performed in the laboratory, it may equally be applied to a system of greater magnitude such as a lake, with only minor changes. This is done, with respect to Lake Vanda, and it is shown that the present unusual character of that lake is consistent with its development as a thermosolutal convecting system, the heat source being entirely absorbed solar radiation.

Chapter 2

Non-convecting lakes

2.1 Lake Bonney: Description and measurements

2.1.1 Introduction

Lake Bonney lies in a drainage basin at the foot of the Taylor Glacier, in the upper part of the Taylor Valley. The lake is nearly 6 km long over-all, but is separated into two lobes by Bonney Riegel, a steep spur which runs nearly across the valley from the southern side. Of the two lobes the western, nearer the glacier, is much the smaller, though it has the larger catchment area, and it is connected with the larger lobe by a narrow and relatively shallow channel. Mountain ranges border the lake to the north and south, shading it to some extent even in midsummer. To the east, the valley floor rises gradually to Nussbaum Riegel, preventing any outflow of water. The annual inflow of meltwater is therefore compensated only by evaporation of the permanent ice cover.

At the time of the author's visit to the lake, two mechanisms had been advanced to explain the high temperatures found in the Victoria Land lakes. The first of these was due to Armitage and House (1962) and ascribed the heating to geothermal effects, either springs of warm water or a high geothermal heat flux. The second theory was that advanced by Wilson and Wellman (1962), who showed that the temperature gradient near the bottom of Lake Vanda varied in a manner consistent with the production of heat by exponentially absorbed solar radiation. The geothermal theory apparently arose from the first investigators' attempts to describe these lakes in the traditional terms which have arisen from studies of temperate lakes. Although solar radiation accounts for a major part of the heat budget of many lakes, heat gained in this way is normally lost when winter cooling of the surface induces convection, and the average annual gain is zero.

In the case of Lake Bonney, the maximum temperature occurs about 20 m above the lake bed. Since the temperature falls at depths greater than this, heat is clearly flowing downwards, and a high upward geothermal heat flux could not account for the observed distribution of temperatures. Angino et al. (1964) suggested that warm water of intermediate density may flow into the lake from springs, float up to a level determined by its density, and there act as a heat source. This theory exploits the fact that the maximum temperature occurs where the density gradient is greatest, since that is the level most likely to provide the appropriate density. It would be expected that the temperature would vary horizontally as well as vertically, being somewhat higher near a spring, and indeed the isotherms near the level of maximum temperature do show some lenticular deviation from the horizontal. Any water originating in the springs would have to be compensated by an increased rate of surface evaporation, but the quantity need not be large. For example, an intrusion of water at 30°C need only amount to 50 gm per cm² of the lake's surface area annually to supply all the heat required, a quantity of the same order as the ablation rate observed on nearby Lake Fryxell (Henderson et al. 1966).

There are two main arguments against the hot spring theory. The first is that no springs are observed outside the lake. This may be fortuitous, but if paths could be melted through the permafrost to allow springs to appear under the lake, it is equally possible for this to happen elsewhere. A spring may be encouraged to appear underwater if another heat source is available to melt the permafrost, but in this case it becomes unnecessary to invoke the spring.

Secondly, the temperature distribution should tend towards a linear reduction with distance above and below the heat source. This is not the case, and it would be difficult to account for the detail of the observed temperature profile on the hot spring theory.

2.1.2 Measurements

The author's expedition to Lake Bonney was intended to give data which would allow the solar heating theory to be tested, and accordingly it was planned to measure temperature, density, chemical content and solar radiation as a function of depth at numerous stations on both lobes of the lake. In fact difficulties over transport prevented completion of the planned program, but sufficient measurements were made in each category to allow a test of the theory as it applies to the eastern lobe of the lake. In all, measurements were made at ten stations, the locations of which are shown on the map of fig.2. In each case a period of at least 12 hours elapsed after drilling a hole before measurements were taken there, to allow any disturbance in the water to decay.

Temperature. Water temperatures were measured with copper-constantan thermocouples. The surface water of the lake was fresh, and the cold junction, which was held in a vacuum flask containing this water and ice, was assumed to be at 0°C .

A Cambridge portable potentiometer was used to measure the thermocouple emf. The slide wire of this instrument was marked in $10 \mu\text{v}$ steps, but calibration by the Physics and Engineering Laboratory, DSIR, showed that interpolation to $\pm 2 \mu\text{v}$ was justified. This implies an ideal limit of error of $\pm 0.05 \text{ C deg}$ for the temperatures, although other factors undoubtedly tended to widen these limits and may have produced readings in error by $\pm 0.1 \text{ C deg}$ on occasion. The most serious threat to accuracy was the strong wind, and it was found necessary to rest the potentiometer on a triangle of wooden pegs fixed in the ice to prevent the galvanometer rocking.

Temperatures were measured at depth intervals of 1.52 m (5 ft) at the ten stations between January 6 and January 9, 1963. The mean profile is given in table I, and the horizontal variation is shown by the isotherms plotted in fig.3.

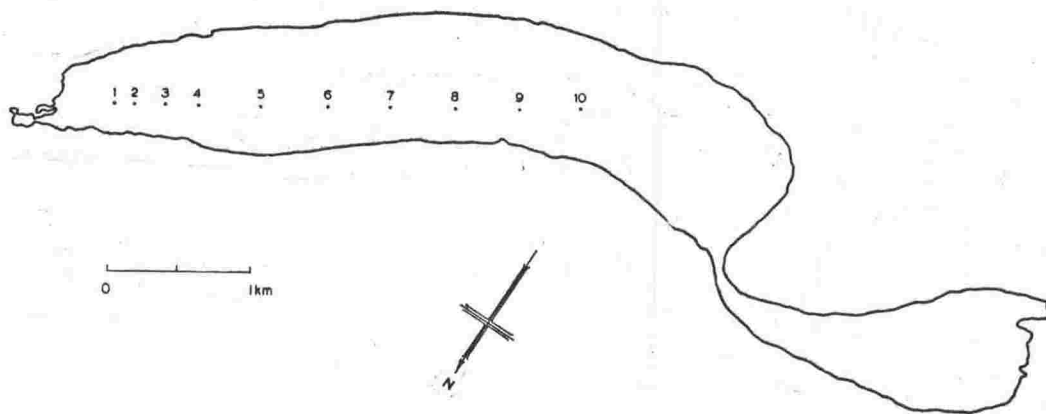


Fig.2. Lake Bonney, showing locations of measuring stations.

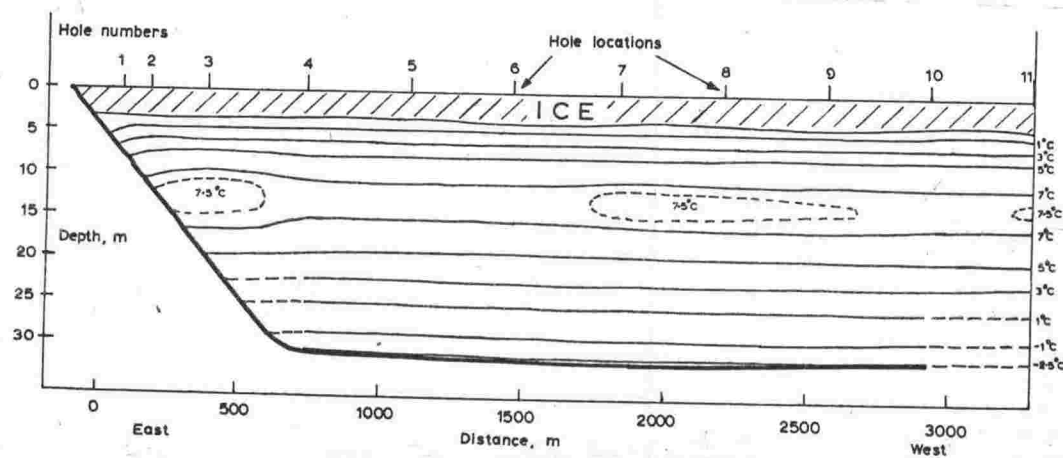


Fig.3. Vertical section of Lake Bonney, showing isotherms.

Table I

Mean temperature profile in Lake Bonney

<u>Depth (m)</u>	<u>Temperature (°C)</u>
4.57	0.94
6.10	3.00
7.62	4.97
9.15	6.22
10.68	7.01
12.20	7.48
13.72	7.52
15.25	7.13
16.78	6.52
18.30	5.69
19.82	4.67
21.34	3.74
22.87	2.66
24.40	1.72
25.92	0.70
27.44	-0.08
28.96	-0.96
30.48	-1.74
31.70	-2.60

Radiation. Radiation measurements were made on only one occasion. This was at station 10 at midday on January 9. Light clouds drifted across the sun at times, but, when possible, readings were taken with the sun clear. The instrument used was a selenium photocell potted in perspex and araldite and coupled directly to the potentiometer. The photocell had maximum response at a wavelength of 550 m μ , which is near that at which water has its maximum transmission.

The results are shown in table II and figure 4. Because of the peaked response of the photocell, readings taken near the surface cannot be compared directly with those taken at other depths. After the light had penetrated some distance, however, the filtering effect of the water restricted the bandwidth present within the acceptance bandwidth of the detector. Thus the logarithmic variation of the readings between 12m and 30m is taken to indicate directly an absorption length of $8.2 \pm 0.6\text{m}$ (that is, an extinction coefficient of $0.12 \pm 0.01 \text{ m}^{-1}$) between those depths.

Table II

Light intensities in Lake Bonney (midday, 9/1/63).

<u>Depth (m)</u>	<u>Photocell output (mV)</u>	
	<u>Lowering</u>	<u>Raising</u>
0	63.0	61.25
1.53	15.55	-
3.05	9.75	8.10
6.10	7.15	6.60
9.15	6.60	6.15
12.20	5.55	5.50
15.25	4.0	4.0
18.30	2.55	2.55
21.34	1.73	1.68
24.40	1.40	1.20
27.44	0.92	0.87
30.48	0.56	0.59

Immediately under ice cover: 7.0 mV (raising).

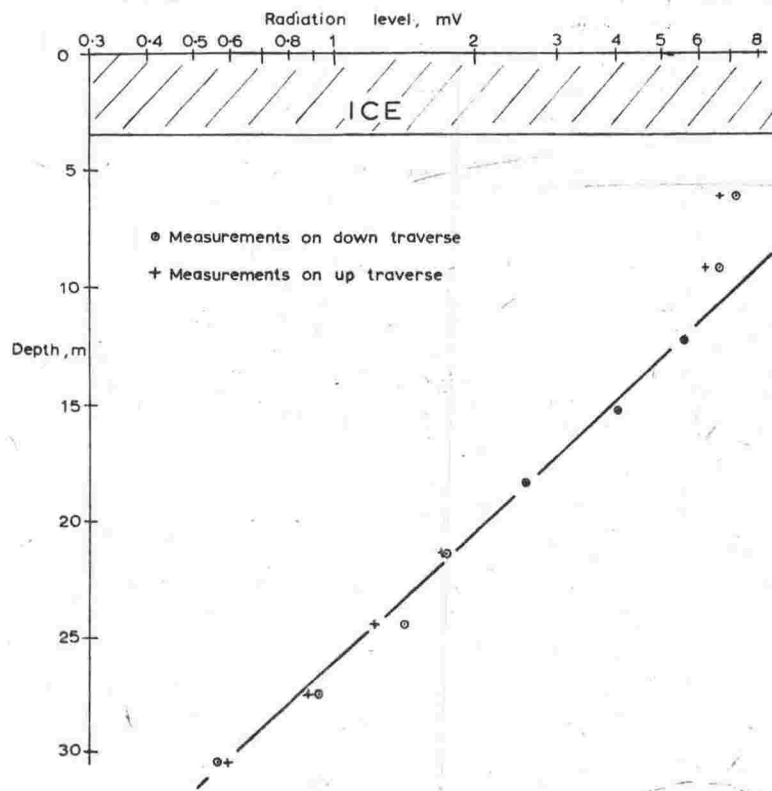


Fig.4. Measured variation of solar radiation with depth in Lake Bonney. The solid line corresponds to an absorption length of 8.2m.

It seems likely that the rough ice acted as a diffusing surface, so that the major part of the radiation in the water was travelling almost vertically downward, nearly along the axis of the detector. A reading taken at the surface is, however, subject to correction not only on account of the bandwidth considerations mentioned above but also because the radiation from the sun was incident from a direction some 56° off axis. While the radiation readings are chiefly of interest in the evaluation of the extinction coefficient, it is also useful to know what fraction of radiation incident on the ice actually penetrates to the water. An attempt was therefore made to correct the readings taken above and immediately below the ice, to evaluate the true ratio of radiation intensities. The corrections are described in Appendix 1, where it is shown that between 1% and 2% of incident radiation penetrated the ice.

Density. Water samples were taken from station 4 at depth intervals of 1.52 m. A hose lowered to the appropriate depth was coupled to a hand pump and a sufficient quantity of water drawn from each depth to ensure that the whole system was thoroughly purged and the sample representative. Later, the density of each sample was measured in the laboratory using calibrated hydrometers. In each case the measurement was made at a temperature sufficiently close to that of the sample in situ, usually within 0.2 C deg, for the density to be equal to that in situ, within the measurement accuracy of ± 0.0005 gm/ml. The results are shown in table III.

Salinity. The electrical conductivity and chloride content of the water samples were measured in the laboratory, and are also shown in table III.

Table III
Results of Laboratory Measurements on Samples Taken from
Various Depths in Lake Bonney

Depth m	Density g/ml	Temper- ature, °C	Electrical Conduc- tivity at 19°C, (ohm cm) ⁻¹ X 10 ³	Chloride Content, ppm
0-3.5	Ice			
4.6	1.0014	1.2	3.40	800
6.1	1.0022	3.0	4.84	1300
7.6	1.0062	4.9	11.75	4320
9.2	1.0096	6.2	16.6	7360
10.7	1.0195	7.0	29.8	16680
12.2	1.0508	7.4	52.8	44750
13.7	1.0885	7.4	66.4	78000
15.2	1.1266	7.1	64.6	119000
16.8	1.1510	6.4	64.6	138000
18.3	1.1660	5.0	66.4	151000
19.8	1.1751	4.6	68.4	164000
21.4	1.1801	3.6	68.4	175000
22.9	1.1846	2.6	68.4	180000
24.4	1.1868	1.5	68.4	180000
25.9	1.1888	0.6	68.4	180000
27.4	1.1895	0.0	68.4	180000
29.0	1.1932	-1.0	68.4	180000
30.5	1.1985	-2.0	68.4	180000

The temperature indicated in column 3 is that at which the density measurement was made.

2.2 Lake Bonney: Analysis

2.2.1 Basis

The in situ densities show that the water in the lake is stably stratified, while the electrical conductivity and chloride measurements show that the increase of density with depth is caused by the increasing salt content. (A later, apparently more accurate, investigation by Hoare et al. (1964) showed a chloride concentration increasing downwards even near the lake bottom, so the apparent constancy of the present results at depth is not inconsistent with this conclusion.) Thus the solar heating hypothesis can be tested on the assumption that heat, produced by the absorption of radiation, is transferred by conduction only, there being no vertical circulation of the water. The isotherms plotted in fig. 3, and similar measurements taken by other investigators, all show that there is very little horizontal variation of temperature except near the lake edge. Thus over most of the lake it may be assumed that the heat flow is vertical, and the relatively small departure of the lake bed from a horizontal planar form may be neglected.

The development of the temperature profile can therefore be represented by the equation governing the conduction of heat in one dimension,

$$\frac{\partial \theta}{\partial t} = K \frac{\partial^2 \theta}{\partial z^2} + \frac{KA}{k} \quad (1)$$

where

- θ = temperature
- t = time
- z = depth
- K = thermal diffusivity
- k = thermal conductivity
- A = rate of heat production per unit volume.

If the radiation is absorbed logarithmically, as is approximately the case in Lake Bonney, and is incident at a rate $Q \text{ cal cm}^{-2} \text{ sec}^{-1}$ at the upper surface of the water (i.e. at $z = 0$), we may write

$$A = \eta Q e^{-\eta z} \quad (2)$$

where z is positive downwards, and η is the extinction coefficient.

2.2.2 Seasonal effects

In equation (2), Q is not constant; in addition to the diurnal effect due to variation of the sun's altitude, there is a large annual fluctuation. Most of the radiation occurs in the 4-month period from November to February, and there is none from mid-April to mid-August.

The quantity of heat absorbed in the lake each year is so small that the annual oscillation of temperature is of little interest in comparison with the long-term trend towards an equilibrium state. Furthermore, the extreme values of the oscillation occur at the beginning and end of the summer heating period. The seasonal effect should thus be minimal in the measurements, which were made only two weeks after midsummer.

An indication of the amplitude of the seasonal oscillation is available in the data of Angino et al. (1964), which show increases of up to 1 C deg between the beginning and end of the 1961-62 summer. Alternatively, the fall which should occur during winter can be estimated by the Schmidt graphical method, which can be used to solve (1) when $A = 0$. This method predicts a maximum fall of about 0.5 C deg if the temperature profile at the beginning of winter was the same as that measured at midsummer. Since the heat flow would be rather greater at the beginning of winter than at midsummer, owing to the extra heating, both figures agree quite well. Thus the seasonal oscillation of temperature is no more than ± 0.5 C deg superimposed on the long-term heating, and this variation is small compared to the lake's existing temperature excess of about 20 C deg over the annual average temperature of the environment. This fact and the timing of the measurements justify the neglect of seasonal effects in the analysis.

2.2.3 Steady state solution

It is instructive to solve (1) first for the equilibrium state, so that the extent to which the lake at present deviates from this state may be seen. With

$$\frac{\partial \theta}{\partial t} = 0$$

and boundary conditions

$$\theta = 0 \quad \text{at} \quad z = 0$$

$$\frac{d\theta}{dz} = 0 \quad \text{at} \quad z = z_m$$

the steady-state temperature distribution is given by

$$\theta = \frac{Q}{k} \left\{ \frac{1}{\eta} - z e^{-\eta z} - \frac{1}{\eta} e^{-\eta z} \right\} \quad (3)$$

in the case of a lake of infinite depth.

Fig. 5 shows a comparison of the observed mean temperature profile with that predicted by (3), where z_m and η are observed values of the depth of the temperature maximum and the extinction coefficient respectively, and $\frac{Q}{k}$ has been chosen to give satisfactory agreement between theory and experiment. Note that the theoretical profile is referred to the depth at which the temperature is zero. The measured profile suggests that the base of the ice cover has been displaced upward from its mean annual level, presumably by a combination of fresh melt-water flowing into the lake and melting of the ice, so the theoretical curve has been related to a lower level.

The value of $\frac{Q}{k}$ used in the profile of fig. 5 was $0.032 \text{ deg cm}^{-1}$. Taking $0.0012 \text{ cal sec}^{-1} \text{ deg}^{-1} \text{ cm}^{-1}$ for the conductivity k , and assuming that 1.5% of radiation incident on the ice penetrates to the water, the incident radiation amounts to $80,000 \text{ cal cm}^{-2} \text{ yr}^{-1}$, which compares well with the Scott Base value of 91,000 (Thompson and Macdonald, 1962). There is reasonable agreement of form between the measured and calculated profiles, and this, together with the satisfactory estimate of radiation intensity, constitutes good evidence in favour of the solar heating theory. However the steady state theory cannot explain the

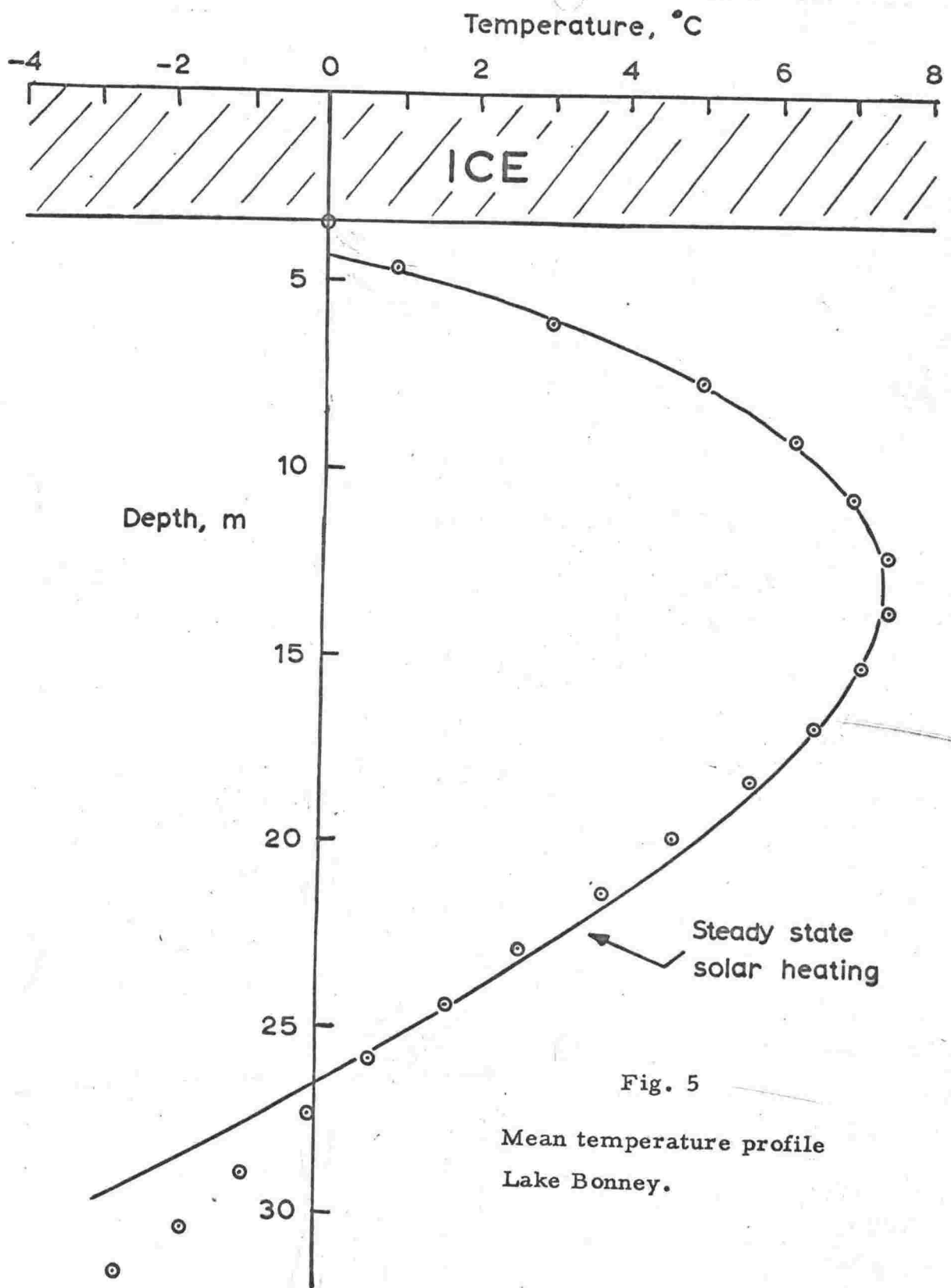


Fig. 5

Mean temperature profile
Lake Bonney.

small decrease in downward heat flow which occurs below a depth of 25m. In order to account for the detail of the temperature profile it is necessary to remove the steady state restriction.

2.2.4 Non-steady state solution

Here again the basic equation to be solved is (1), without restriction on the value of $\frac{\partial \theta}{\partial t}$. Once again attention will be focussed on the long-term effects by assuming Q to be constant. It will also be assumed again that the extinction coefficient η is the same at all depths, though the value in the uppermost 5m of water is uncertain.

2.2.5 Initial conditions

Solution of (1) demands a knowledge of the temperature distribution at time $t = 0$. Fortunately the solution for values of t in the range of interest is not unduly sensitive to the initial distribution, and a satisfactory estimate can be made by reference to the present salt distribution (fig.6). This is of a form similar to that which is to be expected as a result of diffusion from a uniformly concentrated layer of solution into a layer of fresh water. It is therefore inferred that at one time the lake was somewhat shallower than now and of uniformly high salinity, and that fresh water ran in over the brine to bring the surface up to its present level. The fact that the lake is coldest at the bottom implies that this brine was cold.

At the boundary between the fresh water and the salt solution a density gradient would have been established which would have prevented any convection in that region, heat transfer being entirely conductive. By the absorption of sunlight, and because of the low rate of transfer of heat through it, this conductive region would have tended to become heated relative to the water above and below. The heating from above would have further stabilized the lower part of the lake. In the upper part stability would have been induced firstly because fresh water heated from below is stable until its temperature exceeds that of its maximum density, and secondly because while the temperature was below that

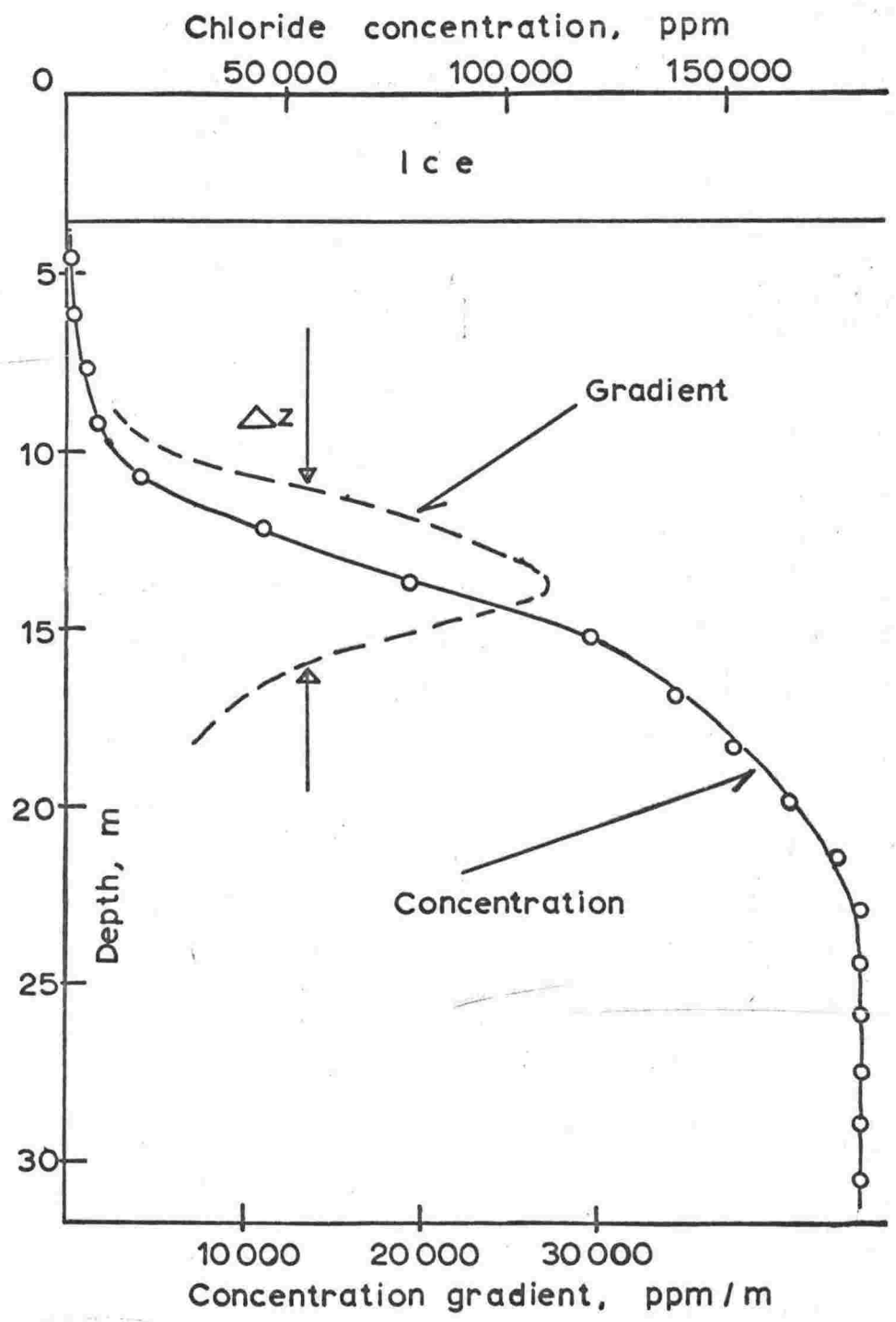


Fig. 6

Chloride concentration profile, Lake Bonney. The gradient of this curve is also shown in part.

limit a stabilizing salt concentration gradient would have been produced by diffusion from the concentrated lower layer.

It is to be supposed that the lake was formerly in equilibrium with its environment, and that the postulated inflow of fresh water produced a relatively rapid transition to a new equilibrium. The nature of such an equilibrium is considered in appendix 2, both generally and as it applies in Lake Bonney. It is shown that a cold brine lake can be in equilibrium with its environment provided the annual inflow is so small that convection is induced in the brine every winter when its upper surface is cooled. Once the ice is separated from the brine by a layer of fresh water which is too thick to be frozen during a winter, annual stirring is not provided, a stable density gradient is set up, and long-term solar heating starts.

The inferred position of the boundary between the primary brine and the fresh layer must be consistent with the present distribution of salt. Fig.6 includes a partial graph of the gradient of chloride concentration, and the boundary must be assumed to have existed where this curve goes through a maximum. Thus the primary brine lake was 18m deep.

The base of the present ice cover was found to lie at an average depth below the free water surface of 3.35m. However the upward heat flow was much less at that level than it was at slightly greater depths, which suggests that water immediately under the ice was being heated relatively rapidly. As in the steady state analysis, it is assumed that this water resulted from the summer thaw and can be neglected in the analysis, and that throughout the period concerned in the analysis the effective 0°C level lay a little below that measured. The magnitude of this offset will be considered later.

While the temperature T_i of the primary brine is an important parameter, initial conditions in the fresh layer are less so. Two simple possibilities present themselves: firstly, that the fresh layer was

initially uniform at 0°C ; and secondly, that there was a linear variation of temperature between the surface at 0°C and the brine boundary at T_i . The second alternative defies the observation that fresh water freezes at 0°C , but takes some account of the presumption that the layer was not in fact formed instantaneously, but arose over perhaps four or five consecutive summers, during which period salt would have diffused upward and lowered the freezing point somewhat. On balance, the second alternative appears more realistic, and is the one adopted.

It is necessary to allow for some minor geothermal effects. This is done most simply by assuming that before the lake increased in depth heat entered from below by means of a temperature gradient in the underlying rock, this gradient extending unchanged to a great depth below the lake. As the lake temperature rose, heat would still have flowed upward under the influence of such a gradient, even though at the bottom of the lake there was a downward net flow of heat. The main result would therefore have been to heat the rock under the lake and reduce the heat loss through the lake bed. Whether the magnitude deduced for this temperature gradient can be interpreted literally is open to doubt. The value is not inconsistent with a geothermal origin but on the other hand it is conceivable that the heat concerned may have been stored in the rock during some previous epoch when the lake was heated. Whatever its true origin, the effect will be referred to as geothermal for the sake of convenience.

2.2.6 Boundary conditions

As well as the condition that the temperature is maintained at 0°C at the level taken as $z = 0$, three other boundary conditions must be satisfied:

(1) The temperature must be continuous at $z = l_1$ and $z = l_2$, where l_1 is the depth to the junction of the primary brine and the fresh water layer, and l_2 is the depth to the lake bed (see fig.10).

(2) Any radiation reaching the bottom of the lake is absorbed there, causing a discontinuity in temperature gradient. Thus, at $z = l_2$,

$$k_2 \frac{\partial \theta_2}{\partial z} - k_3 \frac{\partial \theta_3}{\partial z} = Q e^{-\gamma l_2}$$

where k_2 , θ_2 and k_3 , θ_3 are values in the regions $l_1 < z < l_2$ and $z > l_2$ respectively.

(3) As $z \rightarrow \infty$ the temperature gradient tends to a constant positive value γ .

2.2.7 Solution

The problem divides naturally into three parts, which correspond respectively to the radiation effect, the geothermal effect, and the effect of heat flows which result from the nonuniform initial temperature distribution in the water.

The temperature distributions R, S, and T due to these effects are found separately by solving the basic equation for three different sets of initial and boundary conditions. Superposition of these sets leads to the initial and boundary conditions stated for the problem as a whole, and superposition of the three temperature distributions gives the required total distribution.

The three problems and their solutions are given below, the solutions having been obtained by Laplace transformation. For simplicity, it has been assumed throughout that there is thermal matching between the lake water and the underlying rock, that is,

$$k_2/K_2^{1/2} = k_3/K_3^{1/2}.$$

The effect of this assumption is to remove from the solutions a number of terms which appear to be negligible if the mismatch is not large. Taking the range of values given in the Smithsonian Physical Tables for granite as an indication of probable magnitudes, we get, in cgs units,

$$\begin{aligned} k_2 &= 0.0012 \\ k_3 &= 0.0045 - 0.0050 \end{aligned}$$

$$K_2 = 0.0012$$

$$K_3 = 0.0127$$

Hence

$$k_2/K_2^{1/2} = 0.035$$

and

$$k_3/K_3^{1/2} = 0.040-0.045.$$

The mismatch indicated seems unlikely to affect the accuracy of the calculations seriously.

Solutions will be given here only for the region $0 \leq z \leq l_2$, since this is the region in which measurements are available, and because the expressions for $z > l_2$ are very lengthy.

Radiation part.

$$\frac{1}{K_1} \frac{\partial R_1}{\partial t} = \frac{\partial^2 R_1}{\partial z^2} + \frac{\eta Q}{k_1} e^{-\eta z} \quad 0 \leq z \leq l_1$$

$$\frac{1}{K_2} \frac{\partial R_2}{\partial t} = \frac{\partial^2 R_2}{\partial z^2} + \frac{\eta Q}{k_2} e^{-\eta z} \quad l_1 \leq z < l_2$$

$$\frac{1}{K_3} \frac{\partial R_3}{\partial t} = \frac{\partial^2 R_3}{\partial z^2} \quad z > l_2$$

where

$$K_1 = K_2$$

$$k_1 = k_2$$

$$R_1 = 0 \quad \text{at } z = 0, \quad \text{all } t$$

$$R_1 = R_2 \quad \left. \vphantom{R_1 = R_2} \right\} \text{at } z = l_1, \quad \text{all } t$$

$$\frac{\partial R_1}{\partial z} = \frac{\partial R_2}{\partial z}$$

$$\left. \begin{aligned} R_2 &= R_3 \\ k_2 \frac{\partial R_2}{\partial z} - k_3 \frac{\partial R_3}{\partial z} &= Q e^{-\eta l_2} \end{aligned} \right\} \text{at } z = l_2, \text{ all } t$$

$$R_1 = R_2 = R_3 = 0 \text{ at } t = 0, \text{ all } z.$$

Then the temperature in the water ($0 \leq z \leq l_2$) is given by

$$\begin{aligned} R = \frac{Q}{k_1 \eta} & \left\{ \operatorname{erfc} \left(\frac{z}{2K_1^{1/2} t^{1/2}} \right) + e^{-\eta z} (e^{K_1 \eta^2 t} - 1) \right. \\ & \left. - \frac{1}{2} e^{K_1 \eta^2 t} \left[e^{-\eta z} \operatorname{erfc} \left(\frac{z}{2K_1^{1/2} t^{1/2}} - \eta K_1^{1/2} t^{1/2} \right) + e^{\eta z} \operatorname{erfc} \left(\frac{z}{2K_1^{1/2} t^{1/2}} + \eta K_1^{1/2} t^{1/2} \right) \right] \right\} \\ & + \frac{Q}{2k_1 \eta} \left\{ e^{K_1 \eta^2 t} \left[e^{\eta z} \operatorname{erfc} \left(\frac{l_2 + z}{2K_1^{1/2} t^{1/2}} + \eta K_1^{1/2} t^{1/2} \right) \right. \right. \\ & \left. \left. - e^{-\eta z} \operatorname{erfc} \left(\frac{l_2 - z}{2K_1^{1/2} t^{1/2}} + \eta K_1^{1/2} t^{1/2} \right) \right] + e^{-\eta l_2} \left[\operatorname{erfc} \frac{l_2 - z}{2K_1^{1/2} t^{1/2}} - \operatorname{erfc} \frac{l_2 + z}{2K_1^{1/2} t^{1/2}} \right] \right\} \end{aligned}$$

The first of these two expressions is the solution for an infinitely deep lake ($l_2 \rightarrow \infty$) and the second is the correction for finite depth. The quantity $Rk_1 \eta / Q$ is shown plotted for various values of the time t in Figure 7.

Geothermal part.

$$\frac{1}{K_1} \frac{\partial S_1}{\partial t} = \frac{\partial^2 S_1}{\partial z^2} \quad 0 \leq z < l_2$$

$$\frac{1}{K_3} \frac{\partial S_3}{\partial t} = \frac{\partial^2 S_3}{\partial z^2} \quad z > l_2$$

where

$$S_1 = 0 \text{ at } z = 0, \text{ all } t$$

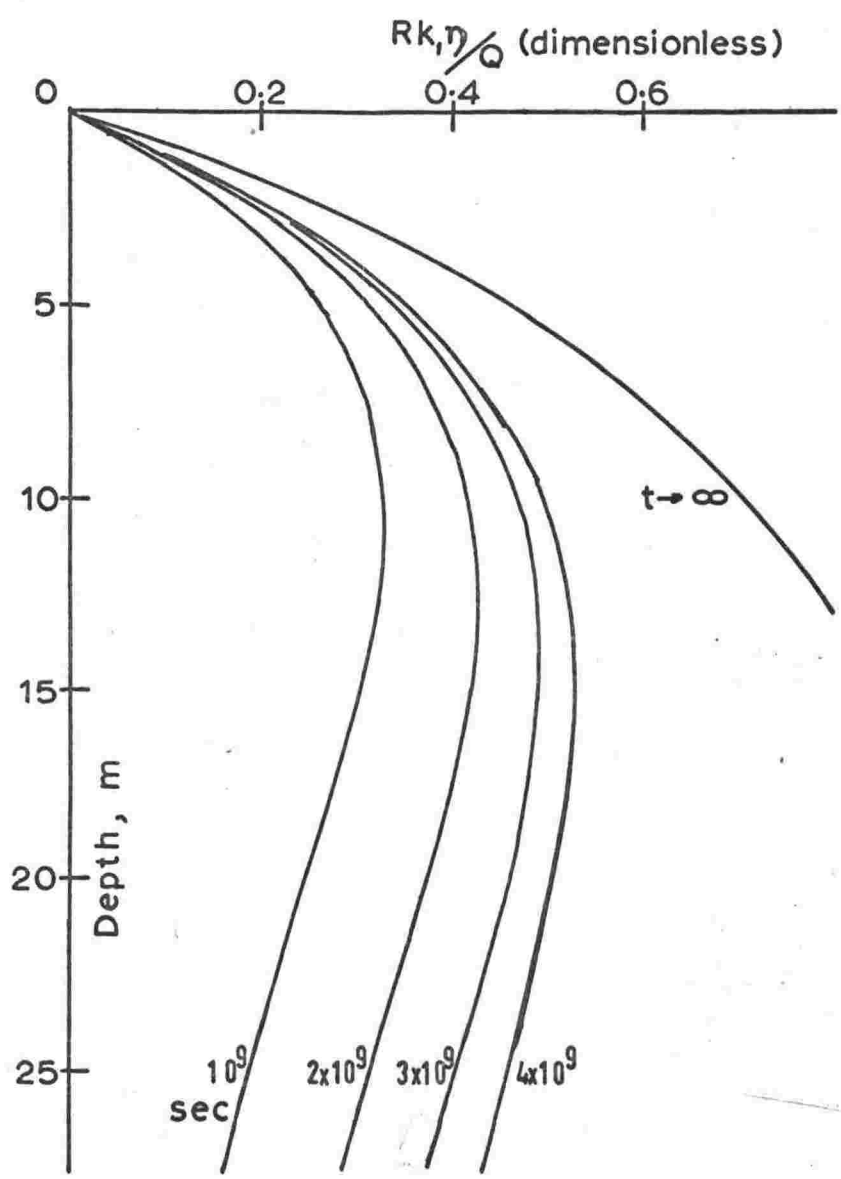


Fig. 7

Increase of temperature with time, due to the absorption of solar radiation.

$$\left. \begin{aligned} S_1 &= S_3 \\ k_2 \frac{\partial S_1}{\partial z} &= k_3 \frac{\partial S_3}{\partial z} \end{aligned} \right\} \text{ at } z = l_2, \text{ all } t$$

$$S_1 = 0 \text{ at } t = 0, z < l_2$$

$$S_2 = \gamma(z - l_2) \text{ at } t = 0, z > l_2$$

Then the temperature in the water is given by

$$S = \gamma(K_3/K_1)^{1/2} \left\{ (K_1 t/\pi)^{1/2} (e^{-(l_2 - z)^2/4K_1 t} - e^{-(l_2 + z)^2/4K_1 t}) + \frac{1}{2}(l_2 + z) \operatorname{erfc} \left[(l_2 + z)/2K_1^{1/2} t^{1/2} \right] - \frac{1}{2}(l_2 - z) \operatorname{erfc} \left[(l_2 - z)/2K_1^{1/2} t^{1/2} \right] \right\}$$

The quantity $S/(\gamma l_2)$ is plotted in Figure 8.

Conduction from initial temperature distribution.

$$\frac{1}{K_1} \frac{\partial T_1}{\partial t} = \frac{\partial^2 T_1}{\partial z^2} \quad 0 \leq z \leq l_1$$

$$\frac{1}{K_1} \frac{\partial T_2}{\partial t} = \frac{\partial^2 T_2}{\partial z^2} \quad l_1 \leq z < l_2$$

$$\frac{1}{K_3} \frac{\partial T_3}{\partial t} = \frac{\partial^2 T_3}{\partial z^2} \quad z > l_2$$

where

$$T_1 = 0 \text{ at } z = 0, \text{ all } t$$

$$\left. \begin{aligned} T_1 &= T_2 \\ \frac{\partial T_1}{\partial z} &= \frac{\partial T_2}{\partial z} \end{aligned} \right\} \text{ at } z = l_1, \text{ all } t$$

$$\left. \begin{aligned} T_2 &= T_3 \\ k_1 \frac{\partial T_2}{\partial z} &= k_3 \frac{\partial T_3}{\partial z} \end{aligned} \right\} \text{ at } z = l_2, \text{ all } t$$

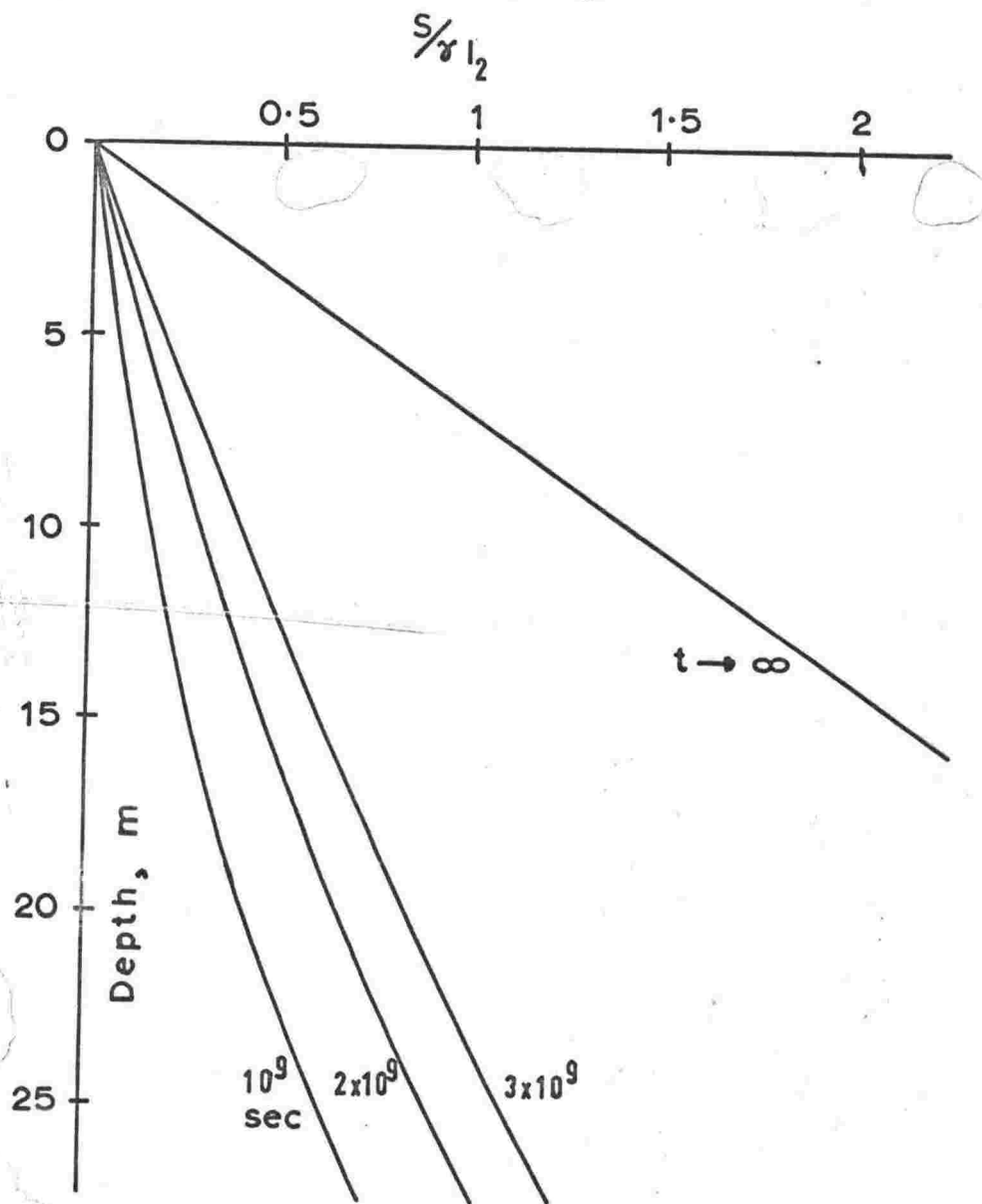


Fig. 8

Increase of temperature with time, due to geothermal flux.

$$T_1 = \frac{z}{l_1} T_i \quad \text{at } t = 0, \quad 0 \leq z \leq l_1$$

$$T_2 = T_3 = T_i \quad \text{at } t = 0, \quad z \geq l_1$$

Then the temperature in the water is given by

$$\begin{aligned} T_1 = & - (T_i/l_1) \left\{ (K_1 t/\pi)^{1/2} \right. \\ & \cdot (e^{-(l_1 - z)^2/4K_1 t} - e^{-(l_1 + z)^2/4K_1 t}) \\ & + \frac{1}{2} (l_1 + z) \operatorname{erfc} \left[(l_1 + z)/2K_1^{1/2} t^{1/2} \right] \\ & \left. - \frac{1}{2} (l_1 - z) \operatorname{erfc} \left[(l_1 - z)/2K_1^{1/2} t^{1/2} \right] - z \right\} \end{aligned}$$

and

$$\begin{aligned} T_2 = & - (T_i/l_1) \left\{ (K_1 t/\pi)^{1/2} \right. \\ & \cdot (e^{-(l_1 - z)^2/4K_1 t} - e^{-(l_1 + z)^2/4K_1 t}) \\ & + \frac{1}{2} (z + l_1) \operatorname{erfc} \left[(z + l_1)/2K_1^{1/2} t^{1/2} \right] \\ & \left. + \frac{1}{2} (z - l_1) \operatorname{erfc} \left[(z - l_1)/2K_1^{1/2} t^{1/2} \right] - l_1 \right\} \end{aligned}$$

The quantity T/T_i is plotted in figure 9.

2.2.8 Evaluation of the parameters

The temperature in the water is

$$\theta(z) = R(z) + S(z) + T(z).$$

θ depends on ten parameters (t , Q , γ , k_1 , K_1 , K_3 , l_1 , l_2 , η , and T_i), and it is not possible to specify the values of these parameters completely. Thus the problem becomes one of choosing values for the parameters which give a theoretical temperature profile $\theta(z)$ which best matches the measured temperatures. It will be seen that the appropriate values accord well with such other evidence as exists, and that they are unique (or at least that each lies within one fairly well-defined range). This provides good evidence that the model advanced to account for the temperature profile is qualitatively correct.

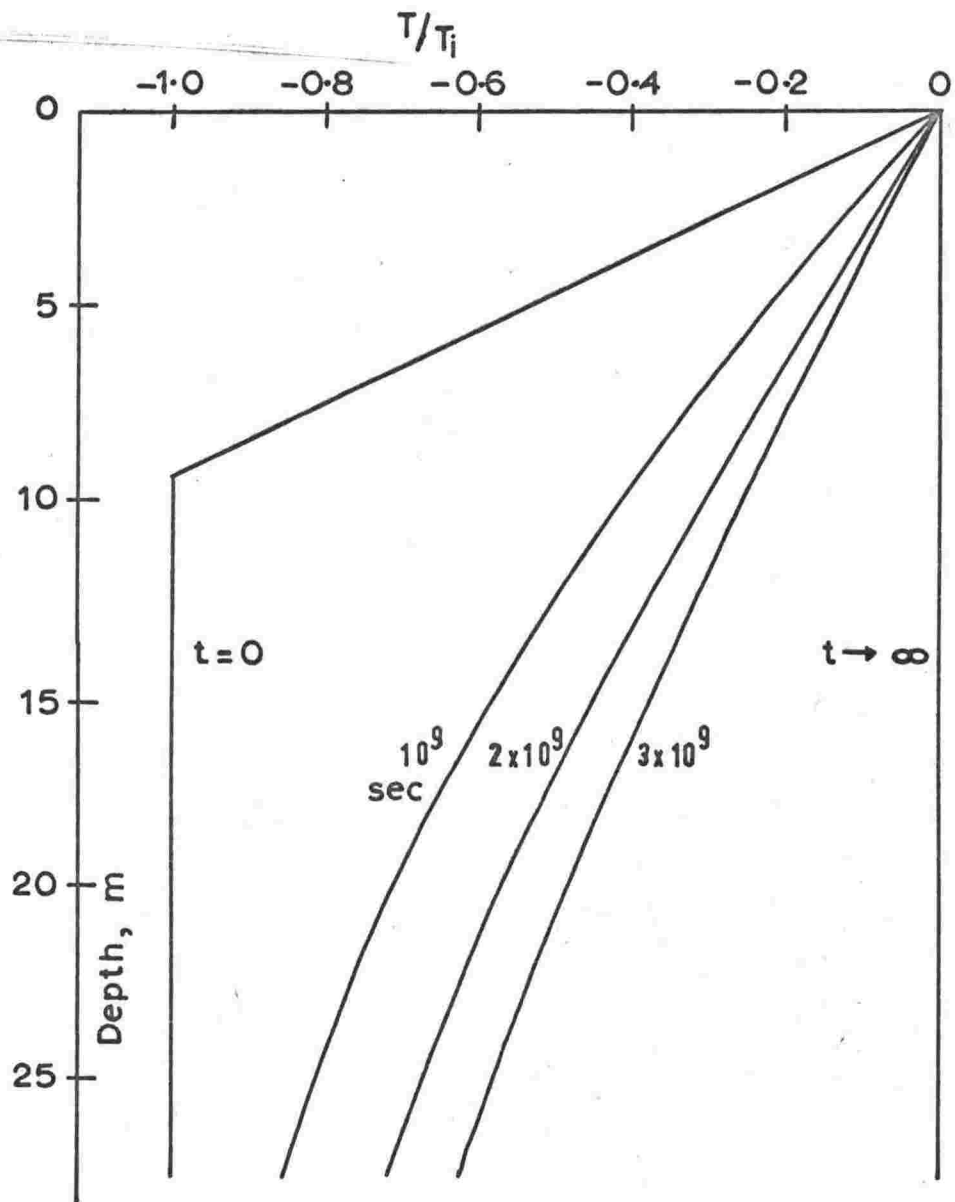


Fig.9

Increase of temperature with time, due to rearrangement of initial temperature distribution.

Two methods were used for evaluating the parameters, one based on manual computation and the other on the use of an electronic digital computer. The manual method was developed before electronic computing facilities became available, and is very tedious in application. However it is of interest, since it shows explicitly the development of the components R, S and T of the solution, and makes it clear that only one set of values for the parameters is admissible. The computer solution is more powerful, in that it allows up to six of the parameters to be optimised simultaneously, compared to three in the manual method; but the latter is a desirable counter to the suspicion that almost any experimental profile could be matched by adjusting enough parameters. Both methods will therefore be described.

2.2.9 Manual optimisation.

This method allows the variation of the three most important parameters, time t , radiation flux Q and geothermal gradient γ . Of the remaining seven, k_1 , K_1 and K_3 can be found from published tables, and the extinction coefficient τ has been measured; this leaves l_1 , l_2 and T_i which warrant further discussion.

l_1 and l_2 are the depths respectively to the antediluvian brine surface and the lake bed, measured from the level at which θ is zero. It has already been mentioned that this level is somewhat below the measured 0°C isotherm. Extrapolation of the measured temperature profile according to the shape of the steady-state solar heating profile near $z = 0$ showed that the level $z = 0$ (at which $\theta = 0$) should be set about 1m below the measured 0°C isotherm. This fixed l_1 and l_2 , as shown in fig.10.

The choice of a value for T_i is somewhat arbitrary. A lower limit is imposed by the freezing point of the primary brine, but this itself is not well defined. The freezing points of samples taken from the lake in 1963 showed that the solution is eutectic at a depth of about

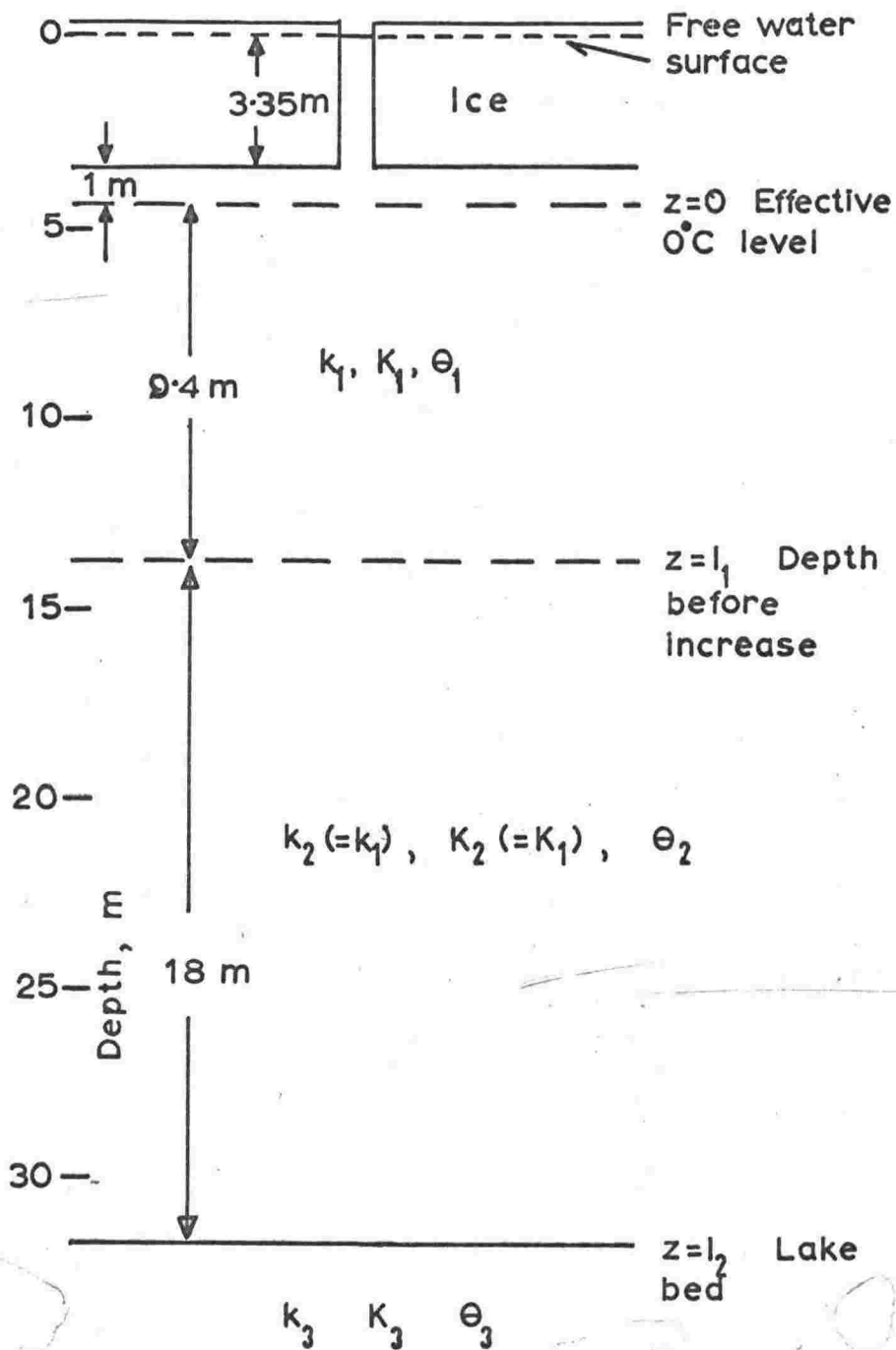


Fig.10

Quantities used in the calculations.

23m, with a minimum freezing point of $-23.5 \pm 0.5^{\circ}\text{C}$. In the case of a sample taken at 30m, salt was deposited at temperatures below $-20.5 \pm 0.5^{\circ}\text{C}$, but it is conceivable that the solution at this depth had become stronger as a result of the dissolution of salt which had been lying on the lake bed when the temperature began to rise. In any case the temperature was probably not even as low as -20.5°C , since it must have been at least as high as the annual average temperature in the region, in order to allow heat produced by the absorption of solar radiation to be conducted out through the ice cover. The average temperature is now about -17°C (Péwé 1960) or -18°C (See Hoare et al., 1965. The value was deduced from measurements in the Canada Glacier near Lake Fryxell.) Hence, if air temperatures have remained fairly constant over the period of interest, T_i was not far from -17°C .

The procedure adopted for optimising t , Q and γ was as follows. First, a series of graphs like that of fig.11 was drawn. In these graphs the value of $(R + T)$ at a particular depth z was plotted as a function of t for one value of Q , six such graphs sufficing to cover the reasonable range of Q . On each graph nine curves were plotted, corresponding to depths taken at intervals of 3.05m (10 ft). Thus each curve in fig.11 indicates the development of temperature at the specified depth which would be expected if the radiation input had the particular value stated and the geothermal flux was zero.

Second, on each of the graphs like fig.11 the temperature observed at each depth was marked on the curve for that depth. The result was the distribution of short bars, the length of each bar being indicative of the experimental uncertainty. If the geothermal flux had actually been zero, the required value of Q would have been that which resulted in all the bars appearing at the same value of t , since it was assumed that all depths had been heating for the same period. Clearly, such a distribution would also have evaluated t .

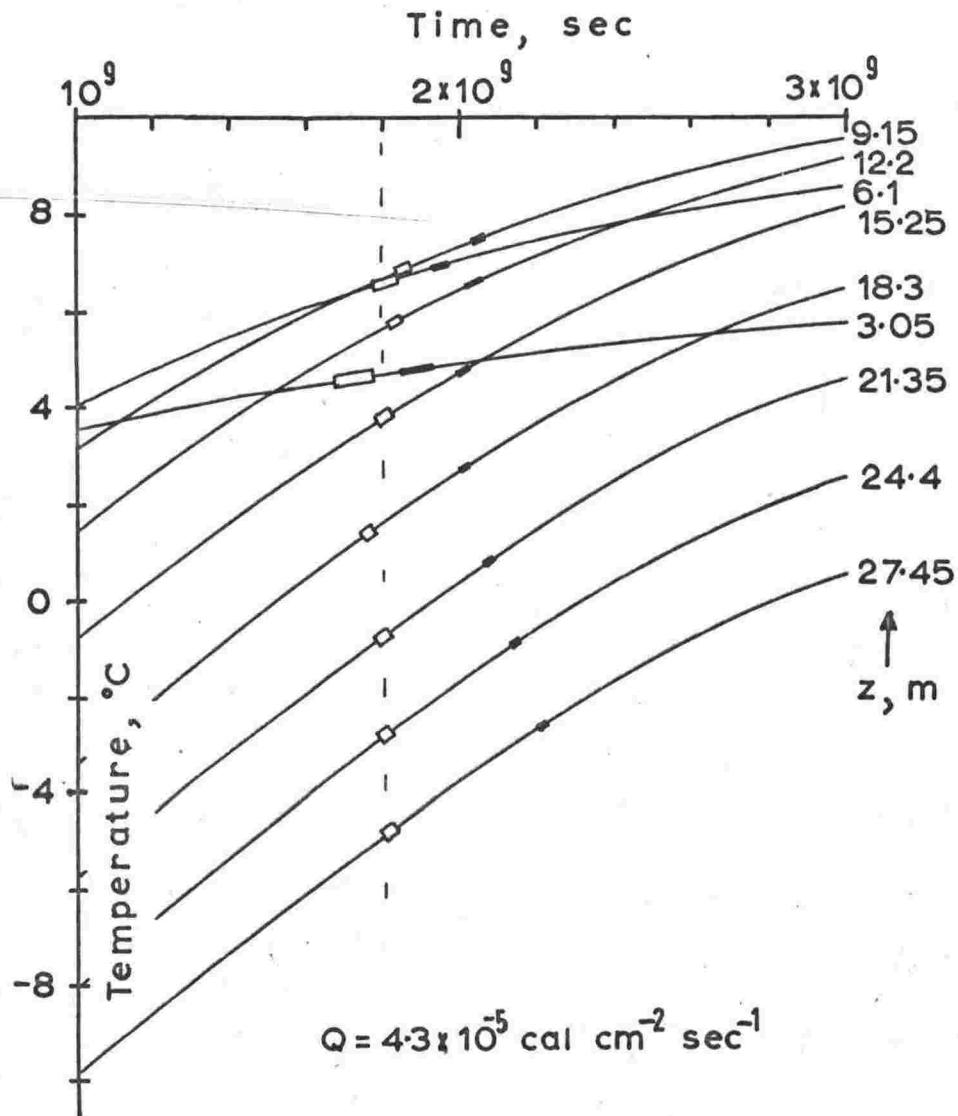


Fig.11

Increase of temperature with time at several depths, due to absorption of solar radiation (Q) and rearrangement of initial temperature distribution. Bars show measured temperatures. Boxes show results of subtracting geothermal effect calculated for $t = 1.8 \times 10^9$ sec.

If the geothermal effect is neglected, there is no value of Q which places all the bars at one value of t . Thus it must be included, but the problem is reduced to finding that distribution $S(z, t)$ which, when subtracted at each depth from the measured temperatures, results in the bars being shifted to lie all at that value of t for which $S(z, t)$ was calculated.

2.2.10 Values.

The best choice of $S(z, t)$ is that given by $\gamma = 0.08 \text{ C deg m}^{-1}$ and $t = 1.8 \times 10^9 \text{ sec}$, applied to the graph for $Q = 4.3 \times 10^{-5} \text{ cal cm}^{-2} \text{ sec}^{-1}$. This choice places the bars in the positions shown by the boxes in fig. 11, which is the graph for this value of Q .

The reason for the uniqueness of this set of values for t , Q and γ can be seen in figs. 7, 8 and 9, which show the growth of R , S and T with time independently. Variation of t affects all three components more at depth than near the surface, while variation of Q and γ alter R and S respectively by fractions which do not change with depth. Thus variation of t cannot be compensated (beyond the limits set by experimental uncertainty) by variation of Q or γ . Again, since R is a maximum at intermediate depths while S is a maximum at the lake bottom, variation of Q cannot be compensated by variation of γ .

Thus, making reasonable allowance for experimental uncertainty, it may be claimed that the solar heating model advanced is consistent with the observed features of the lake, provided

(a) the heating process began $(1.8 \pm 0.2) \times 10^9 \text{ sec}$ ($57 \pm 6 \text{ yr}$) before 1963, i.e. between the years 1900 and 1912;

(b) solar radiation amounting to $(4.3 \pm 0.4) \times 10^{-5} \text{ cal cm}^{-2} \text{ sec}^{-1}$ ($1350 \pm 150 \text{ cal cm}^{-2} \text{ yr}^{-1}$) penetrates the ice cover; and

(c) the geothermal gradient in the area is $0.08 \pm 0.04 \text{ C deg m}^{-1}$, corresponding to a heat flux of $4 \pm 2 \text{ } \mu\text{cal cm}^{-2} \text{ sec}^{-1}$ ($130 \pm 60 \text{ cal cm}^{-2} \text{ yr}^{-1}$).

Discussion of these results will be postponed until after a description of the computer method of optimisation.

2.2.11 Computer optimisation.

The manual method relies on a subjective assessment of the best graphical fit between theory and measurement. In the computer method, the objective least-squares criterion is used; that is, the sum of the squared deviations between calculated and measured temperatures at the various depths is minimised with respect to variation of individual parameters. Symbolically, writing E for the sum of the squared deviations,

$$E = \sum_{n=1}^N \left\{ \theta(z_n) - \phi(h_n) \right\}^2.$$

Here $\theta(z_n)$ is the temperature calculated, while $\phi(h_n)$ is that measured, at the n th depth of measurement. This depth is h_n below the free water surface, and z_n below the theoretical 0°C isotherm. Then if θ , and thus E , depend on several parameters X_i , the criterion for the best fit is that

$$\frac{\partial E}{\partial X_1} = \frac{\partial E}{\partial X_2} = \dots = \frac{\partial E}{\partial X_p} = 0 \quad (4)$$

A primary requirement is, therefore, that any parameter to be varied should show a clearly defined minimum of E .

The first step in developing the computer method was to write a program which calculated E for a large number of combinations of values for the parameters. This gave some idea of the gross behaviour of E , and showed in particular that it was very insensitive to variation of l_1 , the depth to the primary brine surface. This value was therefore fixed by reference to the salinity profile and not included in the optimisation routine. Likewise the physical constants k_1 , K_1 and K_3 were fixed.

The depth scales h and z used for measurement and calculation are offset with respect to each other. Writing

$$d = h - z,$$

d is the "depth shift" and represents the distance that the theoretical 0°C

isotherm lies below the free water surface. E is rather sensitive to d , which is therefore included in the optimisation. However l_2 can be written

$$l_2 = z_{\max} = h_{\max} - d$$

where h_{\max} is the measured depth of the lake. Thus l_2 is not varied explicitly, and the number of parameters to be optimised remains at six - t , Q , γ , d , T_i and η .

The problem of varying P parameters to obtain the best theoretical fit to N experimental observations, where $N > P$, occurs elsewhere. For example, in seismology there may be N instruments which observe a particular earthquake; the problem is to vary such parameters as seismic wave velocity, time of occurrence and coordinates of focus of the earthquake until there is best agreement between the calculated and observed arrival times at the N stations according to a least-squares criterion (see, for example, Bolt, 1960). Or again, in geometrical optics the problem appears as a best choice of positions and radii of curvature of refracting surfaces to give the desired overall behaviour for an instrument (Wynne, 1959; Nunn and Wynne, 1959). The usual method of solution is derived from the condition (4). This criterion supplies P simultaneous equations in P unknowns, which can be solved by standard methods of matrix manipulation to yield the best values of the parameters X_i . The method is necessarily iterative, starting from assumed values for the X_i , since the differentials of the calculated quantity (e.g. θ) with respect to the X_i appear as coefficients in the equations. If these differentials were constant under variation of the X_i , solution of the P equations would yield the best X_i directly. In general, however, the new values X_i are accompanied by slightly different values of $\frac{\partial \theta_n}{\partial X_i}$.

In the present case a different method was used which involved much less algebraic manipulation at the price of rather less efficient convergence towards the final solution. Since good starting values were available for the X_i this was not a serious drawback. In addition, the method readily gave approximate values for $\frac{\partial^2 E}{\partial X_i^2}$, and thus showed the sensitivity of the solution to variation of individual parameters.

The basis of the method was to approximate E near its minimum by the simplest function which possesses a minimum with respect to each of the six parameters:

$$E = E_0 + a_1 (t - t_0)^2 + a_2 (Q - Q_0)^2 + a_3 (\gamma - \gamma_0)^2 \\ + a_4 (d - d_0)^2 + a_5 (T - T_0)^2 + a_6 (\eta - \eta_0)^2$$

Starting values $(t_1, Q_1, \dots, \eta_1)$ were adopted, and small positive and negative increments were chosen so that each parameter could take three values in all (e.g. t_1, t_{1+}, t_{1-}). Then in a six-dimensional space with the parameters as coordinates, thirteen points were defined, grouped around $(t_1, Q_1, \dots, \eta_1)$, by varying each parameter in turn. E was evaluated at each of these points, yielding 13 simultaneous equations of which the first three were

$$E_1 = E_0 + a_1 (t_1 - t_0)^2 + a_2 (Q_1 - Q_0)^2 + \dots + a_6 (\eta_1 - \eta_0)^2 \quad (5/1)$$

$$E_2 = E_0 + a_1 (t_{1+} - t_0)^2 + a_2 (Q_1 - Q_0)^2 + \dots + a_6 (\eta_1 - \eta_0)^2 \quad (5/2)$$

$$E_3 = E_0 + a_1 (t_{1-} - t_0)^2 + a_2 (Q_1 - Q_0)^2 + \dots + a_6 (\eta_1 - \eta_0)^2 \quad (5/3)$$

Since there are only 13 unknowns $E_0, a_1 - a_6$ and $t_0 - \eta_0$, these can be ascertained from the equations. Furthermore, since equations (5/2) to (5/13) differ from (5/1) only by the variation of one of the parameters, the solution is particularly simple; equations (5/2) and (5/3) give a_1 and t_0 , (5/4) and (5/5) give a_2 and Q_0 and so on, and finally (5/1) gives E_0 . Then $t_0 - \eta_0$ are estimates of the coordinates of the minimum of E .

Owing to the approximate nature of the representation of E these estimates

will be in error, but generally less so than the starting ones. The point (t_0, \dots, η_0) is then taken as a new starting point, and the process repeated until E_0 is reduced sufficiently. In practice only about five iterations were required to achieve a satisfactory solution. The Algol program for the scheme, and an example of the output, are given in appendix 3.

In order to reduce the dependence of the solution on measurements made near the surface, which may have been disturbed by the inflow, the uppermost measurement was given a weight of 0.5.

2.2.12 Results.

The best representation of E near its minimum was

$$E = 0.218 + 4.3 \times 10^{-16} (t - 1.78 \times 10^9)^2 + 9.8 (d - 4.67)^2 \\ + 8.2 \times 10^{-4} (Q - 1511)^2 + 3700 (\gamma - 0.0966)^2 \\ + 4.9 (T_i + 16.07)^2 + 5.6 \times 10^4 (\eta - 0.1188)^2$$

This expression can be rewritten as

$$E = 0.0118 + 75.5 (\Delta t/t_0)^2 + 11.9 (\Delta d/d_0)^2 \\ + 104 (\Delta Q/Q_0)^2 + 1.94 (\Delta \gamma / \gamma_0)^2 \\ + 70 (\Delta T_i/T_0)^2 + 43.9 (\Delta \eta / \eta_0)^2,$$

where $\Delta t = t - t_0$ etc., and \bar{E} is the mean square deviation E/N ($N = 18$). The value of \bar{E} can be compared directly with the value obtained for the same quantity in later analyses of other lakes, for which N is different. The coefficients in the second expression are those called b_1 ----- b_6 in table IV, and show that the solution is most sensitive to variation of Q and least to variation of γ . This implies that Q is the parameter which is most closely determined by the optimisation, and γ is that least well determined. The first expression shows that the optimum values are ("manual" values in parentheses):

$$t = 1.78 \times 10^9 \text{ sec} = 57 \text{ yr} \quad (57 \pm 6) \\ Q = 1500 \text{ cal cm}^{-2} \text{ yr}^{-1} \quad (1350 \pm 150) \\ \gamma = 0.10 \text{ C deg m}^{-1} \quad (0.08 \pm 0.04)$$

Table IV
Calculated parameters

Lake and observer	Date of observation	b_1	t_0	b_2	Q_o	$Q_{meas.}$	b_3	γ_0	$k_3 \gamma_0$	b_4	T_{i0}	b_5	γ_0	$\gamma_{meas.}$	b_6	d_0	$\sqrt{\frac{E}{N}}$
Fryxell (Hoare et al.)	Nov 63	6.9	48	7.5	545	-	4.1	0.16	8	8.1	-10	1.4	0.26	1.2	2.3	4.53	0.11
Joyce (Hoare et al.)	Dec 63	14	80	1.7	194		12	.21	10	19	-13	0.57	0.18	0.15	1.9	6.58	0.076
Bonney (East) (Hoare et al.)	Dec 63	82	58	98	1430	1000	2.0	0.098	5	71	-16	41	0.11	0.19 ± 0.02	12	4.82	0.12
Bonney (East) (Shirtcliffe and Benseman)	Jan 63	76	57	104	1510	1500 ± 500	1.9	0.097	5	70	-16	44	0.12	0.12 ± 0.01	12	4.67	0.11
Bonney (East) (S&B, manual analysis)	Jan 63	-	57 ± 6	-	1350 ± 150	1500 ± 500	-	0.08 ± 0.04	4 ± 2	-	-17 (fixed)	-	0.12 (fixed)	0.12 ± 0.01	-	4.35 (fixed)	0.13
Bonney (West) (Hoare et al.)	Dec 63	1.8	43	3.4	507	200	2.2	0.14	7	41	-10	5.6	0.28	0.19	5.4	3.76	0.25

Units:

yrs.

$cal\ cm^{-2}\ yr^{-1}$

$C\ deg\ m^{-1}$

$cal\ cm^{-2}\ sec^{-1}$

$^{\circ}C$

$l^{-1}\ H$

H

$C\ deg$

$$\begin{array}{ll}
 d = 4.67\text{m} & (4.35, \text{fixed}) \\
 T_i = -16^\circ\text{C} & (-17, \text{fixed}) \\
 \gamma = 0.12\text{m}^{-1} & (0.122, \text{fixed}).
 \end{array}$$

The closeness of fit is indicated by the root-mean-square deviation between the N calculated and measured temperatures, i.e. by $\sqrt{\bar{E}}$. This is 0.13 C deg for the manual method, 0.11 C deg for the computer version. Both of these are acceptable when compared to the measurement uncertainty of ± 0.05 C deg, bearing in mind the idealised nature of the model. The calculated temperature profile is shown in fig.12 with the observed mean profile.

2.2.13 Discussion.

It is gratifying that variation of six parameters yields essentially the same result as variation of three, giving confidence that the process yields values which have physical significance. It is, however, fortuitous to the extent that the original choice of -17°C for T_i was not based on firm evidence.

The value given for the geothermal flux is about four times "normal". While this estimate is very rough, and it is not certain that the effect corresponds to geothermal heating as usually understood, the value would not be unreasonable for an area showing some signs of volcanic activity. Indeed, a flux 40 times normal has been found at Scott base (Robertson and Macdonald, 1962), though the proximity of the sea may have affected the temperatures there.

The value given for the radiation flux at the base of the ice cover leads to an estimate of the flux incident on the ice surface if the approximate measurement of 0.015 ± 0.005 for the ratio of the two is accepted. The incident radiation would amount to between 60,000 and 150,000 $\text{cal cm}^{-2} \text{ yr}^{-1}$, which is consistent with the value of 91,000 $\text{cal cm}^{-2} \text{ yr}^{-1}$ measured at Scott Base (Thompson and Macdonald, 1962).

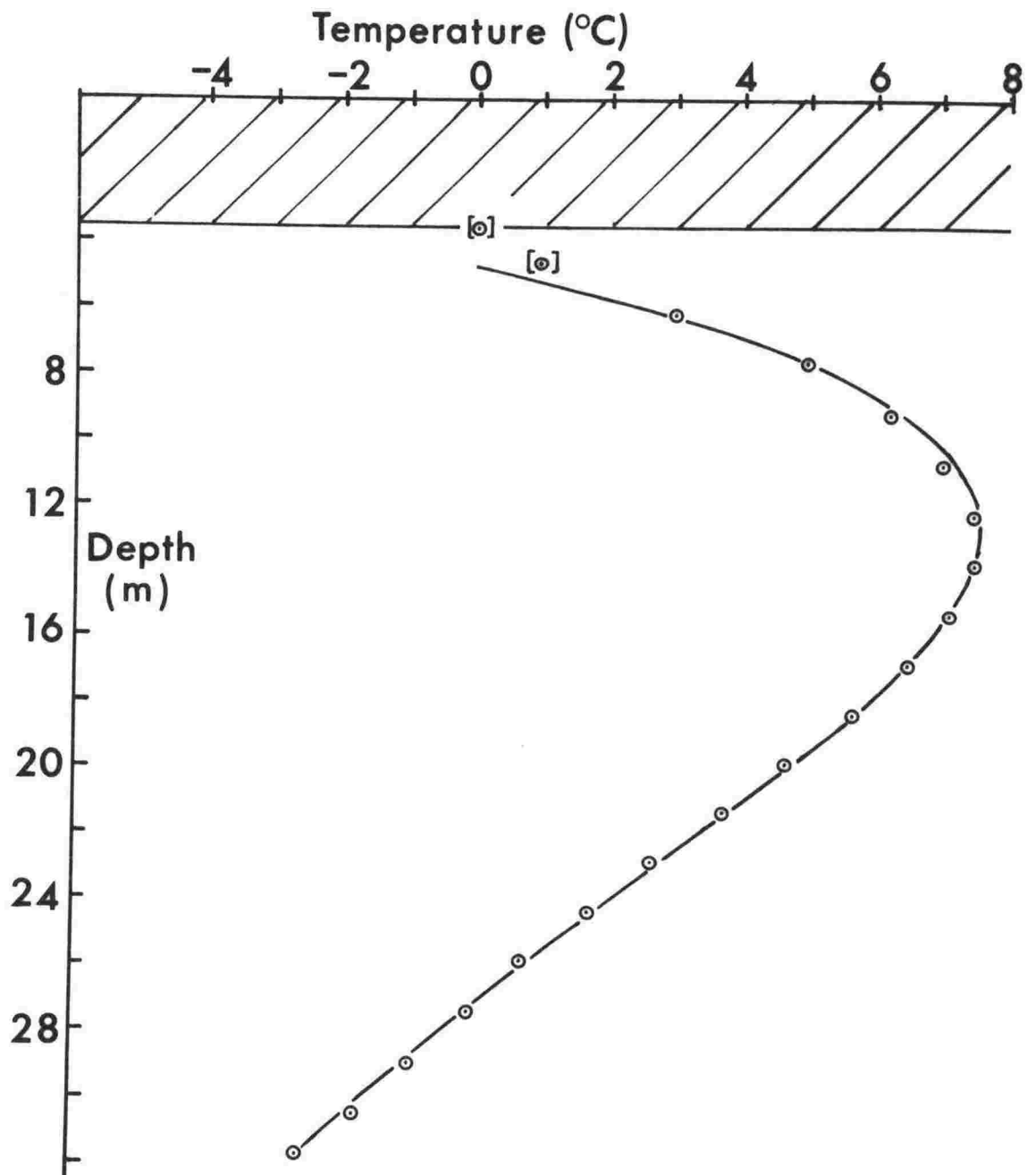


Fig.12 Lake Bonney temperature profile.

The most significant value is that given for the duration of the heating process, and this can be corroborated in two ways. First, the width of the peak in the curve of salt concentration gradient versus depth — that is, the distance between the points where the concentration gradient has half its maximum value — is simply related to the time for which the salt has been diffusing. Ideally, the concentration distribution $C(z, t)$ is given by (Crank, 1957)

$$C(z, t) = \frac{C_0}{2} \operatorname{erfc} \left[\frac{l_1 - z}{2D^{1/2} t^{1/2}} \right]$$

where C_0 is the initial concentration below the boundary and D is the diffusion coefficient for salt in water. Therefore

$$\partial C / \partial z = (C_0^2 / 4 \pi Dt)^{1/2} e^{-(l_1 - z)^2 / 4Dt}$$

This is clearly a maximum at $z = l_1$, and half the maximum value at the depths where

$$e^{-(l_1 - z)^2 / 4Dt} = \frac{1}{2}$$

i.e. at

$$z = l_1 \pm (4Dt \ln 2)^{1/2}$$

The width of the peak is therefore

$$\begin{aligned} \Delta z &= 4 (Dt \ln 2)^{1/2} \\ &= 3.33 (Dt)^{1/2} \end{aligned}$$

Taking $(1.25 \pm 0.25) \times 10^{-5} \text{ cm}^2 \text{ sec}^{-1}$ for the range of coefficients of diffusion of chloride ions in aqueous alkali chloride solutions of the strength found in the lake (Tyrell, 1961), and $5.5 \pm 0.5 \text{ m}$ as the width of the peak, we find that the age of the diffusion is $60 \pm 20 \text{ yr}$. Although the observed chloride concentrations do not correspond exactly to the ideal model assumed, the two are sufficiently alike for the agreement between this age and the thermal age to be significant.

Corroboration of the age is also available from the accounts of the first two parties to visit the lake. The two lobes of the lake are connected by a narrow channel, the width of which was 5.2 m (17 ft) in

1903 (Scott, 1905) and about 31 m (100 ft) in 1911 (Taylor, 1922). Soundings were made in a line across the narrowest part of this channel in February 1964, and these indicate that in order for the channel to be as narrow as 5.2 m the ice surface would have to be 9.2 m lower than its present level (see fig.13). If, in 1903, the ice covering the main lobe was about half its present thickness (see appendix 2), this would have allowed only about 20 m of water beneath the ice, a value very close to that postulated for the previous state of the lake. By contrast, the depth in 1911 must have been close to the present depth, the channel width being 42.3 m in 1963. Thus there is good evidence that the increase in depth, which was postulated as the event which initiated the current phase of the lake's history, took place close to 60 years ago, as calculated.

2.3 Other applications.

Three other lakes in the Taylor Valley have temperature and salinity profiles similar to those of the eastern lobe of Lake Bonney, namely Lake Fryxell (Angino et al., 1962; Hoare et al., 1965), the western lobe of Lake Bonney (Angino et al., 1964; Hoare et al., 1964), and Lake Joyce (R.A. Hoare, pers. comm.). It is of interest to apply the foregoing analysis to these lakes, and also to the measurements by Hoare et al. (1964) of the temperatures in the eastern lobe of Lake Bonney in December 1963; these differ somewhat from those of Shirtcliffe and Benseman (January, 1963).

2.3.1 Lake Fryxell.

This lake is 15 miles east of Lake Bonney, in an enclosed drainage basin near the seaward end of the valley. It is 5 km by 1.5 km in size and is permanently covered by ice about 4.5 m thick. As in Lake Bonney, the increasing salinity with depth prevents convection at all levels. Some light penetrates the ice cover, but the amount has not been reliably measured. Measurements by Hoare et al. with a selenium cell showed that the extinction coefficient in the water was 1.15 m^{-1} , but in matching

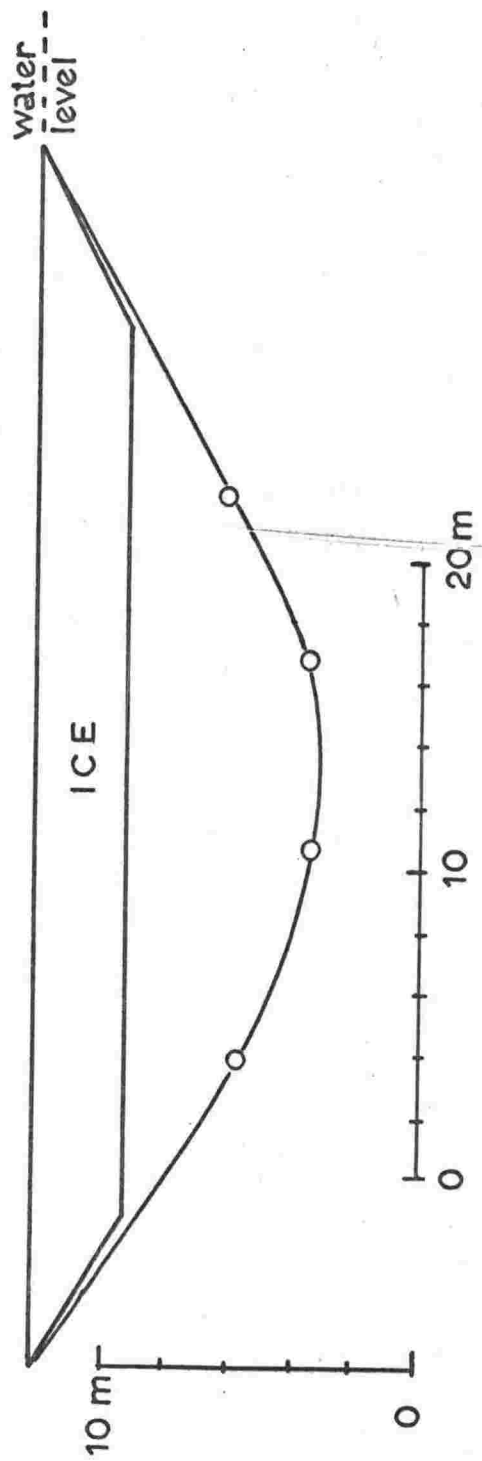


Fig. 13

Bathymetric profile of channel, Lake Bonney.

a theoretical steady-state solar heating profile to the observed temperatures those authors adopted a value of 0.69 m^{-1} , suggesting a lack of confidence in the measurement. An attempt to measure the fraction of incident light penetrating the ice gave an anomalously low value of 0.1%, which was not considered typical for the lake.

The result of the analysis is shown in Table IV and fig.14. The main points of interest are:

(1) The calculated extinction coefficient is much nearer to that found in the other lakes than to that measured in Lake Fryxell. This suggests that the high value actually measured could be a temporary phenomenon. Both this and the anomalously low light penetration of the ice cover could result from a sudden inflow of melt water containing a rather high concentration of suspended material of a brownish colour; the extinction coefficient changing because of the changed spectral composition of light penetrating to the stagnant water, and the change of penetration being accentuated by a tendency for the coloured inflow water to gather in the hole through which the detector was lowered. Whether this could occur without detection is questionable, however.

(2) The calculated fraction of incident radiation penetrating to the level $z = 0$ is about one third of the corresponding value in Lake Bonney. This is consistent with the higher extinction coefficient in Lake Fryxell as indicating either less clarity in both the water and the ice, or a greater difference between the passband wavelengths of the ice and the water.

(3) The temperature of the primary brine exceeds that in Lake Bonney. This reflects the much lower salinity of Lake Fryxell ($\leq 4 \text{ gm/litre}$ of chloride) and the concomitant higher freezing point. In accordance with the arguments advanced in appendix 2 it must be supposed that the ice covering the lake before its increase in depth was thinner than that now present. However this appears inconsistent, since the relatively high primary brine temperature would have led to an excessive loss of heat through such thin ice. An answer to this difficulty can be found by

Temperature (°C)

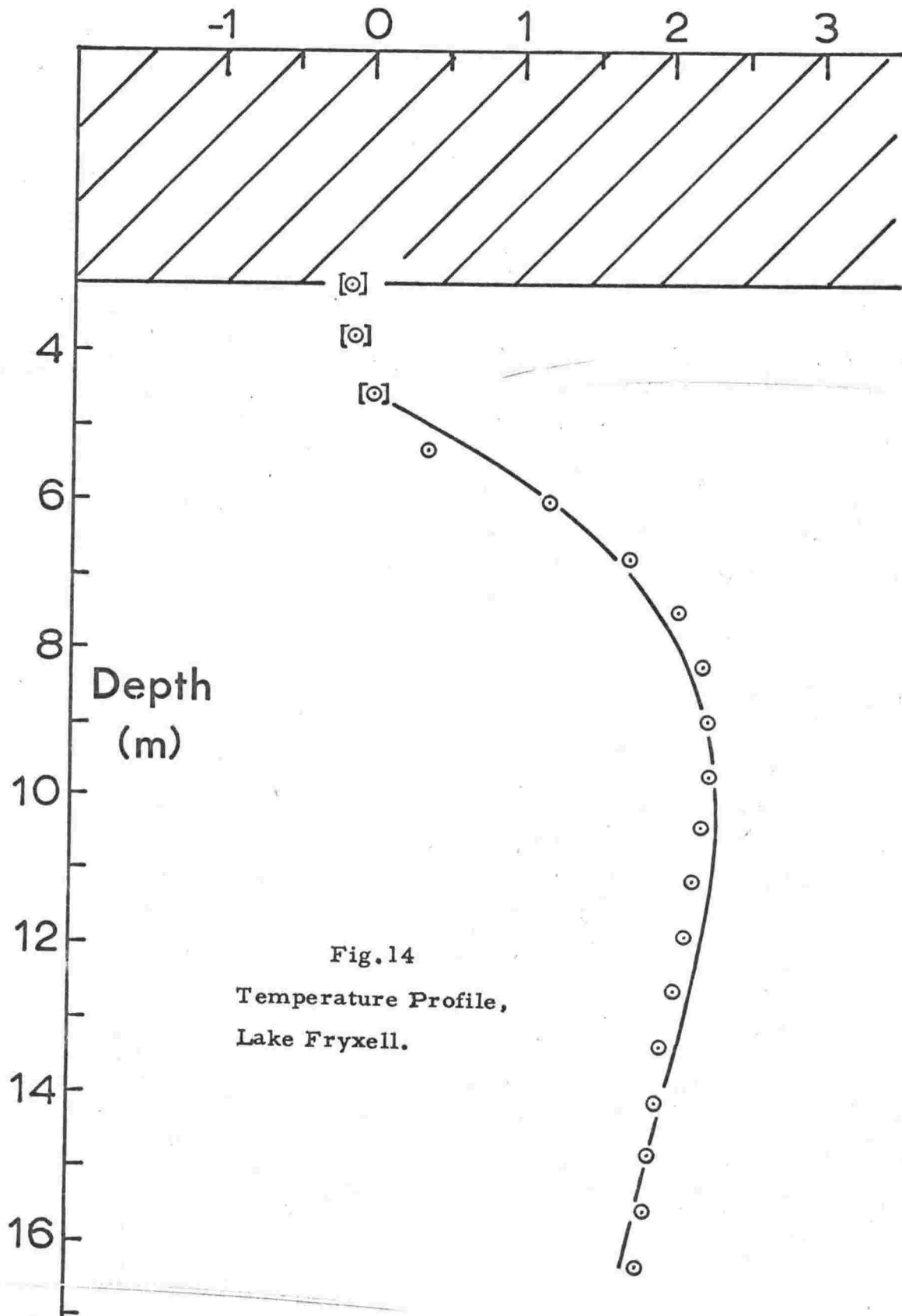


Fig. 14
Temperature Profile,
Lake Fryxell.

considering the stability problem for the case of low initial salinity. The stabilising effect of fresh water flowing over the Fryxell brine would have been much less than that in Lake Bonney, owing to the smaller contrast of salinity. In Lake Bonney there was a sharp boundary between the brine and the thin layer of inflow water, maintained by periodic convection induced partly by downward ice growth in winter; in Lake Fryxell the brine may well have been separated from the ice by a permanent layer of water in which there was a sufficient gradient of concentration to prevent convection, while convection in the brine itself was maintained entirely by the solar heating. The brine would have been insulated from the atmosphere by both the ice and the non-convecting layer, allowing the annual heat loss to balance production. The lake would have been stabilised finally when the inflow of additional water reduced the intensity of radiation reaching the brine below that required to maintain convection. The present salinity profile lends support to this hypothesis by showing a rather less marked maximum in salinity gradient than is the case in Lake Bonney. This could be due to the fact that there was a pre-existing chemocline which increases the apparent age of the present profile.

(4) Table IV includes the coefficients b_1 --- b_6 which show the relative sharpness of the minimum in \bar{E} with respect to the various parameters. These coefficients are generally much lower for Lake Fryxell than for Lake Bonney, so that the parametric values are less well determined. Nevertheless the final agreement between theory and experiment, as represented by the RMS deviation of 0.11 C deg, is quite satisfactory.

2.3.2 Lake Joyce.

Lake Joyce lies beside a lateral extension of the Taylor Glacier, about 10 miles from Lake Bonney and at a somewhat greater altitude. It was investigated by VUW Antarctic Expedition No.8 and appears qualitatively similar to Lake Bonney in its temperature and salinity

profiles, its permanent ice cover and its lack of outflow. The bathymetry is more variable than that of Lake Bonney. There appears to be a small region which is much deeper than the bulk of the lake, and contains more saline water with a higher extinction coefficient. This region was omitted from the analysis, the lake being assumed to have a horizontal bed at a depth of 26 m.

Results are shown in table IV and fig.15. Tolerably good agreement is shown between calculated and measured values of radiation input and extinction coefficient. The calculated parameters are generally less well determined than their values in Lake Bonney, the values of the coefficients b_1 --- b_6 being comparable with those found for Lake Fryxell.

2.3.3 Lake Bonney, eastern lobe (Hoare et al.)

These measurements agree well with those taken 11 months earlier by Shirtcliffe and Benseman, except in the region near and above the temperature maximum. Since this is the region most susceptible to seasonal fluctuation, it is probable that the difference is due to no more than this. Nevertheless, since the analysis neglects seasonal effects, it is remarkable that the parametric values inferred are so similar for the two cases (see table IV and fig.16), even to an increase of 1 year in the age. The main difference is a reduction of 5% in the inferred radiation input, which is scarcely significant. The similarity between the two sets of results shows that the optimising process operates preferentially on the deeper measurements.

2.3.4 Lake Bonney, western lobe.

This lobe is separated from the main, eastern, one by a channel containing only about 5 m depth of water. Thus at depths greater than this the two lobes are chemically and thermally distinct. Superficially the two temperature and salinity profiles are similar, although the temperature maximum in the western lobe is sharper, cooler and shallower than that in the eastern lobe.

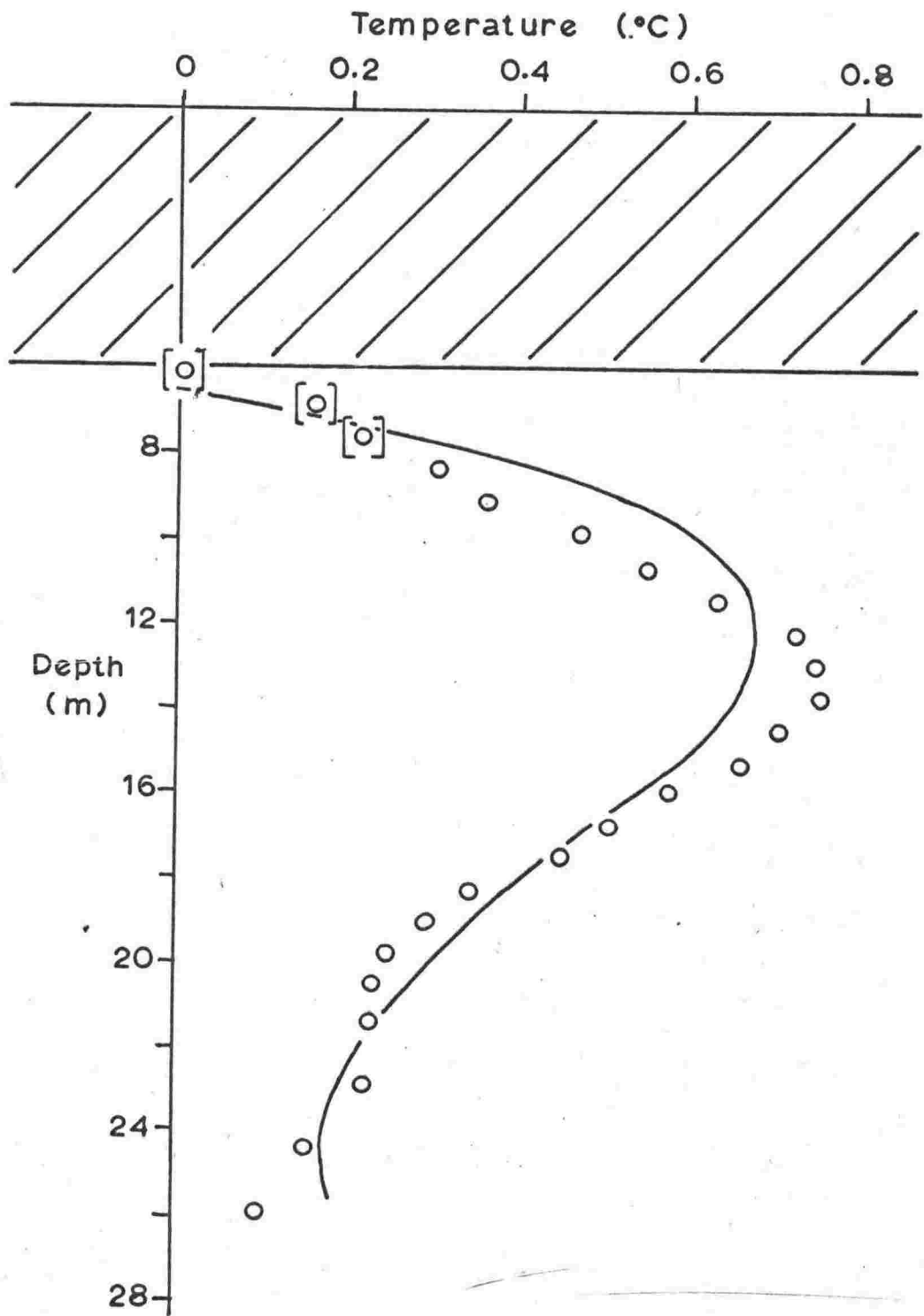


Fig.15

Temperature profile, Lake Joyce.

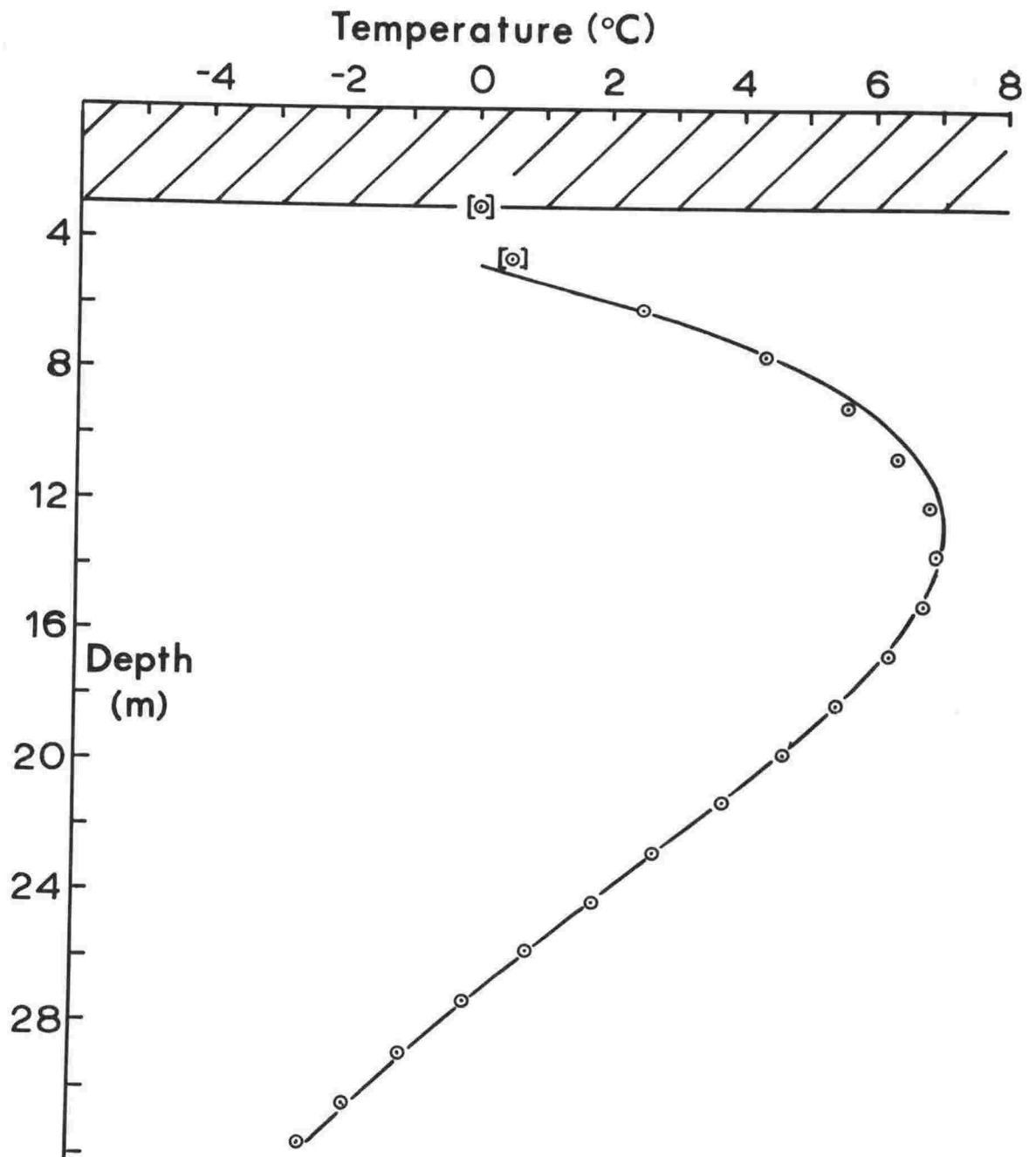


Fig. 16 Lake Bonney temperature profile (measurements by Hoare et al.)

It is clear that the results in this case (see table IV and fig. 17) are significantly worse than those obtained for the other lakes. This failure of the model could possibly be ascribed to two causes. The first of these is associated with the influence of the Taylor Glacier on the temperatures in the lake. The temperature profile examined (in all lakes) was that obtained by averaging at each depth the readings taken at the various stations at that depth. The horizontal variation of temperature is small in the other lakes considered, but in the western lobe of Lake Bonney temperatures measured 150 m from the snout of the glacier average 1.5 C deg, and those measured 300 m from the snout 0.4 C deg, below corresponding values of the mean profile. Thus there is a noticeable horizontal component in the heat flow at least near the glacier. In principle, this will have two effects:

(a) In an otherwise homogeneous fluid, any horizontal temperature variation produces a movement of the liquid, since the condition for hydrostatic equilibrium is that the surfaces of constant density should be horizontal. When the fluid contains a second component, such as a solute, which can also affect its density, hydrostatic equilibrium can exist in spite of horizontal temperature variations provided that the concentration of the second component varies in a compensating way. Such is probably the case here, an upward displacement of the isotherms being accompanied by a downward displacement of the isohals (surfaces of constant salinity). Although this implies a horizontal component of salt diffusion, and a consequent continuous flow to maintain the desired horizontal concentration variation, this flow should be negligibly small. Thus it is probably satisfactory to assume that heat flow is entirely conductive.

(b) The solar heating model assumes one-dimensional heat conduction, with horizontal isotherms. Again, the effect is probably not serious, provided the horizontal component of the heat

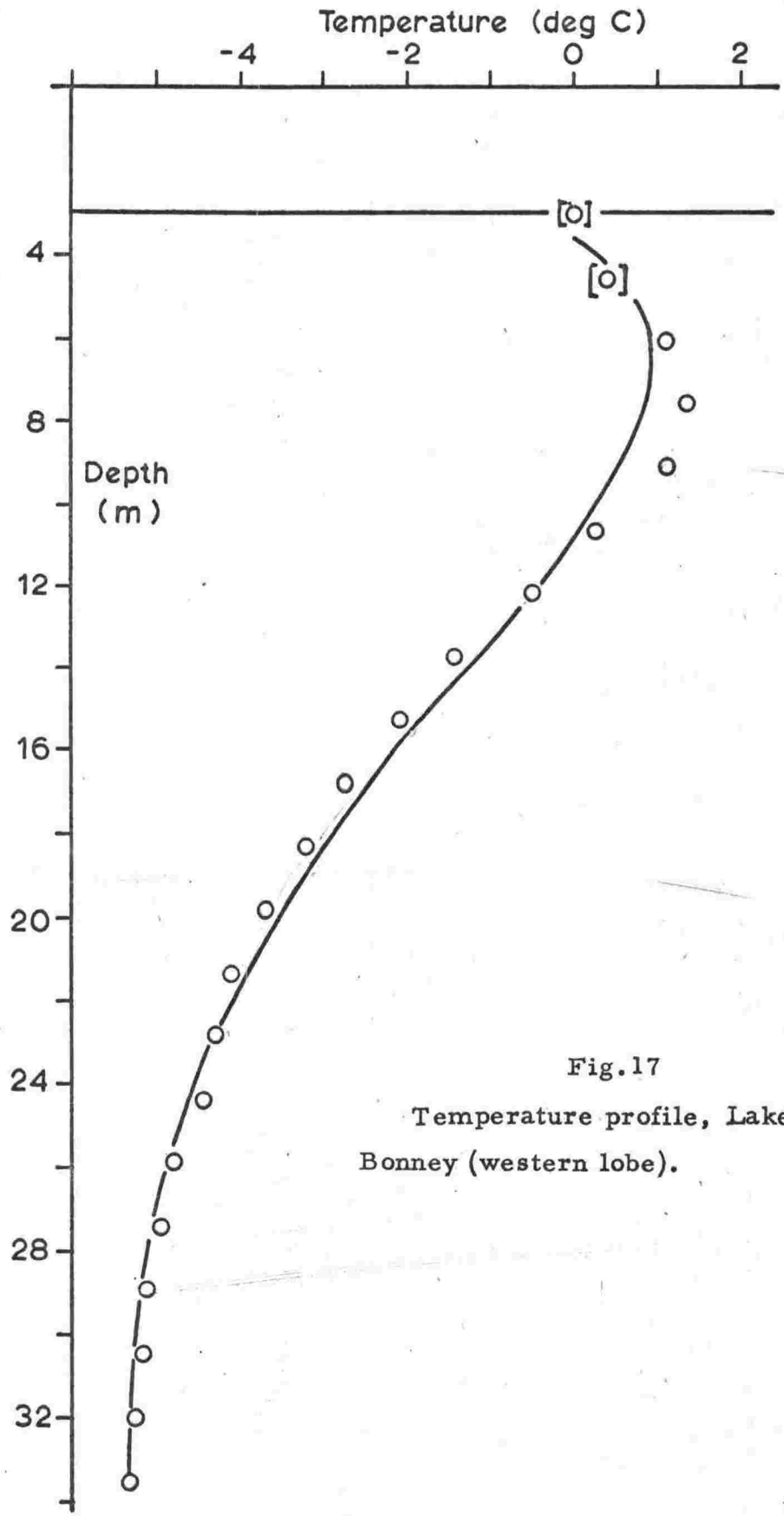


Fig.17
 Temperature profile, Lake
 Bonney (western lobe).

flow is much smaller than the vertical one. The temperature variation indicated suggests a lateral transport of about $3 \text{ cal cm}^{-2} \text{ yr}^{-1}$ near the glacier, which is small compared to the vertical flux at all depths except near the temperature maximum, where the vertical flux is zero. The region where the horizontal flux is dominant is so restricted that the effect is probably negligible.

The second, and more important, reason for the failure of the theory in the case of the western lobe of Lake Bonney is associated with the shallow channel connecting it with the eastern lobe. It is noticeable that at depths down to about 15 m the salinity of the western lobe is greater than that of the eastern lobe, and that there is a sharp salinity gradient in the western lobe at the level of the channel bottom. This implies either that the western lobe has only very recently filled above this level, or that there is a loss of salt from its upper region. The first alternative is certainly untrue, since as has been shown the whole of Lake Bonney has had roughly its present depth at least since the year 1911.

Hence salt is being lost from the upper waters of the western lobe. This implies a flow of water through the channel into the eastern lobe, which can arise in two ways. Firstly, neglecting flow through the channel, the annual depth of inflow to the western lobe is probably greater than that to the eastern lobe, both by virtue of the great collection area of the Taylor Glacier and by virtue of the small surface area of the western lobe when compared with that of the eastern lobe. This difference in inflow must be compensated by a nett flow through the channel from west to east. However the flow would not be steady. Inflow occurs to both lobes in a variable manner, and there are no doubt periods when flow into the eastern lobe exceeds that into the western. During such periods flow in the channel would be from east to west. A second possible cause of flow (in either direction) in the channel is internal waves generated by reversals of direction of the

wind, which apparently blows either up or down the valley most of the time. Thus irrespective of the existence of a mean flow from west to east there must be an exchange of water, and hence of both salt and heat, between the two lobes. By virtue of its smaller volume (about 10%) the western lobe must be more affected by this than the eastern lobe. Since the salinity is higher and the temperature lower in the western lobe, that lobe must experience a nett gain of heat and a net loss of salt in the process, the corresponding fall in temperature and rise in salinity in the eastern lobe being much less marked. Hence the no-flow solar heating model fails when applied to the western lobe, but accounts adequately for conditions in the eastern lobe.

2.3.5 Summary and comment.

A model based on the absorption of sunlight in non-convecting water has been considered in detail, and shown to account for the temperature profile in three lakes in the Taylor Valley. The model assumes a particular origin for the development of the temperatures, and to that extent is speculative. However observations confirm that a rise in level of the required magnitude did occur in at least one of the lakes at the appropriate time. Moreover, insofar as the model requires a particular pre-existing configuration, such an arrangement has been shown to be plausible, particularly in regard to its stability.

The application of the model proceeds by the evaluation of up to six parameters according to the criterion that the calculated temperatures should match those measured as well as possible. The inferred values of the parameters are unique and reasonable, and agree with such reliable observations as exist. Hence it is concluded that the model itself is correct, both in regard to the assumption that no sources of heat exist other than the absorption of sunlight and a geothermal heat flow, and also in regard to the assumed former characters of the lakes.

The correct estimation of those parametric values which can be checked against observation implies that the values are physically significant even when no observations are available to check them. This being so, the process becomes in effect a method of deducing climatic history for the lakes' environments. All three lakes, Joyce, Bonney and Fryxell, appear to have responded to an increase of humidity in their respective regions within the last 50-80 years. Since they are all situated in the Taylor Dry Valley, the climate throughout that valley generally has been becoming less arid over the period.

It is intriguing to speculate on the relative timing of the onset of non-convective heating in the three cases. Lake Joyce, high up the valley, was affected about the year 1885; Lake Bonney, at the foot of the Taylor Glacier, about 1905; and Lake Fryxell, nearest the sea, about 1915. Although the time difference between the Bonney and Fryxell events is barely significant in relation to the uncertainties involved, it seems possible that the climatic effect propagated down the valley from the Polar Plateau.

Chapter 3

Convecting Lakes

3.1 Introduction

The non-convecting lakes already described, together with a few other minor examples from the same area, probably represent the only examples in the world of totally amictic lakes. Even in those lakes elsewhere in which deeper water is stabilised more or less by a solute concentration gradient, the so-called meromictic lakes (Hutchinson, 1957), the upper part is subjected both to turbulent mixing due to wind and also to intermittent gross circulation caused by changes of surface temperature. Other lakes are to be found in Victoria Land which are intermediate in character between the amictic and the meromictic lakes. Although protected from surface disturbance due to either temperature change or wind by a permanent cover of ice, these lakes are subject to some circulation where the gradient of solute concentration is insufficient to maintain stability against the heat flow. In contrast to the meromictic lakes, however, the intermediate class of Victoria Land lakes may be called stratomictic, since continuous convection occurs in a series of layers which may be very thin and which are bounded above and below by regions of high, solute-induced stability.

Details have been published of only two stratomictic lakes, namely Vanda (Wilson and Wellman, 1962; Goldman, 1962; Ragotzkie and Likens, 1964; Hoare, 1966) and Miers (Bell, 1967). Of these, the latter contains relatively little salt (maximum concentration of solutes is less than 300 p.p.m.), and the water temperature exceeds that of maximum density by only a small amount (maximum temperature is 5.25°C), so that the layered convection is not well developed. Lake Vanda, on the other hand, contains a very well-marked series of layers, with thicknesses varying from less than 1 m to about 20 m (Hoare, 1966).

The present study was therefore confined to Lake Vanda, and aimed at clarifying the origin and development of the layered convection in that lake.

3.2 Lake Vanda.

Fig.18 is reproduced from the work of Hoare (1966) and summarises the pertinent data on Lake Vanda. The lake may be divided into two regions; that below a depth of about 50 m, in which transport of heat and solute is due entirely to diffusion, and that above this level where layers of convective transport are separated by stable boundary regions.

Wilson (1964) has shown that the distribution of salt in the lower region is consistent with upward diffusion from a very thin bottom layer for a period of about 1200 years. Thus the time scale for the development of this lake is an order of magnitude longer than that for the Taylor Valley lakes. For this reason no information on age can be obtained from the temperature profile below 50 m since, the diffusion constant for heat being much greater than that for salt, this profile is effectively a steady state one (Wilson and Wellman 1962). The analysis of the Taylor Valley lakes is irrelevant to the problem of Lake Vanda then, except insofar as it has shown firstly that there is no immediate cause to invoke any abnormally high geothermal heat flow, nor any other energy source apart from solar radiation, to explain the high temperatures; and secondly that the depth of the lake is susceptible to climatic changes but otherwise stable. The primary interest in an investigation of Lake Vanda therefore lies in explaining the origin and development of its unusual stratiform nature rather than the elucidation of climatic history in the Wright Valley.

Two origins of the layered convection have been suggested (in discussion) by A.T. Wilson and H.W. Wellman, namely internal waves and changes in lake level. An origin in internal waves presupposes the presence of a solute gradient throughout the lake. The resulting density gradient could support internal waves, which might be excited by

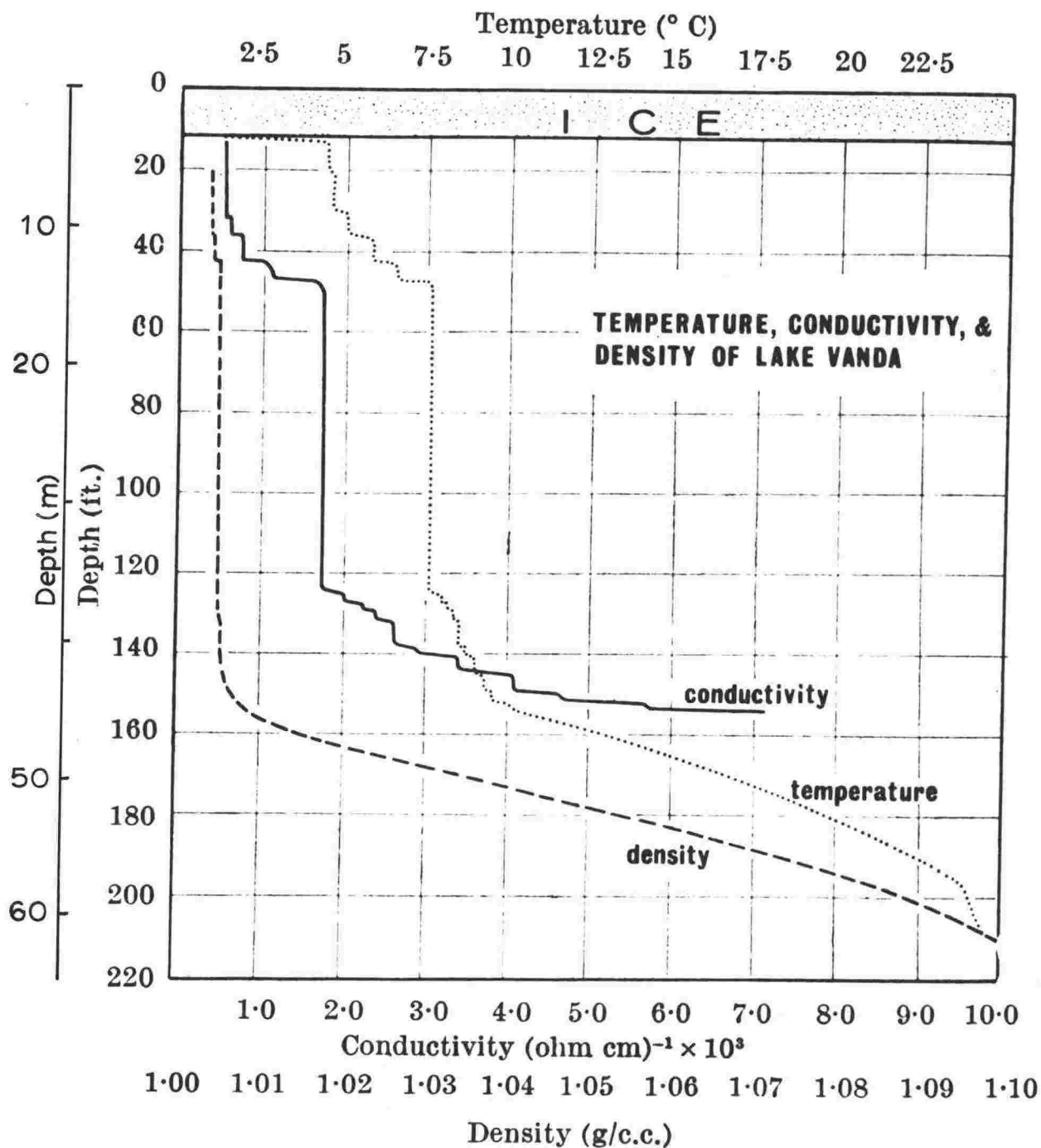


Fig.18 Lake Vanda temperature, conductivity and density profiles. Reproduced from Hoare (1966).

movement of the ice cover by wind. However it is difficult to see how this in itself could produce mixed layers. Provided there is no discontinuity of density, there will be no discontinuity of velocity (Lamb, 1932), and no vortex formation. Once layers had been formed by some other process, a discontinuity of density would be associated with vortex production at the layer boundaries, and the resulting transport of solute would modify the density distribution; but even if it could be shown that this modification tended to maintain the discontinuity (which seems doubtful), diffusion of solute would ensure that a discontinuity of density could not in fact occur. Thus although internal waves are probably present in the lake, and may modify its nature, they could not produce a layered structure from an initially uniform one, and must therefore be discarded as a possible origin.

Mixed layers could have been formed by changes in lake level. If the level fell, in response to a change toward greater aridity in the area, the salt would have remained in solution as evaporation proceeded. Thus if the ice/water boundary fell to a level where the salt concentration was significant, it would have swept the dissolved salt ahead of it until an unstable density profile was produced, when convection would have occurred and produced a mixed layer under the ice. If the lake level subsequently rose the mixed layer might have been perpetuated if the heat flow was sufficient to maintain convection against the stabilising tendency of the underlying salt gradient. If the salt flux into the bottom of the mixed layer slightly exceeded that out of it, the concentration in it would have gradually increased. Then if the lake level fell again, a new mixed layer might have been formed above the old one and of lower concentration. In this way a whole series of layers may in principle have been built up.

In order for changes of lake level to be acceptable as a theory of origin of the layers now present in the lake, it is necessary to show

that each layer could have retained its identity from the time of its formation until the present. It seems unlikely that layers as thin as those near the 50 m level would still retain their identity after a time perhaps as long as 1000 years, during which the salt concentration in them has increased by an order of magnitude. The observations of Hoare (pers. comm.) show that the layers are dynamic in character, so that although the main features are preserved from one summer to the next, differences in detail are apparent even over that time. Thus even if layers had been formed by this process, it is probable that their character would have been so modified by the convective processes in the lake that they would no longer be recognisable. The origin of the present layers therefore lies more with the convective process itself. Indeed, as will be seen in the following sections, this process is capable of producing layers without the assistance of level changes, so it is clearly desirable to investigate convection itself before falling back on level changes to explain the observations.

3.3 Convection.

3.3.1 Basic work.

Thermal convection in a fluid is a process of which the physical basis is obvious, but the details are not. Basically, if the density of an otherwise homogeneous fluid layer is made greater above than below owing to the imposition of a temperature gradient, a flow results in which the lighter fluid floats upwards in some regions and the heavier sinks downwards in others. So long as the temperature difference is maintained, the flow continues.

The first controlled experiments on convection were carried out by Bénard (1900 a, b, c, 1901 a, b), although Thomson (1882) had observed the effect in a layer of hot soapy water cooling from its upper surface. The experiments of Bénard were carried out with liquids having a wide range of viscosity. In each case the liquid layer was thin

(about 1 mm), and was heated uniformly from below by a hot metal plate. These experiments showed that after an initial transient stage in which the structure of the layer was somewhat irregular, the flow was clearly resolved into a cellular pattern. The cells had vertical boundaries and showed a strong tendency to a hexagonal planform, in which flow was upwards in the centre and downwards round the perimeter.

The first theoretical analysis of convection was published by Rayleigh (1916). He cited Bénard's experiments as evidence that the flow pattern is basically cellular. The cause of Bénard convection was assumed to be buoyancy forces, as outlined above, but later authors have shown that in such a shallow layer of fluid the variation of surface tension with temperature provides the major driving force (Pearson 1958, Nield 1964). Nevertheless the flows produced by both effects are very similar (Nield, 1966). Thus although Rayleigh analysed Bénard's experiments on the basis of a false hypothesis as to the driving force, his analysis was correct when applied to buoyancy induced convection, which is the more usual type.

Rayleigh's analysis began with the equations of motion, continuity and heat conduction for the fluid, expressed in an approximate form due to Boussinesq (1903). In this form the fluid is assumed incompressible, and the temperature variation of density insofar as it affects momentum is neglected, only the buoyancy effect being retained. Physical properties of the fluid were assumed to be constant. An additional constraint was an equation of state which assumed a linear variation of density with temperature. These equations were first solved for the equilibrium case in which the velocity was everywhere zero. This solution was then perturbed slightly, and the velocity assumed to grow as $\exp(\gamma t)$ as a result. Assuming γ to be real, that is the flow to be monotonic (non-oscillatory), the stability of the initial equilibrium was then demonstrated by the sign of γ . If $\gamma < 0$ the

perturbation would die away with time, while if $\gamma > 0$ it would grow with time, indicating instability. Rayleigh solved for the case of marginal stability $\gamma = 0$ which separated these two possibilities, and showed that it corresponded to a non-zero temperature gradient. Thus if the temperature gradient was initially zero and then slowly increased (in the direction favouring instability), convection would not immediately ensue, but would occur only when the quantity

$$R = \frac{g \alpha \beta h^4}{\nu K}$$

exceeded some critical value. This value depends on the root-mean-square horizontal wave number, but is a minimum at some wave number, the corresponding critical value being $27 \pi^4 / 4$ (= 657). The non-dimensional group R is now known as the Rayleigh number, and its minimum critical value is the critical Rayleigh number R_c above which convection should occur.

The particular value 657 for R_c follows from the assumption of hydrodynamically free horizontal boundaries with fixed temperatures. This choice of boundary conditions, and the assumption of rectangular rather than hexagonal cells, allows a simple derivation of R_c , but the arrangement is physically unrealistic.

Other boundary conditions do not allow an exact solution for R_c to be obtained so easily (for example, see Low, 1929) and approximate methods have usually been adopted. Jeffreys (1926, 1928) solved for a variety of situations in which one or both horizontal boundaries were hydrodynamically rigid and had either fixed temperature or fixed heat flow (i.e. fixed temperature gradient). More recently, Sparrow et al. (1964) have included both constant temperature and constant heat flow boundaries as opposite extremes of a general "radiation" boundary condition. These and intervening calculations such as those of Pellew and Southwell (1940) show the following general behaviour: If a surface is held at constant temperature, the fluid is more stable than if the heat flux is kept constant at the surface; if a surface is hydrodynamically

rigid, stability is greater than if that surface is free; and a choice of conditions at one boundary such as to produce greater stability will be reinforced by a similar choice at the other boundary. In each case, greater stability is associated with a higher value of R_c . If the lower boundary is rigid (the only practical possibility), variation of the remaining boundary conditions gives values in the range $320 \leq R_c \leq 1707$.

3.3.2 Non-linear temperature profiles.

The calculations of Rayleigh, Jeffreys and Pellew and Southwell assumed a constant temperature gradient throughout the fluid layer. Batchelor (1954) and, in more detail, Morton (1957) considered the effect of a non-linear temperature profile such as may be produced by rapid heating from below, and showed that the critical Rayleigh number was greater than that for a linear profile having the same boundary temperatures, though by only a small amount. Sparrow et al. (1964) showed that when the non-linearity was of the opposite sense, that is when the internal temperatures were greater than those of the linear profile, stability was reduced; this effect was also small provided the non-linearity was not sufficient to reverse the sign of the temperature gradient anywhere.

A more searching analysis by Currie (1967) showed that rapid heating from below could have a marked effect on the critical Rayleigh number. For very slow heating, the value was 1707 (rigid, constant temperature boundaries); as the heating rate increased the value initially diminished to a minimum of 1340, and then increased sharply, without limit.

Debler (1966) showed that a non-linear temperature profile could cause the fluid layer to break up into sub-layers, but only in a very restricted case; it was necessary for the temperature at the upper surface to exceed that at the lower one, and for the maximum temperature to occur within the layer rather above its mid-section. Under these conditions (or analogous ones produced by expansion behaviour such as

that of water near 4°C) the unstable upper part of the layer can drive a separate circulation in the stable lower part.

Another effect of a non-linear temperature profile results from its transient nature. Foster (1965) showed that a non-linear profile resulting from surface cooling of a liquid did not produce detectable motion as soon as some critical temperature difference was exceeded. Instead, a small but observable time lapse occurred during which the rate of growth of instabilities was negligible.

3.3.3 Overstability.

Rayleigh showed that the onset of convective instability was characterised by time-independence of perturbation quantities. When this is the case, the principle of "exchange of stabilities" is said to hold (Jeffreys 1926). Rayleigh effectively proved the validity of this principle for the particular case of stress-free boundaries, and Pellew and Southwell (1940) gave a general proof for any boundary conditions.

The alternative mode of instability was called "overstability" by Eddington (1926). Here the motion which develops from the initial perturbation is oscillatory. As distinct from (monotonic) instability, in which a displacement induces forces which lead the system further from equilibrium, in overstability a displacement from equilibrium induces restoring forces great enough to return the system through equilibrium and beyond the corresponding point on the other side. Although overstability cannot occur in a homogeneous fluid subjected only to a temperature gradient, the imposition of a second constraint on motion can lead to overstability in certain cases. Chandrasekhar (1961) has shown that, in general, a stationary instability occurs when the rate of supply of energy by the thermally-induced buoyancy force can just balance the rate of dissipation by viscosity; while overstability will occur if, at a smaller heat flow, it is possible to balance in a synchronous manner the periodically varying amounts of kinetic energy with similarly varying amounts of dissipation and liberation of energy.

It has been known for some time that overstability may be expected when a homogeneous fluid is subjected simultaneously to an appropriate temperature gradient and to rotation (Chandrasekhar and Elbert, 1955). This type of overstability should occur only in fluids whose Prandtl number P (ratio of kinematic viscosity to thermal diffusivity) is less than 0.677. In accordance with this prediction, Fultz et al. (1954 and 1955) have observed the effect in mercury ($P = 0.025$) but not in water ($P = 7.5$).

According to the theory of Chandrasekhar (1952) it is also possible for overstability to occur when the fluid is electrically conducting and is subjected to a magnetic field as well as heating. In this case, however, no experimental check has been possible, since overstability is only possible when the thermal diffusivity K , the magnetic permeability μ and the electrical conductivity σ are very large; specifically, when $K \mu \sigma > 1$. Under most terrestrial conditions this criterion fails by a wide margin, though it may be met in some stars.

Not surprisingly, in view of the above, overstability can also occur when an electrically conducting fluid is subjected to both rotation and magnetic field when heated from below (Chandrasekhar, 1956). It is found that the system exhibits overstability when sufficiently heated provided the magnetic field is not too intense. Overstability in this category has been observed by Nakagawa (1959) in mercury.

3.3.4 Thermosolutal convection.

The first stability analysis for the case of a fluid containing a vertical gradient of solute concentration in addition to a vertical temperature gradient was given by Vertgeim (1955). This paper considered only the possibility of monotonic instability, when the liquid was contained in a vertical cylinder. The question of monotonic instability for ideal (i.e. stress-free, constant temperature, constant solute concentration) horizontal boundaries was discussed by Stern (1960).

The analysis of Gershuni and Zhukhovitskii (1963) considered both monotonic instability and overstability, but for simplicity they chose the geometry of a plane vertical slot of finite width and infinite height. This gave a simple flow field at the cost of physical reality, but showed that overstability is to be expected under certain conditions.

Other authors have considered the possibility of overstability in a horizontal layer with ideal boundaries (Weinberger 1962, Lieber and Rintel 1963, Walin 1964, Veronis 1965, Sani 1965, Nield 1967). The analysis of this problem is a straightforward extension of Rayleigh's pure-fluid analysis, with the added constraint of a second diffusion equation which describes the diffusion of solute. Gershuni and Zhukhovitskii included the effects of thermal diffusion and diffusive thermal conductivity, but in practice these are generally negligible and the other authors have assumed the two diffusion processes to be independent.

Whereas in a homogeneous fluid convection will occur if the Rayleigh number exceeds a critical value which is unique for a given geometry, when an additional constraint such as a solute gradient is present the critical Rayleigh number is a function of the magnitude of that constraint. In the thermosolutal case the solute effect is expressed through a solutal Rayleigh number R_s , where

$$R_s = \frac{g \eta \gamma h^4}{\nu K}$$

Since R_c is now a function of R_s , it is convenient to present it in graphical form. Fig. 19 is the resulting stability diagram for the thermosolutal extension of the Rayleigh problem, for a case $P_s > P$. Corresponding to monotonic instability and overstability respectively, there are two straight lines on the graph. These have the equations (derived from Nield, 1967)

$$R + \frac{P_s}{P} R_s = 27 \pi^4 / 4 \text{ (monotonic instability)}$$

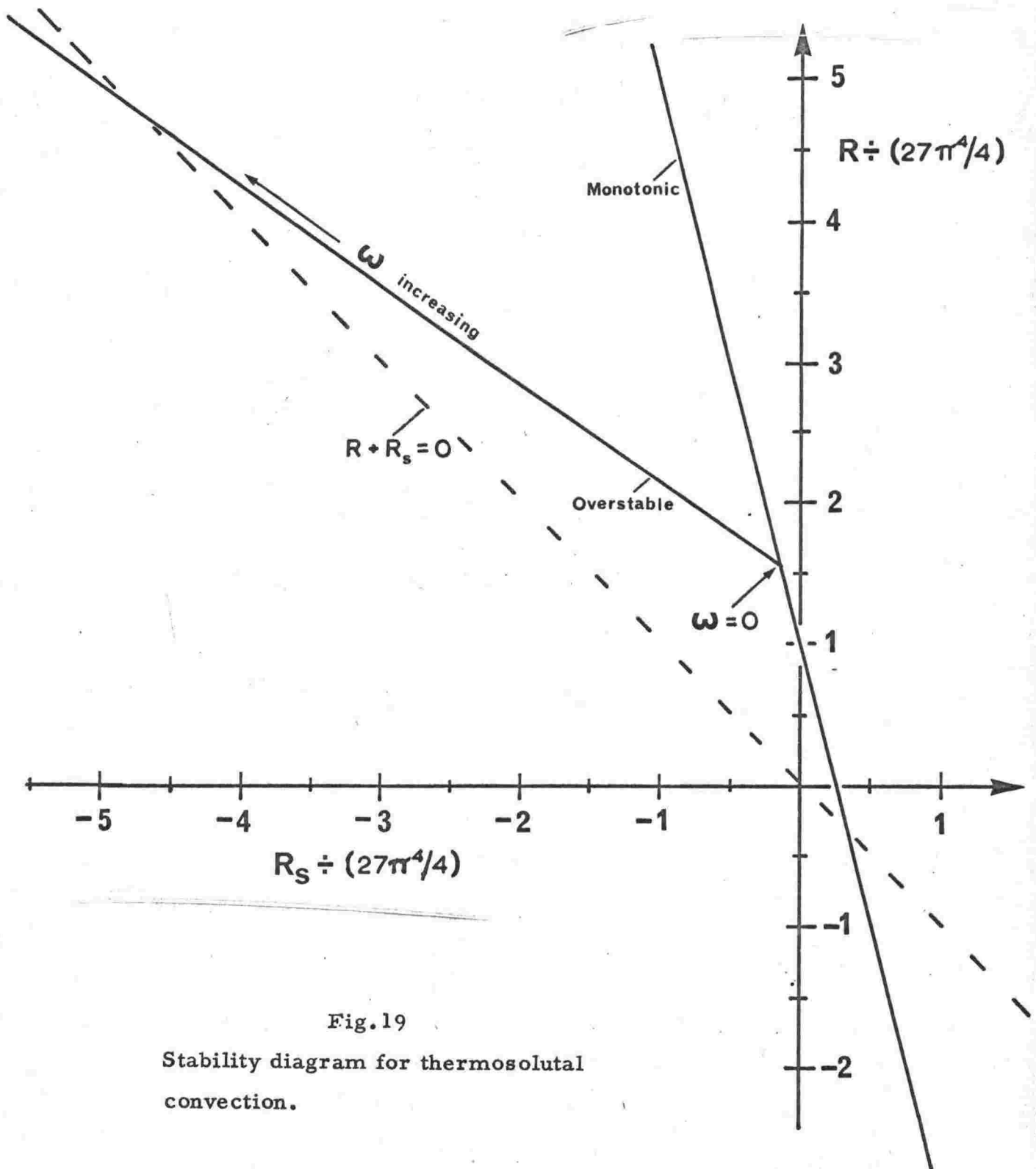


Fig.19
 Stability diagram for thermosolutal
 convection.

and
$$\frac{P_s}{P + P_s} \left\{ \frac{P_s R}{P_s + 1} + \frac{P R_s}{P + 1} \right\} = 27 \pi^4 / 4 \quad (\text{overstability}).$$

For the case of aqueous solutions ($P \sim 10$, $P_s \sim 1000$) the second expression may be approximated by

$$R + \frac{P}{(P + 1)} R_s = 27 \pi^4 / 4.$$

The angular frequency of oscillation ω in the case of overstability is given by

$$\omega^2 = \frac{\nu^2}{3P_s^2 d^4} \left\{ \frac{P_s(P_s - P)}{P(P + 1)} \cdot (-R_s) - \frac{27 \pi^4}{4} \right\}.$$

ω is zero at the intersection of the monotonic instability and overstability lines and increases at points along the overstability line towards more negative R_s , that is towards a stronger stabilising concentration gradient.

The interpretation of the stability diagram is as follows: If R_s is constant and R gradually increased from an initially stable value, overstability is to be expected if the point (R, R_s) crosses the overstability line. If, however, the point crosses the monotonic instability line, whether it has previously passed through the overstability line or not, monotonic convection will ensue.

The line $R + R_s = 0$

is plotted on the stability diagram. Along this line the density gradient in the solution is zero, and below the line the fluid is "gravitationally stable". It is apparent that the condition that density increases downwards is not sufficient to guarantee stability, since both stability lines cross the line of zero density gradient. The possibility of convection occurring under these apparently stable conditions derives from the different diffusion rates for heat and solute. In the monotonic case $R < 0$ and $R_s > 0$, so that (in terms of a heavy solute and a solution which expands on heating) hot, concentrated solution overlies cool, weak solution, the temperature effect predominating in the determination of density. If a mass of liquid starts to fall, it rapidly loses heat to its

surroundings without a corresponding loss of solute ($P_s > P$, i.e. $K > D$), so that the fluid mass becomes more dense than its surroundings and is accelerated. In the overstable case, $R > 0$ and $R_s < 0$, which is the inverse of the previous situation. Here a rising mass of liquid loses heat to its surroundings and experiences a restoring force greater than that which would result if all diffusion were absent, and which continues to operate even when the fluid mass has returned to its original position. Hence an increasing oscillation results.

Not all studies have been concerned with ideal boundaries. Walin (1964) discussed the problem without defining boundary conditions at all, though his solution for the vertical velocity component is that required for ideal boundaries. Nevertheless his paper is of mainly qualitative interest.

Nield (1967) described a method which in principle enables the evaluation of a stability diagram for any set of boundary conditions. Except for the case of ideal boundaries, his calculated results are limited to monotonic instability owing to the tedious algebra involved in overstability. He showed that when the boundary conditions for temperature and solute concentration are formally identical, the stability line is given by

$$R + \frac{P_s}{P} R_s = R_c$$

where R_c is the critical value when the solute is absent, for the same boundary conditions. That is, the ordinary Rayleigh number R is replaced by $R_e = R + R_s P_s / P$, the critical value being unchanged. However, if the boundary conditions for temperature and concentration are different, for example if at a boundary one of these variables and the gradient of the other are held constant, the stability condition is more complex. Because the flow pattern favoured by the temperature distribution is now different to that favoured by the concentration distribution, the two effects are less tightly coupled, resulting in the stability line becoming curved, concave toward the origin.

3.3.5 Finite amplitude effects in thermosolutal convection.

The analyses so far mentioned have been concerned exclusively with the stability problem, neglecting non-linear effects which result from finite velocities. The papers of Veronis (1965) and of Sani (1965) are particularly interesting in that they are attempts to include non-linear effects, and hence to investigate the stability of motions of finite amplitude. Both authors assumed ideal boundaries, but used different approximations in order to make the problem tractable. Veronis assumed, for velocity temperature and concentration, the simplest trigonometrical solutions which would make some allowance for convective redistribution of these quantities. Sani, on the other hand, used series expansions which were formally exact, and truncated the (infinite) series after at most three terms. From the calculations of heat and mass flow, it appears that the latter method is unsatisfactory for overstability, the retention of more terms being required, although it is qualitatively satisfactory for monotonic disturbances.

In spite of their approximate natures, both these studies indicate qualitatively what special effects may be expected to result from the non-linearity of the problem. Both, of course, predict the monotonic instability and overstability previously deduced from linear theory. In addition, they indicate the possibility of sub-critical monotonic convection when $P_s > P$; that is, it is possible for certain disturbances to be maintained at a steady, finite amplitude even though the thermal Rayleigh number is less than that required for either of the cases of "marginal stability". Such convection will not occur, however, unless it is initiated by an appropriate disturbance of sufficient amplitude. Its origin lies in the greater diffusivity of heat compared to that of solute, which results in the solute gradient being deformed by an imposed disturbance more than the temperature gradient. The mid-region of the convecting layer may then have a relatively high temperature gradient and low concentration gradient, favouring convection.

Sani's calculations are concerned almost exclusively with the range $0 \geq R_s \geq -\frac{P(P+1)}{P_s(P_s-P)} \cdot \frac{27}{4} \pi^4$ (for $P_s > P$), that is for values of R_s between zero and the intersection of the monotonic instability and overstability lines on the stability diagram. It appears that the limitations of his method prevent reliable conclusions for greater $|R_s|$. Since this range is very limited for $P_s \gg P$ (as for aqueous solutions), interest in practice centres on much greater $|R_s|$ and his results are of little quantitative value. Where they are valid, however, his calculations agree qualitatively with those of Veronis.

Experimentally, then, if the fluid is not disturbed convection will grow only from the appropriate case of marginal stability, where the required amplitude for initiation tends to zero. However Veronis predicts that the oscillation associated with overstability will quite rapidly reach an amplitude sufficient to initiate the sub-critical monotonic convection. If this was the case, the onset of overstability would be difficult to identify, any form of instability giving rise to monotonic convection.

It is not possible to deduce how long the oscillation would persist, since the time-dependent calculations were performed numerically. However a solution is given for the steady state of the finite amplitude monotonic motion, and this shows that where the conditions are marginal for the occurrence of overstability, the lowest equilibrium amplitude of the temperature disturbance for the monotonic motion is about 5% of the temperature difference across the layer. Thus one might expect to observe overstability as an oscillation which continues for a long time provided the amplitude is much less than this limit.

It is possible to draw more specific conclusions by comparing the analyses of Sani and Veronis. Although the range of validity of the former is limited, within that range the method not only gives solutions for the equilibrium amplitudes of finite amplitude disturbances, but also

permits an evaluation of the stability of such equilibria. In those cases where an increase of equilibrium heat flow (or equilibrium amplitude of disturbance) is associated with a reduction of Rayleigh number, the equilibrium is unstable, and the disturbance is amplified until the equilibrium heat flow is an increasing function of Rayleigh number.

A similar situation is apparent in Veronis' calculations for overstability. His paper includes a sketch of the variation of equilibrium heat flow with Rayleigh number for low amplitude oscillations, which shows higher equilibrium heat flow to be associated with lower Rayleigh numbers. Hence we can expect that, if the Rayleigh number is held constant, any finite oscillation which occurs must be continuously amplified, no matter how small its initial amplitude. Whereas the unstable solution for monotonic flow found by Sani led to a higher equilibrium amplitude of the same type, however, the increasing oscillation will not achieve an equilibrium amplitude, but will lead to monotonic convection.

The reason for this is the relatively rapid redistribution of solute caused by small disturbances. Turning to Veronis' equilibrium solutions for monotonic flow, the ratio

$$r = \frac{\text{convective component of heat flow}}{h \text{ non-convective component of heat flow}}$$

may be compared with the similar ratio for solute transfer (r_s). It is found that, for small disturbances,

$$r_s \doteq \left(\frac{P_s}{P}\right)^2 \cdot r_h \sim 10^4 \cdot r_h \text{ for aqueous solutions,}$$

whereas for large disturbances

$$r_s = r_h.$$

Assuming the situation for overstability to be similar, it is apparent that even though small oscillations would not be expected to provide efficient heat transfer (cf the observations of rotation-induced overstability by Nakagawa and Frenzen, 1955, also Goroff, 1960), they may give a significant solute flow. An increase of solute flow implies an increase

of concentration gradient at the boundaries, where the transfer is entirely conductive. Since the concentrations are fixed at the boundaries, the mid-layer concentration gradient must be reduced. Thus any increase in solute transfer must tend to reduce the solute-induced stability of the mid-layer region. In the absence of the solute gradient, the existing temperature gradient would be highly super-critical to monotonic motions. Hence the convective transfer of solute, even for small disturbances, has a tendency to induce monotonic flow.

3.3.6 Experiments: Marginal stability.

Experimental work on the observation of convective onset has been summarised by Chandrasekhar (1961). Briefly, the experiments fall into three classes according to the method used to observe the onset: heat flow measurement, optical methods, and internal temperature difference measurement.

When a fluid layer transfers heat by conduction only, the heat flow rate increases in proportion to the Rayleigh number. After convection has set in, the total heat flow is the sum of conductive and convective components. For Rayleigh numbers which are not too much in excess of the critical, the convective component is proportional to this excess, so that the total heat flow still varies linearly with R but at a greater rate than during pure conduction. Measurements of heat flow for a series of values of R above and below the critical allow the junction of these lines, and hence the critical Rayleigh number, to be found without direct observation of the vanishingly small effects which occur at marginal stability. This method of finding critical Rayleigh numbers was first used by Schmidt and Milverton (1935), and later by others, notably Silveston (1958). Its use is dependent on the ability to make an external measurement of the heat flow through the liquid layer. This measurement is usually made in terms of the current supplied to an electrical heater, and is essentially indicative of the horizontal-average heat flow. The method is not applicable to thermosolutal overstability, both because the

horizontal average heat transport by this type of convection is very small, and also because there are no stable equilibrium states associated with it.

It is possible to detect the presence of convection optically, since the refractive index of fluids changes with temperature. The presence of a temperature gradient therefore deflects a beam of light which is transverse to the gradient in a manner similar to that which is responsible for a mirage. In the presence of cellular convection, the temperature gradient has a spatial variation which produces a corresponding variation of the light deflection. Several methods have been devised to use this effect, indeed the original work of Bénard is the first example; see also Schmidt and Milverton (1935), Schmidt and Saunders (1938) and Silveston (1958). However such methods depend on effects produced by convection of finite amplitude, and are more suitable for observation of the resulting cellular pattern than of the convective onset itself.

Fultz et al. (1954, 1955) detected the onset of convection by monitoring the temperature difference between two different levels within the layer of fluid. While the disturbance of this temperature difference is vanishingly small at marginal stability, it is possible to take readings for values of heat flow less than and greater than critical, and determine the critical value by interpolation in a manner reminiscent of that of Schmidt and Milverton. The method involves making a continuous record of the temperature difference from the time at which the electrical heater is first switched on. The temperature difference increases from zero towards some equilibrium value. If convection occurs, the recording shows a fluctuation which precedes the attainment of equilibrium, the amplitude of the fluctuation being proportional to the extent to which the heat flow is super-critical; in addition, the equilibrium temperature difference is below that due to conduction alone by an amount proportional to the same excess.

The method of measuring internal temperature differences has three advantages. Firstly, so long as the thermal conditions are not too

far from equilibrium when convection sets in, the temperature difference indicated may be interpreted directly as a measurement of the (almost uniform) temperature gradient throughout the layer. This allows a reasonably accurate measurement of the critical Rayleigh number without the attainment of equilibrium. Indeed, it is not necessary for the system to possess an equilibrium state insofar as the convection is concerned, but the measurement is more accurate if made near the condition of conductive equilibrium.

Secondly, the fluid temperatures are measured at points. Fultz et al. used five thermocouple pairs spaced through the cell so that the temperature difference was an average over a number of sites. In principle, however, the method can measure the disturbance in one confined region, rather than supplying a horizontal average as in the Schmidt-Milverton method. Thus it is suitable for the detection of overstable oscillations, the horizontal-average effect of which is very small.

Finally, a third advantage of this method is that measurements are not confined to the boundaries. Thus it can be used without prior knowledge of the exact whereabouts of the boundaries, and does not require accurate temperature control of the boundaries, both of which features are important in the onset of layered thermosolutal convection, as will be seen. Further, measurement at the boundaries would show only very small convective disturbances if the boundaries were of high conductivity, which is the usual case in practice, since the distortion of the conduction-only temperature profile is a maximum at points within the fluid some short distance from the boundaries, and zero at the boundaries.

3.3.7 Experiments: Finite amplitude.

The vanishingly small effects associated with marginal stability demand relatively sophisticated techniques for their evaluation. Certain gross effects associated with finite amplitude convection can be observed with relative ease and yield useful information.

With regard to pure thermal convection, the chief interest in well-developed flows lies in determining their effect on total heat flow, particularly in regard to studies of turbulence. Heat flow measurements have been made by Malkus (1954a), Thomas and Townsend (1957) and Globe and Dropkin (1959). Malkus found that the convective heat transport varied linearly with Rayleigh number; but that there were several discrete transitions in the character of the convection, at each of which the slope of the line changed, increasing with increasing heat flow. These experiments formed the basis of the theory of Malkus (1954b) and of Malkus and Veronis (1958) in which the transitions were interpreted as steps toward the development of full turbulence. This interpretation was challenged by Elder (1965) who found in similar experiments no evidence that the transitions were due to the successive addition of higher modes on the linear stability theory. Instead, he found that the transitions were due to the broadening of cells, the number of cells present between the vertical boundaries of the apparatus diminishing by one for each transition. Nevertheless, irrespective of the interpretation, the measurements of heat flow as a function of Rayleigh number are valuable, and are substantially confirmed by the later work of Thomas and Townsend and of Globe and Dropkin.

Prior to the observations of Shirtcliffe (1967) which are to be described in the following pages, thermosolutal convection had been studied only in the finite amplitude regime. The first study, by Turner and Stommel (1964), was a rather crude one in which a container of water containing dissolved salt with a stabilising gradient of concentration was heated gently from below. By means of suspended aluminium powder and fluorescein dye it was seen that the resulting convection occurred in layers. The layers were formed in turn starting from the bottom, and slowly increased in thickness after formation. This observation inspired the previously mentioned studies of Walin (1964) and of Veronis (1965), neither of which was successful in explaining the stratiform nature of the convection.

Layered convection has also been observed by Schaafs (1966) to occur in various liquids containing stable solute gradients when these were irradiated by light from above. The effect was observed by means of an optical system, and the photographs published without an explanation of the phenomenon.

The paper by Turner (1965) concerned an experiment designed to elucidate the characteristics of stratiform thermosolutal convection. Instead of allowing the layers to appear in an uncontrolled manner, Turner deliberately produced a two-layer system. Having set up a sharp boundary between the strong and the weak solutions by stirring each, he studied the rate at which salt and heat were transferred across the boundary as a function of the ratio of the contributions of salt and heat to the density difference. The results were published in graphical form without explanation; but a discussion of them in appendix 4 herewith shows that they are consistent with the following behaviour of stratiform thermosolutal convection:

(1) The convecting layers are separated by thin regions in which heat and solute are transferred by diffusion only, no convection penetrating these regions.

(2) The non-dimensional rate at which solute is lifted is proportional to the non-dimensional upward heat flow, the solutal Nusselt number being perhaps $O(10^2)$ times the thermal Nusselt number.

(3) The upward heat flow is described by an effective Rayleigh number R_e , where $R_e = R + \frac{\nu}{\nu + K} R_s$, in the same way as R describes the convective heat flow in pure-thermal convection.

(4) The temperature and solute profiles adjust themselves according to a maximum criterion such as maximum heat flow or maximum R_e .

3.3.8 Summary

Prior to the work to be described in the following pages, information about thermosolutal convection was almost exclusively theoretical, the only exceptions being the observation that it can occur in a layered form, and a crude investigation of the nature of the equilibrium of such layers. Theory predicts that this sort of convection may be initiated in any of three ways: by a disturbance of sufficiently large amplitude, through a state of oscillatory marginal stability, or through a state of monotonic marginal stability. In each case, theory predicts the necessary conditions for each type of initiation, but only for cases of linear profiles of solute and temperature, and usually for physically unrealistic boundary conditions.

The following sections describe experiments designed to check the applicability of the rather idealised theories to real situations, and in particular to the problem of heat transfer in Lake Vanda.

Chapter 4

Laboratory Experiments

4.1 Experimental arrangement.

4.1.1 Background

These experiments had two aims. Firstly, it was hoped to find how thermosolutal convection is initiated, whether through a monotonic or oscillatory marginally stable state or through a sub-critical instability, and if possible to determine the criterion for such convective onset. Secondly, it was hoped to repeat the experiment of Turner and Stommel under conditions which would enable the development of layered convection to be studied in more detail.

The theories of thermosolutal stability have invariably been predicated on linear profiles of both temperature and solute concentration. It is not difficult to approach this thermal condition quite closely, since heat can easily be supplied and extracted through the materials used in constructing the tank which is to contain the fluid. However these materials are generally impermeable to solutes, so that the concentration gradient normal to any such boundary is necessarily zero; and in fact it would be very difficult to establish a near-steady-state flux of solute through a layer of fluid and at the same time control the flow of heat through it. Thus one is forced to carry out experiments using non-linear profiles of concentration, and possibly also of temperature. While it may be argued that non-linearity probably has very little effect in the pure-thermal case provided it is not extreme, and therefore perhaps in this case, the comparison with theory must be viewed with some reservation on this account.

Consider the case of a layer of fluid in which there is a stabilising concentration gradient with impermeable horizontal boundaries, and a linear destabilising temperature profile. Fig. 20 is a sketch of the contributions to density of the concentration and the temperature.

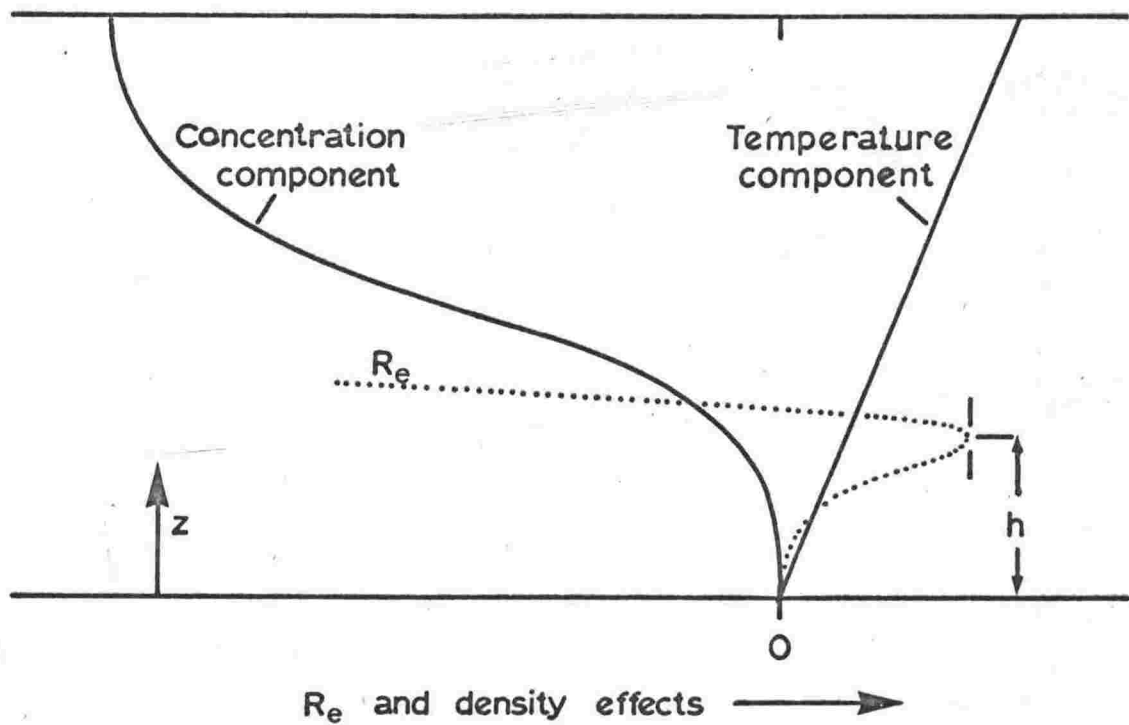


Fig. 20

Temperature and concentration components of a density profile, and the resulting profile of R_e .

Superimposed is a sketch of the variation of R_e with z , when R_e is defined in terms of the temperature and concentration at the lower boundary and those at z . Because $R_e \propto z^3$ it is zero at $z = 0$, and goes through a maximum at some value $z = h$.

It is a natural extension of the discussion of convection in chapter 3 that, if the maximum value of R_e exceeds some critical value, the layer of depth h will become unstable. The critical value of R_e , R_{ec} , will presumably depend on the hydrodynamical conditions at the boundaries of the unstable layer; but in all other types of convection, changing the boundary conditions only changes the critical Rayleigh number without reducing it to zero, and the same behaviour may be expected here. Convection produced in this way may therefore be expected to exhibit the same properties as that considered in the idealised theories, though with some quantitative difference.

In order to measure R_{ec} , it is necessary to evaluate the temperature and concentration at $z = 0$ and $z = h$. Since h is not known before the convection begins, it is necessary in practice to know the complete profiles of concentration and temperature at the critical moment. In fact, as will be seen, h is not well defined until the conditions are much beyond marginal stability. However R_{ec} can be regarded as the maximum of $R_e(z)$ with respect to z at the marginal state, and can be calculated from the profiles of temperature θ and concentration χ .

Since the moment of initiation is not known in advance, it must be possible to specify the profiles $\theta(z)$ and $\chi(z)$ continuously. As far as the solute is concerned, since the boundaries are impermeable the profile at any time can be calculated from that measured at an earlier time provided the diffusion constant is known, at least until convection begins. In order to calculate a temperature profile, however, both an initial profile and some additional information such as the variation of temperature of the heated boundary with time are required, though this problem can be simplified by always starting an experiment with the fluid isothermal.

Minimum requirements for the experiments were, therefore,

- (a) a tank to contain the fluid, with heating facilities underneath,
- (b) a means of measuring the initial concentration profile,
- (c) a continuous recording of the temperature of the tank bottom,
- (d) a sensitive detector of the onset of convection, and
- (e) a means of monitoring the profile of some convenient quantity such as density during the development of layered convection.

4.1.2 Optical equipment.

In practice, (b) and (e) of the foregoing requirements were satisfied by the same equipment. The refractive index of aqueous solutions is a function of both temperature and concentration, but in such a way that it is defined at least approximately by the resulting density. Thus an optical method was used to measure the concentration profile at the start of the experiment, when the liquid was isothermal, and it also gave an approximate density profile at other times.

The basis of the method is indicated in fig. 21 (a)-(c). It is closely related to the "scanning schlieren" method of Longworth (1939, 1946), but has additional components and a different scanning method. For the present purpose Longworth's method had two disadvantages. Firstly, it required a specially modified camera which contained a mechanism for scanning the plate past a slit. It is cheaper, and more convenient in operation, to use a standard camera with an external scanning arrangement. Secondly, the graph produced on the plate was not in the form of a dark (or light) curve drawn on a light (or dark) background, but was a curved boundary between light and dark regions. When analysing such a record, it is more accurate to judge the centre of even a rather broad line than to locate the effective edge of a uniform region, since the edge is seldom sharp, and because its apparent position is likely to depend on the time for which the plate is exposed. Longworth's knife edge was therefore replaced by a horizontal slit placed at the

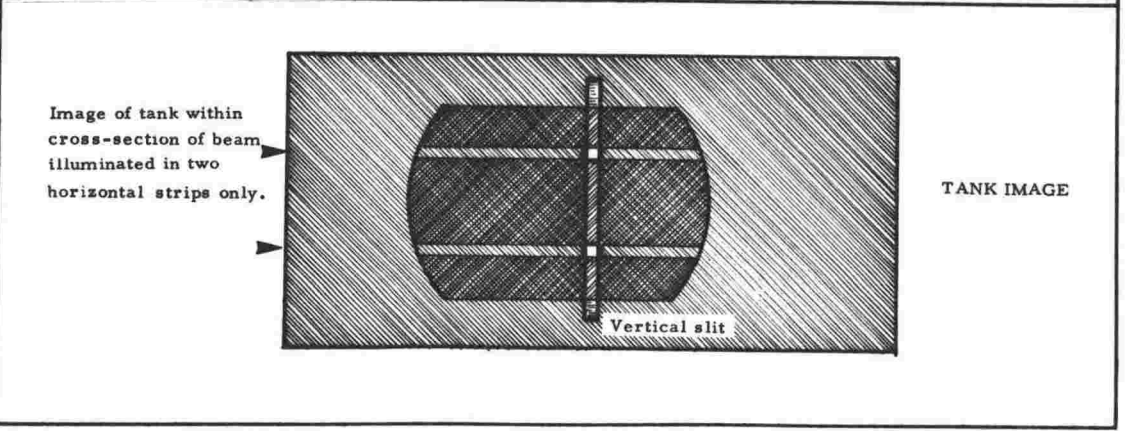
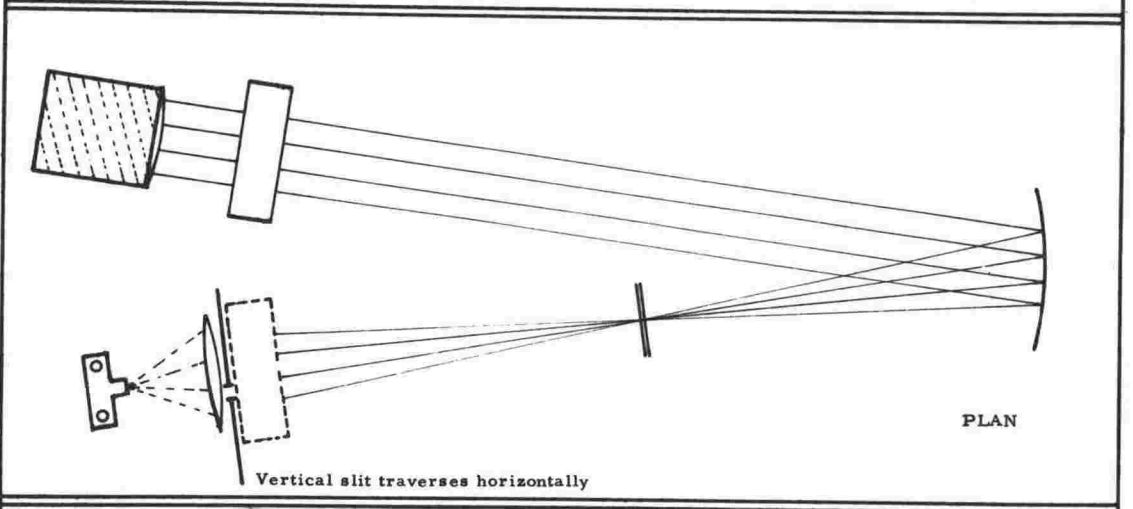
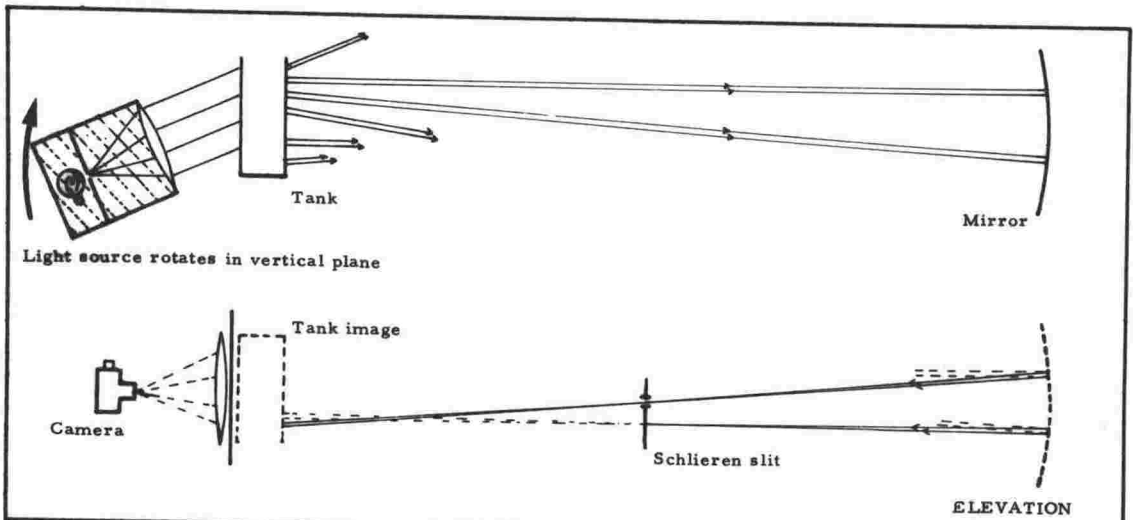
Fig. 21

(a)

The optical system

(b)

(c)



schlieren focus. This gave a record of the same form as that given by the method of Philpot (1938) without the necessity for a large cylindrical lens.

The system operates as follows. If a vertical gradient of refractive index exists at some level in the tank, light travelling nearly horizontally through the tank at that level is deviated through an angle which is nearly proportional to the local refractive index gradient (see Appendix 5 for a detailed analysis). A collimated light beam is incident

these gave satisfactory depth resolution, and the resulting record then took the form of several identical curves offset horizontally from one another.

A further development was to make one of the schlieren slits very wide. This was necessary for the study of well-developed convection, since the turbulent conditions tended to obscure a thin trace. In addition, one edge of this wide slit could be used as a conventional schlieren knife-edge for qualitative investigation of cell shapes and layer development in the convection.

The light source was a 100-W bulb placed behind a small pinhole, and this was followed by a 5-inch diameter Bausch and Lomb three-element collimator lens. These were mounted on a light framework supported by bearings at one end, under the tank, and suspended from a nylon cord at the other. The nylon cord was attached, through pulleys, to the mounting of the large vertical slit, which was moved sideways on an accurate lead screw driven by an electric motor. A complete scan took about 30 seconds, during which time the camera shutter was held open. The camera was an Exakta 35 mm using Ilford HP3 film, with a 100 mm lens mounted on rings so that the tank image filled the field of view. The tank had two sides made of plate glass, chosen for good optical flatness. Internally, it was 25 cm long, 6.4 cm wide and 17 cm high, the largest vertical faces being glass and the ends Tufnol.

In order to ensure even heating of the liquid, the base of the tank was made of brass 1.25 cm thick, and it rested on a bath of oil which was electrically heated. The glass sides could be insulated with plastic foam during experiments, to ensure that heat flow was vertical.

The vertical slit was 1 mm wide, which was the minimum justified by the limits imposed on the resolution by the schlieren slit. In order to give a scale to the final record, cotton threads were put across this slit at intervals of 2 cm. These were illuminated by a lamp which was out of the field of view at the top of the slit construction. The lamp

was supplied through a microswitch which was operated by a cam on a gear wheel in the traverse drive mechanism. Thus the cotton markers were lit briefly at intervals which represented a constant increment of lateral motion of the slit. This produced a grid of points which were accurate indicators of refractive index gradient and approximate indicators of depth.

For qualitative investigations the vertical slit was taken off, and the light source rotated until undeviated light was just passed by the lower edge of the wide schlieren slit. The changeover could be made rapidly, so that a series of frames could be exposed using each method alternately to give the maximum information on a run.

Examples of both applications are shown in Chapter 5 and Appendix 6, which describes the procedure for calibration of the system.

4.1.3 Thermal equipment: instability indicator.

In order to indicate the onset of convection, a pair of thermocouples were used in the manner of Fultz et al. (1955). It was expected that onset would occur as overstability, and that the oscillation would, at least initially, be very small. A galvanometer amplifier was therefore built, of the type described by Sirs (1959). The unit was built in a Cambridge spot galvanometer, two light-dependent resistors being mounted side-by-side in place of the scale. These were placed in a bridge circuit so that movement of the light spot produced a large out-of-balance voltage. Part of this voltage was fed back to give approximately critical damping at reduced gain. The lamp was mounted externally and the unit otherwise encased in polystyrene foam, which served to reduce thermal drift to an acceptable level. To maintain stability, the lamp was supplied from a 12V accumulator. Although much higher gains were feasible, the amplifier was usually operated with a gain of about 4000. The output was recorded on a Moseley strip chart recorder, usually operated with 0-10 mV sensitivity.

It was not known in advance how deep the convecting layer would be. Two pairs of thermocouples were therefore employed, one measuring the temperature difference between 0.5 and 1.0 cm above the tank bottom, the other between 1.5 and 2.0 cm (see fig.22). As heating progressed both these temperature differences became substantial, up to 2 C deg on occasion, giving an e.m.f. up to 80 μ V. Most of this was backed off by a Tinsley vernier potentiometer used as a voltage source, so that the input to the amplifier had a maximum variation of only 2 μ V. The potentiometer, which switched in steps of 1 μ V, had three inputs (apart from the standardising circuit) which could be chosen in turn by a switch. These were connected respectively to the lower thermocouple pair, the amplifier only, and the upper thermocouple pair. The amplifier-only connection was used to short the amplifier input and check the zero drift.

The thermocouples were made of 36 SWG copper and constantan wires mounted between the legs of a perspex H-bracket that fitted inside the tank. The horizontal part of this bracket defined the upper surface of the liquid in the tank and prevented evaporation.

4.1.4 Thermal equipment: bottom temperature.

A miniature-bead thermistor was mounted in contact with the upper surface of the brass slab which formed the base of the tank. This was made one arm of a bridge circuit in which it was balanced against one of 24 resistors chosen by switches. The out-of-balance voltage of the bridge was recorded by a Moseley chart recorder with 0-5 mV sensitivity, giving a lateral displacement of about 1 inch per C deg. over the temperature range 0°C to 70°C.

Each of the 24 ranges was calibrated separately against a mercury-in-glass thermometer. This thermometer, which had been calibrated by D.S.I.R. Physics and Engineering Laboratories, had divisions at 0.1 C deg intervals, and readings were interpolated to 0.01 C deg. The resulting graphs of bridge output, as read on the chart

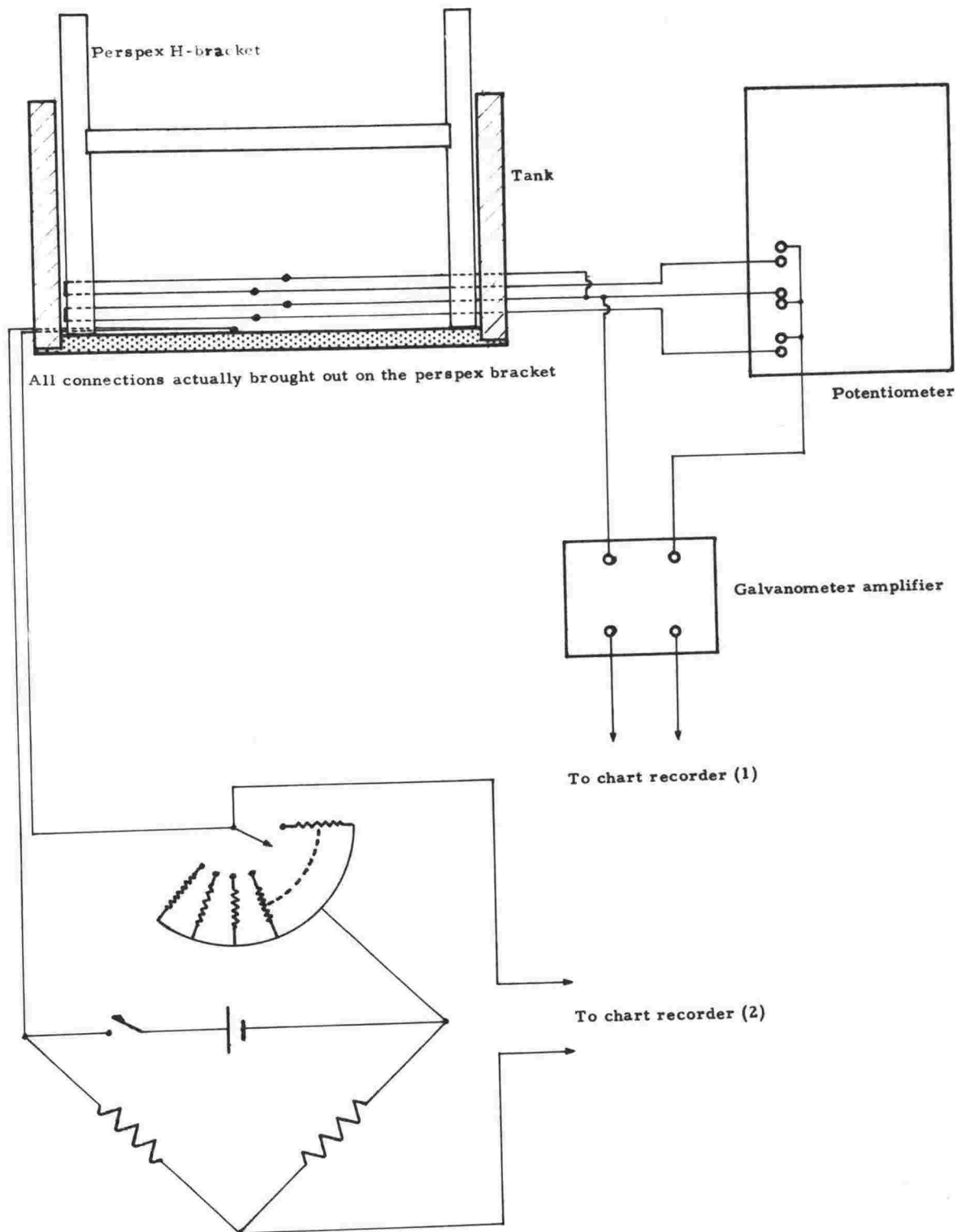


Fig.22 Temperature measuring system.

recorder, against thermistor temperature were accurately linear. Only exceptional points departed from this relationship by more than 0.01 C deg, though the slopes of the lines decreased slowly with rising temperature.

4.2 Experiments.

4.2.1 Stability

These experiments were run in three series, the tank being refilled at the start of each. The method of filling was that later advocated by Mowbray (1967), in which a series of layers are set up, of which the successive concentrations increase downwards. The stepped nature of the initial concentration profile decayed quite rapidly by diffusion, so that in the central region of the tank the concentration increased uniformly with depth. Sugar was again used as the solute, as in calibration, and the concentration was initially zero at the top of the tank.

Each experiment of a series began with the liquid isothermal. A concentration gradient profile was measured under these conditions, so that at any later time in the experiment up to the onset of convection the profile could be deduced from a knowledge of the diffusion constant. In practice, change in the profile during this period was very small.

After the concentration gradient profile had been measured, the heater was switched on and the current adjusted to give the desired rate of increase of temperature at the bottom of the tank. Both this temperature and the amplified output of the differential thermocouples were recorded continuously throughout the experiment. Both records showed an increase with time; the former was kept on scale by switching to successively lower balance resistors in the bridge circuit, the latter by switching in successively greater bucking potentials from the potentiometer. The rate of rise of both records fell off with time, and the heating rate was modified from time to time to maintain progress towards marginal stability. It was not known in advance when this condition would occur in the case of the first run of a series. Thereafter the steady decrease of concentration gradient in the tank, which resulted from diffusion and such limited convection as occurred during individual

experiments, was accompanied by a steady decrease in the temperature gradient necessary to bring about marginal stability. Thus for runs other than the first of a series it was possible to predict roughly the critical output of the differential thermocouple. As this condition was approached the rate of increase of temperature gradient was maintained at a modest value.

Marginal stability was reached in different runs after times varying from 15 minutes to nearly 3 hours, depending on the heating rate and the magnitude of the concentration gradient.

4.2.2 Results.

When marginal stability was reached, it was invariably marked by the appearance of an oscillation superimposed on the steady rise in output of the differential thermocouple. This result is consistent with the theories discussed in chapter 3, although it was not certain in advance that overstability would be observable.

The ease with which the onset of the oscillation could be detected depended on two factors, the rate of change of output of the thermocouples before the oscillation was superimposed, and the position of the thermocouples in relation to the cellular structure of the convection. Fig. 23 shows the important section of the record in a particular clear case (run S8), in which the heating rate was low and the thermocouples were apparently located advantageously. (This record was published in Shirtcliffe (1967).)

The temperature gradient near the bottom of the tank was about $2\text{ C}^{\circ}\text{ cm}^{-1}$ at this time. The heating rate was increased slightly at the point marked A, while at that marked B the sensitivity of the recorder was reduced by a factor 50. As marginal stability approached, the record became increasingly noisy. The appearance of the oscillation was followed by a rapid growth of its amplitude, and after about 12 minutes it became increasingly disordered.

Fig. 23.

Section of differential thermocouple record, run S8, near marginal stability. The quantity plotted against time is the differential output of two copper-Constantan thermocouples placed 0.5 and 1.0 cm above the tank bottom. Heating rate was increased slightly at A. Left-hand voltage scale applies up to B, right-hand scale thereafter.

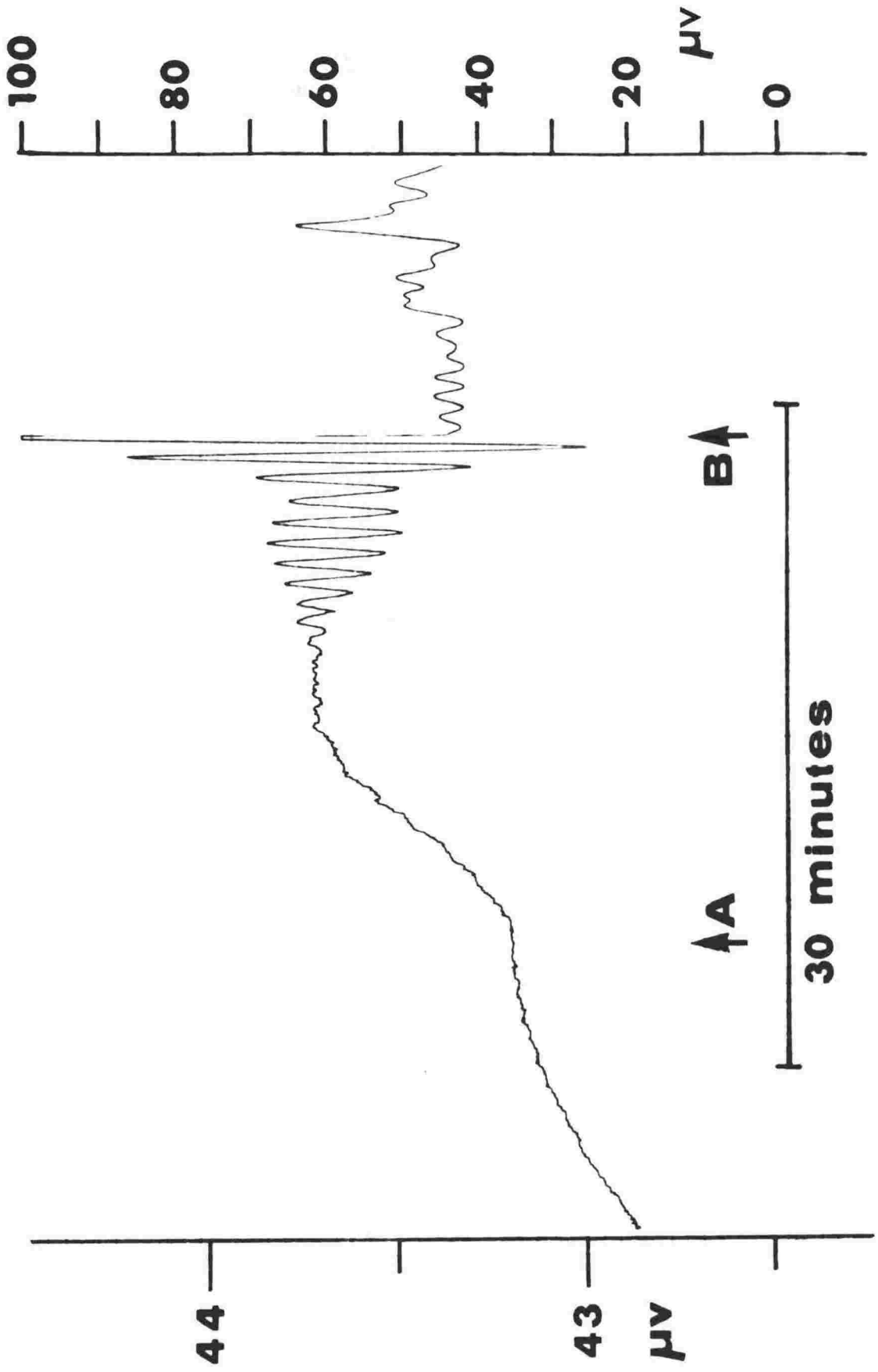
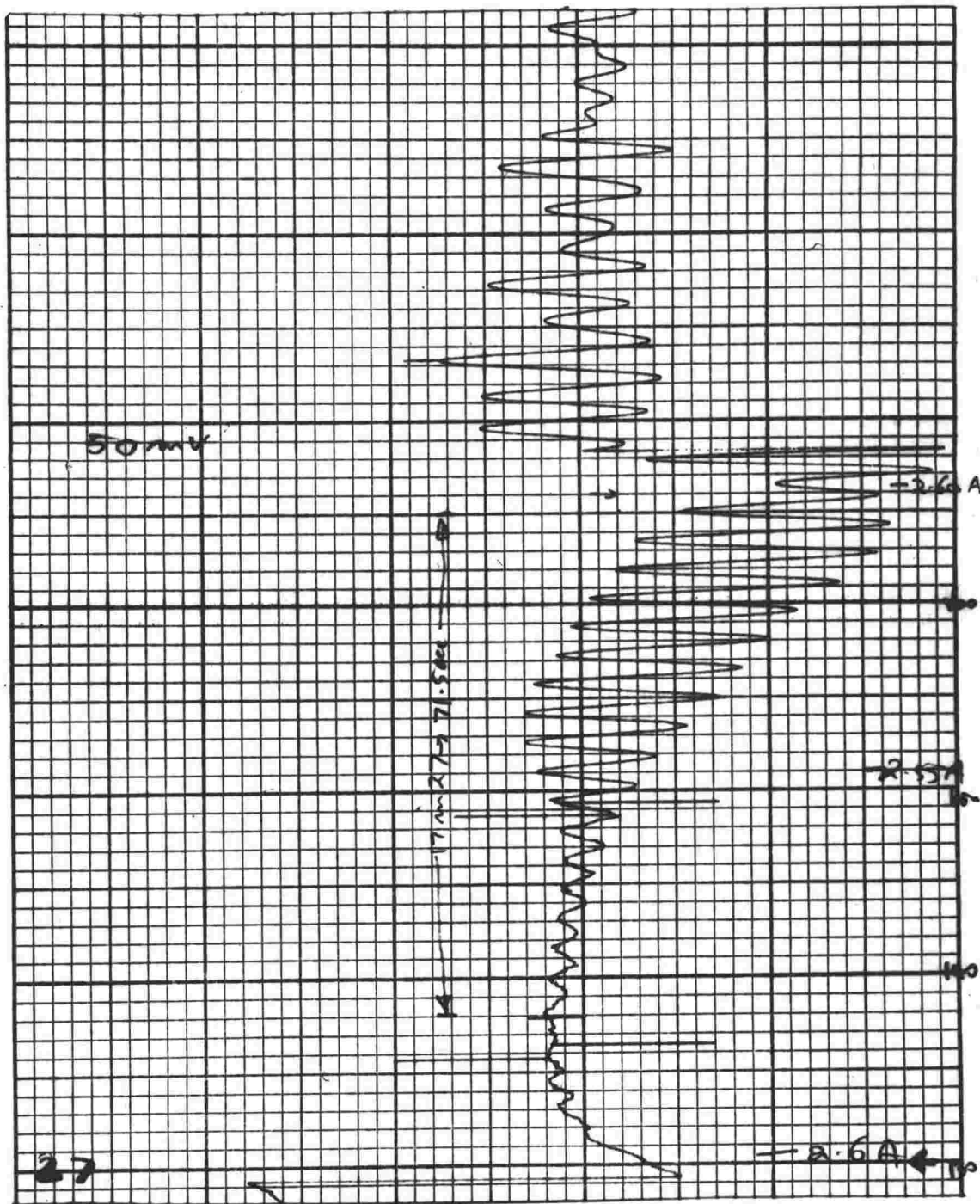


Fig. 24

Section of differential thermocouple record, run S4. Amplitude of sudden change at start is $1 \mu\text{v}$. Output initially is $27 \mu\text{v}$. Sensitivity reduced by factor 5 at marking "50 mV". 17 cycles of oscillation in 20.25 min. show mean period of 71.5 sec.



About the time that the oscillation became large, that is just after B, it became possible to observe cells at the bottom of the liquid. These could be seen by direct observation of the tank, and in this and other runs a record was kept of their development. The cells in this run were initially quite separate and 0.75 cm high. They grew rapidly (in about 30 seconds) to 1.0 cm, while at the same time other cells formed about 0.7 cm in height, and then all the cells steadied at a height of 0.8 cm. About 5 minutes after they first appeared, the layer of cells had increased in thickness to about 1.0 cm, the individual cells being about 1.5 cm wide at the base. One of the initial cells was situated so that it enclosed the lower thermocouple, which presumably explains the clarity of the temperature record.

In order to provide a range of thermal and solutal conditions under which the overstability was observed, a total of 15 runs were made in the three series. The results of the other runs differed from those of run 8 mainly in showing the onset of overstability less distinctly. However two other runs gave additional information.

Fig. 24 shows a section of the thermocouple record for run S4. In this instance an attempt was made to vary the heating rate in such a way as to prolong the period of small oscillations. The result was a period of nearly 10 minutes during which the amplitude of the oscillations was approximately constant. In order to maintain zero growth rate it was necessary to reduce the temperature gradient continuously, at a rate of 0.2% per minute. Presumably, therefore, the difference in concentration between bottom and top of the convecting layer was being reduced at about the same rate. Diffusion alone would have changed the concentration contrast by only about .006% per minute. Hence even this low amplitude oscillation was apparently transferring solute 30 times faster than pure diffusion would. The corresponding figure for the convective heat flow could not be determined but was apparently small. This result is consistent with the prediction of Veronis (1965) that the

increase in solute transfer rate due to small-amplitude (monotonic) convection would be $(K/D)^2$ (i.e. about 10^4) times as great as that for heat.

Fig. 25 shows the tops of the cells formed at an early stage of a typical run (run S 15). These pictures were taken by removing the large vertical slit and using the optical system as a standard schlieren device. The light source was set so that the system would pass only that light which had penetrated the tank in a region where the refractive index was increasing downwards at more than a certain rate. Thus the image of the lowest part of the tank, where the density (and hence refractive index) actually decreased downwards, was not illuminated. The cell tops were illuminated, and hence were regions in which the density increased downwards more rapidly than in surrounding liquid at the same level. This is consistent with the observation that solute was transferred more rapidly than heat by the convection; in terms of their respective effects on the density, the build-up of solute at the top of the cell exceeded that of heat, producing a relatively stable density gradient there.

The sequence in fig. 25 (a)-(e) shows that the cells were independent and dynamic. They migrated sideways, and in addition were continually appearing and disappearing. The system only revealed those in which the solute flux was sufficiently high at a given time; so it is not known whether the whole layer was populated by cells of which only a few were sufficiently active at any time, or whether their apparent independence was genuine. The first alternative seems more reasonable hydro-dynamically, though there is evidence that the second is actually true. In either case the situation was clearly not the orderly array of rectangular contiguous similar cells assumed by the theories of this type of convection.

4.2.3 Periods of the oscillations.

The measured periods of the oscillations just after marginal stability are shown in table V. In each case, the measurement was made

(a)

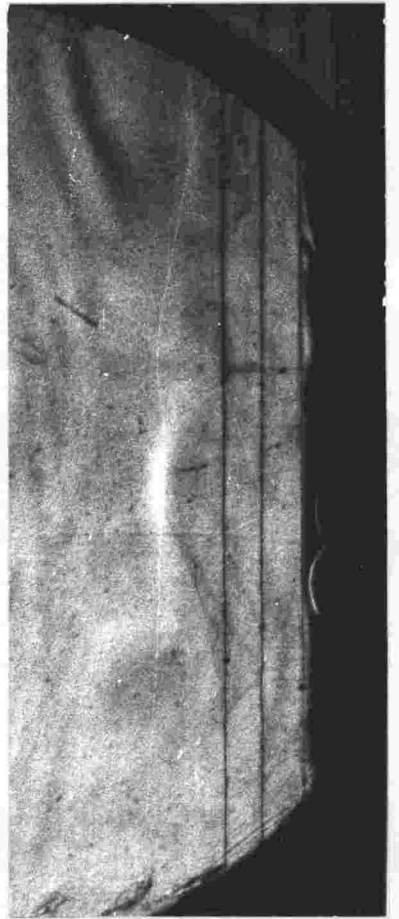
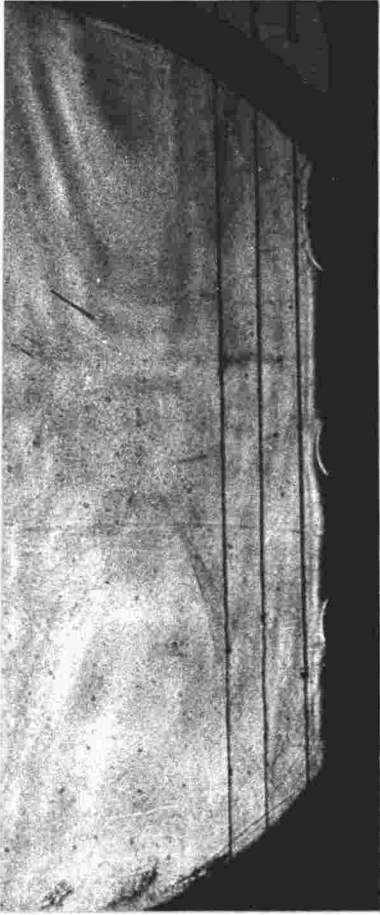
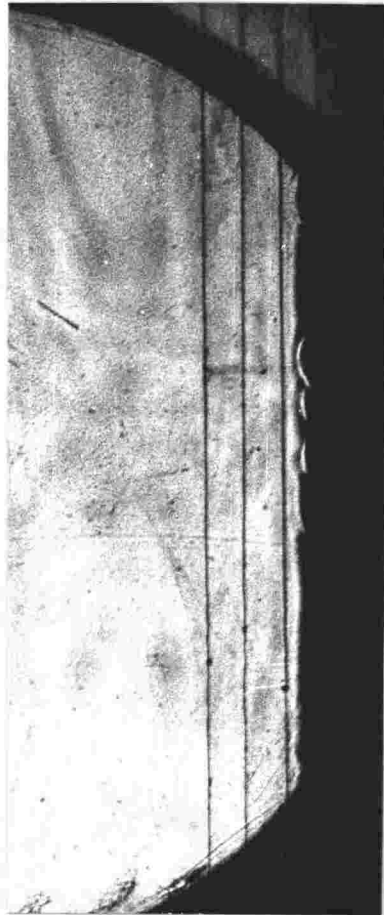
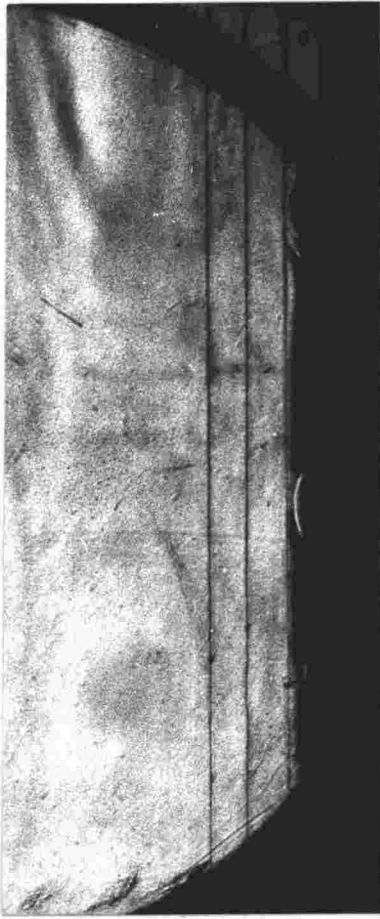
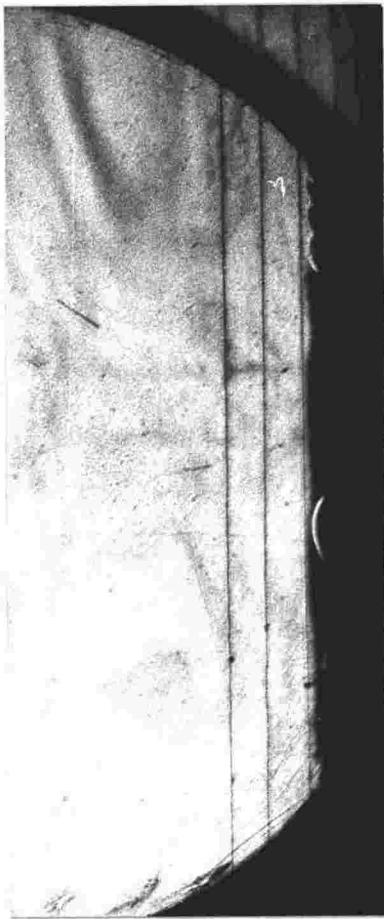
(b)

(c)

(d)

Fig. 25

Schlieren observations of cell tops, run S15. Only the lower part of the field of view is shown. The three thermocouple wires visible are 1.0, 1.5 and 2.0 cm above the tank bottom. (a) was taken 9 min., and (e) 17 min., after oscillation began.



over as many complete cycles as possible until the oscillation became irregular. This number of cycles varied from 2 to 20, producing a range of uncertainties in the periods.

Table V

Observed periods of overstable oscillations.

Run	Period (sec)
S1	53 \pm 5
S2	85 \pm 2
S3	73 \pm 2
S4	69 \pm 2
S5	45 \pm 2
S6	48 \pm 5
S7	56 \pm 2
S8	55 \pm 2
S9	53 \pm 1
S10	32 \pm 2
S11	30 \pm 5
S12	47 \pm 1
S13	65 \pm 5
S14	53 \pm 2
S15	59 \pm 4

4.2.4 Turner-Stommel layers.

It was not planned to investigate the development of convection in layers in great detail, but simply to seek a deeper qualitative insight into the phenomenon. In the event it was found possible to describe the process through a relatively straightforward model, which made the experiment semi-quantitative.

The elements of the process could be deduced from the observations described in the previous section. Convection occurred initially in a thin bottom layer for the reason outlined at the beginning of this chapter. Having begun, it transferred solute relatively quickly

to the top of this layer, forming a stable upper boundary through which both heat and solute could pass by diffusion only. The development of the convection would have increased the rate at which heat and solute were supplied to this boundary. This extra heat flow would have become apparent rather earlier than the extra solute in a region somewhat above the boundary, owing to the greater diffusion constant of heat. If the concentration gradient was sufficiently small in this region, the additional heat supply would have induced convection in it, there being then two layers rather as in Turner's (1965) experiment. Repetition of this process could have produced a further succession of layers provided the heat flow was sufficient to counteract the concentration gradient at the higher levels.

This picture of the origin of layered convection was tested in four experiments, runs T1 to T4:

Run T1. A rather low heating rate was chosen, similar to those used in the stability experiments. Convection began $\frac{1}{2}$ hour after the heater was switched on. Fig. 26 shows the profile measured after convection had continued for $3\frac{1}{2}$ hours. The disturbed layer, initially 1 cm deep, had increased slowly to 2.5 cm over this period, and was surmounted by a thin boundary region containing a highly stable density gradient.

Apparently the heating rate here was too low for convection to occur in a second, higher layer. The disturbed layer was of uniform composition and slowly lost solute upwards at a rate determined by upward diffusion out of the boundary region. As the concentration in the convecting layer fell, the boundary was maintained by its motion upwards into liquid of lower concentration.

An interesting feature of this profile is that the density gradient was apparently unstable only at the bottom of the convecting layer. When convection occurs in a homogeneous liquid heated from below, the density gradient is unstable at the top of the layer as well as the bottom.

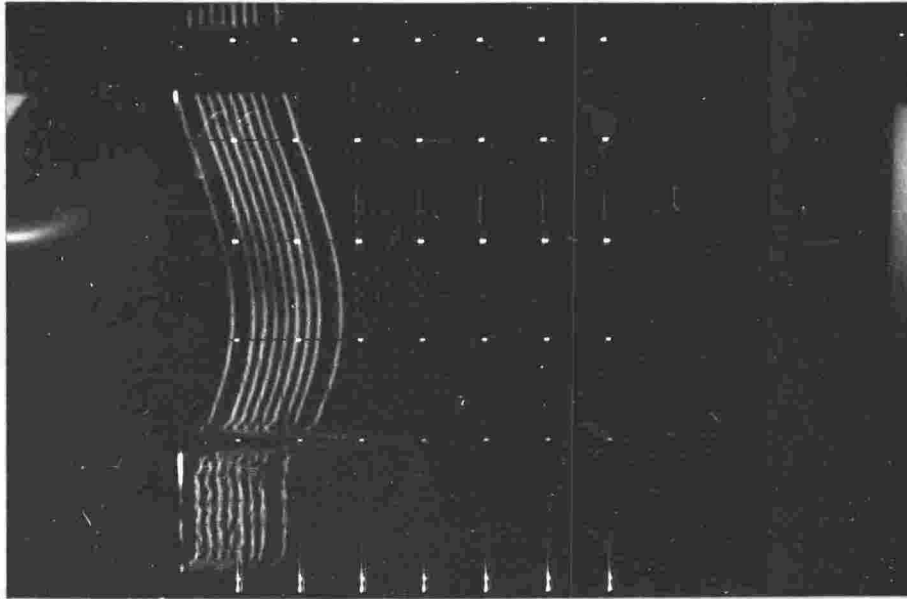


Fig.26

Density gradient profile, run T_1 , after heating for 3.5 hrs.

Run T2. This run was made 6 days after T1, without refilling the tank. The concentration gradients were therefore somewhat less intense. The heating rate was 50% greater than for T1. Convection began after 15 minutes heating with a layer depth of 1.2 cm. Fig. 27 shows the situation 50 minutes later, with a second layer of cells just appearing. The bottom layer was here 2 cm deep, and the new cell tops are visible about 0.5 cm above it. Fig. 28 shows a profile taken 12 minutes later, the lower layer having increased in depth slightly. The (approximately) zero density gradient in the second layer is clearly shown.

This experiment was continued until convection had persisted for 2 hours, at which stage there were still only two convecting layers, respectively 3 cm and 0.5 cm deep.

Run T3. The same tank filling was used, after allowing 3 days for the profile to become smooth again after T2. Heating rate was increased by a further 50%. Convection began after 7 minutes in a layer 1.5 cm deep, and the experiment ran for a further 4 hours. A second layer was formed 25 minutes after convection began, when the lower layer was 2 cm deep. A third layer occurred after a further 90 minutes, when the lowest layer was 3.5 cm deep, and was rapidly followed by two more layers of which the uppermost occupied the top 2 cm of the cell.

Towards the end of this run schlieren observation showed a monotonic, rather than oscillatory, motion of liquid elements in the lowest layer. Profiles taken about this time all showed that the density gradient was unstable immediately under the stable boundary at the top of this layer, as well as at the bottom.

Run T4. The tank was refilled before this run to provide greater concentration gradients, and the heating rate was 80% greater than that used for T3. Convection began in a layer 0.8 cm deep 10 minutes after heating began, and the experiment continued for 2 hours.

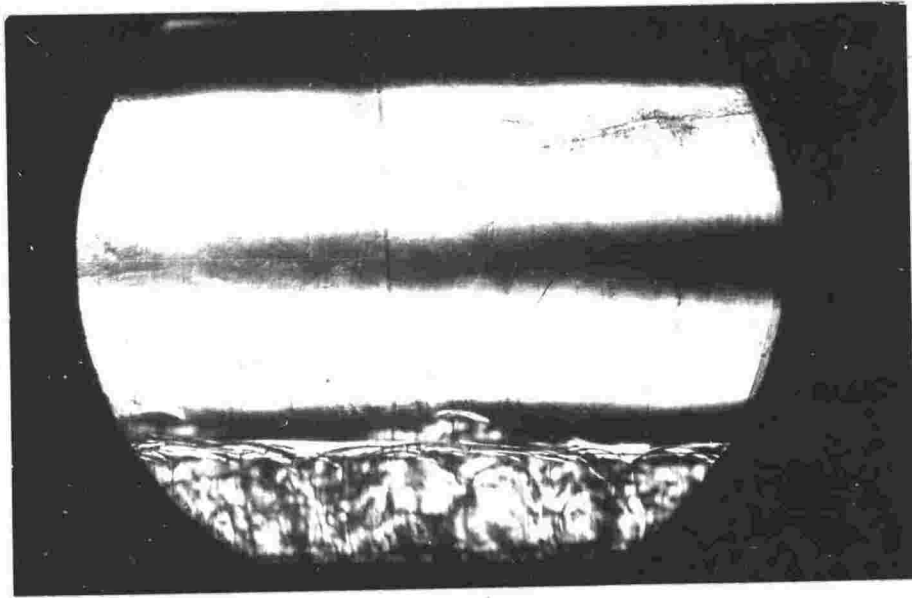


Fig. 27 Schlieren observation, run T2, after heating for 50 min.

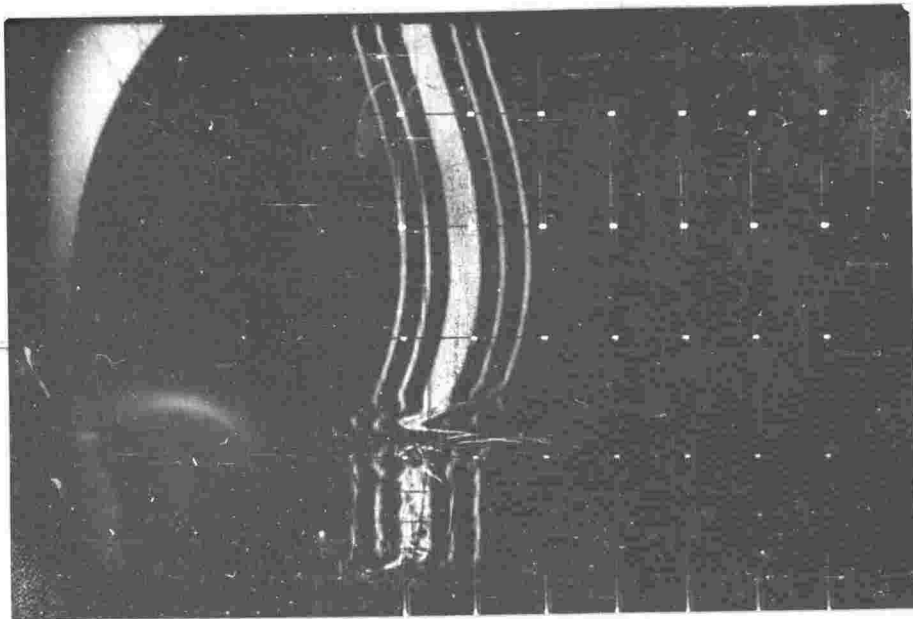


Fig.28 Profile, run T2, 62 min.

The sequence of profiles and schlieren observations in fig.29 covers the whole experiment. The first profile was taken before heating began, and shows the initial disposition of concentration gradient. The last profile was taken 95 minutes after the heater was switched off; since the temperature profile decays much more rapidly than the concentration profile, this is substantially indicative of the distribution of concentration gradient at the end of the experiment.

Intermediate observations were made at the indicated times after heating began. The second layer first appeared after 21 minutes, the cells showing a tendency to occur preferentially over the more active cells in the bottom layer.

After 40 minutes there was still no clear pattern of motion in the bottom layer. Instead, throughout the field of view rising elements could be seen which dissipated before reaching the upper boundary of the layer. A steady motion developed after about 45 minutes, from which time the profiles began to show an unstable density gradient at the top of the layer.

A third layer appeared at about 50 minutes. At 60 minutes the flow in the bottom layer was apparently such as to give a cool region in the centre of the field of view. This tendency for a variation of vertical heat flow across the tank persisted, and at those positions where there was greatest disturbance in the bottom layer there was also the greatest disturbance in the other layers above. Other layers developed as the records show, until the fluid was finally broken into about eight layers.

4.2.5 Expansion of sugar solutions.

Sugar was chosen as the solute for all the experiments because the physical properties of its aqueous solution are well tabulated, and because the more usual (and equally widely available) common salt was liable to introduce galvanic effects in the thermocouple detection system.

0 min

27 min

23 min

32 min

Fig. 29

Sequence of observations, run T4. The observations were made at the indicated times after heating began.



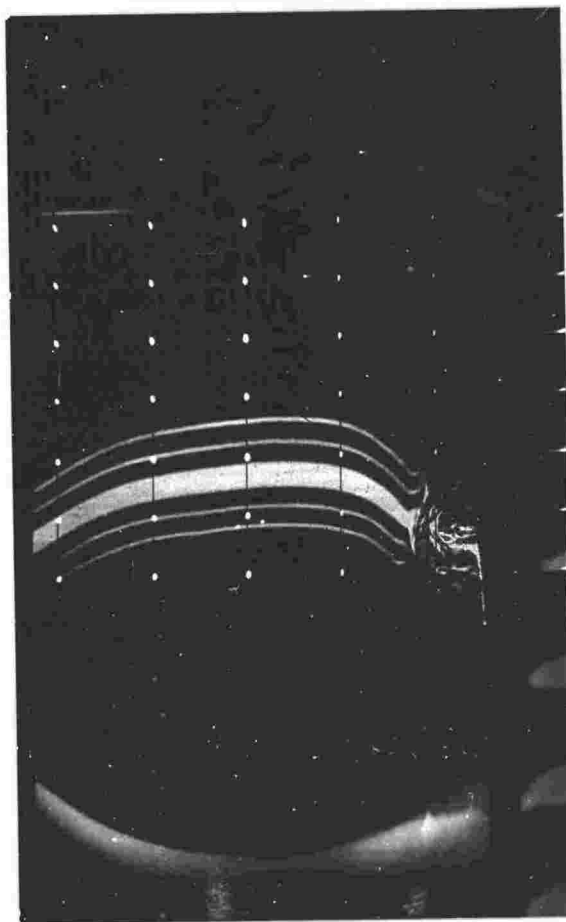
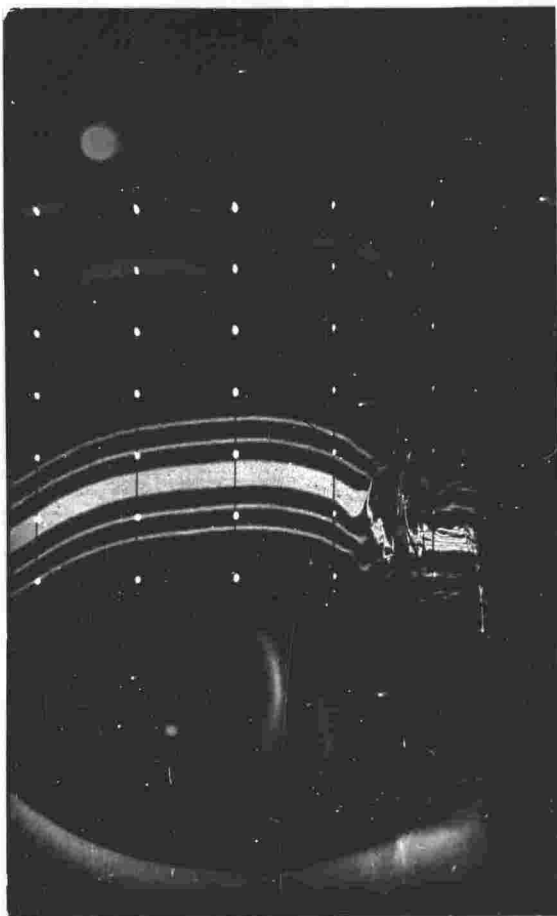
34 min.

44 min

42 min

53 min

Fig. 29 (cont.)



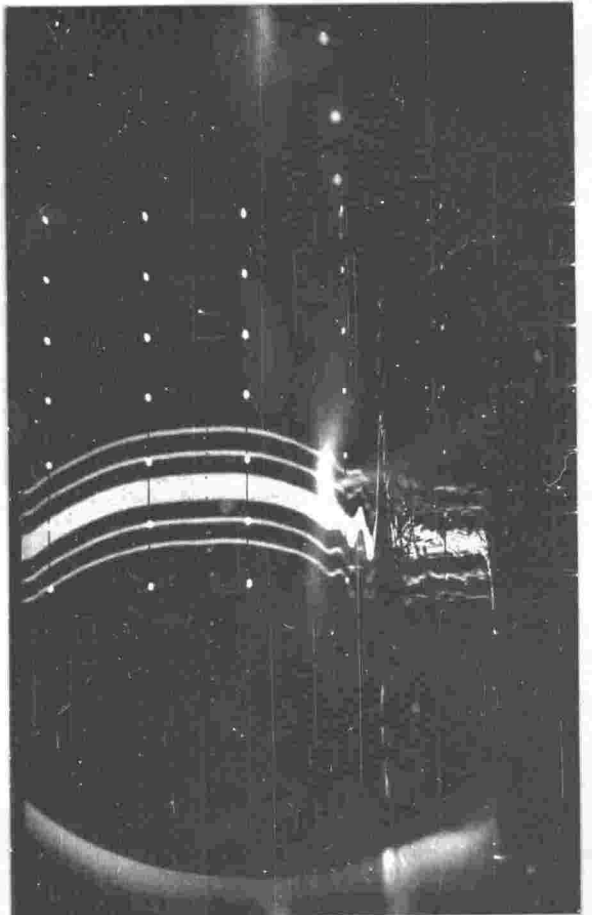
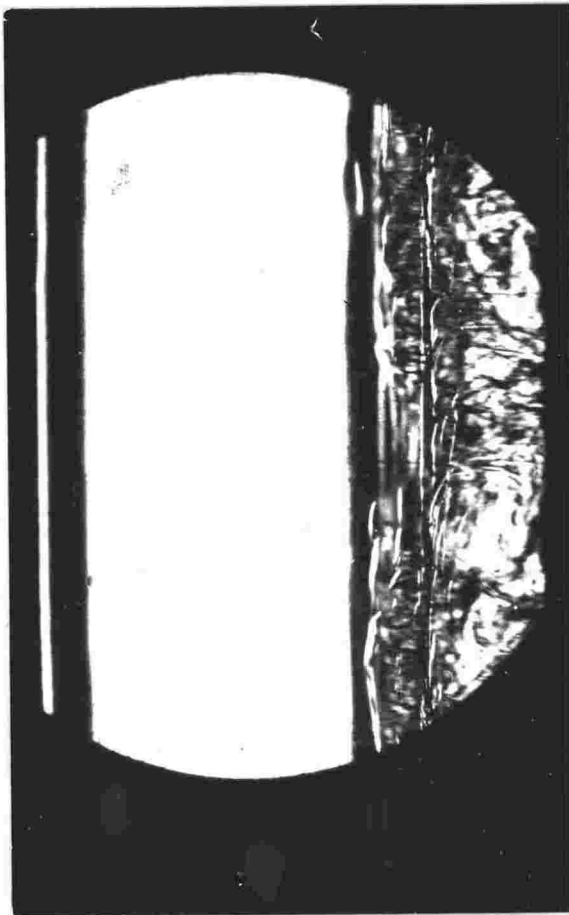
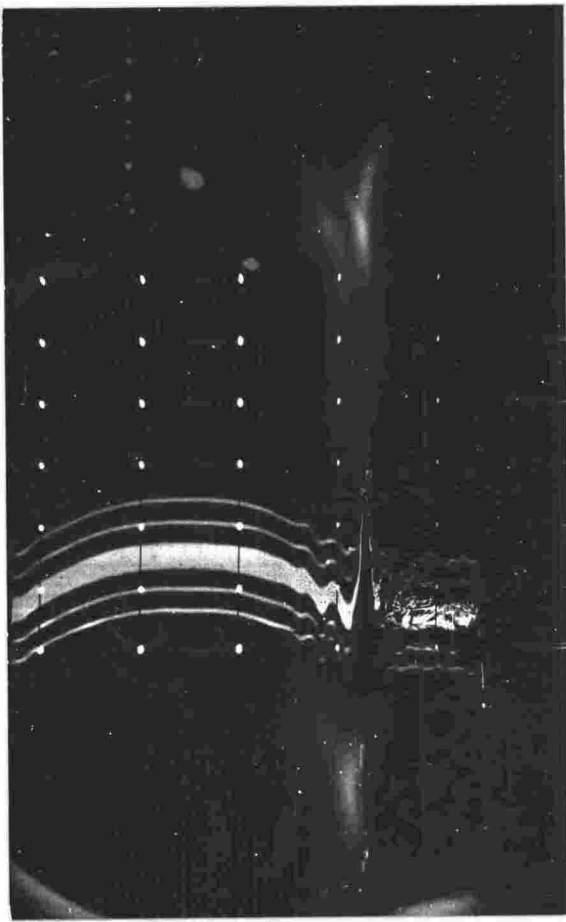
62 min

71 min

63 min

76 min

Fig. 29 (cont.)



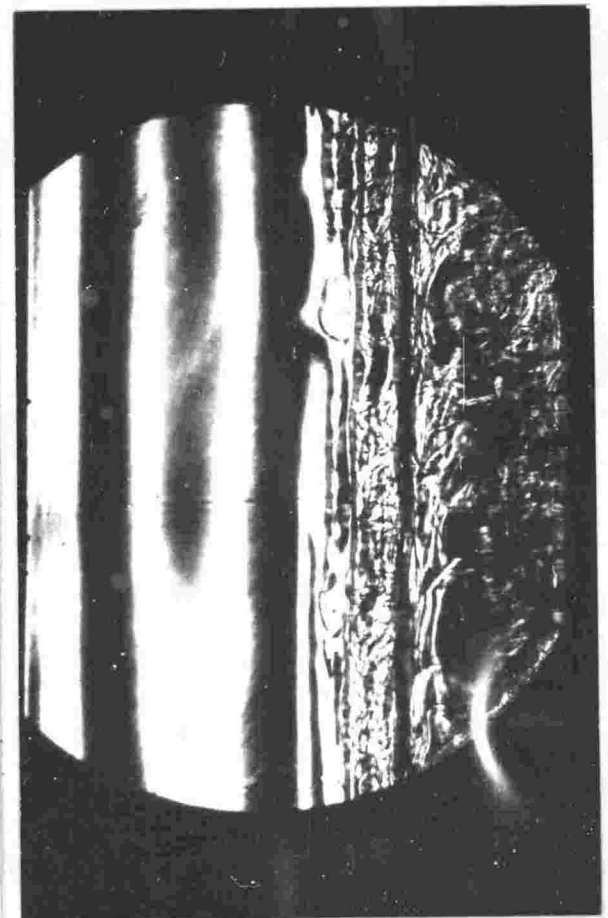
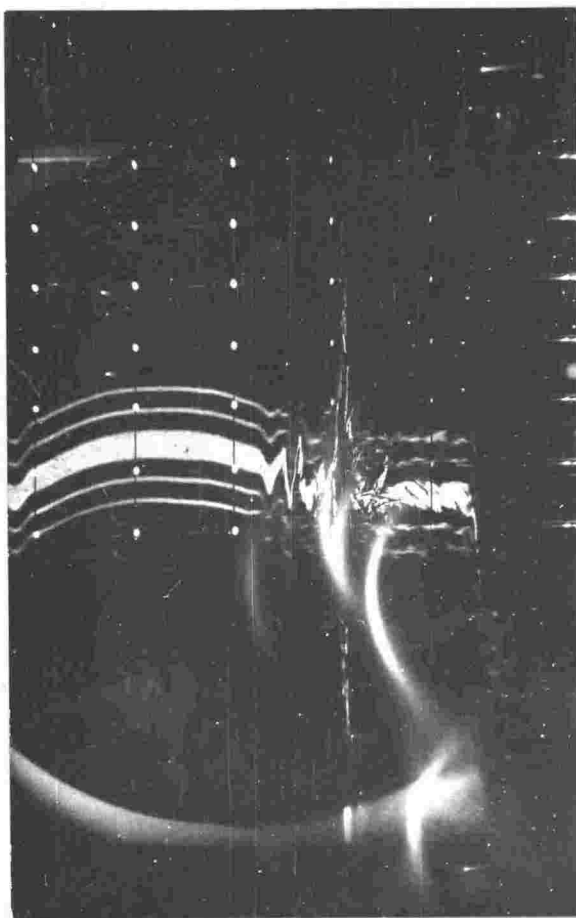
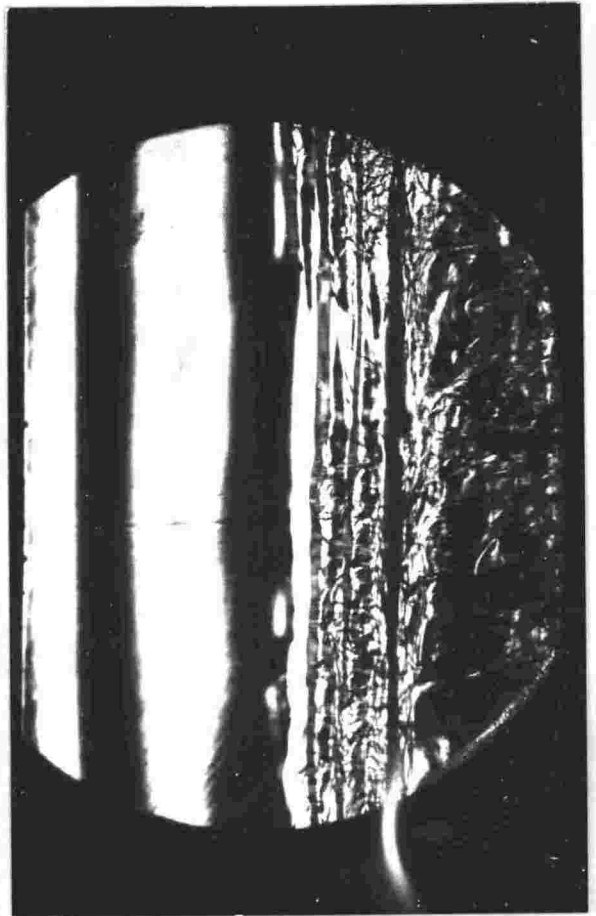
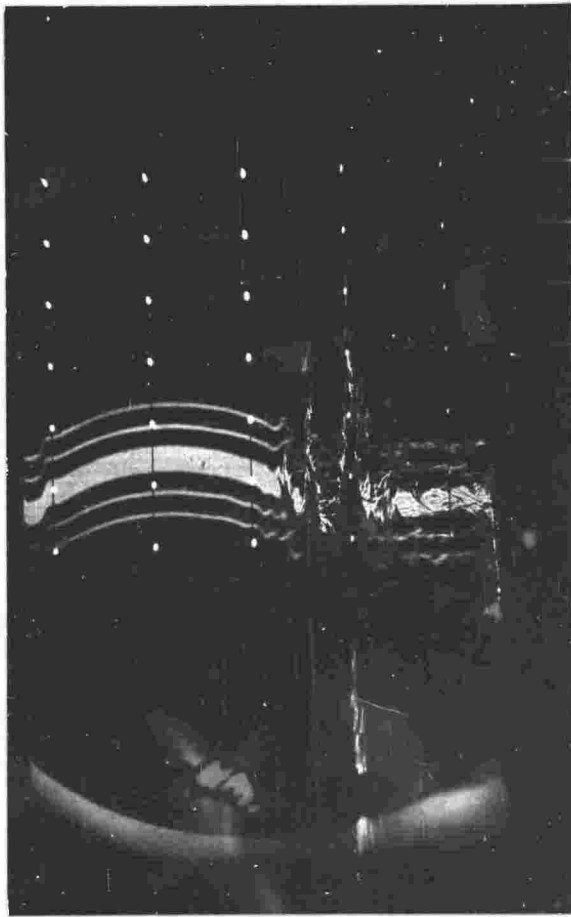
84 min

91 min

90 min

96 min

Fig. 29 (cont.)



97 min

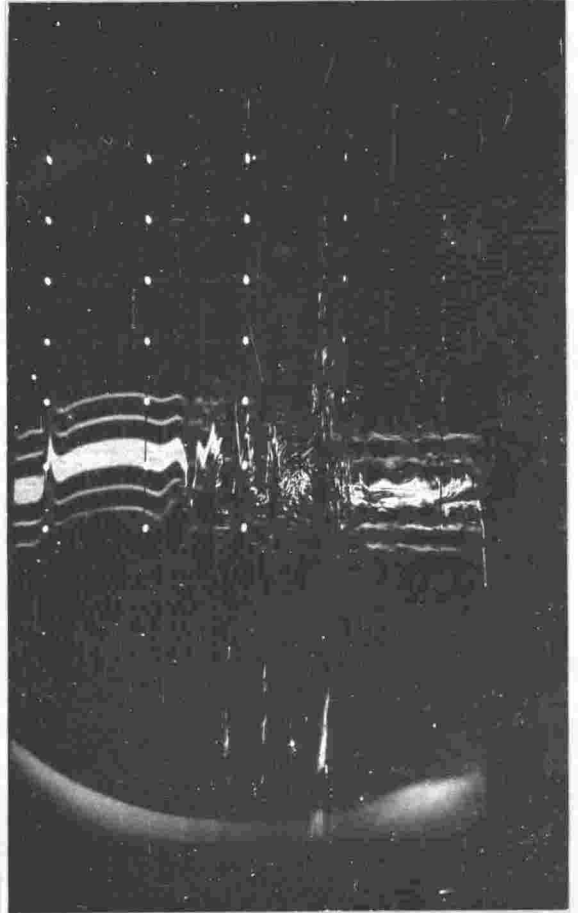
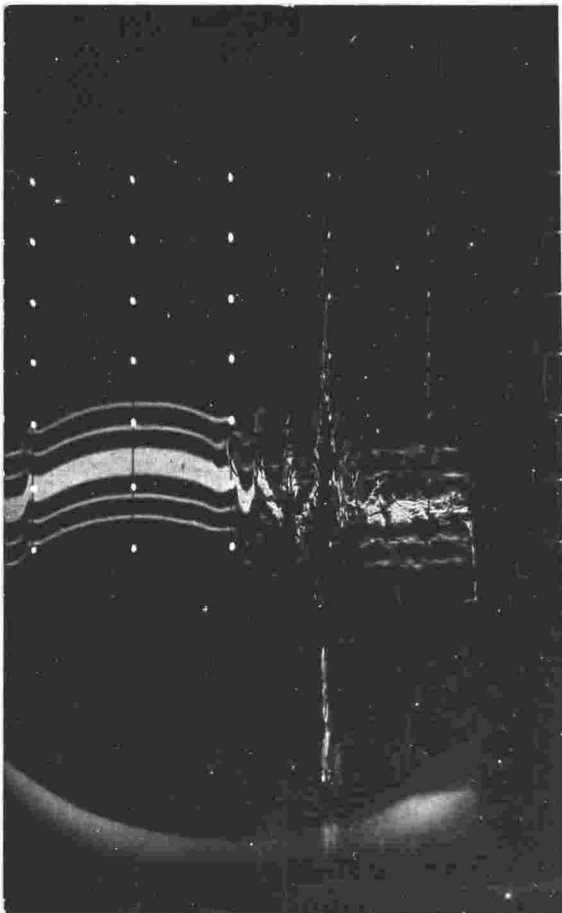
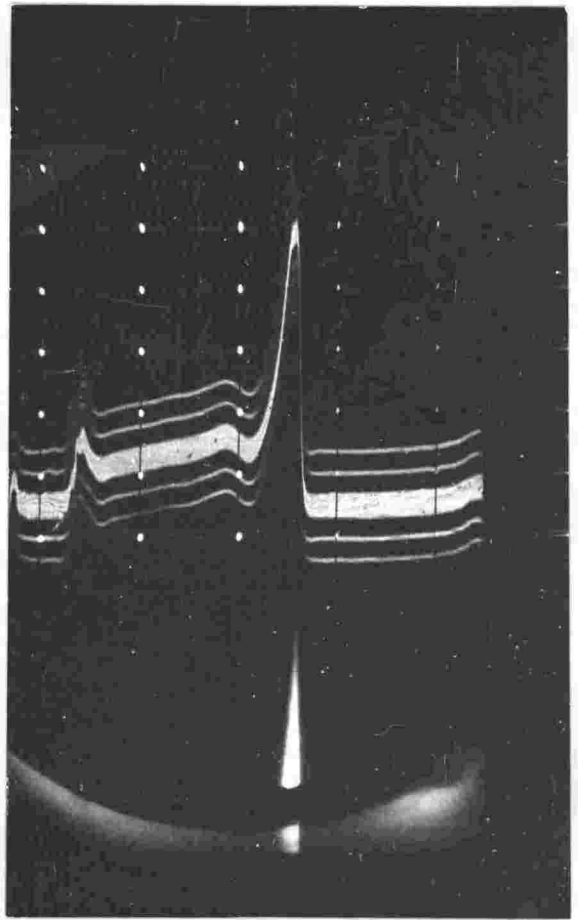
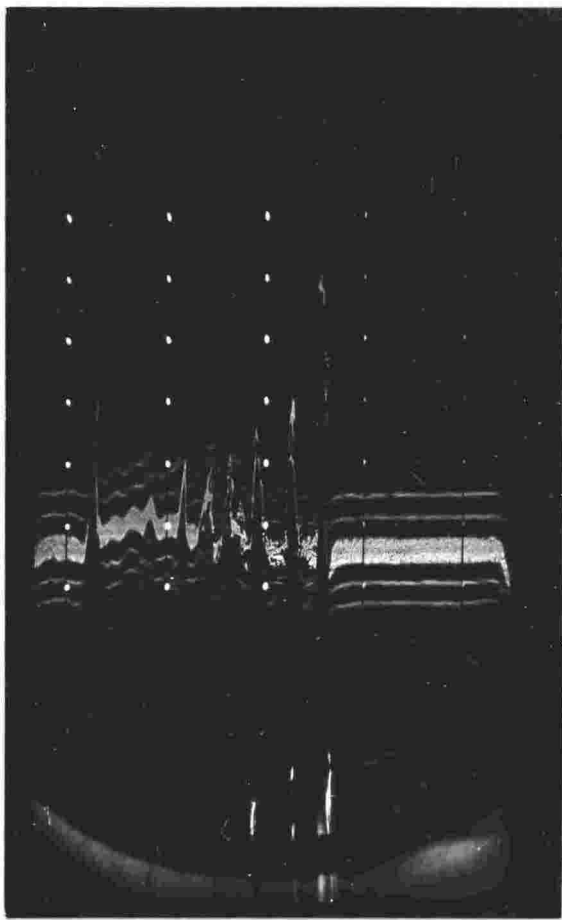
139 min

112 min

222 min

(95 min after heating was stopped)

Fig. 29 (cont.)



One property of sugar solutions on which adequate information was not available, however, was their coefficient of expansion as a function of temperature and concentration. In order to carry out the analysis of the stability experiments, therefore, it was necessary to measure this quantity.

The apparatus consisted of a specific gravity bottle of 60 cm³ volume, to the stopper of which was fused a 1-m length of precision capillary tube with 0.05 cm diameter bore. The bottle was immersed in a water bath in a thermos flask, with the capillary tube protruding through the stopper. The water bath was electrically stirred and could be electrically heated, and its temperature was monitored (to ± 0.01 C deg) by the same thermistor arrangement as had been used in the stability experiments. A scale, checked against a NPL - calibrated steel rule, was mounted on the capillary tube.

A solution of known concentration was placed in the bottle, and the height to which it rose in the capillary tube measured as a function of temperature. Writing V for the effective volume of the bottle, A for the cross-sectional area of the tube, z for height up the tube, θ for temperature, α_g for the expansion coefficient of glass and α for that of the liquid, the apparent change of volume of the liquid between two readings is given by

$$\delta v_{app} = V (\alpha - \alpha_g) \delta \theta = A \delta z.$$

i.e.

$$\frac{\delta z}{\delta \theta} = \frac{V}{A} (\alpha - \alpha_g).$$

The experiment was first carried out using distilled water, for which $\alpha(\theta)$ was accurately tabulated (e.g. International Critical Tables). The resulting graph of $\frac{\delta z}{\delta \theta}$ versus α , shown in fig. 30, yielded values for $\frac{V}{A}$ (3.05×10^4 cm) and α_g (1.1×10^{-5} per C deg).

The procedure was repeated using 5% and 10% solutions of sugar, giving a table of α versus θ for each over the temperature range

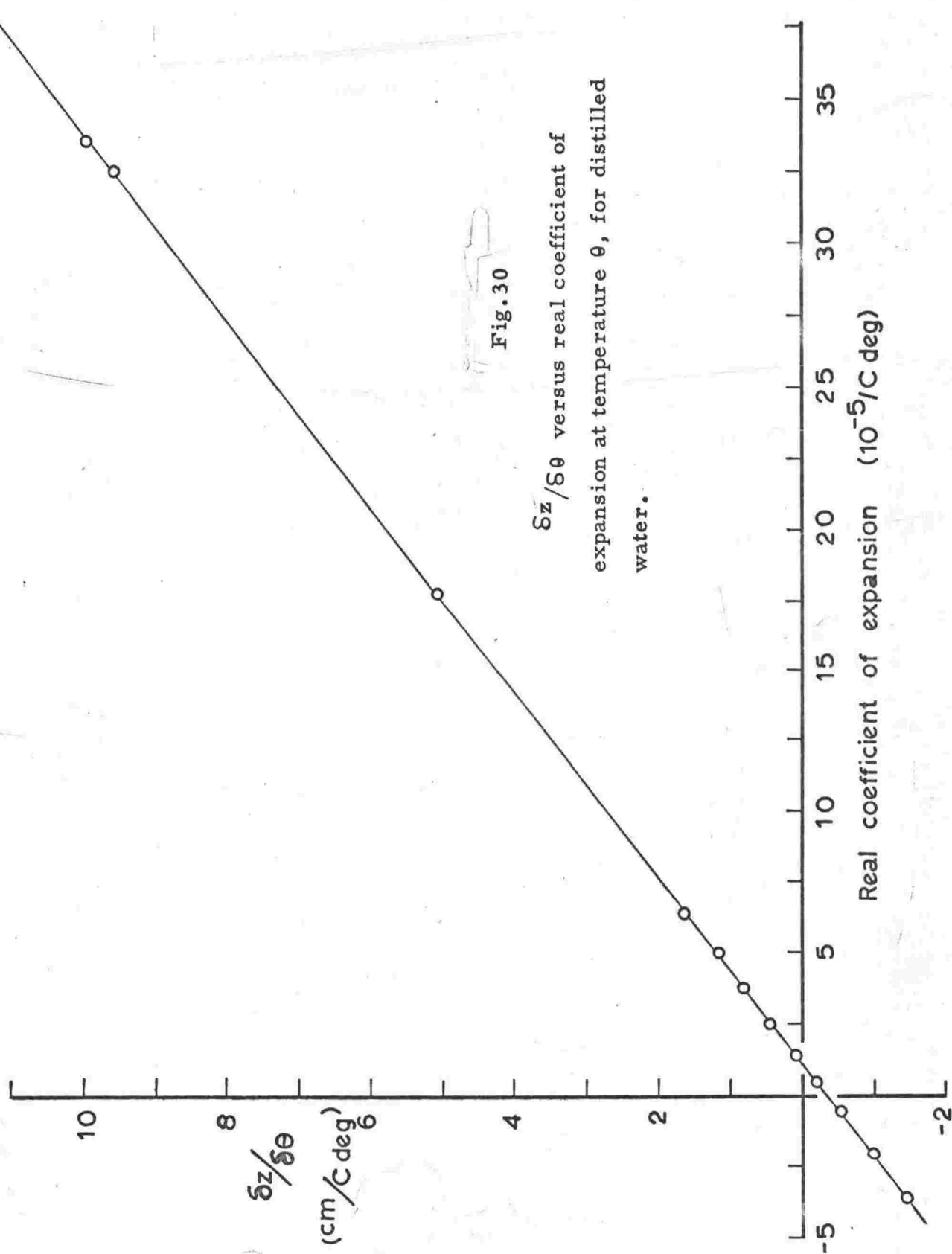


Fig. 30

$\frac{\delta z}{\delta \theta}$ versus real coefficient of expansion at temperature θ , for distilled water.

0 - 35°C. Best-fit power series approximations were then computed for both these tables, and also for that pertaining to pure water. It was found adequate to represent each by a cubic expression. The three cubics were then combined into one expression for the expansion coefficient as a function of both temperature and concentration. Writing x for concentration (in fraction by weight), the resulting expression was

$$10^5 \alpha = -6.674 + 77.65 x + 178.6 x^2 \\ + (1.758 + 0.168 x - 59.36 x^2) \theta \\ - (0.02316 + 0.119 x - 3.237 x^2) \theta^2 \\ + (0.000188 + 0.00195 x - 0.0492 x^2) \theta^3.$$

The measurements, together with this approximation, are shown graphically in fig.31.

4.3 Analysis and discussion

4.3.1 Stability experiments.

The idealised theories predict that the boundary of marginal stability in the (R, R_s) plane is the line

$$R + r R_s = R_{ec}$$

where r is a constant determined by the nature of the convection (see appendix 4). For the overstability exhibited in all the experiments, r takes the value $P/(1 + P)$, which for the solutions used was always close to 0.88.

Appendix 7 describes an Algol program which was used to process the experimental data and calculate, for each experiment, corresponding values of R and R_s at marginal stability. Both R and R_s are functions of the depth of the convecting layer. The program therefore evaluated R , R_s and $R_e (= R + r R_s)$ at depth intervals of 0.1 cm, and the critical values of R and R_s were taken to be those at the depth where R_e was a maximum.

The resulting stability diagram is shown in fig.32, from which it may be concluded that the theoretical linear relationship is approximately

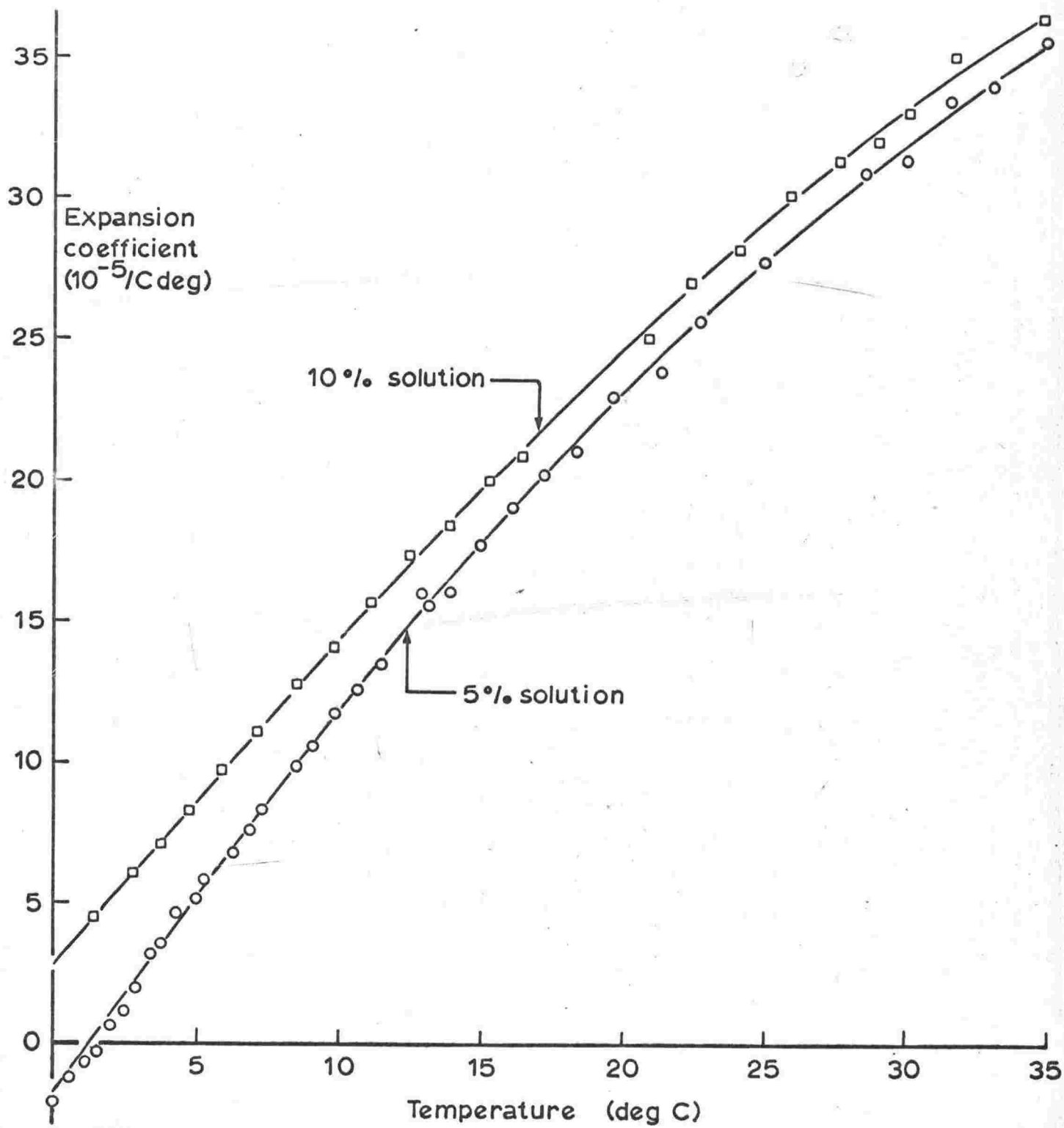


Fig.31

Temperature variation of expansion coefficient of sucrose solutions, with best-fit cubic representations.

obeyed. However the experimental points show a marked tendency to occur at excessive values of R when R is large, and to approach the predicted relationship (with R_{ec} approximately 2500) only for small R . This departure from the predicted relationship is probably real.

4.3.2 Accuracy.

The uncertainty associated with the points on the stability diagram has several causes. Uncertainty in the thermal expansion coefficient and its solutal analogue amounts to $\pm 1\%$ in R and R_s independently; and that in $(K \nu)$, which is the denominator in both R and R_s , amounts to $\pm 5\%$ in R and R_s jointly. A further uncertainty of 1-2% in R and 1% in R_s independently arises from measurement of temperature and concentration respectively. The greatest uncertainty, amounting to about $\pm 10\%$, arises from uncertainty in the depth of the convecting layer; but this affects both R and R_s in such a way that the locus of possible positions (R, R_s) is nearly parallel to the trend of the graph, and does not greatly modify the result. The only remaining possible source of error is the determination of the time of onset of overstability. Except in runs (notably S1) where the heating rate was excessive, this uncertainty is negligible, particularly as this effect also acts almost along the trend of the graph.

4.3.3 Interpretation.

It is not possible to regard the graph as simply indicating that the value $P/(1 + P)$ used for r was wrong. Firstly, P varied somewhat from run to run as it depends on both concentration and temperature; but correction of the points in fig.32 to a common value of P does not affect the results systematically, and this variation may be ignored. Secondly, if a different value is assigned to r - for example unity - this effects the calculations of convecting depth in such a way that the same disparity remains between the experimental points and the new line $R + r R_s = R_{ec}$.

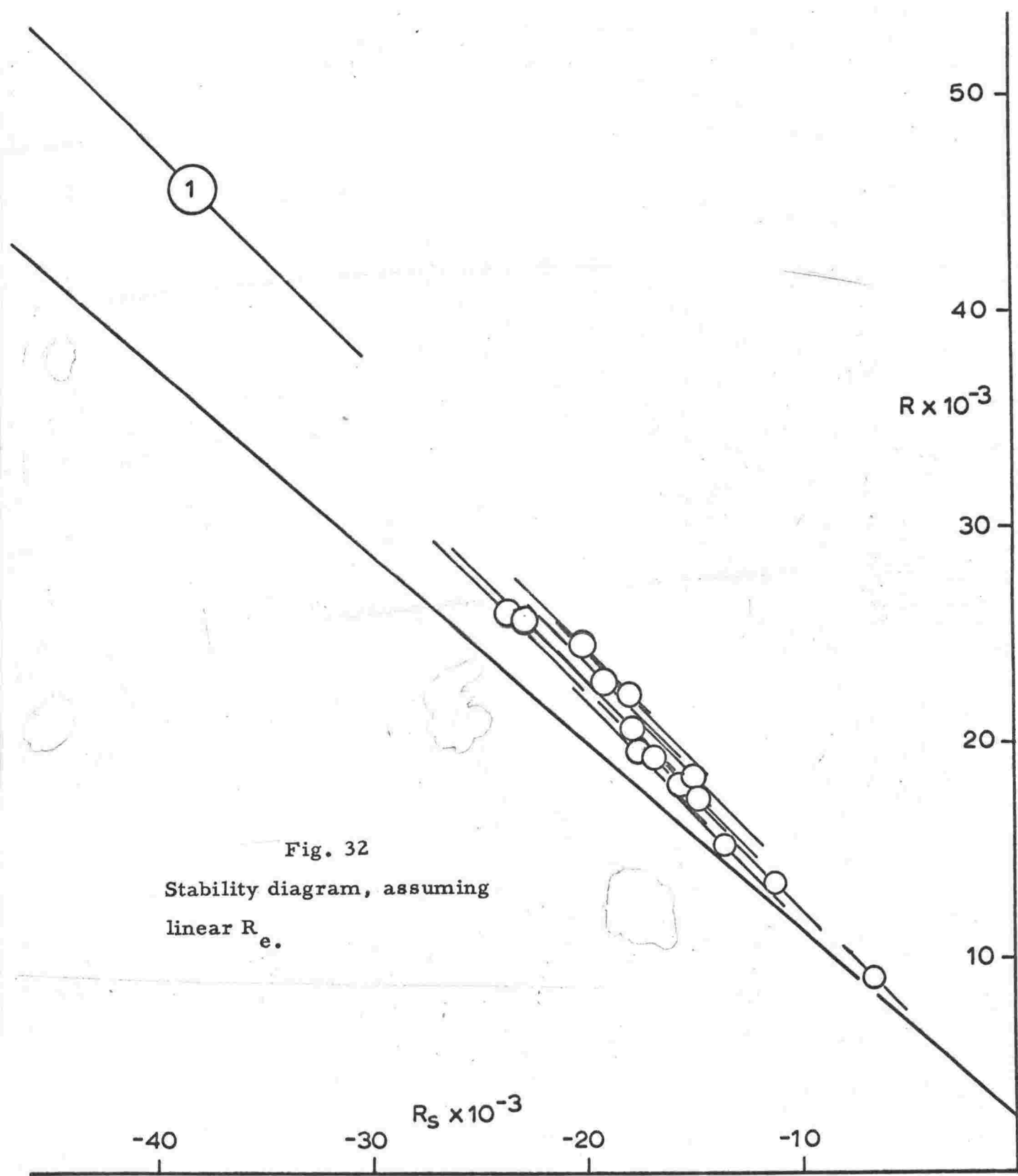


Fig. 32
 Stability diagram, assuming
 linear R_e .

Finally, calculation of the temperature profile is heavily dependent on a knowledge of K . But variation of K would change all the values of R by much the same fraction, and would have the same effect as a change in r . In any case, the only significant uncertainty in K is the effect of concentration on it, and this is of minor importance; and the calculated temperature differences between 0.5 and 1.0 cm agree, within experimental uncertainty, with those measured by the differential thermocouple.

Thus it seems very probable that, although the theoretical linear stability criterion is approximately correct, it is not exact; and that the true criterion is represented by a curve rather than a line in the (R, R_s) plane. This result accords with the study made by Nield (1967) of the case of a monotonic instability. The curvature can result from the fact that the temperature and the concentration are subjected to formally different conditions at the lower boundary.

In view of the method used to calculate R and R_s , it is not possible to decide directly from fig.32 what form the non-linearity of the stability criterion takes. To do this satisfactorily it would be necessary to have an independent measure of the depth of the convecting layer. The only measure available is the record of observations of cell heights. These were not very accurate, and were measured sufficiently long after convection began to throw doubt on their relevance to the marginally stable state. However the graph of R versus R_s , where these are the quantities calculated at marginal stability for the level later occupied by the tops of the observed cells, is displayed in fig.33, and shows reasonably systematic results. The boundary of stability is undoubtedly curved, and is represented quite well by the equation

$$R(1 + 2.5 \times 10^{-6} R) + 0.88 R_s = R_{ec}$$

where R_{ec} is about 5000.

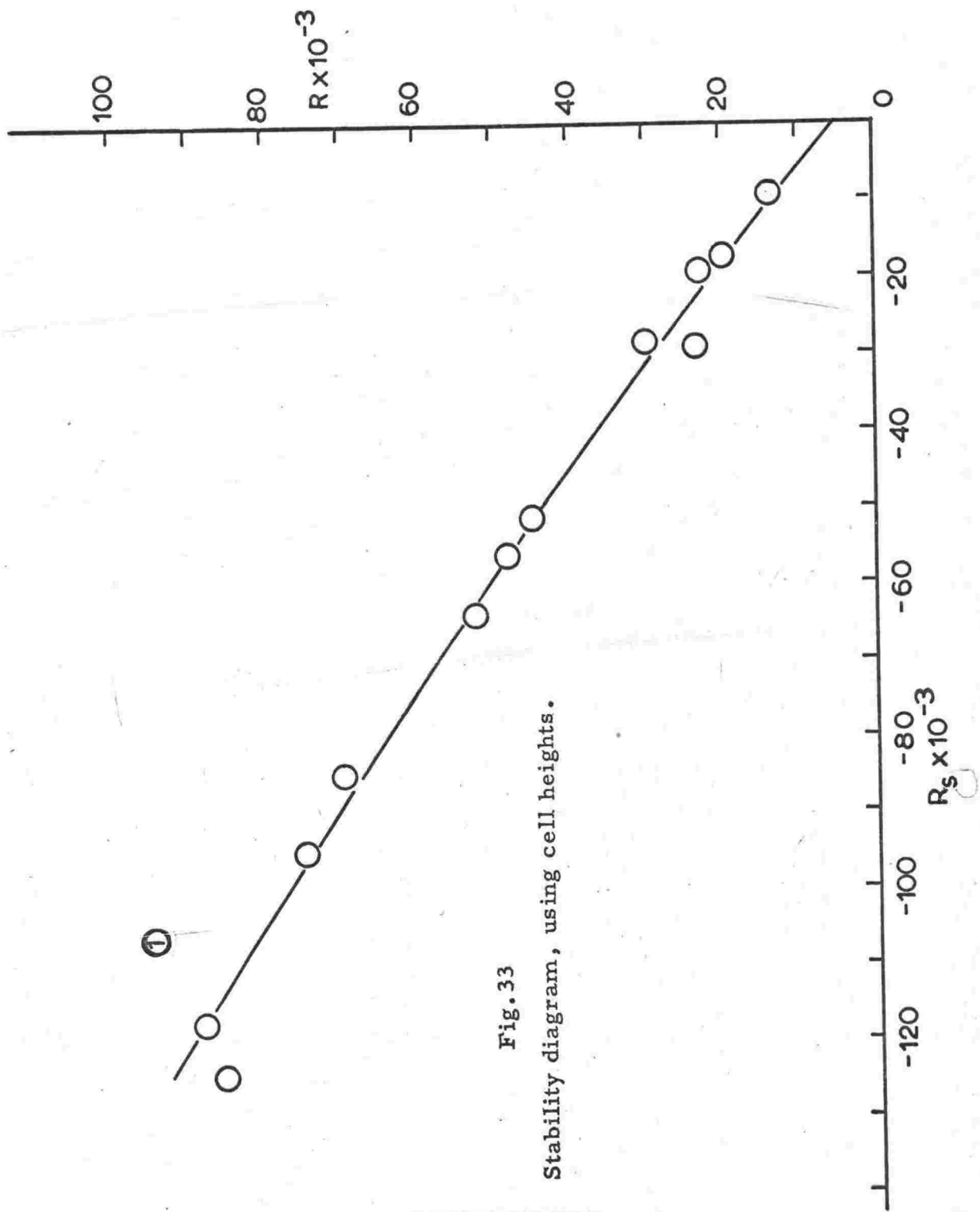


Fig. 33
Stability diagram, using cell heights.

With this relationship as a guide, a search was made for a similar one which would give better agreement with that derived from the experiments, where the assumed relationship was used, as previously, to determine the convecting depth. To ensure that R_e had a maximum in the region of interest, a cubic term had to be included. Fig. 34 shows the stability diagram which resulted from assuming that its form would be

$$R (1 + 4 \times 10^{-6} R - 10^{-11} R^2) + 0.88 R_s = R_{ec},$$

together with the graph of this expression for $R_{ec} = 5000$.

Agreement is still not complete, but the data do not justify a more intensive search for a better fit. One virtue of this choice is that it gives good agreement in the main between calculated convecting depths and observed cell heights, as shown in table VI. Discrepancies are mainly associated with the fact that the maximum of R_e is now rather broad, so that the depth h is ill-defined.

Table VI

Comparison of observed cell heights with calculations of layer depth using non-linear stability criterion.

<u>Run</u>	<u>Calculated (cm)</u>	<u>Observed (cm)</u>
1	1.4	1.4
2	1.2	1.4
3	1.2	1.2
4	1.3	1.3
5	1.0	0.8
6	1.0	0.7 - 1.0
7	1.0	0.7 - 1.0
8	1.1	0.8
9	1.1	0.9
10	1.0	0.9 - 1.1
11	0.8	0.9
12	0.8	0.5 - 1.0

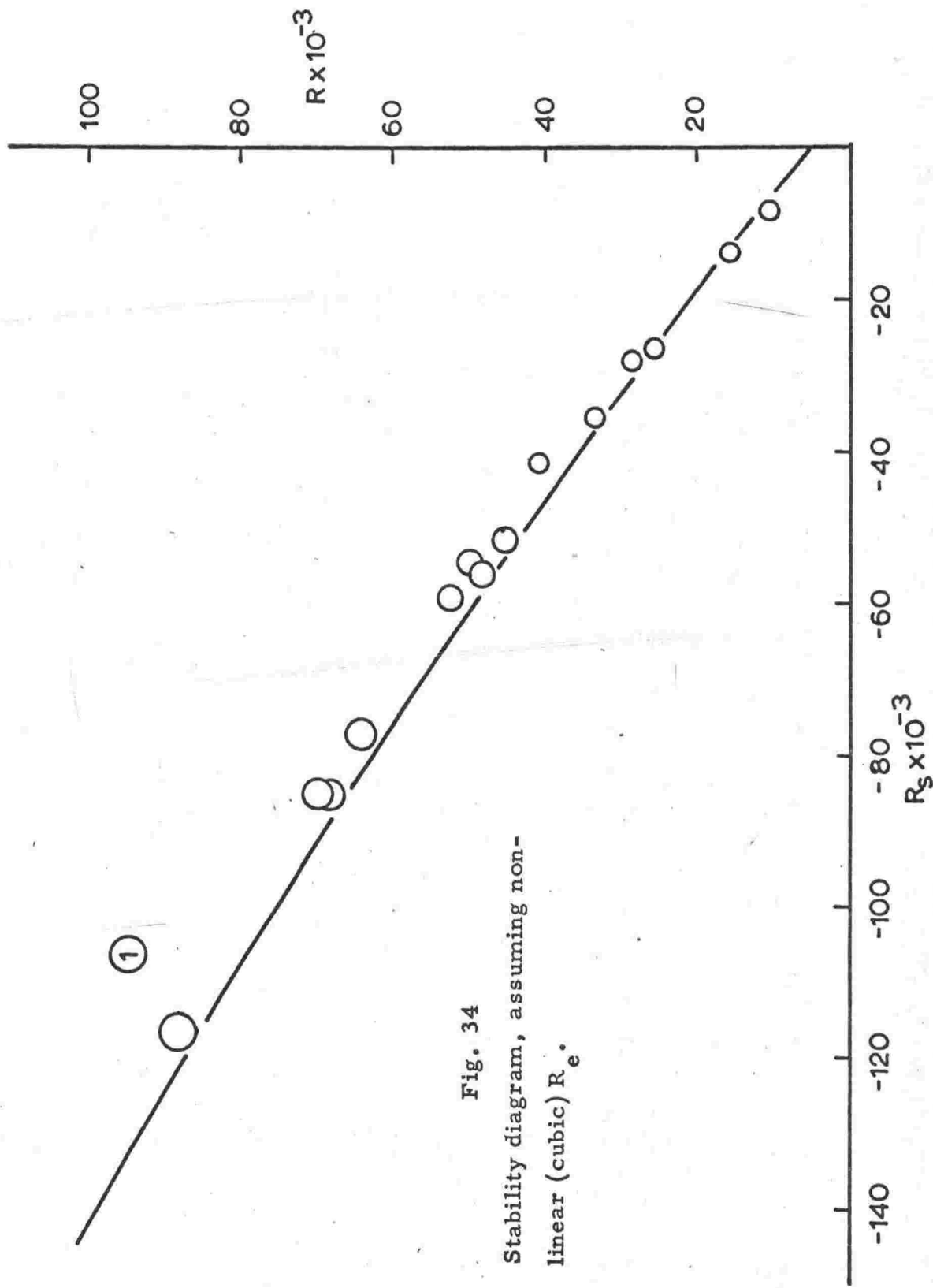


Fig. 34
 Stability diagram, assuming non-linear (cubic) R_e .

<u>Run</u>	<u>Calculated (cm)</u>	<u>Observed (cm)</u>
13	0.8	1.0
14	0.9	0.9
15	0.8	0.8

The results of run S1 do not conform with the general pattern. No source of error could be found to account for this, so it might be associated with the particularly high rate of heating used on this occasion, which led to a very markedly non-linear temperature profile. In the case of monotonic pure-thermal convection, Currie (1967) has predicted that very rapid heating may have a substantial effect on R_c .

4.3.4 Value of R_{ec} .

Although the data do not supply an unequivocal value of R_{ec} , it is likely that the value is higher than expected. The overstable layer had been expected to behave as though its lower boundary was plane and rigid, and its upper boundary approximately plane and stress-free. By analogy with pure thermal convection, R_{ec} would then have been about 1200 (D.A. Nield, pers. comm.), or perhaps as high as 1700 if the upper boundary was effectively rigid. A higher value implies that, in the thermosolutal case, more work has to be done against friction by the buoyancy force. The only possible cause for this seems to be that the cells which formed first were independent of one another, and not contiguous as suggested by studies of pure thermal convection. In this case the buoyancy force in a cell would cause sympathetic motions in a relatively large volume of liquid in addition to the oscillation in the cell itself, against the frictional effect of viscosity.

4.3.5 Periods of the oscillations.

The period expected for each run may be calculated from the formula given in chapter 3, but is a function of the convecting depth. The observed periods, quoted in Table VI, are repeated in Table VII, together with the periods calculated according to the three methods of evaluating

this depth; by taking the maximum of the linear R_e , the maximum of the cubic R_e , or the observed cell depth. In each case, the depth is taken to the nearest 0.1 cm.

Table VII
Periods of the overstable oscillations

<u>Run</u>	<u>Observed period (sec.)</u>	<u>Calculated period (sec.)</u>		
		<u>Linear R_e</u>	<u>Cubic R_e</u>	<u>Cell height</u>
S1	53 ± 5	56	49	49
S2	85 ± 2	63	59	53
S3	73 ± 2	58	50	50
S4	69 ± 2	55	48	48
S5	45 ± 2	39	35	39
S6	48 ± 5	41	36	43 - 36
S7	56 ± 2	41	37	44 - 37
S8	55 ± 2	41	35	41
S9	53 ± 1	43	37	40
S10	32 ± 2	29	24	26 - 23
S11	30 ± 5	31	29	27
S12	47 ± 1	35	33	41 - 30
S13	65 ± 5	59	59	49
S14	53 ± 2	43	40	40
S15	59 ± 4	45	45	45

There is a strong tendency for the calculated periods to be less than the observed ones. This tendency is least obvious if the linear R_e is used to calculate the convecting depth, since it generally gives the smallest of the three depth estimates.

This discrepancy between calculated and observed periods is presumably associated with the difference between the actual form of the cells and that assumed in the theory. For a given solute distribution, the period is determined by the thermal diffusivity and viscosity, solute diffusion being negligible. Since it increases with the viscosity of the

liquid, the observation of excessive values may be ascribed to the same cause as the high R_{ec} , namely the high viscous damping of the motion when the cells are not in contact.

4.3.6 Turner-Stommel layers.

The results of the layer-forming experiments are generally consistent with the mechanism discussed. Each convecting layer is separated from its neighbour by a stable boundary region of finite thickness, through which heat and solute must be transferred principally by diffusion, vertical circulation in this region being prevented by the density gradient.

With regard to the formation of a new layer in an initially stable region, the profiles from run T4 in particular show the development (fig. 29). The upper limit of a convecting layer is indicated by the rise of density gradient in the boundary region. Where the region above this is initially stable, the density gradient at the upper limit of the boundary region diminishes with time, owing to the heat flux being greater than the solute flux (in terms of density effect). This leads to the formation of the new layer.

The profile taken at 71 minutes in run T4 shows an interesting effect which possibly modifies the formation of new layers. There are five curves recorded simultaneously, displaced laterally about 0.4 cm apart across the tank image. In the region where the third layer is forming, these show a variation of conditions across the field of view. At the left hand side the density gradient shows a more marked minimum and maximum respectively at the positions of the new third layer and its boundary with the second. Similar behaviour is shown in other profiles, notably that at 139 minutes; and there is also an indication, particularly in the latter, that layers are present and being formed in regions where the density gradient is noticeably stable.

These effects may result from the variation of vertical heat flow across the tank, which has been referred to. Thus the layers and boundaries may form in accordance with the postulated mechanism where

the heat flow is high, but only approximately obey it elsewhere. Alternatively, they may result from the presence of internal waves excited by the underlying motion. In this latter case the formation of a new layer might be somewhat modified by the motion and the possible associated mixing.

Standing internal waves would represent a limitation of the laboratory experiments, since they are maintained by the walls of the tank. Their effect is likely to diminish as the size of the vessel increases, and in a lake they might have no significant influence. It is likely that they were not important in these experiments, since the layer development was in accordance with prediction, at least qualitatively; but they provide an element of doubt as to the extent to which quantitative analysis is justified.

No direct analysis of these experiments has been attempted. Instead, a numerical model of the process was developed, and this is described in the next chapter. It was applied to the conditions of runs T3 and T4 and found to give quite similar results to those obtained in the experiments, showing that the model was adequate.

Chapter 5

Lake Vanda

5.1 A model of the Turner-Stommel layers.

5.1.1 Introduction.

The sequential development of convecting layers in the presence of a solute gradient has obvious relevance to the study of Lake Vanda. The formation of the first Turner-Stommel layer has been described in some detail, but the onset of convection in subsequent layers is more complex. Presumably a similar criterion for marginal stability in terms of thermal and solutal Rayleigh numbers applies as to the first layer, but the fluxes of heat and solute are now due in part to the convection in the adjacent layer. The convective fluxes through an existing layer depend on R and R_s for the layer, and in turn modify R and R_s . Marginal stability in the first layer can be predicted on the basis of diffusion and a knowledge of the boundary fluxes of solute and heat; the development of temperature and concentration gradients in a region where any other layer is about to form will depend as well on R and R_s in the adjacent existing layer, and this (R, R_s) depends in turn on that in the other layers.

To predict accurately the development of a series of layers would therefore be very difficult, both because of this interdependence between the layers, and also because no satisfactory theory is available to describe the dependence of the solute and heat fluxes on R and R_s . It is therefore necessary to seek a limited representation of the system which is sufficiently tractable to allow calculation.

The model adopted was a crude one, and was not expected to yield accurate results. Nevertheless it reproduced the behaviour of laboratory experiments closely enough for the similarity to be apparent, and it certainly showed qualitatively the formation of layers, justifying the ideas expressed in these pages as to their origin.

5.1.2 The model.

The basis of the model was the representation of both diffusive and convective transfer of solute and heat as diffusion, the relevant diffusion constant being increased in an appropriate way when convection was present. The problem was thus converted to one of diffusion in one dimension through a series of slabs of variable diffusivity and with mobile boundaries. In this form it was amenable to numerical, though not analytical, solution.

Malkus (1954) made very comprehensive measurements of the variation of heat flow with Rayleigh number in pure thermal convection. The interpretation of Turner's (1965) experiments given in appendix 4 shows that the parameter which takes the place of R in the case of fully developed thermosolutal convection is R_e , where

$$R_e = R + r R_s,$$

and the appropriate value of r is $P/(1 + P)$, to a reasonable approximation. It was therefore assumed that Malkus' heat flow measurements were relevant to the thermosolutal case if this (linear) R_e was substituted for R .

The measurements effectively gave the thermal conductivity of the convecting layer as a function of R . In the model, the thermal diffusivity of a slab was assumed to have this same dependence on the value of R_e in the convecting layer which the slab represented. The relationship assumed was

$$R_e \geq R_{ec} : K_m = K_c \left\{ 1 + 0.72 (R_e/R_{ec})^{1/3} (1 - R_{ec}/R_e) \right\}$$

$$R_e < R_{ec} : K_m = K_c.$$

Here K_m is the modified, and K_c the true, thermal diffusivity. This expression matches Malkus' results within 3% at all the transition points, and has the correct cube-root dependence for high R_e .

The method of solution was based on a numerical solution of the heat conduction equation due to Du Fort and Frankel (1953). This is an explicit scheme which, in its simplest form, without heat sources

and with constant diffusivity, is stable for any mesh spacing. This type of stability was required for two reasons. Firstly, an increase in diffusivity K has the same effect on the solution as an increase in the time increment, and K increased markedly during the calculation; and secondly the calculation was a very long one and it was necessary to minimise the number of steps in time required to complete it. Some stability problems were encountered, owing to the combination of spatial and temporal variations of K . These and their solution are described in appendix 8.

The model operated as follows. The basic information required was a set of coordinates of a concentration gradient profile, which were subjected to harmonic analysis and integrated in the usual way. In addition, an initial temperature, and the coefficients of a cubic expression defining the growth of temperature with time at the bottom boundary, were required. The initial temperatures and concentrations at a large number (usually 200) of equally-spaced levels in the "tank" were thus calculated. The development of these values with time was then calculated for successive equal time increments by a simple numerical scheme for a small number (usually 10) of time steps. This simple scheme was stable only for small time increments, but gave a new profile in terms of the immediately preceding one only, and was a useful "starting" scheme. The "running" scheme involved both the two preceding profiles; the initial and final profiles of the starting scheme were used as the first two for the running scheme, which allowed much greater time increments.

Once the running scheme had been established, the profiles were scanned after each pair of time increments to determine whether R_e was positive (i.e. potentially unstable) between any two neighbouring levels. Starting at any such point, the upper and lower bounds of a search layer were extended until R_e was maximised. Then if this

maximum value exceeded R_{ec} all the levels within the layer were assigned a new K , in accordance with the relationship given above, and a new D .

The question of how to assign the modified value of D (diffusion constant for the solute) in the presence of convection was decided by experiment, bearing in mind the evidence given in chapters 3 and 4 that the effect of convection on the solute transfer rate is initially much larger than the corresponding thermal effect. In modelling tank experiments it was found satisfactory to write

$$R_e \geq R_{ec}: \quad D_m = K_m - K_c + D_c$$

$$R_e < R_{ec}: \quad D_m = D_c.$$

Since $K_c \sim 10^2 D_c$, the solute transfer rate was increased about 100 times more than the thermal flux when convection began. This lies between the limits of 1 and 10^4 suggested by Veronis for large- and small-amplitude convection respectively.

The results of a run in which the conditions modelled those of experiment T4 are shown in fig.35. The graphs of temperature and concentration show clearly the way in which an initially smooth density profile is broken into steps by the convection, the density contrast between adjacent steps being maintained by the low diffusion constant of the solute in the non-convecting regions. The concentration profiles also show the way in which two layers may amalgamate. The two layers present up to 79 minutes have a steadily decreasing concentration difference. By 99 minutes this has diminished to the point at which convection has occurred over the whole region, speedily extinguishing any remaining contrast.

5.1.3 Limitations

Limitations of the numerical model are evident in all the graphs. Firstly, the temperature and concentration profiles are represented as having constant gradients throughout a convecting layer. This is certainly not the case after monotonic convection has been

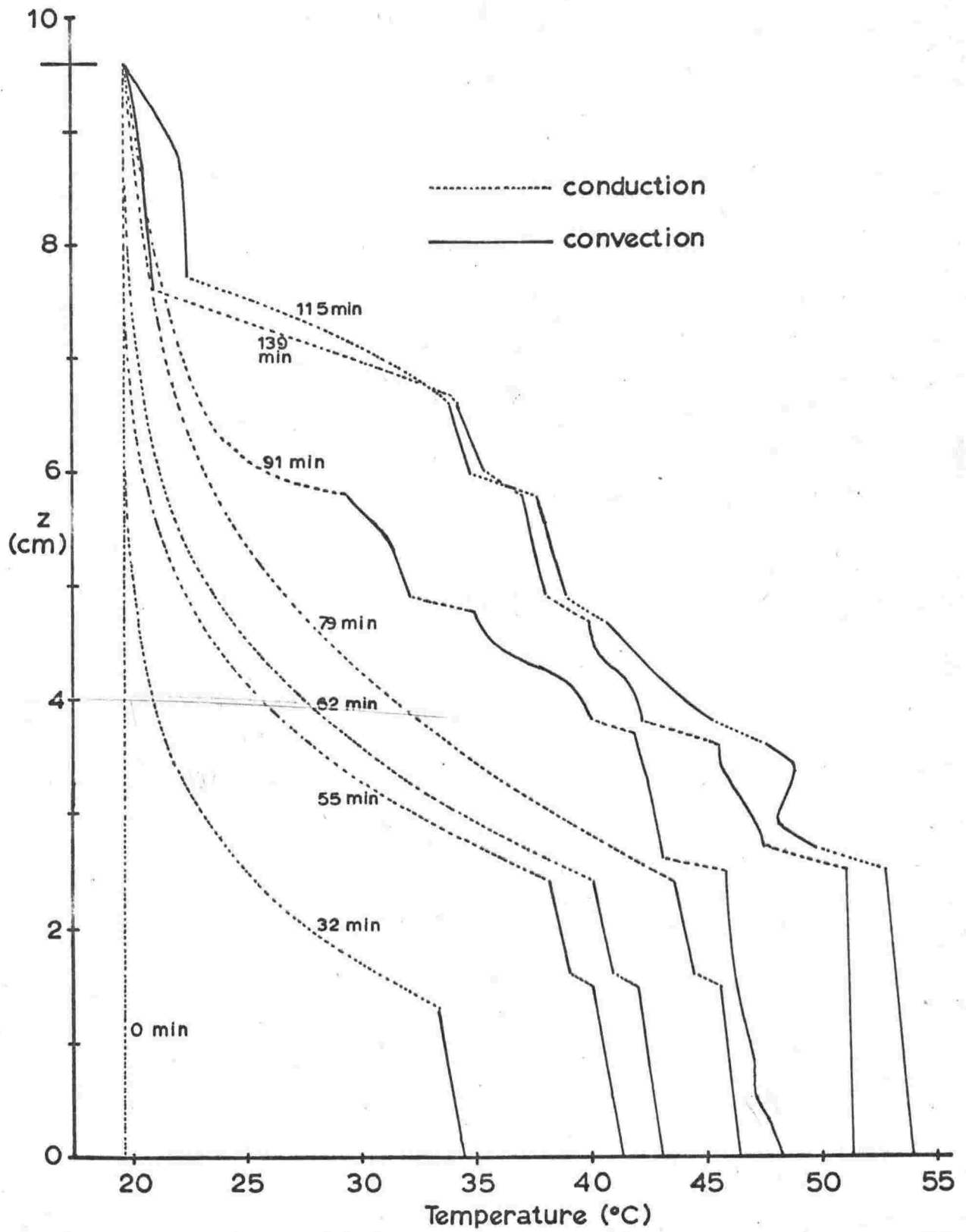


Fig. 35(a)

Numerical model, run T4. Calculated temperature profiles.

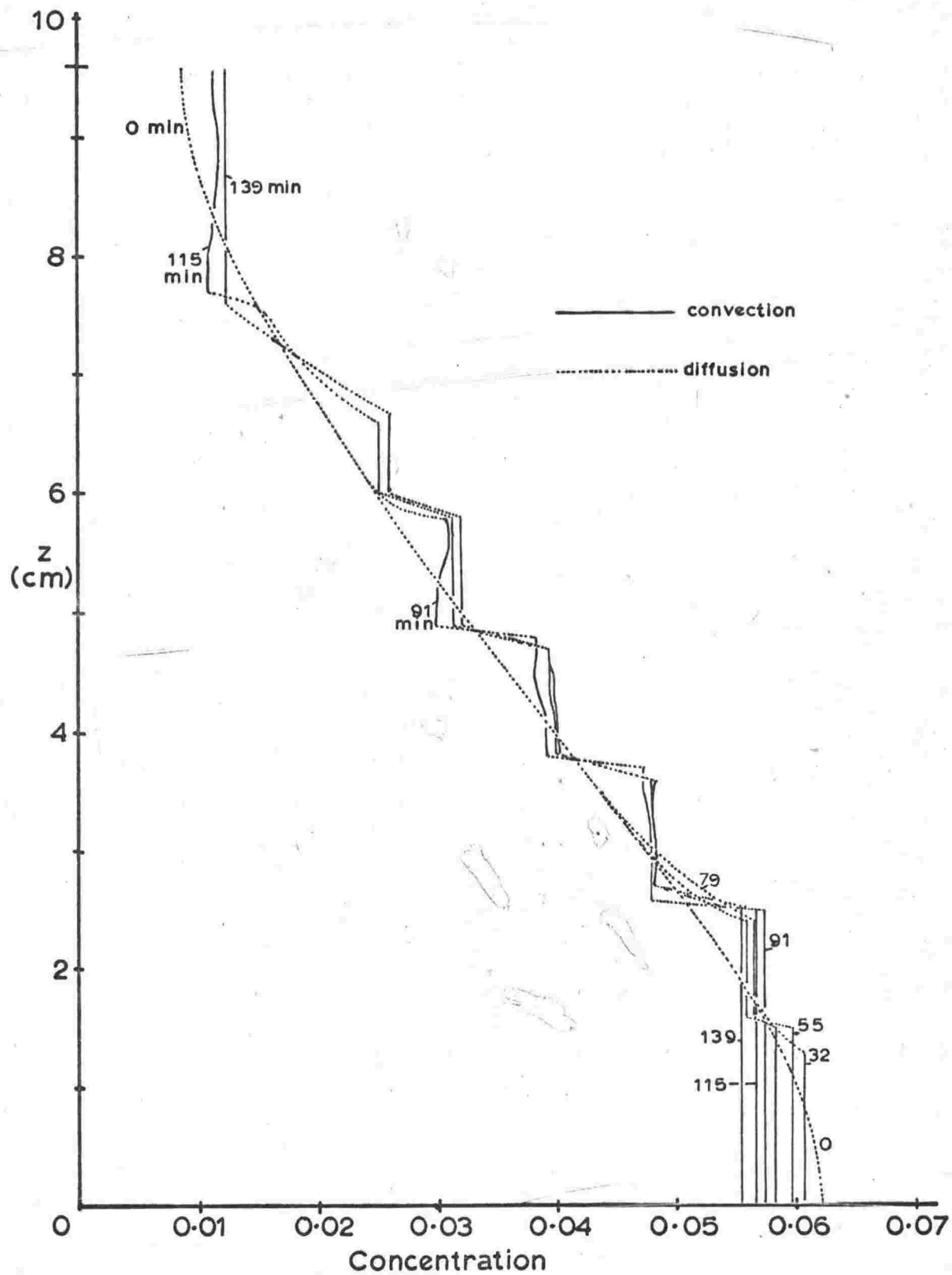


Fig. 35(b)

Numerical model, run T4. Calculated concentration profiles.

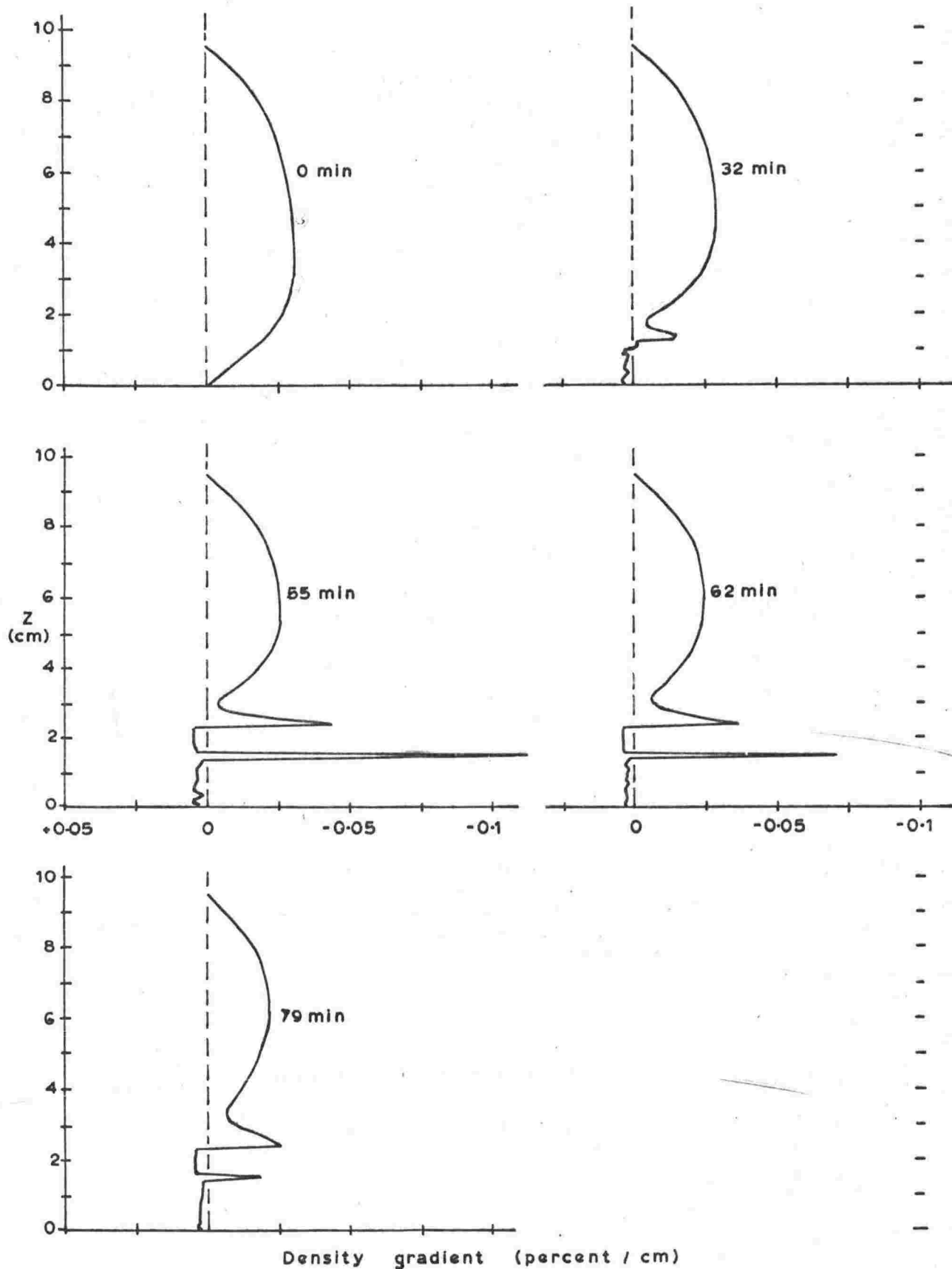


Fig. 35(c) Numerical model, run T4. Calculated density gradient profiles for times shown.

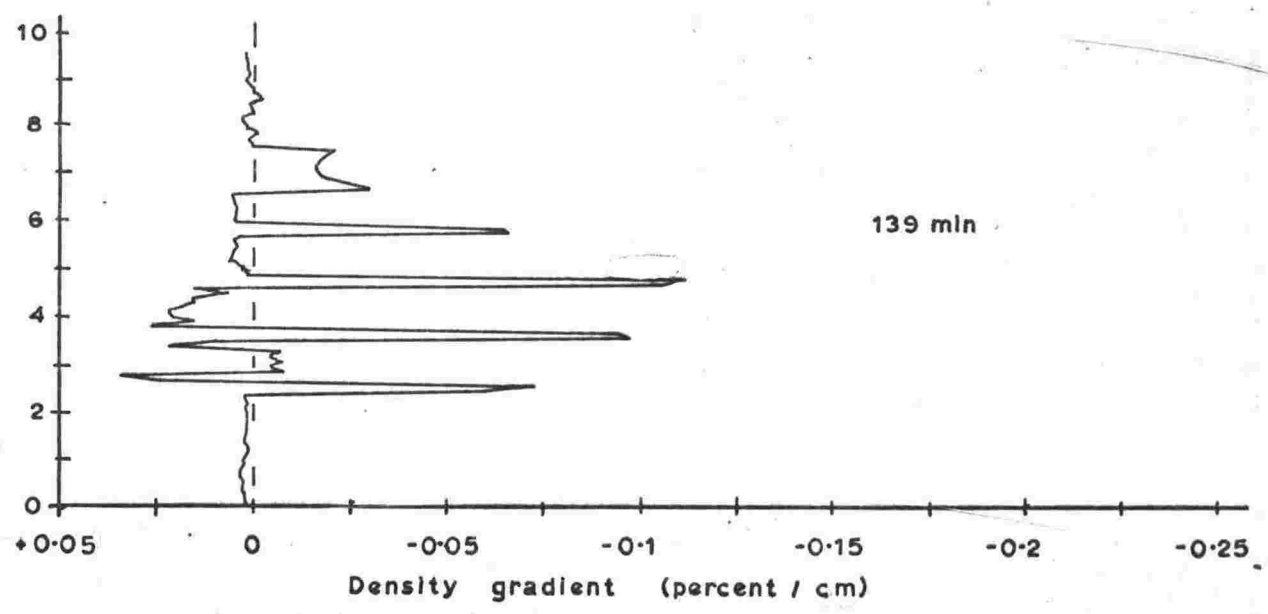
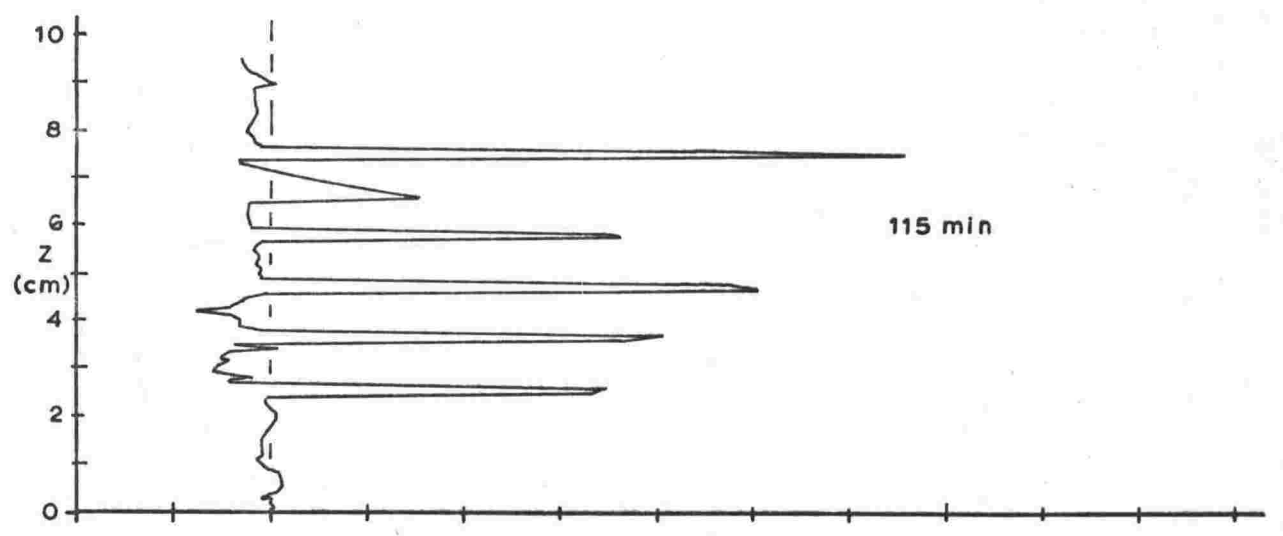
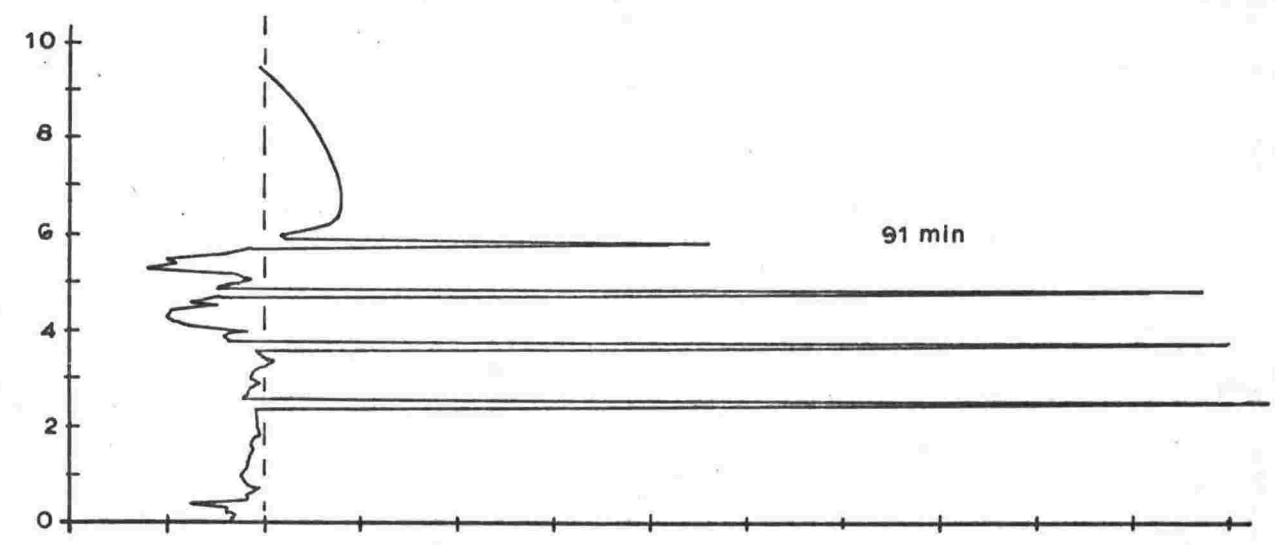


Fig. 35(c) (cont.)

established. The experimental profiles show that there is then a considerable gradient of density, and hence of temperature, in the boundary layers at top and bottom of the convecting region, and effectively zero gradients between (see for example T4 at 139 minutes). On the other hand, before the convection becomes monotonic, constant internal gradients may be a reasonable approximation.

The second limitation is less basic, and concerns simply the accuracy with which the computations were carried out. While the numerical scheme is apparently stable, it is not free from errors, which apparently arise mainly when diffusion constants are reassigned. Such errors are shown by the non-linearity of the temperature profiles of some convecting layers, and in a few cases by concentration profiles as well. They are particularly evident in the density gradient profiles, where their magnitudes are emphasised by the differentiation. They do not seem serious enough to affect the results significantly.

A further limitation of the method, not shown by these graphs, is that the time-development of the temperature and concentration profiles within a convecting layer is not well represented. Diffusion in a system of scale length h and diffusion constant K has a characteristic time $t = h^2/K$. The time development of convection has been studied for a particular configuration by Foster (1965), the characteristic times being of order $10^{-3} h^2/K$, where K is here the thermal diffusivity. It is not possible to deduce a general expression from Foster's results, but it seems very likely that the dependence on h of the characteristic time for the growth of convection differs from that for diffusion. Now K in the model was chosen initially to provide the correct heat transfer rate in the steady state. Foster's results show that this requirement is incompatible with a realistic representation of the time-development of the profile within a convecting layer, and furthermore it seems likely that the degree of incompatibility depends on the scale of the system in some way.

To meet this difficulty, the dependence of K on R_e in the model was increased until reasonable results were obtained. The graphs shown for the model of experiment T4 were obtained by increasing by a factor 10 the convective component of K_m and D_m , that is,

$$R_e \geq R_{ec} \left\{ \begin{array}{l} K_m = K_c \left\{ 1 + 7.2 (R_e/R_{ec})^{1/3} (1 - R_{ec}/R_e) \right\} \\ D_m = K_m - K_c + D_c \end{array} \right.$$

While the agreement between the experimental and the model results is quite close, the difficulties discussed above limit the quantitative validity of the method. Although a continued search for better ways of evaluating K_m and D_m , and longer computations using a finer mesh spacing, would yield more impressive results than those exhibited, the limit of credibility has probably been reached. The important point is that the model is based on a simple description of the convective process entirely in terms of Rayleigh numbers, but reproduces the behaviour observed in experiments quite well. To the extent that this description is valid, the dimensionless character of the Rayleigh numbers removes any problems of scale, and the model method may therefore be applied to a system of any size.

5.2 The development of Lake Vanda.

5.2.1 Basis of the investigation.

Lake Vanda is clearly separable into two regions, respectively above and below a plane about 17 m above the lake bed. Conventional limnology does not provide suitable nomenclature, so they will be called simply the upper and lower regions. Of these, the lower region has apparently not experienced mixing for something over 1000 years (Wilson, 1964), during which time salt (mainly calcium chloride) has been diffusing upwards from the lake bed. The temperatures are high, and their profile is maintained in equilibrium by the absorption of sunlight (Wilson and Wellman, 1962). The upper region is occupied

by a series of convecting layers in which there are relatively low temperatures and salt concentrations.

The primary aim of this investigation is to establish a reasonable theory of origin of the layers in the upper region. In a sense this has already been done, since it has been shown that the combination of a stabilising solute gradient and a destabilising temperature gradient can lead to layers in a system of any size. Since this effect is inevitably present in such a system, it becomes unnecessary to invoke any other mechanism for the formation of the layers.

However it is possible to take the matter further. Wilson's (1964) results show that, near the lake bed, the salt concentration varies very nearly as would be expected after upward diffusion for 1300 years; while nearer the top of the lower region the concentrations become increasingly too small compared with this theoretical profile. (It was presumably because of this departure that Wilson gave his age estimate as 1200 years.) The departure could be explained if the diffusion, instead of taking place in a region whose upward extent was unlimited, was subjected to a boundary condition whereby, at about 20 m above the lake bed, the concentration was maintained at some very low value. Such a boundary condition requires extraction of solute at about the 20 m level and hence a sink of solute above it.

The situation described above is consistent with the following picture of the development of the lake: From about 1300 years ago, when the lake consisted of a dry salt bed or a shallow saline pool, its level has been rising more or less steadily, and sufficiently rapidly to offer little impediment to the upward diffusion of salt. At the same time, the absorption of solar radiation has produced and maintained high temperatures in the lake by the mechanism familiar from the study of Lake Bonney. Throughout the process, there have been gradients of both temperature and salinity in the lake, a potential source of

layered convection. Such convection would have occurred where the concentration gradient was small enough to be overcome by the destabilising effect of the temperature gradient, that is, some way above the lake bed. It would have transferred salt upwards rapidly, into the relatively large volume of nearly fresh water, thus maintaining the boundary condition required near the top of the lake's lower region.

5.2.2 Application of the numerical model.

In order to check this view of Vanda's development, the numerical model was suitably modified and a series of computations performed with the aim of reproducing the temperature and salinity profiles currently observed in the lake. In addition to the problems already met in simulating the tank experiments, this application introduced three further difficulties:

(1) The source of heat was now not conduction through the lower boundary, but the exponential absorption of downward radiation. Thus the heat conduction equation contained a source term, and this made the numerical scheme unstable. The solution of this problem is dealt with in appendix 8.

(2) (a) The scale of this system was much greater than that of the first. This had two effects, the more fundamental of which concerned the problem of the time-development of profiles within a convecting layer. It was found that no method of assigning diffusivities to convecting regions which tolerably represented the steady-state transfer rate, gave an acceptable rate of development of the profile towards that state. Deep convecting layers were found to approach a state of uniform concentration and temperature with characteristic times of order 100 years, which was not realistic. Since the calculations here covered a period of several hundred years of real time, compared with as many minutes in the former case, it was assumed that the time occupied by any convecting layer in reaching its fully-developed state was negligibly small. Thus wherever the criterion

for the onset of convection was surpassed, the temperatures and concentrations within the layer were immediately made uniform throughout the layer, and equal to the mean of the previous values. Thermal diffusivities were assigned according to the original scheme (p 88), and solute diffusion constants according to

$$D_m = K_m D_c / K_c,$$

the latter being in accordance with Veronis' (1965) estimate for large-amplitude convection.

(2)(b) The second effect of the scale of the problem was less basic. Storage in the (Elliott 503) computer was limited, and the vertical extent of the system could not be divided into more than about 500 steps; the minimum convenient depth increment was therefore about 20 cm, compared with 0.05 cm in the tank model. Depths of convecting layers, and also of the conducting regions separating them, were quantized in the model in units of twice the depth increment. The resulting 40 - cm unit was barely adequate to represent the many layers whose actual depths are about 1 m, and was certainly too large to represent the stable boundary regions satisfactorily.

(3) Given that the investigation was to be based on a particular history for the lake, there were still many possible variations of detail, and the system was much less determinate than in the case of the laboratory experiments. There the depth of liquid was constant, the initial solute distribution was known, and the temperature of the heated boundary was known as a function of time throughout the experiment. Here, only the final depth and profiles were known.

In these circumstances, rather sweeping approximations were inevitable. It was assumed that the depth of the lake had increased in only two stages, the second of which consisted of an instantaneous addition of sufficient fresh water at 0°C to bring the level up to that now observed. The first stage was assumed to have ended with the lake having an intermediate depth, a salinity profile due to diffusion from

the bed into a semi-infinite medium for an appropriate time (usually 1000 years), and a steady-state solar-heated temperature profile. Computation was then limited to the second stage of development, reducing the computing time considerably.

The development of convection in this system was obviously influenced more by the variable expansion coefficient of aqueous solutions than was the case in the tank experiments, since the temperatures and concentrations developed through conditions of maximum density. A repetition of the measurements of expansion coefficient carried out for sugar solutions was not justified. Instead, the expansion coefficient was assumed to vary with temperature in the same way at all concentrations, but subject to a shift of the temperature origin as the concentration changed. The temperature of maximum density (zero expansion coefficient) of calcium chloride solutions was available as a function of concentration (International Critical Tables), and gave the appropriate variation of temperature origin with concentration. This probably represented the expansion coefficient quite well in the important region near its zero, and with tolerable accuracy elsewhere, since the concentrations were never high in the convecting regions.

5.2.3 Results.

A number of calculations were performed with different initial conditions. These invariably exhibited convecting layers whose depths varied from less than 1 m up to more than 30 m, and the distribution of these was frequently rather similar to that observed in Lake Vanda. Typically, when a considerable depth of fresh water at 0°C was added to the stable, heated, pre-existing lake, the temperature of this water rose quite rapidly, since the heat loss from the top was initially zero. This led to convection as soon as the temperatures had risen past the stable configuration imposed initially by the inverted expansion behaviour of fresh water at low temperatures. As a result of the increased rate at which heat was lost once convection had penetrated to the surface, the

temperatures in the upper part of the lake then tended to decline somewhat. Since the upper surface was held at 0°C , and the heat flow through the bottom was adjusted to give a temperature there of about 25°C , temperatures within the lake were maintained between these limits. In the upper, convecting, part of the lake the steady state appeared to involve an oscillation of temperature which was dictated by the migration of layer boundaries. Since the total solute content was conserved, however, the behaviour of the concentration profile was more regular. After the initial period of rather intense convection, which conveyed solute upwards relatively quickly, the profile showed a continuing upward transfer at a decreasing rate.

While the general behaviour of the model was that indicated, interest centred on the reproduction of the profiles actually observed. The details of the profiles produced by the model varied greatly according to the initial conditions assumed, of which there was a great variety of choice. In consequence the degree of similarity between model and measured profiles depended largely on the patience and insight of the programmer in devising more successful combinations. Since the former at least was limited, the process was continued only to a point where the likeness was readily apparent; as with the laboratory experiments, better results could no doubt be achieved.

The quantities which had to be allocated at the beginning of each calculation were the following:

- (i) The initial concentration at $z = 0$.
- (ii) The time for which the solute had been diffusing in the first phase of development.
- (iii) The depth of the lake during the first phase.
- (iv) The temperature at infinite depth at the end of the first phase; the temperature profile at this time was taken as that in the upper part of an infinitely deep lake heated to equilibrium by the absorption of solar radiation, the heat flow tending to zero at great depth.

- (v) The intensity of solar radiation under the ice.
- (vi) The heat flow in or out of the lake bed.

For most of the calculations (ii) was set at 1000 years, though values of 850 and 1200 years were tried, and (v) was set at 2×10^{-4} cal cm⁻² sec⁻¹ (6300 cal cm⁻² yr⁻¹) in accordance with the measurement of Wilson and Wellman (1962). (vi) was chosen by trial and error so that the temperature at $z = 0$ tended towards a value not too far from 25° C with increasing time. Thus the problem was effectively narrowed down to finding the best simultaneous choices for (i), (iii) and (iv).

Fig. 36 shows the development of the profiles for the most satisfactory case, in which the quantities were set as follows:

- (i) 14% by weight
- (ii) 1000 years
- (iii) 30 m
- (iv) 35° C
- (v) 2×10^{-4} cal cm⁻² sec⁻¹
- (vi) 3×10^{-6} cal cm⁻² sec⁻¹ out of the lake.

The observed values are those of Hoare (1966); the concentration profile is that which, if the solute were entirely CaCl₂, would give the density profile published therein. Apparently reasonable agreement between calculated and observed concentration profiles is given by assuming a time of about 250 years for the duration of the lake's second phase, that is, 1250 years in all. Agreement between the temperature profiles is somewhat marred by excessive calculated temperatures. Nevertheless, overall, agreement is quite good, and certainly constitutes evidence in favour of the hypothesis that the layers formed entirely as a result of convective effects initiated by absorbed sunlight.

5.2.4 Conclusion

The development of thermosolutal convection on the laboratory scale has been described adequately in terms of a numerical model, which

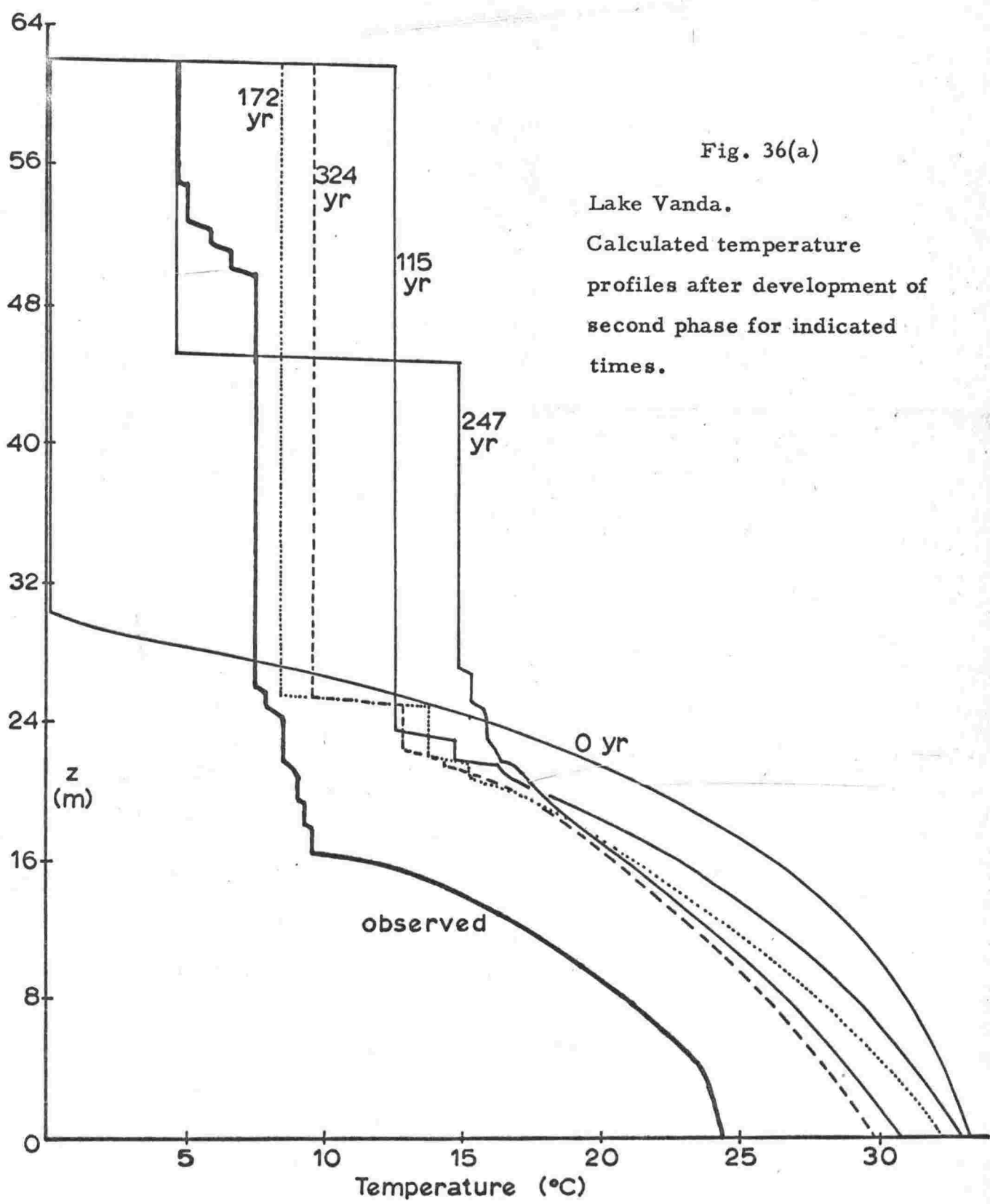


Fig. 36(a)

Lake Vanda.
 Calculated temperature
 profiles after development of
 second phase for indicated
 times.

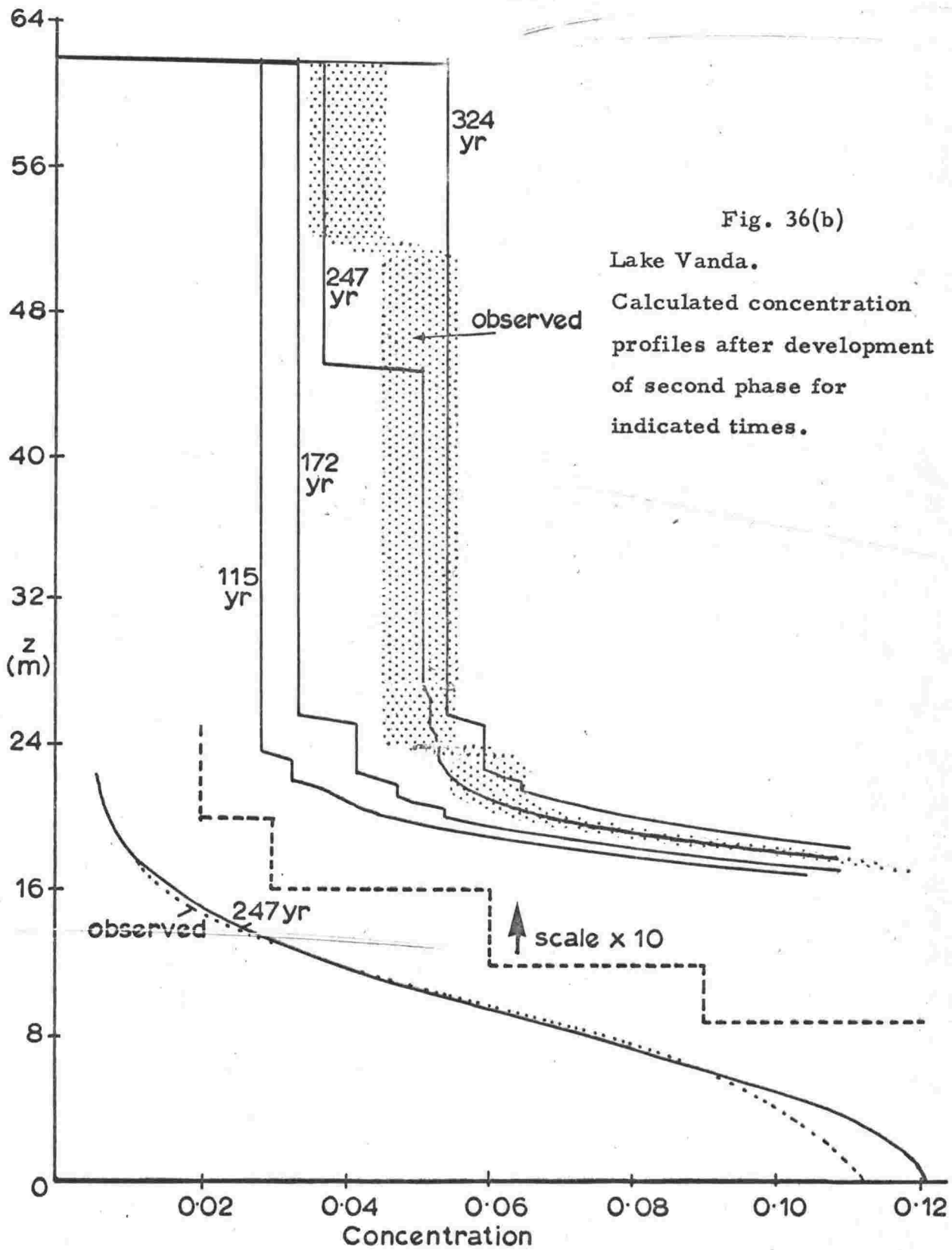


Fig. 36(b)

Lake Vanda.

Calculated concentration profiles after development of second phase for indicated times.

is dependent on scale in minor respects only. The same model has therefore been applied to the problem of Lake Vanda. In this way it has been shown that the present layered structure of that lake could have been caused in the following way: About 250 years ago the lake was only 30 m deep, and was solar heated in much the same way as Lake Bonney is now, though to higher temperatures. At that time the lake filled up quite rapidly to its present level by the addition of fresh water at 0°C . The present structure would then have resulted from convection, and no other mechanism need be invoked.

It does not seem possible to press the investigation far enough to deduce any significant climatic information from the analysis of Lake Vanda, beyond the general observation that during the last 1250 years the area has been less arid than it was before. It is clear that the model is unable to resolve any detail of factors such as the variation of intensity of solar radiation in the past; this is partly because heat transfer is quite rapid in relation to the times involved, so that thermal detail tends to be lost, and partly because of the inherent inaccuracy of the model itself. The concentration profile proceeds much more slowly towards its equilibrium state, but the information it contains is of less climatic interest, and the inaccuracy of the calculation is important here also.

Appendix 1

Correction of radiometer readings.

Near the surface of the lake, three corrections had to be made to the measurements of radiation intensity using the selenium photocell radiometer. These corrections were for spectral response, directional response and ice albedo, and will be considered individually.

Spectral response.

The spectral response correction was calculated graphically. The intensity distribution of sunlight under the ice was assumed to correspond to that under 3 m of pure water, no reliable information on the transmission properties of ice being available. This distribution was calculated using values of extinction coefficient for pure water given in the Smithsonian Physical Tables. The intensity distributions above and below the ice were then modified according to the spectral response of the photocell, which was published by the manufacturer. Graphical integration then showed that above the ice the output of the photocell was 37% of that of an instrument whose sensitivity at all wavelengths was equal to the peak sensitivity of the photocell, while the corresponding figure under the ice was 72%.

Directivity.

The directional correction for the surface reading was estimated by measuring the relative response of the instrument as a function of direction, in the laboratory. The results are shown in fig. A1, from which it can be seen that the response at an off-axis angle of 56° is about 35.5%.

Albedo.

A further correction is needed for the surface reading, to allow for the reflective nature of the ice surface. Ideally, the surface reading should have been taken with the photocell buried a short distance below the ice surface, but this was not practicable, and consequently a correction must be made for the albedo. This was about 50% at the time (R. Ragotzkie, pers. comm.), but is probably dependent on the nature of the ice surface, which is very variable (Hoare et al., 1964).

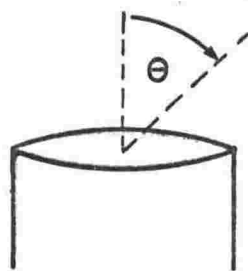
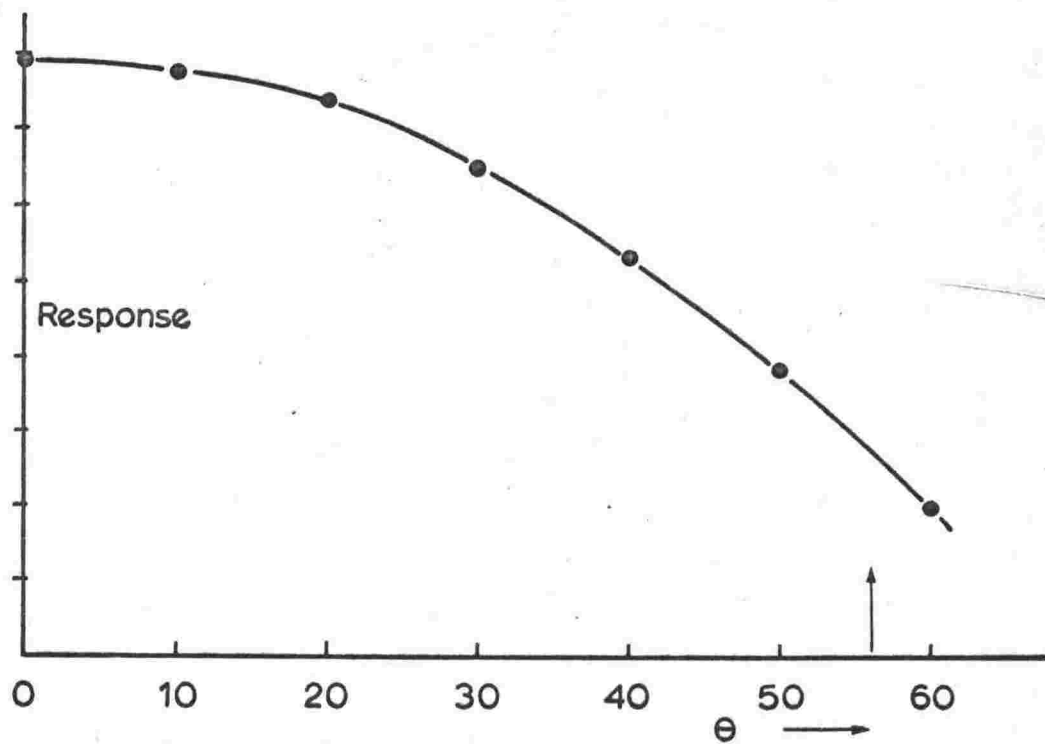


Fig. A1

Directivity of the radiometer. Arrow indicates direction of sun during measurements in Lake Bonney.

Total.

Neglecting the albedo correction, the fraction of the incident radiation which penetrates the ice is thus the observed ratio ($7.0/61.25 = .113$) multiplied by the ratio of the spectral corrections ($.37/.72$) and by the surface directional correction (0.355), that is, 0.020 . The albedo correction is variable, but may reduce this value to 0.01 . Thus between 1% and 2% of incident radiation penetrates the ice. This figure may be compared with values obtained by other investigators, on this and other lakes, in table AI.

Table AI.

Measurements of the fraction of incident radiation which penetrates the ice cover of various lakes.

Lake Bonney

Shirtcliffe and Benseman (1964) Jan. 1963	1.5 ± 0.5% ^a
Hoare et al. (1964) Dec. 1963	1.1% ^b
Hobbie and Mason (reported by Likens and Ragotzkie, 1964) Jan. 1963	21% ^{ac}

Lake Fryxell

Hoare et al. (1965) Nov. 1963	0.1% ^{bd}
-------------------------------	--------------------

Lake Vanda

Wilson and Wellman (1962) Dec. 1961	6% ^b
-------------------------------------	-----------------

Notes:

- a. Photocell measurement.
- b. Bolometer measurement.
- c. Apparently uncorrected.
- d. Not considered typical.

Appendix 2

The equilibrium between a Victoria-Land lake and its environment.

The Victoria-Land lakes are characterized by high salinity at depth, a permanent ice cover which transmits some sunlight, and a periodic inflow of low-salinity water which is balanced not by outflow but by ablation of the ice cover. In order for the lakes to contain a liquid phase in a region of average temperature -17°C , either the salinity must be sufficiently high to reduce the freezing point below this, or a source of heat must exist to maintain a high temperature. Generally, the lakes are maintained at temperatures well above freezing point. In the analysis of these thermal conditions, an implicit assumption is that the level of the lake, and the thickness of the ice cover which to some extent governs radiation input and heat output, can both remain nearly constant for considerable periods. It is also claimed that quite rapid changes of level can take place from time to time, so that a lake occasionally undergoes a rapid transition from one state of equilibrium to another. The following discussion justifies this picture.

If the lake is to be permanently ice-covered in spite of a continual loss through ablation of the surface, ice must be formed at the ice/water boundary at a similar rate. If, in addition, the water level is to be constant, the rate of evaporation must be balanced by the rate of inflow of fresh water.

Assume initially that inflow, freezing and evaporation are continuous processes. Let the rate of inflow of water be V_i , the rate of ice formation be V_f , and the rate of loss of ice through evaporation be V_e , where V_i , V_f and V_e are volumes of water (equivalent) per unit time. Then if the water depth in the lake is W , and the ice thickness I , the total depth below the ice surface is $D = W + I$ and

$$\frac{dw}{dt} = \frac{V_i - V_f}{s} = \frac{V_i}{s} - f$$

$$\frac{dI}{dt} = \frac{V_f - V_e}{s} = f - e$$

$$\frac{dD}{dt} = \frac{V_i - V_e}{s} = \frac{V_i}{s} - e$$

where t is time, s the area of the lake, f is the thickness of water frozen in unit time and e is the equivalent water thickness lost as evaporation from the ice surface in unit time. Note that the quantities determined by particular thermal and climatic conditions are respectively f and e , not V_f and V_e . Then when the lake is in equilibrium with its surroundings,

$$\frac{dW}{dt} = \frac{dI}{dt} = \frac{dD}{dt} = 0$$

i.e.
$$\frac{V_i}{s} = f = e.$$

The stability of this equilibrium can be tested by considering the response of the system to various disturbances. Consider first an increase in aridity caused, for example, by an increase in mean wind speed. This would have the effect of increasing the evaporation rate both on the lake and in the environment. Thus e would rise while V_i , which represents the residue of environmental melt water which is not evaporated, would fall. Hence

$$\frac{dD}{dt} = \frac{V_i}{s} - e < 0$$

and the lake level would fall. However as it did so the surface area s would become smaller, until $\frac{V_i}{s}$ rose sufficiently to give equilibrium again.

Since e would rise without an associated change in f ,

$$\frac{dI}{dt} = f - e < 0$$

and the ice would get thinner. However as the thinning progressed the temperature gradient in the ice would increase, leading to greater heat extraction and an increase in f . Hence the ice thickness would tend to stabilize at some smaller value. Similarly,

$$\frac{dW}{dt} = \frac{V_i}{s} - f < 0$$

initially, so that the water depth would be reduced. Arguments similar to the above show that a temporary increase in V_i not associated with a climatic change would lead to a temporary increase in water depth followed by a gradual return to the original level, while a permanent change in inflow rate not associated with a climatic change would displace the equilibrium towards greater water depth, without changing the ice thickness. (This last possibility would require some catastrophic event to alter the drainage pattern significantly, and is unlikely.) Hence so long as the climate in the region is constant, the lake will probably remain in a stable state, but the water depth and ice thickness are sensitive to climatic changes.

Lake Bonney.

It has been shown that the depth of water in Lake Bonney increased by about 10 m between 1903 and 1911. In terms of the foregoing discussion it is possible to deduce the probable state of the lake before that time.

A permanent increase in depth would be caused by an increase in inflow, probably resulting from a decrease in aridity in the region. More arid conditions would have been associated with thinner ice, higher rates of evaporation and ice production, and smaller inflow. A limit can be placed on the change in area of the lake by reference to the bathymetric map of Angino et al (1964). While the paucity of data induces doubt as to the accuracy of this map, it suggests that a depth increase of 10 m would have been accompanied by an areal increase of about 20%. Thus in the equilibrium equation

$$\frac{V_i}{s} = f = e,$$

if s was formerly 20% less while f and e were greater, V_i was formerly less by a fraction less than 20%, and the change in f and e was less than 20%. The relationship between climatically induced fluctuations of inflow

and ablation is uncertain, but, in the absence of reliable information, suppose that the changes in them have the same relative magnitudes.

$$\text{i.e. } \frac{\delta e}{e} \doteq - \frac{\delta V_i}{V_i} .$$

$$\text{Then, as } \frac{\delta V_i}{V_i} - \frac{\delta s}{s} = \frac{\delta e}{e} = \frac{\delta f}{f} ,$$

$$\frac{\delta s}{s} \doteq 2 \frac{\delta V_i}{V_i} .$$

That is, a 20% increase in area implies approximately a 10% increase in inflow and a 10% decrease in evaporation and freezing rates. Thus e and f were not greatly different from their present values.

It has been shown that in its former state the water in Lake Bonney was of nearly uniform salinity and relatively cold, the calculated temperature being about -16°C . Since this temperature is only about 1 Cdeg above the present mean annual temperature, the ice cover at that time must have been much thinner in order to allow the extraction of heat liberated both by the absorption of radiation and by the production of ice. It is not immediately clear that the ice could have been sufficiently thin, without completely melting every summer, a situation which did not apply in Dec. 1903 (Scott 1905).

A possible configuration which meets the foregoing requirements is illustrated in fig. A2. At this point it is necessary to drop the pretence that inflow, evaporation and freezing are continuous processes, and to remember that the first two of these occur predominantly in the summer, while the third is limited to the winter. (The equilibrium analysis still holds provided quantities are averaged over an annual cycle.) In the summer, then, the fresh inflow water, together with some melt water from the ice cover, would have formed a thin layer between the ice and the brine. The ice/water boundary would have been at 0°C , so a considerable temperature gradient would have existed in the upper region of the brine, the mean temperature of which would have been about -16°C .

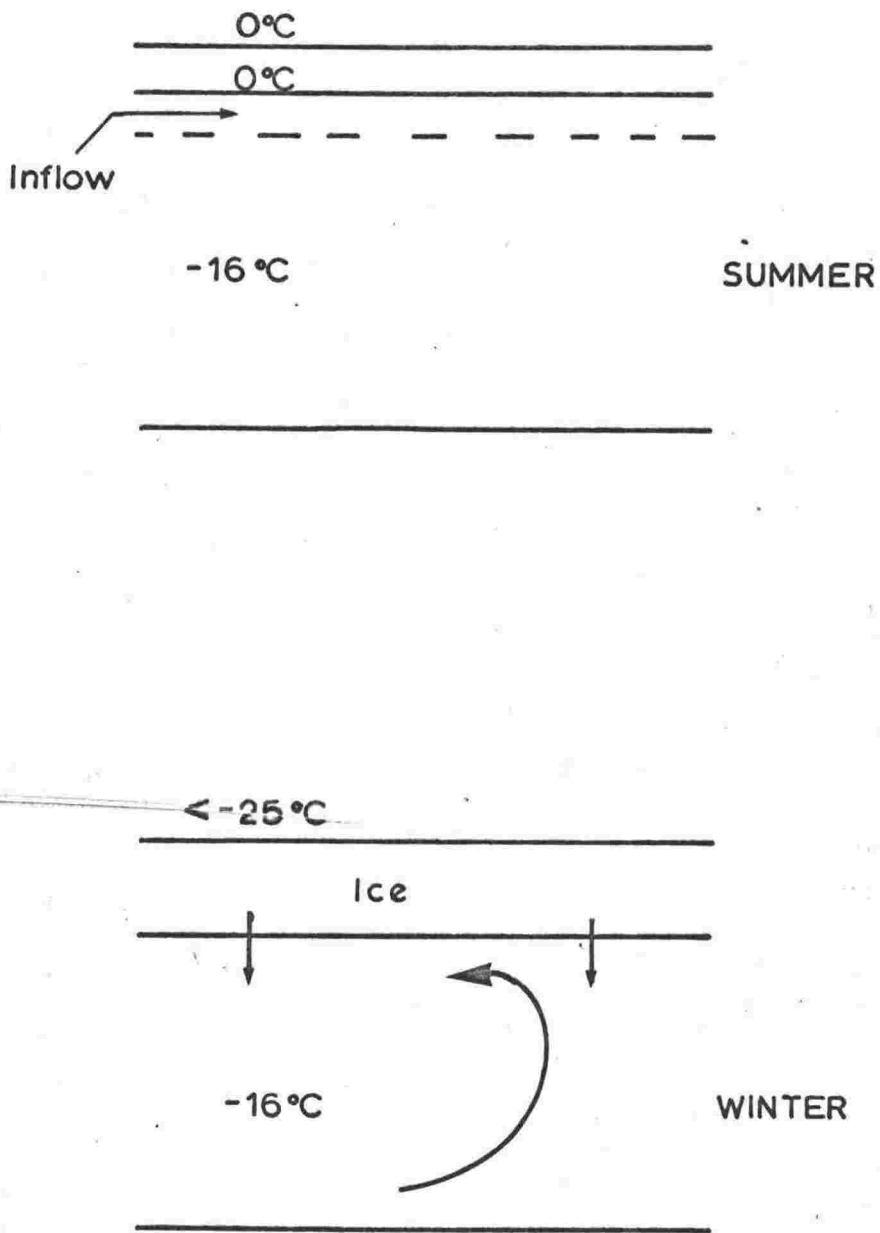


Fig. A2

Hypothetical former state of Lake Bonney.

This would have inhibited convection in the brine, so that the effect of this heating would not have penetrated far into the brine within the duration of a summer. During this period some solar heating would have occurred in the brine. At the beginning of winter the ice surface temperature drops to a very low value - for 6 months of the year it is below -25°C (Pewe 1960). This would have extracted sufficient heat from the ice to freeze all the interstitial water and then cause the lower boundary to migrate downwards just as at present, through the fresh layer. This layer would have contained a salt gradient after its period of contact with the brine, so the temperature of the ice/water boundary would have fallen as the boundary moved downwards. This would have inhibited the extraction of heat and further migration of the boundary, but if the "fresh" layer was sufficiently thin the ice could have grown down to a level where the freezing point was below -16°C . At about this point convection would have occurred throughout the brine, owing to the cooling of its upper surface. Further downward migration of the ice would have been resisted by the large thermal capacity of the convecting brine, the temperature of which would not have fallen much further. The average temperature of the ice/water boundary over an annual cycle would therefore have been about -8°C .

It has been seen that inflow and freezing rates at this time were not very different from their present values. Thus the total heat to be extracted through unit area of the ice annually was likewise similar to the present, the average temperature difference across the ice being perhaps half as great as now. Thus the system could have been in equilibrium if the ice was about half as thick as it is now.

Appendix 3.Algol program to optimise parameters in a theoretical
temperature profile.

Pages 1 and 2 of the program (UPHSO4) set up the procedures required and print out the starting data and headings. Calculation begins on page 3 with the assignment of values in the parameter matrix. The calculation of an individual profile is begun at the bottom of page 3 and completed at the top of page 4; this section is used many times to give the many estimates of E (sum of squared deviations between calculated and measured profiles) required.

Page 4 contains two precautions against malfunction: (a) If the variation of E with a parameter is nearly linear, the new value chosen for the parameter is not that which minimises E, but that which gives the smallest E at one of the trial points. (b) If the new value for the parameter lies outside the range of trial values, the nearest trial value is used instead. This is necessary since the approximate representation of E is too inaccurate for greater corrections to be justified. Another precaution, built into the procedure "fill", is that the trial points lie at unequal distances on each side of the central point in the variation of each parameter. This avoids an indeterminacy arising when the central point is very close to the minimum of E.

On page 5 the new values of the parameters are assigned, the sequence is restarted where appropriate, and the values are printed out. If the RMS deviation is reduced to an acceptable level (defined by the input data) the profile is printed out. Alternatively, if this criterion is not surpassed within an acceptable number of trials (also defined in the input data) the last profile is printed out, with an indication to this effect. The example of printout given below is one such case.

UPHSO4 ;

```

begin real
  E, t, to, t1, ds, ds0, rho, rho0, rho1, rho, rho0, rho1, sigma, sigma0, signal, tau, tau0, eta1, eta, eta0, eta1, w, one,
  two, three, four, five, six, seven, eight, nine, ten, eleven, R, S, T, T1, T2, temp, l1, l2, X, v, inc, accept;
  integer a, i, j, L, m, M, N, p, P, Q, r, V ;
  array ptrs[1:13, 1:7], best[1:13], profile[1:200], y[1:200, 1:2], z[1:200] ;
  integer array A[1:40] ;
  switch SA:=repeat ;
  procedure fill(ptr, n, m, x0, x1) ;

```

```

  comment Assigns values to parameter matrix ;
  value m, x0, x1 ;
  real x0, x1 ;
  integer n, m ;
  array ptr ;
  for n:=1 step 1 until 13 do
  begin if n=2*m-1 then ptr[n, m]:=x0+x1 else
  if n=2*m-2 then ptr[n, m]:=x0-.8*x1 else
  ptr[n, m]:=x0

```

```

  end ;
  real procedure Gauss(x); value x; real x;
  comment Calculates the integral from -infinity to x of
  exp(-0.5*x^2) dx/sqrt(2*pi);

```

```

  begin real y, z, w;
  if x=0 then z:=0 else
  begin y:= abs(x)/2;
  if y > 3 then z:=1
  else if y < 1 then
  begin w:= y*y;

```

```

  z:=((((((0.000124818987*w
  -0.001075204047)*w
  +0.005198775019)*w
  -0.019198292004)*w
  +0.059054035642)*w
  -0.151968751364)*w
  +0.319152932694)*w
  -0.531923007300)*w
  +0.797884560593)*y*2

```

```

  end
  else

```

```

begin y:=y-2;
z:=((((((-0.0000452555659*y
+0.000152529290)*y
-0.00001938132)*y
-0.000676904986)*y
+0.001350604284)*y
-0.000794620620)*y
-0.002034234874)*y
+0.006549791214)*y
-0.010557625006)*y
+0.011630447319)*y
-0.009279453341)*y
+0.00535579108)*y
-0.002141265741)*y
+0.000535310849)*y
+0.999936657524

```

```
end
```

```
end; Gauss := if x > 0 then (z+1)/2 else (1-z)/2
```

```
end Gauss;
```

```
real procedure solve(x1,x2,x3,x1,x2,x3);
```

```
comment Evaluates coefficient in equation for E;
```

```
value x1,x2,x3,x1,x2,x3;
```

```
real x1,x2,x3,x1,x2,x3;
```

```
solve:=((x3-x1)*(x2-x1)-(x2-x1)*(x3-x1))/((x2-x3)*(x2-x1)*(x3-x1));
```

```
P:=M:=m:=1;
```

```
Q:=6;
```

```
instrng(A,m);
```

```
read t0,t1,ds0,ds1,rho0,rho1,sigma0,sigma1,tau0,tau1,eta0,eta1,a,l1,K,r,accept;
```

```
for J:=1 step 1 until a do for L:=1,2 do read y[J,L];
```

```
lineprinter;
```

```
topoform;
```

```
print SUP%504EL?Variation of six parameters to minimize standard deviation between calculatedEL??,
```

```
Band measured temperatures in solar heated lake of Bonney typeEL2??;
```

```
m:=1;
```

```
outstring(A,m);
```

```
print CEL5?TRIAL VALUE OF AGEES21??,sameline,scaled(3),t0,SES4?INCREMENTES5??,
```

```
t1,ELS15?DEPTH SHIFTES13??,freepoint(4),ds0,SES21??,
```

```
ds1,ELS15?SOLAR FLUXES14??,3.153609*K*eta0*rho0,SES21??,3.153609*K*eta0*
```

```
rho1,ELS15?GEOTHERMAL GRADIENTES5??,sigma0*.3072,SES21??,sigma1*.3072,ELS15?FIRST?,
```

```
E TEMPERATURES7??,-tau0,SES21??,tau1,ELS15?EXTINCTION COEFFICIENTES2??,eta0,SES21??,
```

```
eta1,CEL2?TEMPERATURE MEASURED AT DEPTHESES??,y[1,1],SES?M WASES??,y[1,2],SES?DEG C?;
```

```

for J:=2 step 1 until a do
  print SLS30??,sameline,freepoint(4),y[J,1],S9S9??,y[J,2] ;
  print SLS2?FIRST DEPTH OF LAKES5??,sameline,freepoint(3),11,S9L?DIFFUSIVITYES5??,
  scaled(2),K,SLS5?STANDES14?AGES17?DEPTRES13?SOLARES13??,
  SGEOTRES13?FIRSTES12?EXTICINELS2?DEVNES34?CHIFFES13?FLUXES14?GRADES14??,
  STEMPES13?COEFFELES?DEG CES14?SECES13?MES15?LY/YRES13?DEG/MES13?DEG?,
  SSS?CS14?WEL2?? ;

repeat:fill(ptrs,i,2,t0,t1) ;
  fill(ptrs,i,3,ds0,ds1) ;
  fill(ptrs,i,4,rho0,rho1) ;
  fill(ptrs,i,5,sigma0,sigma1) ;
  fill(ptrs,i,6,tau0,tau1) ;
  fill(ptrs,i,7,ota0,ota1) ;
  for V:=1 step 1 until Q do
    begin for N:=1, 2*V, 2*V+1 do
      begin t:=ptrs[N,2] ;
        ds:=ptrs[N,3] ;
        rho:=ptrs[N,4] ;
        sigma:=ptrs[N,5] ;
        tau:=ptrs[N,6] ;
        eta:=ptrs[N,7] ;
        if M=1 then
          begin for p:=1 step 1 until a do z[p]:=yfp,1]-ds ;
            E:=0 ;
            L2:=z[a]
          end ;
          for p:=1 step 1 until a do
            begin if p=1 then w:=.5 else w:=1.00 ;
              if M=2 then z[p]:=.3043*p ;
                one:=2*(1-Gauss(z[p]/sqrt(2*K*t))) ;
                two:=exp(-eta*z[p])*(1+exp(i*(ota*t2)*t)) ;
                three:=Gauss(z[p]/sqrt(2*K*t))-eta*sqrt(2*K*t)
                  + Gauss((12-z[p])/sqrt(2*K*t)+eta*sqrt(2*K*t)) ;
                four:=Gauss(z[p]/sqrt(2*K*t)+eta*sqrt(2*K*t))
                  - Gauss((12+z[p])/sqrt(2*K*t)+eta*sqrt(2*K*t)) ;
                five:=Gauss((12+z[p])/sqrt(2*K*t)) - Gauss((12-z[p])/sqrt(2*K*t)) ;
                R:=one - two + three * exp(K*(eta*t2)*t - eta * z[p])
                  + four * exp (K*(eta*t2)* t + eta * z[p]) + five * exp (-eta*t2) ;
                six:=exp(-((12-z[p])2)/(4*K*t)) - exp (-((12+z[p])2)/(4*K*t)) ;

```

```

seven:=(12+z[p])* Gauss ((12 + z[p])/sqrt(2*K*t));
eight:=(12-z[p])*Gauss ((12-z[p])/sqrt(2*K*t));
S:= six * sqrt (K*t/3.1416)-seven + eight + 2 * z[p];
nine:= exp(-((11-z[p])^2)/(4*K*t)) - exp(-((11+z[p])^2)/(4*K*t));
ten:=(11+z[p])*(1-Gauss((11+z[p])/sqrt(2*K*t)));
eleven:=abs(11-z[p])*(1-Gauss (abs(11-z[p])/sqrt(2*K*t)));
T1:=nine*sqrt (K*t/3.1416)+ten-eleven-z[p];
T2:=T1+z[p]-11;
if z[p] < 11 then T:= T1/11 else T:=T2/11;
temp:= rho * R + sigma * S + tau * T;
if M = 2 then print freepoint (4), z[p], prefix(ESS5??), z[p]+ds, temp;
if M=1 then
  begin E:=E+w*(temp-y[p,2])^2;
  if N=1 then profile[p]:=temp;
  if p=a then ptrs[N,1]:=E
  end;
end profile;
if M=2 then stop;
end three profiles;
best[1]:=ptrs[1,1];
best[2*v]:=solve(ptrs[1,v+1], ptrs[2*v,v+1], ptrs[2*v+1,v+1], ptrs[1,1], ptrs[2*v,1], ptrs[2*v+1,1]);
if best[2*v]*(ptrs[2*v+1,v+1]-ptrs[1,v+1])^2 < 10^-4 then
  begin if ptrs[2*v,1] > ptrs[2*v+1,1] then best[2*v+1]:= ptrs[2*v+1,v+1]
  else best[2*v+1]:= ptrs[2*v,v+1]
  end else
  begin v:= checkr((ptrs[1,v+1]+ptrs[2*v,v+1])/2 - (ptrs[2*v,1]-ptrs[1,1])/
    (2*(ptrs[2*v,v+1]-ptrs[1,v+1]) * best[2*v]));
  if v < ptrs[2*v,v+1] then best[2*v+1]:=ptrs[2*v,v+1] also
  if v > ptrs[2*v+1,v+1] then best[2*v+1]:=ptrs[2*v+1,v+1] else best[2*v+1]:=v;
  end;
inc:=ptrs[2*v+1,v+1] - ptrs[1,v+1];
fill(ptrs,i,v+1,best[2*v+1],inc);
end set of profiles;
print freepoint(4),sqrt(best[1]/a),sameline,ESS3??,scaled(2),best[2],ESS??,scaled(3),best[3],
ESS3??,scaled(2),best[4],ESS??,scaled(3),best[5],ESS3??,scaled(2),best[6]/(K*3.153609
*best[13])^2,ESS??,freepoint(4),best[7]*K*3.153609*best[13],ESS3??,scaled(2),best[8]*10.6,
ESS??,freepoint(4),best[9]/3.255,ESS3??,scaled(2),best[10],ESS??,freepoint(4),-best[11],
ESS3??,scaled(2),best[12],ESS??,freepoint(4),best[13],ELL??;
if P<r then

```

```

begin
  ds0:=best[5] ;
  rho:=best[7] ;
  sigma0:=best[9] ;
  tau0:=best[11] ;
  eta0:=best[13] ;
  p:=p41 ;
  goto repeat
end also
begin print f$LS?BEST CALCULATED TEMPERATURE AT DEPTHS??, sameline, freepoint(4),
  y[1,1], f$S2?IS$S2??, profile[1], f$S2?DEVIATIONS2??, profile[1]-y[1,2] ;
  for p:=2 step 1 until a do print f$LS38??, sameline, freepoint(4), y[p,1], f$S6??,
  profile[p], f$S13??, profile[p]-y[p,2] ;
  print f$LS?FULL CALCULATED PROFILE$ES3?Z$S6?DEPTHS6?TEMP$EL??;
  M:=2 ;
  Q:=1 ;
  a:=12/.3048 ;
  t0:=best[3] ;
  ds0:=best[5] ;
  rho0:=best[7] ;
  sigma0:=best[9] ;
  tau0:=best[11] ;
  eta0:=best[13] ;
  goto repeat ;
end
end else
begin print f$LS?THIS PROFILE MAY NOT SATISFY THE CRITERIA$EL?BEST CALCULATED TEMPERATURE AT #?,
  f DEPTHS2??, sameline, freepoint(4), y[1,1], f$S2?IS$S2??, profile[1], f$S2?DEVIATIONS2??,
  profile[1]-y[1,2] ;
  for p:=2 step 1 until a do print f$LS38??, sameline, freepoint(4), y[p,1], f$S6??, profile[p],
  f$S13??, profile[p]-y[p,2] ;
  print f$LS?FULL CALCULATED PROFILE$EL2S3?Z$S6?DEPTHS6?TEMP$EL??;
  M:=2 ;
  Q:=1 ;
  a:=12/.3048 ;
  t0:=best[3] ;
  ds0:=best[5] ;
  rho0:=best[7] ;
  sigma0:=best[9] ;
  tau0:=best[11] ;
  eta0:=best[13] ;
  goto repeat
end
end

```

UPHS04
 VARIATION OF SIX PARAMETERS TO MINIMIZE STANDARD DEVIATION BETWEEN CALCULATED
 AND MEASURED TEMPERATURES IN SOLAR HEATED LAKE OF BONNEY TYPE
 LAKE FRYXELL HOARE DATA

TRIAL VALUE OF AGE 1.75e+09 INCREMENT 2.00e+08
 DEPTH SHIFT 4.600
 SOLAR FLUX 567.6
 GEOTHERMAL GRADIENT .0922
 FIRST TEMPERATURE -12.00
 EXTINCTION COEFFICIENT .3000

TEMPERATURE MEASURED AT DEPTH 5.300 M HAS .3600 DEG C
 6.000 1.180
 6.750 1.720
 7.450 2.040
 8.200 2.210
 8.950 2.250
 9.700 2.250
 10.40 2.200
 11.15 2.150
 11.90 2.090
 12.60 2.030
 13.35 1.940
 14.10 1.910
 14.80 1.860
 15.55 1.840
 16.30 1.800

FIRST DEPTH OF LAKE 4.00
 DIFFUSIVITY 1.20e-07

STAND DEVN	AGE	DEPTH SHIFT	SOLAR FLUX	GEOTH GRAD	FIRST TEMP	EXTCTN COEFF						
DEG C	SEC	M	LY/YR	DEG/M	DEG C	/M						
4.587	1.6e-12	1.67e+09	1.4e+03	4.30e+00	2.4e-03	463.3	2.9e+03	.1229	1.2e+00	-10.36	2.0e+07	,2615
.3786	9.8e-15	1.58e+09	-3.3e+01	3.98e+00	4.1e-04	557.7	2.9e+03	.1536	1.4e+00	-10.00	3.0e+05	,2834
.1395	2.0e-15	1.50e+09	4.0e-01	4.38e+00	3.8e-04	577.2	2.7e+03	.1592	1.3e+00	-10.01	1.1e+04	,2755
.1444	1.2e-16	1.46e+09	2.1e+00	4.67e+00	3.6e-04	567.5	2.5e+03	.1571	1.3e+00	-10.02	3.2e+03	,2664
.1140	4.6e-17	1.47e+09	2.0e+00	4.63e+00	4.0e-04	549.3	2.5e+03	.1583	1.3e+00	-10.02	1.0e+03	,2603
.1074	4.5e-17	1.50e+09	2.1e+00	4.54e+00	4.1e-04	536.1	2.6e+03	.1587	1.3e+00	-10.03	8.8e+02	,2570
.1107	4.9e-17	1.51e+09	1.8e+00	4.53e+00	3.9e-04	545.0	2.6e+03	.1588	1.3e+00	-10.03	3.3e+02	,2628

UPHS04; typical output (page one).

THIS PROFILE MAY NOT SATISFY THE CRITERIA
 BEST CALCULATED TEMPERATURE AT DEPTH 5.300 IS

DEPTH	TEMP	DEVIATION
3.048	4.831	.3125
3.096	5.136	.0393
3.144	5.440	-.1061
3.192	5.745	-.1677
3.240	6.050	-.1485
3.288	6.355	-.0497
3.336	6.660	.0125
3.384	6.964	.0631
3.432	7.269	.0678
3.480	7.574	.1255
3.528	7.879	.1210
3.576	8.184	.1087
3.624	8.488	.0427
3.672	8.793	-.0173
3.720	9.098	-.0757
3.768	9.403	-.1469
3.816	9.708	
3.864	10.01	
3.912	10.32	
3.960	10.62	
4.008	10.93	
4.056	11.23	
4.104	11.54	
4.152	11.84	
4.200	12.15	
4.248	12.45	
4.296	12.76	
4.344	13.06	
4.392	13.37	
4.440	13.67	
4.488	13.97	
4.536	14.28	
4.584	14.58	
4.632	14.89	
4.680	15.19	
4.728	15.50	
4.776	15.80	
4.824	16.11	
4.872	16.41	

FULL CALCULATED PROFILE

Z	DEPTH	TEMP
3.048	4.831	.2665
3.096	5.136	.6058
3.144	5.440	1.7980
3.192	5.745	1.0886
3.240	6.050	1.230
3.288	6.355	1.450
3.336	6.660	1.573
3.384	6.964	1.683
3.432	7.269	1.846
3.480	7.574	1.914
3.528	7.879	2.025
3.576	8.184	2.066
3.624	8.488	2.160
3.672	8.793	2.188
3.720	9.098	2.248
3.768	9.403	2.285
3.816	9.708	2.298
3.864	10.01	2.313
3.912	10.32	2.311
3.960	10.62	2.287
4.008	10.93	2.292
4.056	11.23	2.277
4.104	11.54	2.261
4.152	11.84	2.233
4.200	12.15	2.198
4.248	12.45	2.188
4.296	12.76	2.115
4.344	13.06	2.106
4.392	13.37	2.029
4.440	13.67	2.024
4.488	13.97	1.947
4.536	14.28	1.944
4.584	14.58	1.874
4.632	14.89	1.861
4.680	15.19	1.810
4.728	15.50	1.731
4.776	15.80	1.766
4.824	16.11	1.693
4.872	16.41	1.617

UPHSO4; typical output (page two).

Appendix 4Interpretation of the experiment of Turner (1965).

In this experiment a tank contained two layers of common salt solution, the lower layer being concentrated and the upper layer weak. The interface between these layers was maintained by the convection occurring within each layer, owing to the supply of heat at the base. The aim of the experiment was to study the properties of the interface, on the assumption that these could be observed in isolation from the properties of the convecting layers above and below. A dimensional analysis suggested that the experimental data should be analysed with respect to a stability parameter $S = \frac{\gamma \Delta C}{\alpha \Delta T}$, the ratio of the contributions of solute and heat to the density difference between the layers.

The experiment involved measuring the rates of transfer of heat and solute across the interface. This was achieved by insulating the tank, including the upper water surface, and observing the rate of increase of temperature and solute concentration in the upper layer, for a range of heating rates (3:1) and values of the stability parameter (7:1). The heat flux was expressed in terms of the "solid plane value", which is the heat flux that would have been expected if the layers were separated by a solid, plane, perfectly conducting boundary, and the results are shown in fig.A3. The solute flux was expressed in terms of the ratio between effective turbulent transfer coefficients for solute and heat, and the results are plotted in fig.A4. Finally, the ratio between the potential energy changes due to the transfer of solute and of heat was evaluated, and its dependence on the stability parameter is shown in fig.A5.

The most striking result is that concerning potential energy changes. Turner pointed out that some self-limiting mechanism must be operating to control the coupled diffusion of salt and heat, since the ratio of potential energy changes becomes constant for $S \geq 2$, but he offered no suggestions as to its nature.

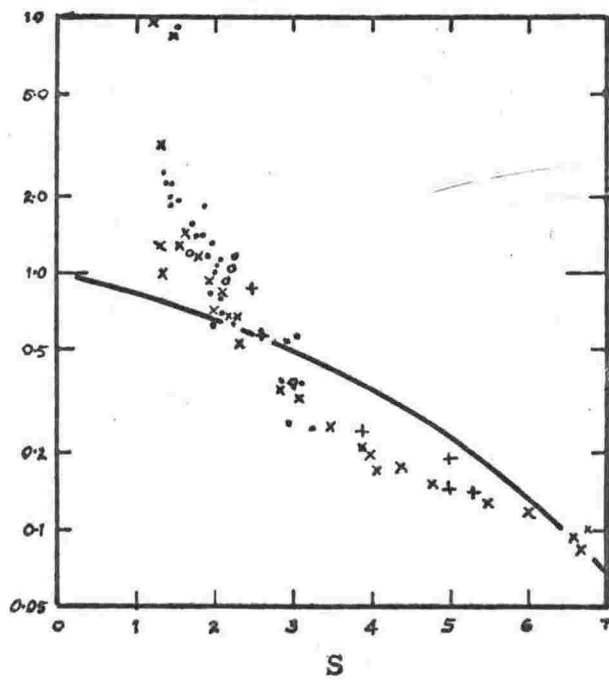
Fig. A3

The measured heat flux across the interface between two liquid layers, compared with the value calculated for solid planes. Different symbols refer to different heating rates. Experimental points reproduced from Turner (1965).

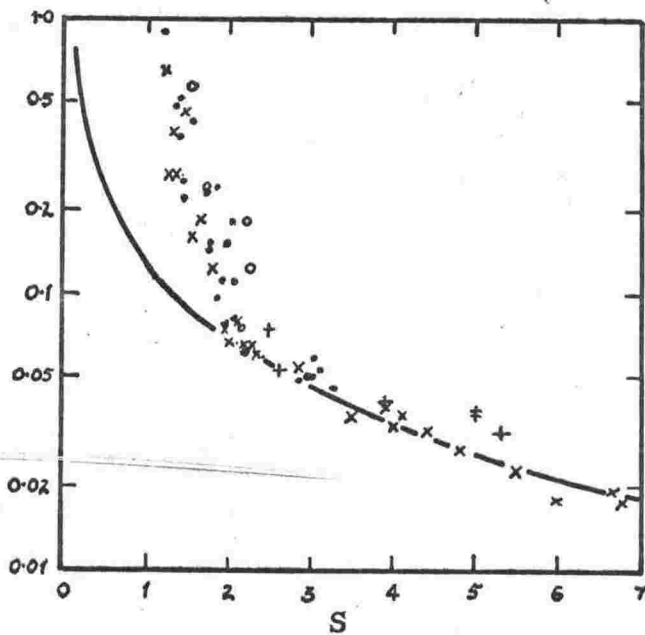
Fig. A4

The ratio of the turbulent transfer coefficients for salt and heat, as a function of the stability parameter s . (Turner, 1965.)

Ratio of measured heat flux
to solid plane value.



Ratio of turbulent
transfer coefficients



In order to explain these results, it is necessary to consider the system as a whole, and not just the interface. The following theory is crude, but gives some insight into the problem. Two regimes are of interest.

Stability $S > 2$.

In order for steady convection to occur it has been seen that the density must be less at the bottom of the layer than at the top. The difference is very small, less than 1 part in 10^4 for the conditions quoted by Turner, and for the present purpose it may be neglected. Hence if a large density difference exists between the layers, it is clear that the convection occurs in two regions of substantially constant density, with a region between them which contains a high density gradient and which is not penetrated by the convection. This situation is sketched in fig. A6. The mid-layer differences of concentration and temperature measured by Turner are ΔC and ΔT respectively, but the temperature difference driving the convection in the lower layer is rather less than ΔT , and the corresponding concentration difference is less than ΔC . Several choices may be made to approximate these actual differences, and all seem to lead to the same qualitative behaviour. The most straightforward choice is that the temperature difference between bottom and top of the lower convecting layer is $(\Delta T - \delta\theta)$, and that the corresponding concentration difference is $\frac{1}{2}(\Delta C - \delta x)$.

The thickness ϵ of the conducting layer appears to be less than 0.2 cm under the conditions of the experiments, and may therefore be assumed to be much less than h , the half-depth of the system. Consequently, quasi-steady state conditions apply at all times. Thus the solute and heat fluxes through the conducting region equal those through the lower layer. Writing H_1 and H_2 for the heat fluxes through the bottom layer and conducting region respectively, and F_1 and F_2 for the corresponding solute fluxes,

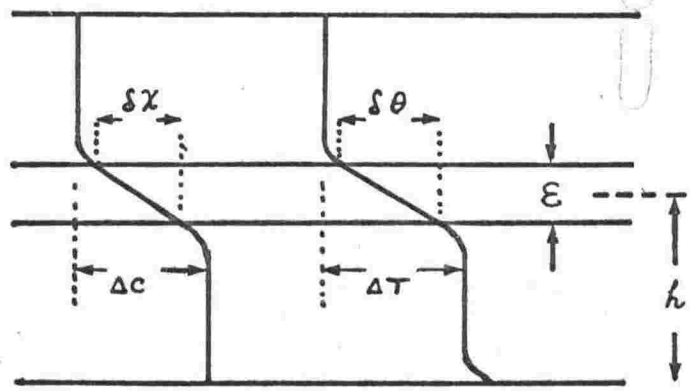
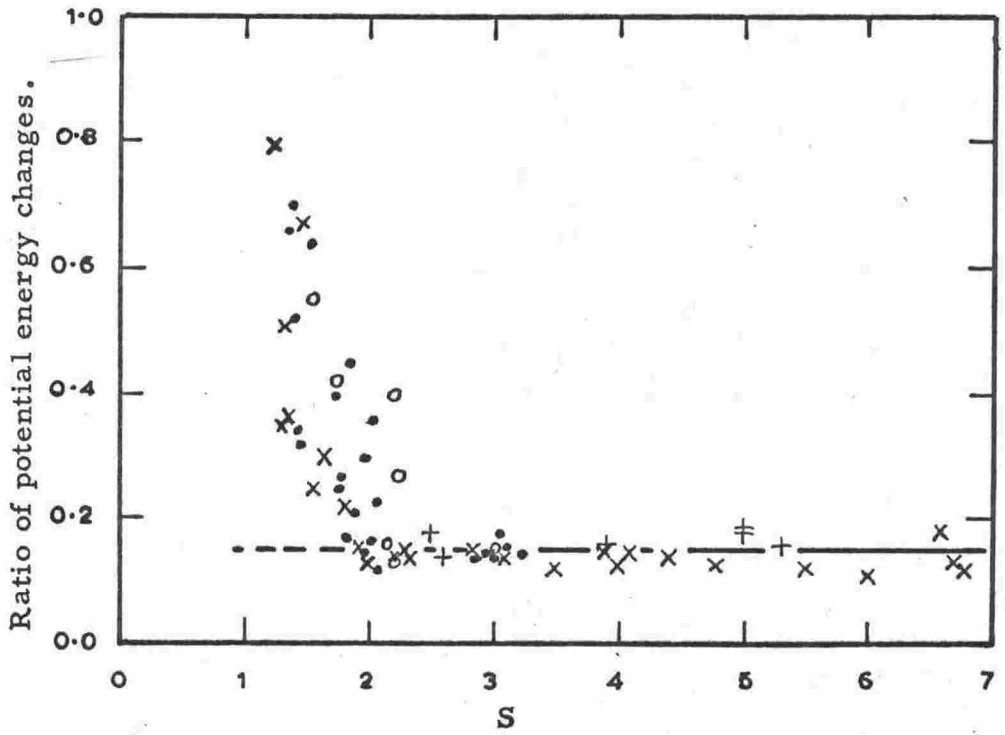
$$H_1 = H_2, \quad F_1 = F_2.$$

Fig. A5

The ratio of potential energy changes due to the transfer of salt and heat across the interface, as a function of the stability parameter. (Turner, 1965.)

Fig. A6

Hypothetical profiles of concentration and temperature during Turner's experiment.



These conditions are not sufficient to make the system determinate. Three assumptions may be made concerning the convection; firstly, following Malkus (1954b), we may assume that the heat flow is a maximum for the given boundary temperatures and concentrations, and secondly, we may impose the condition that the non-dimensional solute flow (i.e. a solute Nusselt number N_s) is proportional to the thermal Nusselt number N_h . Finally, we note that the criterion for the onset of convection in a thermosolutal system is found from the corresponding criterion for the pure-thermal system having the same geometry by substituting $(R + rR_s)$ for R , where r is a constant determined by the nature of the instability; it therefore seems appropriate to regard $(R + rR_s)$ ($= Re$, say) as the parameter which describes the heat flow, just as R does in the pure-thermal case. (We could maximise Re instead of H_1 , with similar results.)

Accordingly, we may modify Turner's treatment by writing for the lower layer

$$N_h = a (Re)^{1/3} = \frac{H_1}{k_h \frac{\Delta T - \delta \theta}{h}}$$

where a is a numerical constant and $k_h = \rho cK$ is the thermal conductivity.

Also

$$Re = \frac{gh^3}{\nu K} \left\{ \alpha (\Delta T - \delta \theta) - \frac{r\eta}{2} (\Delta C - \delta x) \right\}$$

$$\therefore H_1 = ak_h \left(\frac{g}{\nu K} \right)^{1/3} (\Delta T - \delta \theta) \left\{ \alpha (\Delta T - \delta \theta) - \frac{r\eta}{2} (\Delta C - \delta x) \right\}^{1/3} \quad (1)$$

Then differentiation shows that H_1 is a maximum when

$$3 \frac{\Delta C - \delta x}{\Delta T - \delta \theta} + \frac{\delta x}{\delta \theta} = \frac{8\alpha}{r\eta} \quad (2)$$

Now $N_s = \psi N_h$,

where ψ is a numerical constant.

$$\begin{aligned} \text{Then } F_1 &= \psi \frac{k_s}{2k_h} \frac{\Delta C - \delta x}{\Delta T - \delta \theta}, \quad H_1 = \psi \frac{k_s}{2k_h} \cdot \frac{\Delta C - \delta x}{\Delta T - \delta \theta} \cdot H_2 \\ &= \psi \frac{k_s}{2k_h} \cdot \frac{\Delta C - \delta x}{\Delta T - \delta \theta} \cdot \frac{k_h \delta \theta}{\epsilon} \\ &= F_2 \\ &= \frac{k_s \delta x}{\epsilon} \end{aligned}$$

$$\therefore \delta x = \frac{\psi}{2} \frac{\Delta C - \delta x}{\Delta T - \delta \theta} \delta \theta \quad (3)$$

and, from (2),

$$\delta \theta = \frac{\psi + 6}{8\psi\alpha} \eta r \delta x \quad (4)$$

From (3) and (4)

$$\delta x = \frac{16\psi\alpha\Delta T}{(\psi+6)(2-\psi)\eta r} \left\{ 1 - \frac{r(\psi+6)}{16} \cdot S \right\}$$

$$\text{and } \delta \theta = \frac{2\Delta T}{(2-\psi)} \left\{ 1 - \frac{r(\psi+6)}{16} \cdot S \right\}$$

Substituting in (1) gives

$$H_1 = a k_h \left(\frac{g\alpha}{\nu K}\right)^{1/3} \left(\frac{\psi}{\psi+6}\right)^{1/3} \left(\frac{\psi}{\psi-2}\right) \left\{ 1 - \frac{r(\psi+6)}{8\psi} \cdot S \right\}^{4/3} (\Delta T)^{4/3}$$

Writing Turner's solid plane heat flow as H_p ,

$$H_p = a k_h \left(\frac{g\alpha}{\nu K}\right)^{1/3} (\Delta T)^{4/3}$$

$$\therefore \frac{H_1}{H_p} = \left(\frac{\psi}{\psi+6}\right)^{1/3} \left(\frac{\psi}{\psi-2}\right) \left\{ 1 - \frac{r(\psi+6)}{8\psi} \cdot S \right\}^{4/3}$$

Here ψ and r are as yet undetermined.

However r must be one of $\frac{P_s}{P}$, $P/(P+1)$ and $\frac{P}{P_s}$ (Veronis, 1965).

Within this limitation, the only satisfactory choice for r is $r = \frac{P}{P+1} \neq 0.9$, and the best value for ψ is ill-defined but ≥ 20 . The curve corresponding to $\psi = 30$, $r = 0.9$ is superimposed on Turner's data in fig. A4 and fits fairly well for $2 \leq S \leq 7$. The reason for failure at high S is probably a failure of the heat flow law. As S increases the effective

Rayleigh number Re decreases, reducing the turbulence of the convection. When $Re \lesssim 10^5$ the law

$$N_h = a (Re)^{1/3}$$

may be expected to fail, invalidating the analysis.

With regard to the "ratio of turbulent transfer coefficients for solute and heat", this theory (for $S > 2$) predicts that

$$\begin{aligned} \frac{F_2}{\Delta C} \cdot \frac{c \rho \Delta T}{H_2} &= \frac{\Delta T}{\Delta C} \cdot \frac{\rho c k_s}{k_h} \frac{\delta x}{\delta \theta} \\ &= \frac{\Delta T}{\Delta C} \cdot \frac{D}{K} \cdot \frac{8 \psi \alpha}{(\psi + 6) r \eta} \\ &= \frac{D}{K} \cdot \frac{8 \psi}{r(\psi + 6)} \cdot \frac{1}{S} \end{aligned}$$

Similarly, the "ratio between the potential energy changes due to the transfer of solute and of heat" is given by

$$\begin{aligned} \frac{\rho c \eta F_2}{\alpha H_2} &= \frac{\eta}{\alpha} \cdot \frac{D}{K} \frac{\delta x}{\delta \theta} \\ &= \frac{\eta}{\alpha} \cdot \frac{D}{K} \cdot \frac{8 \alpha \psi}{r \eta (\psi + 6)} \\ &= \frac{D}{K} \cdot \frac{8 \psi}{r (\psi + 6)} \end{aligned}$$

These two are plotted on Turner's data in figs. A5 and A6, implying a value for D/K of 0.02. This is about twice the correct value, but the qualitative behaviour is well represented.

Stability $S < 2$.

At low stability, the conducting layer has become very thin, and the predictions of the theory are sensitive to the original assumptions as to the distributions of temperature and concentration. In fact the layer thickness is reduced to zero for some stability $1 < S \leq 2$, and not $S = 1$ as implied by Turner, owing to the temperature increment at the bottom of the lower layer which has no counterpart in the solute profile. Thus this theory may be expected to give useful results only for $S \geq 2$.

It seems likely, then, that the change of behaviour shown in Turner's results at $S = 2$ is a result of the reduction to zero of the conducting layer depth at about that point. That being so, the sharp rise in heat and salt flows for $S < 2$ is accounted for by the initiation at $S \doteq 2$ of convection over the whole tank depth, instead of in separate layers. The stability parameter then no longer represents the state of the boundary between two layers, but merely relative readings at two depths in one convecting layer. The convection may be expected to equalize the temperatures, and also the concentrations, at the two levels quite rapidly, which would have been interpreted as increasingly high flow rates occurring for continuously decreasing S .

Appendix 5

Optics of the scanning schlieren system.

This study may be broken into two parts; an analysis of the deviation imposed on the light when it traverses the tank, which is a matter of ray optics, and a consideration of the maximum resolution which can be expected, which is determined by diffraction.

(a) Ray paths through the tank.

Fermat's principle states that

$$\delta \left\{ \int_A^B n \, ds \right\} = 0$$

where A and B are fixed end points of a family of possible ray paths, n is the local refractive index and ds is an element of ray path length. From this it may be shown (see for example, Kelso 1964) that

$$\frac{d}{ds} \left(n \frac{dx}{ds} \right) - \frac{\partial n}{\partial x} = 0, \quad (1)$$

with similar equations in y and z . Then, in a horizontally stratified medium in which

$$n = n(z)$$

with z vertical, it can be shown that any ray is confined to a vertical plane. If the light is incident normally on one of the glass walls of the tank, such a plane will be a cross section of the tank perpendicular to these walls. Let the x - direction be normal to the glass walls. Then from (1),

$$n \frac{dx}{ds} = n_0 \left(\frac{dx}{ds} \right)_0 = a, \text{ say,} \quad (2)$$

where a is a constant and the subscript zero refers to the plane $x = 0$.

Since the path is entirely in the (x, z) plane,

$$\left(\frac{dz}{dx} \right)^2 = \left(\frac{ds}{dx} \right)^2 - 1$$

and hence, from (2),

$$\left(\frac{dz}{dx}\right)^2 = \frac{n^2 - a^2}{a^2}$$

If the origin is chosen so that the ray is horizontal at $x = 0$,

$$\left(\frac{dz}{dx}\right)_0 = 1$$

and

$$a = n_0$$

Hence

$$\frac{dz}{dx} = \left(\frac{n^2}{n_0^2} - 1\right)^{\frac{1}{2}}$$

and

$$\frac{d^2z}{dx^2} = \frac{n}{n_0^2} \frac{\partial n}{\partial z}$$

Now the curvature ρ of the ray is given by

$$\begin{aligned} \rho &= \frac{d^2z}{dx^2} / \left\{ 1 + \left(\frac{dz}{dx}\right)^2 \right\}^{3/2} \\ &= \frac{n}{n_0^2} \frac{\partial n}{\partial z} \end{aligned} \quad (3)$$

To a first approximation, since the ray departs only slightly from the horizontal, we can write

$$n = n_0$$

so that

$$\rho = \frac{1}{n_0} \left(\frac{\partial n}{\partial z}\right)_0$$

In traversing the tank, the change in inclination of the ray is given by

$$\begin{aligned} \Delta \left(\frac{dz}{dx}\right) &\doteq X \rho \\ &= \frac{X}{n_0} \left(\frac{\partial n}{\partial z}\right)_0 \end{aligned} \quad (4)$$

where X is the distance between the vertical boundaries of the liquid. Refraction at these boundaries increases this deviation by a factor n_0 .

Hence, since the scanning schlieren system actually plots the deviation $\Delta \left(\frac{dz}{dx}\right)$ versus z , this represents $\left(\frac{\partial n}{\partial z}\right)_0$ versus z to a first approximation. In order to check the error introduced by assuming this to be exactly true, a second approximation may be

obtained to (4) by expanding n and $\frac{\partial n}{\partial z}$ in a Taylor series round $x = 0$, and recalling that

$$\left(\frac{dz}{dx}\right)_0 = 0$$

Then, neglecting higher-order terms,

$$n_x = n_0 \left\{ 1 + \frac{x^2}{2n_0^2} \left(\frac{\partial n}{\partial z}\right)_0^2 \right\}$$

and

$$\left(\frac{\partial n}{\partial z}\right)_x = \left(\frac{\partial n}{\partial z}\right)_0 \left\{ 1 + \frac{x^2}{2n_0^2} \left(\frac{\partial^2 n}{\partial z^2}\right)_0 \right\}$$

Substituting these values into (3),

$$\rho_x = \frac{1}{n_0} \left(\frac{\partial n}{\partial z}\right)_0 \left\{ 1 - \frac{x^2}{n_0^2} \left(\frac{\partial n}{\partial z}\right)_0^2 + \frac{x^2}{2n_0} \left(\frac{\partial^2 n}{\partial z^2}\right)_0 \right\}$$

Now

$$\Delta \left(\frac{dz}{dx}\right) = \int \rho ds, \text{ where the integration is taken over the whole path in the tank.}$$

$$= \int_0^X \rho dx, \text{ very nearly. (Here the fact that the system uses rays which are horizontal on exit from the tank has been used.)}$$

$$= \frac{x}{n_0} \left(\frac{\partial n}{\partial z}\right)_0 \left\{ 1 - \frac{x^2}{3n_0^2} \left(\left(\frac{\partial n}{\partial z}\right)_0^2 - \frac{n_0}{2} \left(\frac{\partial^2 n}{\partial z^2}\right)_0\right) \right\}$$

In practice $\left(\frac{\partial n}{\partial z}\right)_0^2 \ll n \frac{\partial^2 n}{\partial z^2}$, so the deviation is

$$\Delta \left(\frac{dz}{dx}\right) = \frac{x}{n_0} \left(\frac{\partial n}{\partial z}\right)_0 \left\{ 1 + \frac{x^2}{6n_0} \left(\frac{\partial^2 n}{\partial z^2}\right)_0 \right\}$$

Once again, the total deviation, including the effect of refraction at the vertical boundaries, is n_0 times this.

It may be seen that the error involved in assuming that the measured profiles directly indicate $\left(\frac{\partial n}{\partial z}\right)$ versus z , subject to some

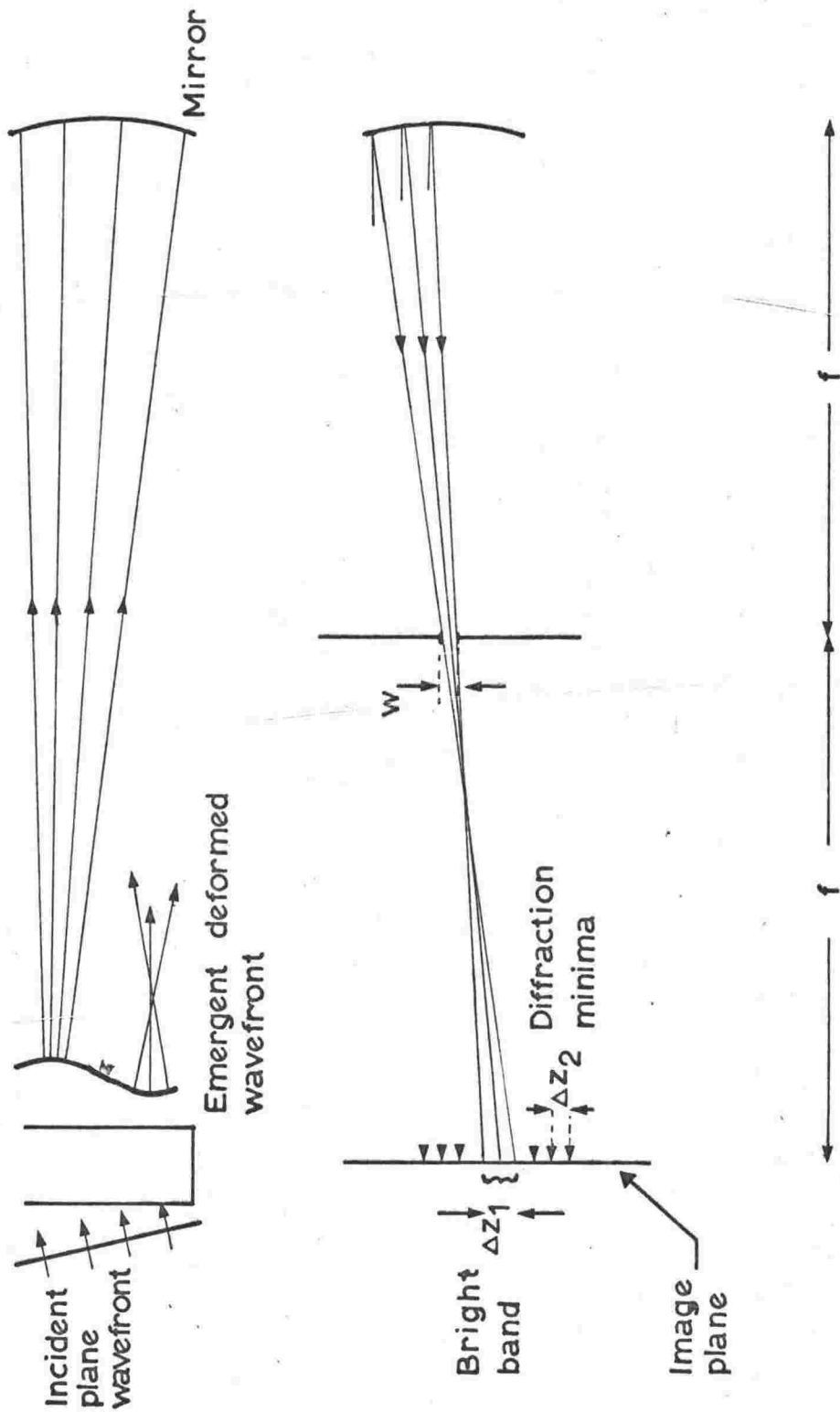


Fig. A7. Origin of diffraction effects.

gained from reducing w past the value for which $\Delta z_1 = 2 \Delta z_2$, since if w is smaller than this limit the bright band becomes just the central maximum of the diffraction pattern and increases in width as w diminishes.

The difference in angular deviation experienced in the tank by rays just passing the two sides of the slit is very nearly w/f , where f is the focal length of the concave mirror. The vertical separation of neighbouring levels in the tank leading to this difference in deviation is given by

$$\frac{w}{f} = \frac{X}{n} \frac{\partial^2 n}{\partial z^2} \Delta z_1$$

i.e.

$$\Delta z_1 = \frac{wn}{fX} \frac{\partial^2 n}{\partial z^2}$$

Also

$$\Delta z_2 = \frac{f \lambda}{w}$$

where λ is the wavelength of the light. Then the depth resolution is optimum when

$$\Delta z_1 = 2 \Delta z_2,$$

i.e. when

$$w = f \left(\frac{2 \lambda X}{n} \frac{\partial^2 n}{\partial z^2} \right)^{\frac{1}{2}}$$

Here the value of $\frac{\partial^2 n}{\partial z^2}$ is the maximum which may be encountered, since this gives the minimum Δz_1 for a particular w . The appropriate value is about 10^{-3} cm^{-2} , which corresponds to a slope of 1 pip cm^{-1} in the profile. This yields an optimum slit width of about 0.15 cm for a focal length f of 213 cm , and a corresponding value $\Delta z_2 = 0.07 \text{ cm}$.

Appendix 6Calibration of the optical system and determination of its accuracy.

For calibration the tank was filled with two layers of approximately equal depth, the upper one being fresh, air-free water and the lower one a solution of sugar in similar water. The strength of the sugar solution was about 5% by weight, characteristic of the solutions used in the experiments, and was accurately known. The fresh water was first put in the tank, and the solution was then poured very slowly through a tube having its outlet at the bottom of the tank. About 30 minutes were required to pour about 750 cm^3 of solution, and the resulting boundary between the two layers was very sharp.

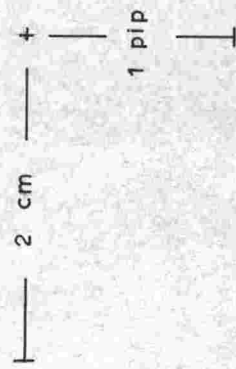
The refractive index gradient at the boundary of the two layers was initially too great for the equipment to record it. Useful records were obtained after about 20 hours, after which a recording of the profile was made at intervals, initially of about 12 hours, over a period of several days.

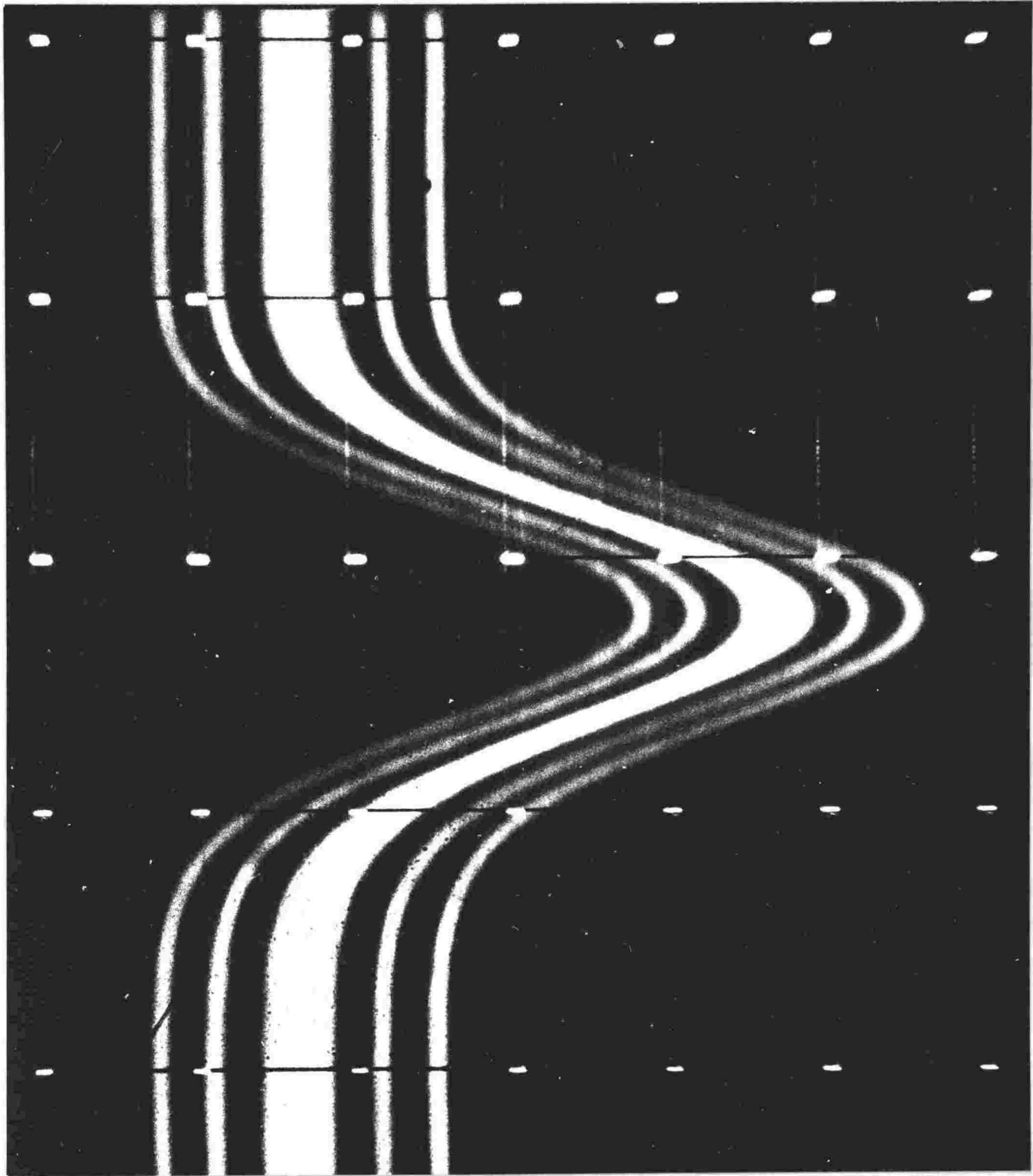
A typical recording of a profile is shown in fig. A8, each curve being a graph of refractive index gradient against depth. The top and bottom boundaries of the tank were impermeable to solute, so the refractive index gradient was zero there. Thus the base-line of zero refractive index gradient was simply the line joining the ends of the profile. Calibration involved comparing the area (expressed in "pip-cm" where a pip is the arbitrary unit of the profile) between the profile and the base line, with the known concentration difference between top and bottom of the tank. This necessitated recording the profile before the boundary concentrations had been significantly changed by diffusion.

Integration of the profile was accomplished by approximating the profile by a function and integrating the latter. Since the curve went to zero at both ends, a Fourier sine series was used, the fundamental wavelength being twice the total depth of the liquid. To calculate the coefficients for a series of $N-1$ harmonics, at least N coordinates equally spaced in depth had to be measured.

Fig. A8

Concentration gradient profile from a calibration run; the result of diffusion of a 4.4% aqueous sucrose solution into water for 18.5 hrs.





A large (10" x 8") print was made of each profile. This was placed in a framework attached to a lead screw which had divisions every 0.001 cm. The print was arranged so that the lead screw moved it parallel to the depth axis. A travelling microscope was then used to measure the coordinate perpendicular to this motion. For profiles recorded at the beginning of the series, up to 100 points on the curve were evaluated, but this was reduced to about 30 for later profiles in which the higher harmonics were negligible.

The calibration procedure was carried out four times, and showed that 1 pip on the profile was equivalent to a concentration gradient of 0.695 (percent by weight) per cm.

System errors.

Harmonic analysis of the profiles provided a convenient estimate of the random errors associated with the system. At the most, ten harmonics were required to represent a profile. At higher orders the amplitudes were not zero, however, but distributed as would be expected for white noise. That is, the amplitude of each harmonic appeared to fluctuate about zero in succeeding profiles, all harmonics having the same standard deviation. These amplitudes were presumably indicative of the noise in the system, that is, the random errors of measurement. In a series of ten consecutive profiles, the root-mean-square amplitude of the top ten harmonics was 0.0016 pips. This may be compared with the fundamental amplitude which was seldom less than 1.0 pips, so that the uncertainty in it due to random errors was about 0.2%. The integral under the profile had a similar uncertainty.

Another approach to the estimation of errors was to study the decay of individual harmonic amplitudes with time. Writing h for the depth of liquid in the tank and t for time, the k th harmonic should have decayed as $\exp(-k^2 \pi^2 Dt/h^2)$. Fig. A9 shows the decay of A_1 for the same series of profiles as mentioned in the last paragraph (other harmonics showed similar behaviour). It appears from this graph that the amplitude is liable to error within the limits ± 0.01 pips.

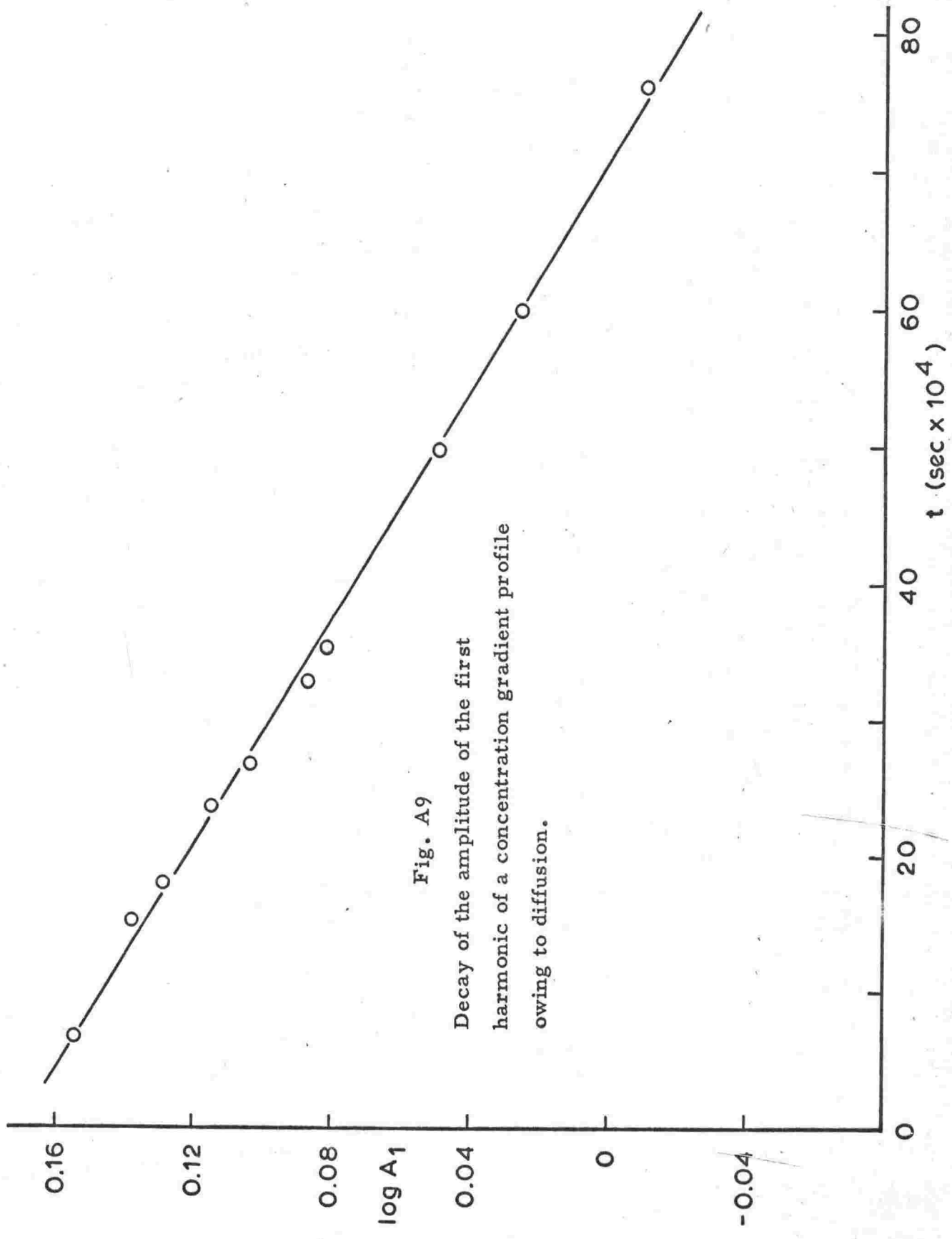


Fig. A9

Decay of the amplitude of the first harmonic of a concentration gradient profile owing to diffusion.

This is about twice the estimate of purely random errors if the limits of error are interpreted as three times the r.m.s. error. This increase is probably due to the fact that the errors in measurements of the coordinates of succeeding points on the profile tended to be correlated.

The slope of the line in fig. A9 should be $(-D k^2 \pi^2 \log e/h^2)$, indicating a value for D of $5.25 \times 10^{-6} \text{ cm}^2 \text{ sec}^{-1}$. This may be compared with the measurements of Gosting and Morris (1949) and of Irani and Adamson (1958), which both gave a value $5.226 \times 10^{-6} \text{ cm}^2 \text{ sec}^{-1}$ for very dilute solutions at 25°C .

Calibration errors.

In addition to the errors associated with the measuring system, inaccurate estimation of the concentration contrast between bottom and top of the tank would have introduced errors in calibration.

Uncertainty in the concentration of the solution which initially formed the lower layer in the tank was negligible at $\pm 0.1\%$. However the important quantity for calibration was the difference in concentration between top and bottom tank surfaces at the time when the profile was measured, and this would have been slightly less than the original concentration contrast owing to diffusion in the interim. By making the boundary between the layers as sharp as possible this change was reduced to a minimum, and the harmonic analysis of the profile provided a convenient check. Owing to the decay of individual harmonics with time, the area S under a profile was given by

$$S = (2h/\pi) \sum_{k=1,3,5,\dots} (A_{k0}/k) \exp(-\pi^2 k^2 Dt/h^2)$$

Hence

$$\frac{\partial S}{\partial t} = - (2\pi D/h) \sum k A_k$$

where A_{k0} is the amplitude of the k th harmonic at time zero. It was a simple matter, then, to check that $\frac{\partial S}{\partial t}$ was sufficiently close to zero for the boundary concentrations to be assumed equal to their initial values.

A minor problem was encountered when the tank was first filled. Because each of the two layers was initially homogeneous, only quite small temperature gradients sufficed to induce convection in them. As shown by the experiments of Turner (1965), considered in appendix 4, this would have transported solute across the boundary and distributed it throughout the upper layer. This would have reduced the concentration contrast, and hence the apparent sensitivity of the system. The effect was reduced to negligible proportions by thermostating the room containing the equipment.

Appendix 7

Analysis of results of stability experiments.

The input data for program UPHSO5f consisted mainly of two arrays. The first of these, g, contained the readings taken at N equally spaced points along the isothermal concentration gradient profile. The other input array, mV, contained readings of the out-of-balance voltage of the thermistor bridge every 45 seconds during the experiment. These readings were converted to temperatures T by the linear relationships found for the various bridge ranges during calibration.

After reading in this data, the program calculated the N-1 harmonic coefficients A_k , and the concentration at the bottom of the tank. For each specified time, the Rayleigh numbers were then calculated and printed for a series of levels between (Z=) 0.4 and 1.7 cm from the tank bottom. The thermal Rayleigh number R was calculated from the sequence of temperatures measured at Z = 0. The temperature θ at Z at time t is given by (Carslaw and Jaeger, 1959)

$$\theta = \frac{Z}{2(\pi K)^{1/2}} \int_0^t T(\lambda) \frac{\exp\left(-\frac{Z^2}{4K(t-\lambda)}\right)}{(t-\lambda)^{3/2}} d\lambda$$

where T is the temperature at Z = 0. In order to calculate the integral with sufficient accuracy, the readings of T were interpolated linearly to intervals of 4.5 seconds when $Z \leq 1.5$ cm.

A typical printout is shown in fig. A10. The first column shows that the results apply to the time 187×45 seconds after the start of the temperature record, and the second column gives the corresponding temperature T. The fourth and fifth columns contain respectively the temperature θ and the concentration (in pip-cm) at the level given in the third column. The remaining three columns contain R, $-R_g$ and $(R + 0.88 R_g)$ respectively.

UPHSO5f ;

```
begin real c0,conc,Z,IF,scale,grav,alpha,beta,gamma,chi,temp,time,t,D,K,Knu,R,Rs,T,q,g1 ;
integer n,k,N,p,m,q,r,L,curvemax,range ;
array A[1:100],G[1:200],g[1:200],T[1:300],mv[1:300];
integer array curve[1:5],title[1:15] ;
m:=1;
instring(title,m) ;
read N,scale,D,time,chi,p,t,conc,gamma,grav,range,curvemax ;
for n:=1 step 1 until curvemax do read curve[n];
G[1]:= G[N+1]:= 0;
read g1;
for n:=2 step 1 until N do
begin read g[n] ;
G[n]:=(g[n]-g1)/scale ;
G[2*N+2-n]:=-G[n]
end ;
for n:=1 step 1 until p do
begin read mv[n];
if n>2 then begin if abs(mv[n]-mv[n-1])>1.0 then range:=range+1 end;
if range= 6 then T[n]:= 17.135 + .823*mv[n] else
if range= 7 then T[n]:= 19.66 + .842*mv[n] else
if range= 8 then T[n]:= 22.44 + .864*mv[n] else
if range= 9 then T[n]:= 25.51 + .888*mv[n] else
if range=10 then T[n]:= 28.24 + .907*mv[n] else
if range=11 then T[n]:= 31.255 + .932*mv[n] else
if range=12 then T[n]:= 34.56 + .984*mv[n]
end;
for n:=1 step 1 until 100 do A[n]:=0 ;
for k:=1 step 1 until N-1 do
begin for n:=1 step 1 until 2*N do A[k]:=A[k]+G[n]*sin(3.14159*(n-1)*k/N)/N ;
A[k]:=A[k]*exp(-D*9.8696*time*k12/93.509)
end ;
c0:=0 ;
for k:=1 step 1 until N-1 do
c0:=c0+chi*9.67*A[k]/(3.14159*k) ;
c0:=c0+conc ;
beta:= chi*(0.389 + 0.055*c0) ;
lineprinter; topofform;
m:=1 ;
outstring(title,m);
```

```

print  $\epsilon$ 1?concentration is ?, sameline, freepoint(5), c0,  $\epsilon$ 1s2?m $\epsilon$ s7?Tmfs7?depthfs6?tempfs6?IF?,
 $\epsilon$ 1s10?R $\epsilon$ s13?R $\epsilon$ s11?Re $\epsilon$ L2??;
for q:=1 step 1 until curvemax do
begin
m:=curve[q];
Tq:=T[m];
K:=0.00135*(1+0.00309*Tq-0.214*c0);
Knu:=0.000605*(1+0.00337*Tq-0.601*c0+22.8*c0*c0)/(25+Tq);
alpha:=(-6.674+77.65*c0+178.6*c0*c0+(1.758+0.168*c0-59.36*c0*c0)*Tq
-(0.02316+0.1185*c0-3.237*c0*c0)*Tq*Tq+(1.875+19.45*c0-491.9*c0*c0)*Tq*Tq*Tq*c0-5;
print  $\epsilon$ 1L2??;
for Z:=0.4 step 0.1 until 1.71 do
begin
temp:=0;
if Z<1.51 then for n:=1 step 1 until m-1 do
begin
if n=m-1 then L:=9 else L:=10;
for r:=1 step 1 until L do temp:=temp+(T[n+1]*r/10+T[n]*(1-(r/10))-T[1])*t
*exp(-Z*r/(4*K*t**(m-n-r/10)))/(10*(t**(m-n-r/10))11.5)
end
else
for n:=2 step 1 until (m-1) do temp:=temp+(T[n]-T[1])*exp(-Z12/(4*K*t**(m-n)))
/(((m-n)11.5)*sqrt(t));
temp:=T[1]+Z*temp/(2*sqrt(3.14159*K));
R:=(grav*alpha*(T[m]-temp)*Z13/Knu);
IF:=0;
for k:=1 step 1 until N-1 do IF:=IF+9.67*A[k]*(1-cos(3.14159*Z*k/9.67))/(k*3.14159);
Rs:=(grav*beta*IF*Z13/Knu);
print digits(3),n,prefix( $\epsilon$ 1s4??),freepoint(4),T[m],Z,temp,IF,scaled(4),R,Rs,(R-gamma*Rs)
end
end;
restart
end
end;

```

TWENTY OCTOBER
 CONCENTRATION IS
 M DEPTH .04562
 TM

			TEMP	IF	R	RS	RE
187	21.35	.4000	20.81	.0103	5.709#02	1.247#02	4.611#02
187	21.35	.5000	20.69	.0166	1.372#03	3.931#02	1.026#03
187	21.35	.6000	20.57	.0247	2.807#03	1.015#03	1.914#03
187	21.35	.7000	20.45	.0350	5.130#03	2.283#03	3.121#03
187	21.35	.8000	20.33	.0477	8.635#03	4.639#03	4.553#03
187	21.35	.9000	20.22	.0629	1.365#04	8.710#03	5.983#03
187	21.35	1.000	20.11	.0808	2.053#04	1.535#04	7.016#03
187	21.35	1.100	20.00	.1016	2.965#04	2.568#04	7.053#03
187	21.35	1.200	19.90	.1253	4.144#04	4.113#04	5.248#03
187	21.35	1.300	19.80	.1521	5.633#04	6.348#04	4.699#02
187	21.35	1.400	19.70	.1820	7.477#04	9.490#04	-8.736#03
187	21.35	1.500	19.61	.2152	9.724#04	1.380#05	-2.418#04
187	21.35	1.600	19.52	.2516	1.242#05	1.958#05	-4.808#04

Fig.A10
 Typical print-out from program UPHS05

Appendix 8Numerical model of layered thermosolutal convection(a) Program UPHS06b.

This version of the model represented the tank experiments. The program is shown below and has been described in Chapter 5. The first two pages are concerned with setting up sub-routines, reading in the relevant starting data, and calculating the concentration profile. The third page contains the starting and running solutions of the diffusion equation which enable calculation of successive temperature and concentration profiles. The remainder of the program contains the logic necessary to search the profiles for layers which are potentially unstable, to decide whether the criterion for marginal stability has been surpassed, and if so to re-assign the diffusion constants for heat and solute.

The forms of the starting and running solutions are shown in fig. A11. The boundary conditions imposed on temperature (θ) and concentration (C) were similar for both solutions:

Upper boundary (j = jmax)

$$C_{j_{\max}} = C_{j_{\max}-1} \text{ (starting)} = C_{j_{\max}-2} \text{ (running)}$$

$$\theta_{j_{\max}} = \text{constant} = \theta_h.$$

Lower boundary (j = 0)

$$C_0 = C_1 \text{ (starting)} = C_2 \text{ (running)}.$$

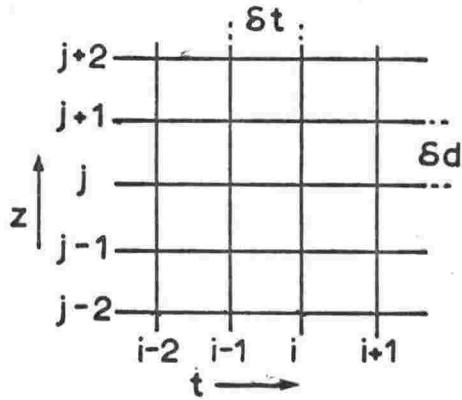
$$\theta_0 = \theta_h + (\text{lin})t + (\text{sq})t^2 + (\text{cu})t^3$$

where t is time, and θ_h is room temperature.

Note that the running solution uses alternate mesh points only. Both the current and immediate past profiles were therefore stored in one one-dimensional array. The stability test was made after each pair of time increments.

Provided the diffusion constant does not vary, it can be shown (see, for example, Du Fort and Frankel, 1953) that the running solution is stable for all values of $\lambda' \text{ Km}$. Experimentally, variation of K with

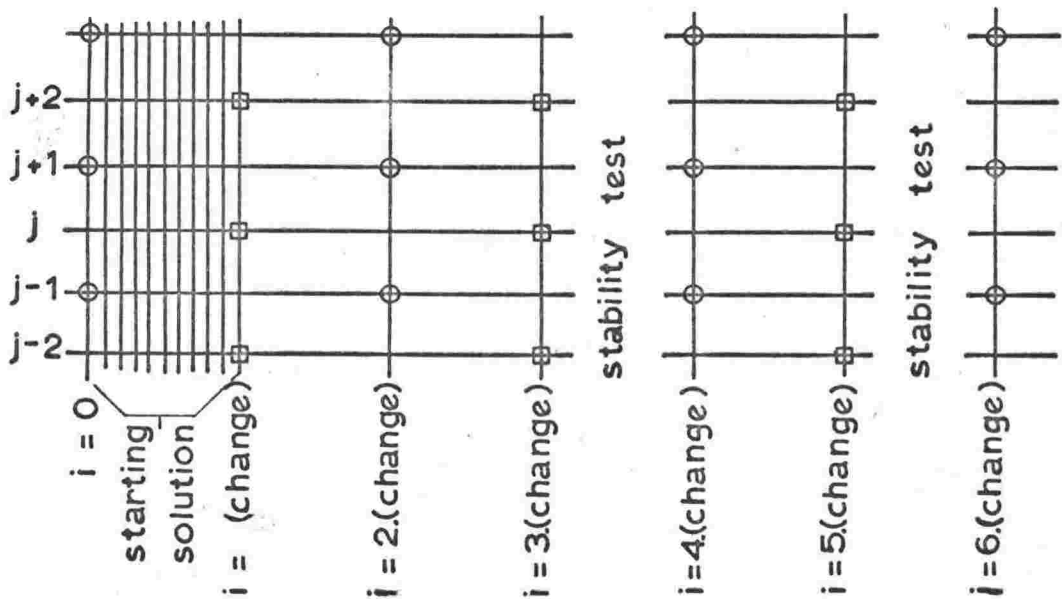
Starting solution



$$\theta_{i,j} = \theta_{i-1,j} + \frac{\lambda}{2} \{K_j(\theta_{i-1,j+1} - \theta_{i-1,j}) - K_{j-1}(\theta_{i-1,j} - \theta_{i-1,j-1})\}$$

$$\lambda = 2\delta t / (\delta d)^2$$

Running solution



$$\theta_{i,j} = \frac{\theta_{i-2,j}(1 - \lambda'K_m) + (\theta_{i-1,j+1}K_j + \theta_{i-1,j-1}K_{j-1})\lambda'}{1 + \lambda'K_m}$$

$$\lambda' = \lambda (\text{change})$$

$$K_m = \frac{K_j + K_{j-1}}{2}$$

Fig. All. Starting and running solutions in the numerical model of layered convection.

space and with time simultaneously led to some instability, although the problem was not serious in this version of the program where the mesh size could be kept small. It was found quite adequate to limit the rate at which the diffusion constant could grow, by assigning new values in the manner shown on the fifth page of the program. Instead of using the new value actually calculated (i.e. K_{mod} or D_{mod}) a mean was taken between this and the previous value, heavily weighted in favour of the latter. Note that once the running solution was established, the arrays "thetai" and "conci" contained the immediate past values of K and D ; they were used initially to store the input profiles of temperature and concentration for use in setting up the running solution.

(b) Program UPHS06C.

This version was basically similar to the previous one, with certain necessary modifications to the input data and the running solution to represent Lake Vanda instead of the tank experiments. Apart from the differences mentioned in Chapter 5, there were three main changes in this version:

- (i) Since this physical situation was one in which convection from time to time decayed back to conduction, in addition to the more usual case of convection developing from conduction, the method of assigning K and D had to be altered slightly. The change allowed the averaging process to occur whether the diffusion constant was increasing or decreasing.
- (ii) As pointed out in Chapter 5, the heat equation now contained a source term. If the running solution is considered for the special case of an initially isothermal medium of infinite extent, it is easy to see that the increase of temperature will not be described correctly by including the source term in the difference equation. This comes about through the use of the last two profiles in deducing the next one. The

second of these contains higher temperatures than the first due to the source term, and this increase is extrapolated to the new profile, which would therefore contain higher temperatures than the second even if the source term were now omitted; addition of the source term increment therefore magnifies the rate of increase and produces instability.

This problem was overcome by adding the source term increment separately. After each pair of profile calculations, the appropriate increment was added to every term, the older of the two profiles receiving the same increment as the younger (except that the increment was a function of depth).

- (iii) In order to reduce the time needed for a run, this version of the program had to be operated with a rather large mesh spacing. This aggravated the stability problems. The solution seemed to be most unstable to an error which took the form of a wave on the profile. In order to damp this wave, temperatures at $(j + 2)$ and $(j - 2)$ were introduced into the solution for (j) , in addition to those at $(j + 1)$ and $(j - 1)$ which were already included. To do this $\theta_{i-2,j}$ was replaced by

$$0.05 (\theta_{i-2, j+2} + \theta_{i-2, j-2}) + 0.90 \theta_{i-2, j}$$

except near $j = 0$ where the original form was retained. The solution for the concentration profile received the same treatment.

```

begin comment layer formation in non-radiative case with isothermal start. Given bottom temperatures.
Top boundary constant temperature;
real c, depth, deltat, time, deltat, sigma, grav, nu, beta, Re1, Re2, Re3, Rec, t, th, thd1, thd2,
thetaconv, chd1, chd2, conconv, lambda, Kcond, Kmean, Dcond, Dmean, Dmod, Dmod, lin, sq, cu, g1,
scale, c0, cav ;
integer i, ipmax, imax, inext, j, jmax, jl, ju, change, k, l, m, n, p, q, r ;
array theta[0:499], conc[0:499], K[0:499], D[0:499], thetai[0:499], conc1[0:499], AA[1:30], GG[1:60],
g[1:60];
integer array iprint[1:20] ;
switch ss:=A,B,C,E,F,G,X ;
real procedure alpha(u) ;
value u ;
integer u ;
begin c:=conc[u] ;
t:=theta[u] ;
alpha:=(-6.6739+77.645*c+178.58*c*c
+(1.7577 +0.168*c -59.36*c*c)*t
-(0.023157 +0.11852*c-3.2368*c*c)*t*t
+(0.0001875 +0.0019453*c-0.04919*c*c)*t*t*t)*10-5
end;
procedure printemps ;
begin print f$12??, digits(6), i, sameline, f$S?time steps, total time?, scaled(4), deltat*i,
f$S?sec f$L?? ;
for q:=0 step 20 until 20*(jmaxdiv20) do
begin print f$12?? ;
prefix(f$S2??) ;
print freepoint(3), deltat*q/100, f$S?metres f$2?? ;
for p:=0, p+2 while p<18 and (q+p) <= jmax do print freepoint(5), theta[q+p] ;
print f$1S16?? ;
for p:=0, p+2 while p<18 and (q+p) <= jmax do print freepoint(5), conc[q+p] ;
print f$1S16?? ;
for p:=0, p+2 while p<18 and (q+p) <= jmax do print freepoint(5), K[q+p] ;
print f$1S16?? ;
for p:=0, p+2 while p<18 and (q+p) <= jmax-2 do print freepoint(5),
100*((alpha(q+p)+alpha(q+p+2))*(theta[q+p]-theta[q+p+2])/2
- beta*(conc[q+p]-conc[q+p+2]));
print f$12?? ;
end
end ;

```

```

real procedure gradient(w) ;
  value w ;
  integer w ;
  gradient:=(alpha(w)+alpha(w+2))*(theta[w]-theta[w+2])/2 -sigma*beta*(conc[w]-conc[w+2]) ;
real procedure Re(x,y) ;
  value x,y ;
  integer x,y ;
  Re:=grav*((alpha(x)+alpha(y))/2)*(theta[x]-theta[y])-checkr(sigma*beta*(conc[x]-conc[y])) ;
  *(deltad*(y-x))1/3/(Kcond*0.225*((1+3*conc[x])/(25+theta[x])+(1+3*conc[y])/(25+theta[y]))) ;
read depth,deltad,time,deltat,ipmax,change,grav,sigma,beta,Rec,Kcond,lin,sq,cu,N,scale,c0 ;
lineprinter ;
topoform ;
imax:=checki(entier(time / deltat)) ;
jmax:=entier(depth / deltat) ;
inext:=1 ;
lambda:=2*deltat/(deltad)1/2 ;
read th ;
GG[1]:= GG[N+1]:= 0 ;
read g1 ;
for n:= 2 step 1 until N do
begin read g[n] ;
  GG[n]:= (g[n] - g1)/scale ;
  GG[2*N + 2 - n]:= -GG[n]
end ;
for n:= 1 step 1 until 30 do AA[n]:= 0 ;
for k:= 1 step 1 until N-1 do for n:= 1 step 1 until 2*N do
  AA[k]:= AA[k] + GG[n]*sin(3.14159*(n-1)*k/N)/N ;
for j:=0 step 1 until jmax do
begin thetai[j]:=theta[j]:=th ;
  conc[j]:= 0 ;
  for k:= 1 step 1 until N-1 do
    conc[j]:= conc[j]-0.00705*9.67*AA[k]*(1-cos(3.14159*j*deltad*k/9.67))/(k*3.14159) ;
  K[j]:=Kcond ;
  D[j]:=Dcond
end ;
cav:= 0 ;
for j:= 0 step 1 until jmax do cav:= cav+conci[j]/(jmax+1) ;
for j:= 0 step 1 until jmax do conc[j]:= conc[j]-cav+c0 ;

```

```

for i:=1 step 1 until change, 2*change step change until imax do
begin if checki(i) < change then
begin checks(ε11?) ;
for j:=1 step 1 until jmax-1 do
begin thd2:=theta[j] + lambda*(K[j]*(theta[j+1]-theta[j]) - K[j-1]*(theta[j]-
theta[j-1]))/2 ;
chd2:=conc[j]+lambda*(D[j]*(conc[j+1]-conc[j]) - D[j-1]*(conc[j]-conc[j-1]))/2 ;
if j>1 then
begin theta[j-1]:=checkr(thd1) ;
conc[j-1]:=chd1
end else
begin theta[0]:=checkr(th+lin*i*deltat+sq*(i*deltat)^2 + cu*(i*deltat)^3) ;
conc[0]:=chd2
end ;
thd1:=thd2 ;
chd1:=chd2
end ;
theta[jmax]:=th ;
theta[jmax-1]:=thd2 ;
conc[jmax]:=conc[jmax-1]:=chd2 ;
if i=change then for j:=1 step 2 until jmax-1 do theta[j]:=thetai[j]
end else
begin checks(ε12?) ;
r:=1 ;
for j:=r step 2 until jmax-1 do
begin Kmean:=(K[j]+K[j-1])/2 ;
Dmean:=(D[j]+D[j-1])/2 ;
theta[j]:=(theta[j]*(1-change*lambda*Kmean) + (theta[j+1]*K[j]+theta[j-1]*K[j-1])
*change*lambda)/(1+change*lambda*Kmean) ;
conc[j]:=(conc[j]*(1-change*lambda*Dmean) + (conc[j+1]*D[j]+conc[j-1]*D[j-1])
*change*lambda)/(1+change*lambda*Dmean)
end ;
if r=1 then
begin i:=i+change ;
r:=2 ;
goto X
end ;
theta[0]:=checkr(th + lin*i*deltat + sq*(i*deltat)^2 + cu*(i*deltat)^3) ;
theta[jmax]:=th ;

```

```

end ;
  if i > change then for j:=0 step 1 until jmax-1 do
  begin
    thetai[j] := K[j];
    concil[j] := D[j];
    K[j]:= Kcond;
    D[j]:= Dcond
  end;
  for j:=0 step 2 until jmax-4 do
  begin if checkr(gradient(j)) > 0 then
    begin l:=jl:=j;
      A:  l:=l+2;
        if gradient(l) > 0 and l < jmax-2 then goto A else
          begin m:=n:=0;
            ju:=checki(l);
            Re1:=checkr(Re(jl,ju));
            checks(EB?);
            if ju=jmax then
              begin Re2:=Re1-1;
                n:=1;
                goto C
              end ;
            Re2:=Re(jl,ju+2);
            if Re1 < Re2 then
              begin checks(EC?);
                if n=2 then
                  begin Re1:=Re2+1;
                    n:=1;
                    ju:=ju+2;
                    goto C
                  end else
                    begin ju:=ju+2;
                      n:=1;
                      goto B
                    end
                end else
                  begin if n#1 and ju-ju+1>2 then
                    begin ju:=ju-2;
                      n:=2;
                      goto B
                    end else if jl=0 then goto G else

```



```
end ;  
if i>imax then  
begin printemps ;  
stop  
end ;  
if i>iprint[inext] then  
begin printemps ;  
inext:=inext+1  
end  
  
end  
end ;
```

```

begin comment layer formation in radiative case with two-layer start;
  real c,c2, depth, deltat, eta, Q, time, deltat, sigma, grav, nu, beta, Re1, Re2, Re3, Rec, t, t2,
  thd1, thd2, thetaconv, chd1, chd2, conconv, lambda, Kcond, Dcond, Kmean, Dmean, Kmod, Dmod,
  botflo, oldepth, oldtemp, oldconc, shift, alph, alph2, toth, totc ;
  integer h, i, ipmax, imax, inext, j, jmid, jmax, jl, ju, change, l, m, n, p, q, r, s ;
  array theta[0:499], conc[0:499], K[0:499], D[0:499], thetai[0:499], conc1[0:499], radiant[0:499];
  integer array iprint[1:20] ;
  switch ss:=A,B,C,E,F,G,X ;
  procedure printemps ;
    begin print EL2??, digits(6), i, sameline, EL2time steps, total time?, scaled(4), deltat*i,
      EL2sec ie ?, deltat*i/(365.25*86400), EL2years EL?? ;
    for q:=0 step 20 until 20*(jmaxdiv20) do
      begin print EL2?? ;
        prefix(EL2??) ;
        print freepoint(3), deltat*q/100, EL2metres EL2?? ;
        for p:=0, p+2 while p<18 and (q+p) <= jmax do print freepoint(5), theta[q+p] ;
        print EL216?? ;
        for p:=0, p+2 while p<18 and (q+p) <= jmax do print freepoint(5), conc[q+p] ;
        print EL216?? ;
        for p:=0, p+2 while p<18 and (q+p) <= jmax do print freepoint(5), K[q+p] ;
        print EL2?? ;
      end
    end ;
  real procedure gradient(w) ;
  value w ;
  integer w ;
  begin c:= conc[w] ;
    c2:= conc[w+2] ;
    t := theta[w] ;
    t2:= theta[w+2] ;
    alph:= (-6.1832+ 1.5903*(t+c*shift)- 0.01256*(t+c*shift)12)*10-5 ;
    alph2:= (-6.1832+ 1.5903*(t2+c2*shift)- 0.01256*(t2+c2*shift)12)*10-5 ;
    gradient:=(alph+alph2)*(t-t2)/2 -sigma*beta*(c-c2)
  end ;

```

```

real procedure Re(x,y) ;
  value x,y ;
  integer x,y ;
  begin c:=conc[x];
  c2:=conc[y];
  t := theta[x];
  t2:= theta[y];
  alpha:= (-6.1832+ 1.5903*(t+c*shift) - 0.01256*(t+c*shift) t2)*10-5;
  alpha2:=(-6.1832+ 1.5903*(t2+c2*shift)-0.01256*(t2+c2*shift) t2)*10-5;
  Re:=grav*(((alpha+alpha2)/2)*(t-t2)-checkr(sigma*beta*(c-c2)))*(deltad*(y-x) t3/
  (Kcond*0.229*((1+1.3*c+10.0*c f2)/(26+t) +(1+1.3*c2+10.0*c2 t2)/(26+t2))))
  end;
read depth,oldepth, oldtemp, oldconc, eta, Q, deltat,time,deltat,ipmax,change,grav,sigma,beta,
Rec,Kcond,Dcond,shift,botflo ;
lineprinter ;
topoform ;
imax:=checki(entier(time / deltat)) ;
jmax:=entier(depth / deltat) ;
inext:=1 ;
lambda:=2*deltat/(deltat) t2 ;
botflo:= botflo + Q*exp(-eta*deltad*jmax) ;
for j:= 0 step 1 until jmax do radiant[j]:= 2.0*eta*Q*deltat*exp(-eta*deltad*(jmax-j)) ;
jmid:= entier(oldepth/deltad) ;
for j:=0 step 1 until jmid do
begin thetai[j]:=theta[j]:=oldtemp*(1-exp(-0.001*(jmid-j)*deltad)) ;
conc[j]:=conci[j]:=oldconc*exp(-10.5*10-7 *(deltad*j) t2) ;
K[j]:=Kcond ;
D[j]:=Dcond
end ;
for j:= jmid +1 step 1 until jmax+1 do
begin thetai[j]:= theta[j]:= 0 ;
conci[j] := conc[j] := 0 ;
K[j]:= Kcond ;
D[j]:= Dcond
end ;
for ni:=1 step 1 until ipmax do read iprint[n] ;

```

```

begin if checki(i) < change then
  begin checks (£I1?) ;
  for j:=1 step 1 until jmax-1 do
    begin thd2:=theta[j] +0.5* lambda*(K[j]*(theta[j+1]-theta[j]) -K[j-1]*(theta[j]-
      theta[j-1])) ;
    chd2:=conc[j]+lambda*(D[j]*(conc[j+1]-conc[j]) -D[j-1]*(conc[j]-conc[j-1]))/2 ;
    if j>1 then
      begin theta[j-1]:=checkr(thd1) ;
      conc[j-1]:=chd1 ;
    end else
      begin theta[0]:=checkr(thd2) ;
      conc[0]:=chd2 ;
    end ;
    thd1:=thd2 ;
    chd1:=chd2 ;
  end ;
  theta[0]:= checkr(theta[1]+deltad*botflo/K[0]) ;
  theta[jmax]:=0 ;
  theta[jmax-1]:=thd2 ;
  conc[jmax]:=conc[jmax-1]:=chd2 ;
  if i-change then for j:=1 step 2 until jmax-1 do theta[j]:=theta[i[j] ;
  end else
  begin checks (£I2?) ;
  r:=s:=1 ;
  for j:=r step 2 until jmax-1 do
    begin Kmean:=(K[j]+K[j-1])/2 ;
    Dmean:=(D[j]+D[j-1])/2 ;
    theta[j]:=((s-1)*0.05*(theta[j+2]+theta[j-s])+(0.90+0.1*(2-s))*theta[j])*
      /(1+change*lambda*Kmean)+(theta[j+1]+theta[j-1])*change*lambda*Kmean)
    conc[j]:=((s-1)*0.05*(conc[j+2]+conc[j-s])+(0.90+0.1*(2-s))*conc[j])
      *(1-change*lambda*Dmean)+(conc[j+1]+conc[j-1])*change*lambda*Dmean)
      /(1+change*lambda*Dmean) ;
    s:=2 ;
  end ;
  if r=1 then
    begin i:=i+change ;
    r:=2 ;
    goto x
  end ;

```

```

for j:=1 step 1 until jmax-1 do theta[j]:=theta[j]+2*change*radiant[j]
  /(1+change*lambda*(K[j]+K[j-1])/2) ;
theta[0]:=theta[2]+2*deltad*botflo/K[0] ;
theta[jmax]:=theta[jmax+1]:=0 ;
conc[0]:=conc[2] ;
conc[jmax+1]:=conc[jmax]:=conc[jmax-2] ;

end ;
if i>change then for j:=0 step 1 until jmax-1 do
  begin
    thtai[j] := K[j] ;
    conc[i][j] := D[j] ;
    K[j] := (Kcond+K[j])/2 ;
    D[j] := (Dcond+D[j])/2 ;

  end ;
if i > change then for j:=10 step 2 until jmax-4 do
  begin
    if checkr(gradient(j)) > 0 then
      begin
        l:=j+1 ;
        A:
        if gradient(1) > 0 and 1 < jmax-2 then goto A else
          begin
            m:=n:=0 ;
            ju:=checki(1) ;
            Re1:=checkr(Re(jl,ju)) ;
            checks(EB?) ;
            if ju=jmax then
              begin
                Re2:=Re1-1 ;
                n:=1 ;
                goto C
              end ;
            Re2:=Re(jl,ju+2) ;
            if Re1 < Re2 then
              begin
                checks(FC?) ;
                if n=2 then
                  begin
                    Re1:=Re2+1 ;
                    n:=1 ;
                    ju:=ju+2 ;
                    goto C
                  end
                else
                  begin
                    ju:=ju+2 ;
                    n:=1 ;
                    goto B
                  end
                end
              end
            end
  end

```

```

end else
begin if n#1 and ju-jl>2 then
begin ju:=ju-2 ;
n:=2 ;
goto B
end else if jl=0 then goto G else
begin n:=0 ;
Re1:=checkr(Re(jl,ju)) ;
checks(£E?) ;
if ju-jl=2 then begin Re3:=Re1-1 ;
checks(£F?) ;
goto F
end else Re3:=Re(jl+2,ju) ;
checks(£F?) ;
if Re1 < Re3 then
begin if n=2 then
begin Re1:=Re3 +1 ;
n:=1 ;
jl:=jl+2 ;
checks(£F?) ;
goto F
end else
begin jl:=jl+2 ;
n:=1 ;
goto E
end
end else
begin if n=1 or jl=0 then goto G else
begin jl:=jl-2 ;
n:=2 ;
goto E
end
end ;
m:=m+1 ;
checks(£G?) ;
j:=ju-2 ;
if Re1 > Rec then
begin Kmod:= Kcond*(1+0.72*(Re1/Rec)†0.3333*(1-(Rec/Re1))) ;
Dmod:= Kmod*Dcond/Kcond ;
for l:=jl step 1 until ju-1 do

```

```

begin K[1]:= (Kmod + thetai[1])/2 ;
D[1]:= (Dmod + conc[1])/2
end ;
totc:= totc+ 0 ;
for l:= j1 step 2 until ju do
begin toth:= toth+theta[1] ;
totc:= totc+conc[1]
end ;
totc:= 2*totc/(ju-jl+2) ;
totc:= 2*totc/(ju-jl+2) ;
for l:= j1 step 1 until ju do
begin theta[1]:= toth ;
conc[1] := totc
end
end
end
end
theta[jmax] := 0 ;
if i>imax then
begin printemps ;
stop
end ;
if i>iprint[inext] then
begin printemps ;
inext:=inext+1
end
end
end
end ;

```

Acknowledgements.

This project began with an expedition to Lake Bonney (VUWAE7), and it is a pleasure to express my gratitude to the other members of that team, R.F. Benseman and K.B. Popplewell, for their energetic assistance both in preparation and in execution of the task. (In particular, I am grateful to the latter for making the measurements of chloride concentration.) The opportunity to mount the expedition was due to Prof. R.H. Clark, without whose initiative VUW Antarctic field work would not have been possible. I am grateful to him, and also to the other VUW personnel who have been concerned with the Victoria Land lakes, and with whom I have had many useful and stimulating discussions; particularly Prof. A.T. Wilson, Prof. H.W. Wellman and Dr R.A. Hoare. To Dr Hoare I am indebted also for the unpublished data concerning Lake Joyce. The bathymetric measurements of February 1964 were made by A. Heine.

With regard to the work on convection, I am grateful to Dr D. Nield for a number of helpful discussions, and previews of his publications, concerning the theory of thermosolutal convection. I wish to acknowledge also the patience with which Dr R.B. Payne assisted a tyro programmer to overcome the difficulties of machine computation.

Thanks are due to Prof. D.A. Christoffel for the interest he has maintained in the whole project, while allowing his student considerable freedom in the manner of its prosecution.

I am grateful to the NZ University Grants Committee and the VUW Internal Research Committee for financial assistance; to the Physics and Engineering Laboratory, D.S.I.R., for technical assistance (including the measurements of density and conductance for Lake Bonney water samples); and to Antarctic Division of D.S.I.R., the Royal New Zealand Navy, the U.S. Navy and U.S.A.R.P. personnel for logistic support.

Finally, I would like to record my gratitude to my wife, without whose sympathetic encouragement this work would not have reached completion.

References

- Angino, E.E., K.B. Armitage and J.C. Tash (1962) Chemical stratification in Lake Fryxell, Victoria Land, Antarctica. Science 138 (3536) 34-36.
- Angino, E.E., and K.B. Armitage (1963) A geochemical study of Lakes Bonney and Vanda, Victoria Land, Antarctica. J. Geol. 71 (1) 89-95.
- Angino, E.E., K.B. Armitage and J.C. Tash (1964) Physicochemical limnology of Lake Bonney, Antarctica. Limnol. Oceanog. 9 (2) 207-217.
- Armitage, K.B., and H.B. House (1962) A limnological reconnaissance in the area of McMurdo Sound, Antarctica. Limnol. Oceanog. 7 (1) 36-41.
- Batchelor, G.K. (1954) Heat convection and buoyancy effects in fluids. Quart. J. Roy. Meteorol. Soc. 80 339-358.
- Bell, R.A.I. (1967) Lake Miers, South Victoria Land, Antarctica. N.Z.J. Geol. Geophys. 10 (2) 540-556.
- Bénard, H. (1900a) Étude expérimentale du mouvement des liquides propagent de la chaleur par convection. Régime permanent: tourbillons cellulaires. Compt. Rend. 130 1004-1007.
- Bénard, H. (1900b) Mouvements tourbillonnaires a structure cellulaire. Étude optique de la surface libre. Compt. Rend. 130 1065-1068.
- Bénard, H. (1900c) Tourbillons cellulaire dans une nappe liquide. Rev. Gen. Sci. Pures Appl. 11 1261-1271 and 1309-1328.
- Bénard, H. (1901a) Tourbillons cellulaires dans une nappe liquide. J. Phys. Radium 10 254-266.
- Bénard, H. (1901b) Les tourbillons cellulaires dans une nappe liquide transportant de la chaleur par convection en régime permanent. Ann. Chim. Phys. 23 62-144.
- Bolt, B.A. (1960) The revision of earthquake epicentres, focal depths and origin-times using a high-speed computer. Geophys. J. 3 (4) 433-440.
- Bousinesq, J. (1903) Théorie analytique de la chaleur. Paris, Gauthier-Villars.
- Carslaw, H.S. and J.C. Jaeger (1959) Conduction of heat in solids. Oxford, Clarendon Press, 2nd ed.
- Chandrasekhar, S. (1952) On the inhibition of convection by a magnetic field. Phil. Mag. 43 501-532.

- Chandrasekhar, S. (1956) The instability of a layer of fluid heated below and subject to the simultaneous action of a magnetic field and rotation. Proc. Roy. Soc. (London) A 237 476-484.
- Chandrasekhar, S. (1961) Hydrodynamic and hydromagnetic stability. Oxford, Clarendon Press.
- Chandrasekhar, S., and D.D. Elbert (1955) The instability of a layer of fluid heated below and subject to Coriolis forces. Proc. Roy. Soc. (London) A 231 198-210.
- Crank, J. (1957) The mathematics of diffusion. Oxford, Clarendon Press.
- Currie, I.G. (1967) The effect of heating rate on the stability of stationary fluids. J. Fluid Mech. 29 (2) 337-347.
- Debler, W.R. (1966) On the analogy between thermal and rotational hydrodynamic stability. J. Fluid Mech. 24 165-176.
- Du Fort, E.C., and S.P. Frankel (1953) Stability conditions in the numerical treatment of parabolic differential equations. Math. Tab., Wash. 7 135-152.
- Eddington, A.S. (1926) Internal constitution of the stars. London, Cambridge University Press.
- Elder, J.W. (1966) Thermal turbulence. Proc. 2nd Australasian Conf. Hydraulics and Fluid Mech., Univ. of Auckland, 1965 B 293-311.
- Foster, T.D. (1965) Stability of a homogeneous fluid cooled uniformly from above. Phys. Fluids 8 (7) 1249-1257.
- Fultz, D., Y. Nakagawa and P. Frenzen (1954) An instance in thermal convection of Eddington's "overstability" Phys. Rev. 94 1471-1472.
- Fultz, D., Y. Nakagawa and P. Frenzen (1955) Experiments on overstable thermal convection in mercury. Proc. Roy. Soc. (London) A 231 211-225.
- Gershuni, G.Z., and E.M. Zhukhovitskii (1963) On the convective instability of a two-component mixture in a gravity field. PMM (Translated) 27 (2) 441-452.
- Globe, S., and D. Dropkin (1959) Natural convection heat transfer in liquids confined by two horizontal plates and heated from below. J. Heat Transfer 81 156-165.
- Goldman, C.R. (1962) Primary productivity studies in Antarctic lakes. In Biologie Antarctique (Premier Symposium). Paris, Hermann.

- Goroff, I.R. (1960) An experiment on heat transfer by overstable and ordinary convection. Proc. Roy. Soc (London) A 254 537-541.
- Gosting, L.J., and M.S. Morris (1949) Diffusion studies on dilute aqueous sucrose solutions at 1 and 25° with the Gouy interference method. J. Am. Chem. Soc. 71 1998.
- Henderson, R.A., W.M. Prebble, R.A. Hoare, K.B. Popplewell, D.A. House and A.T. Wilson (1966) An ablation rate for Lake Fryxell, Victoria Land, Antarctica. J. Glaciol. 6 (43) 129-134.
- Hoare, R.A. (1966) Problems of heat transfer in Lake Vanda, a density stratified Antarctic lake. Nature 210 (5038) 787-789.
- Hoare, R.A., K.B. Popplewell, D.A. House, R.A. Henderson, W.M. Prebble and A.T. Wilson (1964) Lake Bonney, Taylor Valley, Antarctica: A natural solar energy trap. Nature 202 (4935) 886-888.
- Hoare, R.A., K.B. Popplewell, D.A. House, R.A. Henderson, W.M. Prebble and A.T. Wilson (1965) Solar heating of Lake Fryxell, a permanently ice-covered Antarctic lake. J. Geophys. Res. 70 (6) 1555-1558.
- * Hutchinson, G.E. (1957) A treatise on limnology. New York, John Wiley and Sons.
- Irani, R.R. and A.W. Adamson (1958) Transport processes in binary liquid systems. I. Diffusion in the sucrose-water system at 25°. J. Phys. Chem. 62 1517-1521.
- Jeffreys, H. (1926) The stability of a layer of fluid heated below. Phil. Mag. 2 (series VII) 833-844.
- Jeffreys, H. (1928) Some cases of instability of fluid motion. Proc. Roy. Soc. (London) A 118 195-208.
- Kelso, J.M. (1964) Radio ray propagation in the ionosphere. New York, McGraw-Hill.
- Lamb, H. (1932) Hydrodynamics. 6th edition. New York, Dover Publications.
- Lieber, P. and L. Rintel (1963) Convective instability of a horizontal layer of fluid with maintained concentration of diffusive substance and temperature on the boundaries. Inst. Eng. Res., Univ. Calif., Berkeley, MD-63-6.
- Longworth, L.G. (1939) A modification of the schlieren method for use in electrophoretic analysis. J. Am. Chem. Soc. 61 529-530.
- Longworth, L.G. (1946) Optical methods in electrophoresis. Ind. Eng. Chem. (Analytical) 18 (4) 219-229.

- Low, A.R. (1929) On the criterion for stability of a layer of viscous fluid heated from below. Proc. Roy. Soc. (London) A 125 180-195.
- Malkus, W.V.R. (1954a) Discrete transitions in turbulent convection. Proc. Roy. Soc. (London) A 225 185-195.
- Malkus, W.V.R. (1954b) The heat transport and spectrum of thermal turbulence. Proc. Roy. Soc. (London) A 225 196-212.
- Malkus, W.V.R. and G. Veronis (1958) Finite amplitude cellular convection. J. Fluid Mech. 4 225-260.
- Morton, B.R. (1957) On the equilibrium of a stratified layer of fluid. Quart. J. Mech. App. Math 10 433-447.
- Mowbray, D.E. (1967) The use of schlieren and shadowgraph techniques. J. Fluid Mech. 27 (3) 595-608.
- Nakagawa, Y. (1959) Experimental observations of overstable cellular convection. Proc. Roy. Soc. (London) A 253 212-217.
- Nakagawa, Y. and P. Frenzen (1955) A theoretical and experimental study of cellular convection in rotating fluids. Tellus 7 1-21.
- Nield, D.A. (1964) Surface tension and buoyancy effects in cellular convection. J. Fluid Mech. 19 (3) 341-352.
- Nield, D.A. (1966) Streamlines in Benard convection cells induced by surface tension and buoyancy. Z. Angew. Math. Phys. 17 226-232.
- Nield, D.A. (1967) The thermohaline Rayleigh-Jeffreys problem. J. Fluid Mech. 29 (3) 545-558.
- Nunn, M. and C.G. Wynne (1959) Lens designing by electronic digital computer : II. Proc. Phys. Soc. 74 316-329.
- Pearson, J.R.A. (1958) On convection cells induced by surface tension. J. Fluid Mech. 4 489-500.
- Pellew, A. and R.V. Southwell (1940) On maintained convective motion in a

- fluid heated from below. Proc. Roy. Soc. (London) A 176
312-343.
- Péwé, T.L. (1960) Multiple glaciation in McMurdo Sound region, Antarctica:
a progress report. J. Geol. 68 498-514.
- Philpot, J.St L. (1938) Direct photography of ultracentrifuge sedimentation
curves. Nature 141 (3563) 283-284.
- Ragotzkie, R.A. and G.E. Likens (1964) The heat balance of two Antarctic
lakes. Limnol. Oceanog. 9 (3) 412-425.
- Rayleigh, Lord (1916) On convection currents in a horizontal layer of fluid,
when the higher temperature is on the under side. Phil. Mag. 32 (192)
529-546.
- Robertson, E.I. and W.J.P. Macdonald (1962) Electrical resistivity and
ground temperature at Scott Base, Antarctica. N.Z.J. Geol. Geophys. 5
(5) 797-809.
- Sani, R. (1965) On finite-amplitude roll-cell disturbances in a fluid
layer subjected to both mass and enthalpy transfer. Am. Inst. Chem.
Eng. J. 11 (6) 971-980.
- Schaafs, W. (1966) Schichtbildungen in Konzentrationsgefallen bei
Einstrahlung von Lichtenergie. Kolloid-Z. Z. Polym. 212 (2) 146-155.
- Schmidt, R.J. and O.A. Saunders (1938) On the motion of a fluid heated
from below. Proc. Roy. Soc. (London) A 165 216-228.
- Scott, R.F. (1905) The voyage of the Discovery. London, Macmillan.
- Scott, R.F. (1913) Journals of Capt. Scott in Scott's last Expedition
(ed. L. Huxley). London, Macmillan.
- Shackleton, E.H. (1909) The heart of the Antarctic. London, Heinemann.
- Shirtcliffe, T.G.L. (1964) Lake Bonney, Antarctica; cause of the elevated
temperatures. J. Geophys. Res. 69 (24) 5257-5268.

- Shirtcliffe, T.G.L. (1967) Thermosolutal convection: observation of an overstable mode. Nature 213 (5075) 489-490.
- Shirtcliffe, T.G.L. and R.F. Benseman (1964) A sun-heated Antarctic lake. J. Geophys. Res. 69 (16) 3355-3359.
- Silveston, P.D. (1958) Warmedurchgang in waagerechten Flüssigkeitsschichten. Forsch. Gebiete Ingenieurw. 24 59-69.
- Sirs, J.A. (1959) Galvanometer feedback systems. J. Sci. Instr. 36 (5) 223-227.
- Sparrow, E.M., R.J. Goldstein and V.K. Jonsson (1964) Thermal instability in a horizontal fluid layer: effect of boundary conditions and non-linear temperature profile. J. Fluid Mech. 18 513-528.
- Stern, M. (1960) The "salt-fountain" and thermohaline convection. Tellus 12 172-175.
- Taylor, T.G. (1922) The physiography of the McMurdo Sound and Granite Harbour region in Scientific reports of the British Antarctic (Terra Nova) expedition 1910-1913. London, Harrison and Sons.
- Thomas, D.B. and A.A. Townsend (1957) Turbulent convection over a heated horizontal surface. J. Fluid Mech. 2 (5) 473-492.
- Thompson, D.C. and W.J.P. Macdonald (1962) Radiation measurements at Scott Base. N.Z.J. Geol. Geophys. 5 (5) 874-909.
- Thomson, J. (1882) On a changing tessellated structure in certain liquids. Proc. Glasgow Phil. Soc. 13 464-468.
- Turner, J.S. (1965) The coupled turbulent transports of salt and heat across a sharp density interface. Int. J. Heat Mass Transfer 8 759-767.
- Turner, J.S. and H. Stommel (1964) A new case of convection in the presence of combined vertical salinity and temperature gradients. Proc. Nat.

Acad. Sci. U.S. 52 (1) 49-53.

Tyrell, H.J.V. (1961) Diffusion and heat flow in liquids. London, Butterworths.

Veronis, G. (1965) On finite amplitude instability in thermohaline convection. J. Marine Res. 23 (1) 1-17.

Vertgeim, B.A. (1955) On the conditions of appearance of convection in a binary mixture. PMM 19 (6) 747-750.

Walin, G. (1964) Note on the stability of water stratified by both salt and heat. Tellus 16 (3) 389-393.

Weinberger, H. (1962) Stability criteria for liquid systems with temperature and salt concentration gradients. Report, National Physical Laboratory of Israel.

Wilson, A.T. (1964) Evidence from chemical diffusion of a climatic change in the McMurdo Dry Valleys 1200 years ago. Nature 201 (4915) 176-177.

Wilson, A.T. and H.W. Wellman (1962) Lake Vanda as a solar energy trap. Nature 196 (4860) 1171-1173.

Wynne, C.G. (1959) Lens designing by electronic digital computer : I. Proc. Phys. Soc. 73 777-787.

*House, D.A., R.A. Hoare, K.B. Popplewell, R.A. Henderson, W.M. Prebble and A.T. Wilson (1966) Chemistry in the Antarctic. J. Chem. Education 43 (9) 502-505.

Symbols

(Numbers in parentheses indicate chapters or appendices where a particular definition applies)

- A: Rate of heat production/unit volume (2).
 Cross-sectional area of capillary (4).
- A_k : Amplitude of k th harmonic.
- a: Numerical constant.
- b_i : i th coefficient in expression for \bar{E} .
- C: Concentration.
- c: Specific heat.
- D: Diffusion constant for solute.
 Depth below ice surface (A2).
- d: Depth offset between z and h scales.
- E: Sum of squared deviations between calculated and measured temperatures.
- \bar{E} : Mean squared deviation (E/N).
- e: Thickness of ice (water equivalent) evaporated in unit time.
- F: Solute flux.
- f: Thickness of water frozen in unit time (A2).
 Focal length of concave mirror (A5).
- g: Acceleration due to gravity.
- H: Heat flux.
- h: Fluid layer depth (3, 4).
 Half-depth of tank contents (A4).
- I: Ice thickness.
- K: Thermal diffusivity.
- k: Thermal conductivity (2).
 Order of harmonic (A6).
- k_h : Thermal conductivity (A4).
- k_s : Solute conductivity.
- l_1 : Depth to junction of fresh water layer and primary brine.

- l_2 : Depth to lake bed.
 N : Number of temperature measurements in a profile.
 N_h : Thermal Nusselt number.
 N_s : Solutal Nusselt number.
 n : Refractive index.
 P : Number of parameters being optimised (2).
 Prandtl number (ν/K) (3).
 P_s : Solutal Prandtl (or Schmidt) number (ν/D).
 Q : Incident radiation intensity (at $z = 0$).
 R : Radiation part of temperature solution (2).
 Rayleigh number.
 R_c : Critical Rayleigh number.
 R_s : Solutal Rayleigh number.
 R_e : Effective thermosolutal Rayleigh number.
 R_{ec} : Critical effective Rayleigh number.
 r : Coefficient of R_s in R_e .
 r_h (r_s): $\left[\begin{array}{l} \text{convective component of heat (solute) flow} \\ \text{non-convective component of heat (solute) flow.} \end{array} \right]$
 S : Geothermal part of temperature solution (2).
 Stability parameter (A4).
 Area of lake (A2).
 ds : Element of ray path.
 T : Part of temperature solution resulting from rearrangement of initial temperature profile (2).
 Temperature (A4).
 T_i : Temperature of primary brine.
 t : Time.
 V : Volume of specific gravity bottle.
 V_i : Inflow rate (volume of water in unit time).
 V_f : Freezing rate (volume of water in unit time).
 V_e : Evaporation rate (volume of water in unit time).
 W : Water depth in lake.

- w: Schlieren slit width.
 X: Horizontal light path length in liquid.
 X_i : i th parameter (P parameters in all).
 z: Depth below 0°C isotherm (positive downwards) (2).
 Height up capillary (4).
 z_m : Depth of temperature maximum.
 α : Thermal expansion coefficient.
 β : Temperature gradient (positive unstable).
 γ : Geothermal temperature gradient (2).
 Perturbation time coefficient (3).
 Concentration gradient (positive unstable) (3).
 ϵ : Thickness of conducting layer.
 τ : Extinction coefficient (2).
 Solutal analogue of thermal expansion coefficient ($\rho = \rho_0(1 + \eta C)$) (3).
 θ : Temperature.
 λ : Wavelength of light.
 μ : Magnetic permeability.
 ν : Kinematic viscosity.
 ρ : Density.
 Curvature of ray (A5).
 σ : Electrical conductivity.
 $\theta(h)$: Temperature measured at depth h below free water surface.
 x : Concentration.
 ψ : Numerical constant.
 ω : Angular frequency.

Polar Plateau

Taylor Glacier

L. Bonney

Ferrar Glacier

"A VERY CURIOUS VALLEY"